DISSERTATIONS IN
FORESTRY AND
NATURAL SCIENCES

Niko Penttinen

Photonic adsorption studies in liquid

devices, models, and an ellipsometric approach

Publications of the University of Eastern Finland
Dissertations in Forestry and Natural Sciences No 180

UNIVERSITY OF
EASTERN FINLAND

NIKO PENTTINEN

Photonic adsorption studies in liquid

devices, models, and an ellipsometric approach

Publications of the University of Eastern Finland
Dissertations in Forestry and Natural Sciences
No 180

Academic Dissertation
To be presented by permission of the Faculty of Science and Forestry for public examination in the Auditorium AU100 in Aurora Building at the University of Eastern Finland, Joensuu, on August, 21st, 2015,
at 12 o'clock noon.

Department of Physics and Mathematics

Printing:
Grano Oy
Joensuu, 2015

Editors:
Prof. Pertti Pasanen, Prof. Kai-Erik Peiponen
Prof. Matti Vornanen, Prof. Pekka Kilpeläinen

Distribution:
University of Eastern Finland Library / Sales of publications
julkaisumyynti@uef.fi
http://www.uef.fi/kirjasto

ISBN: 978-952-61-1818-5 (printed)
ISSNL: 1798-5668
ISSN: 1798-5668

ISBN: 978-952-61-1819-2 (PDF)
ISSN: 1798-5676 (PDF)

Author's address:
University of Eastern Finland
Department of Physics and Mathematics
P.O.Box 111
FI-80101 Joensuu
FINLAND
email: niko.penttinen@emso.fi

Supervisors:
Kai-Erik Peiponen
University of Eastern Finland
Department of Physics and Mathematics
P.O.Box 111
FI-80101 Joensuu
FINLAND
email: kai.peiponen@uef.fi

Reviewers:
Tom Kuusela
University of Turku
Department of Physics and Astrology
Vesilinnantie 5
FI-20500, Turku
Finland
email: tom.kuusela@utu.fi

Jarl. B. Rosenholm
Åbo Akademi
Fysikaalisen kemian laitos
Porthaninkatu 3-5
FI-21500, Turku
Finland
email: jarl.rosenholm@abo.fi

Opponent:
Tommy Nylander
Lund University
Department of Chemistry
Box 117
SE-22100 Lund
Sweden
email: tommy.nylander@fkem1.lu.se

ABSTRACT

Any liquid environment contains a vast amount of variables, some of which might still be unknown to this day. While this environment has been under intensive study for decades and instrumentation constantly improves, the fundamental questions about the chosen models and variables remain. This creates a wide variety of discussion but very few standard approaches.

There are two main foci in this study: an extensive study of the literature and an ellipsometric approach in detecting particle adsorption. The study on literature serves as a base for discussion, which is mostly considering what is and isn't a plausible photonic model in adsorption.

The empiric part of the study concentrates on analyzing primal signal changes observed in a liquid environment. The equipment used is constructed seeking to create a simple ellipsometric build that works in particle adsorption detection. A multi–fiber spectrometer is successfully used as a detector, and indicates that by recording parallel signals from a system, a benefit could be achieved in both analyses and signal improvements.

Different numerical adsorption models are constructed, calculated, compared, and further discussed. Discussion on the background of the adsorption phenomenon and measurement analysis strongly indicate, that the liquid environment should be handled with care. The vast amount of variables involved create a challenge to photonic approaches, which are highly sensitive to selected models and material properties. This study progresses through device level challenges, basic general ellipsometric theory, and calculated models seeking to present matters to be considered.

Universal Decimal Classification:
(043), 510:535.5, 514:532.6, 532.6, 532.6:539.6, 535.3, 535.5, 535:602, 542.6:543.4, 542.6, 543.4, 681.7
PACS Classification:
06.60.Sx, 07.05.Tp, 42.25.Ja, 42.25.Hz, 82.37.-j, 87.14.E-

Library of Congress Subject Headings:
Optics, Adsorption, Photonics, Biophysics, Polarization (Light), Ellipsometry, Polarimetry, Liquids, Proteins, Nanoparticles

Preface

These four years after my master's thesis have been immensely diverse. It seems that I could fit a lifetime into every individual year that has passed. Last one of those years was filled, among other projects, by this study and writing work. The topic of this work has been under scientific research work for decades, but still there are things to do. This long history, and perhaps arguably ambiguous results, makes the whole subject hard to believe in. However, I am grateful to Finnish Culture Fund and to the Foundation of Alfred Kordelin for the two years of funding my research. This goes to show, that there are still entities that see the science as a diverse tool in understanding all parts of the nature.

I would like to thank the SiB–Labs color group of Joensuu for being a splendid work environment for the last two years that I have been working there. Especially, I would like to thank Tapani and Markku who contacted me, hired me as a coder, and who also continued to see the scientist in me. Essentially you are the ones who most likely made it possible for me to continue working on my thesis. Furthermore, Tapani, and Ville, I really enjoyed our daily coffee discussions and your company in general. In addition, I would also like to thank Kai-Erik for guiding me through the PhD bureaucracy.

A big thank you also to the lab personel who helped me. Especially Tommi, who's is responsible for the measurement cuvette for this study. You always produce better than I ever ask. It really shows that you care what you do, which I really appreciate.

I would also like to thank my family and friends. Especially mentioning Stanislav Hason, who has been helping in purchasing both molecules and surfaces for my studies as well as being a co–author and a friend. And Martti, I really enjoyed our co–operations both at work and during free time. Also, Martti, thanks for the nanoparticles for my few measurements.

Finally, Anni. We have been together nearly a decade. I would like to thank you from the bottom of my heart. You bear my long days at work, cranky behavior, and your smile still greets me when I come home. Your empathy and love is unmatched by no one I have ever met. Nothing can top that. Thank you.

in Joensuu, June 27, 2015

Yours,

Niko Penttinen

"Critical analysis further finds that it is not generally possible to style any particular researcher's work as 'right' or 'wrong'; the best is the same as the rest – different. Consequently, there seems little purpose in a systematic review of this literature jumble until and unless it can be discovered how it comes to be that this collection of work, performed by so many highly qualified researchers over so many years with increasingly powerful analytical tools, has become so internally inconsistent."

Erwin Vogler

Protein adsorption in three dimensions

Biomaterials 33(5), 2012

OTHER WORKS

I have also performed other studies during my post–graduate period. These publications, excluding conference papers, consist of *eight* multidisciplinary journal papers published in peer–reviewed journals either about measurements in a liquid environment, or about general spectral material measurement and analyses. However, despite these previous journal papers, it cannot be addressed enough, that this study stands on its own as an independent work. Furthermore, in the moment this thesis was printed, four more journal paper work were actively undergoing.

Contents

1 INTRODUCTION **1**

1.1 Motivation 1
1.2 Putting things into perspective 2
1.3 Aim and structure of this study 4

2 ADSORPTION FUNDAMENTALS AND PHOTONIC RESEARCH **7**

2.1 Approach to adsorption in this study 7
2.2 A few words on biomaterials 8
2.2.1 Material response and properties 9
2.2.2 Actual materials 10
2.2.3 Proteins? 12
2.3 Interatomic forces 12
2.3.1 Force between charges 12
2.3.2 van der Waals 13
2.3.3 Evaluation of the forces 15
2.3.4 Atomic Force Microscopy 16
2.3.5 Impact on adsorption 17
2.4 Liquid media 17
2.4.1 Hydration forces 19
2.5 Variables in adsorption 22
2.5.1 Material porosity 23
2.5.2 Intermediate factors affecting adsorption . . . 24
2.5.3 Reversibility of adsorption 37
2.5.4 Isotherm and kinetics 38
2.5.5 Interfering 43
2.5.6 Sample characterization 45
2.5.7 Conclusion 46
2.6 Nanoparticles 47
2.6.1 General 47
2.6.2 Synthesis 48

2.6.3 Toxicology 49
2.6.4 Photonic interests 50
2.6.5 Atomic models 50
2.6.6 Conclusion 51
2.7 Photonic methods 51
2.7.1 Method types 51
2.7.2 Reflection and ellipsometry 53
2.7.3 Total Internal Reflection 55
2.7.4 Surface Plasmon Resonance 56
2.7.5 Other methods 57
2.7.6 General photonic results of previous studies . 61
2.7.7 Conclusion 64

3 THEORY **69**
3.1 General photonics theory 69
3.2 Polarization 73
3.2.1 Polarization 73
3.2.2 Stokes parameters 74
3.2.3 Fresnel equations and Snell's law 77
3.2.4 Setup in the reflection observations 81
3.2.5 Jones formalism 82
3.2.6 Jones formalism output in PSA reflection . . . 83
3.2.7 Irradiance of the reflected field 85
3.3 Ellipsometric parameters 86
3.3.1 Ellipsometric and Stokes parameters 87
3.3.2 Discussion of the nature of Ψ and Δ measurements 88
3.3.3 Polarization dependent output of systems . . 89
3.4 Thin film reflection 92
3.4.1 Single film reflection 92
3.4.2 Ellipsometric parameters 93

4 MATERIALS AND METHODS **95**
4.1 Devices and computer programs 95
4.1.1 Devices 95
4.1.2 Programs 95

4.2 Surfaces and particles 95
4.2.1 Surfaces 95
4.2.2 Particles, molecules, and solutions 98
4.3 Measurements 104
4.3.1 Measurement setup 104
4.3.2 Quality of the sensor used 106
4.3.3 Liquid environment measurements 107
4.4 Models 109
4.4.1 What is a model anyway? 109
4.4.2 Need for mathematical modeling 110
4.4.3 Models in different photonic systems 113
4.4.4 Models used in this study 116
4.4.5 Photometric evaluations 120
4.4.6 Model challenges 125
4.4.7 Conclusion 127

5 RESULTS AND DISCUSSION 129
5.1 Characterization of the used samples 129
5.1.1 Contact angle and topography 129
5.1.2 Atomic force microscope observations 131
5.1.3 Titanium heating 132
5.1.4 Justifying the numerical models 134
5.2 Observed kinetics 138
5.2.1 Temporal signal challenges 139
5.2.2 HSA protein isotherm 143
5.2.3 HPF protein kinetics 148
5.2.4 Signal from numerical models 155
5.2.5 Model–predicted adsorption and model goodness 159
5.3 Discussion 166
5.3.1 Errors and possible contamination sources . . 166
5.3.2 Results 168
5.3.3 Effect of the model 171
5.3.4 Device selection 174
5.3.5 Surface characterization 175

5.3.6 Accuracy and repeatability of the study 176
5.3.7 Future 178

6 CONCLUSIONS **181**

A ON PROTEIN CHEMICAL COMPOUND NAMES **183**

B PROTEIN SHAPE AND SCALE **185**

C INTERFERING ELECTRIC FIELDS **187**

D ELLIPSOMETRIC EQUATIONS **191**

BIBLIOGRAPHY **194**

NOTATIONS

A	Amplitude of a field	
$\mathbf{J}$	General Jones operator	
i	Complex unit number, $i^2 = -1$	
E	Electric field	
d	Thickness of material	[m]
r	Fresnel coefficient for reflection	
R	Reflectance	
t	Fresnel coefficient for transmission	
T	Transmittance	
x	Coordinate direction x	
y	Coordinate direction y	
z	Coordinate direction z	
s	Denotes S-polarization ($\perp$)	
p	Denotes P-polarization ($\parallel$)	
N	Complex refractive index	
M	Amount / repetition count	
t	Time	[s]
*	A complex conjugate	
α	Rotation angle	[°] / [rad.]
θ	Photon incident angle on an interface	
θ_C	Water contact angle	[°] / [rad.]
λ	Photon wavelength	[m]
Ψ	Ellipsometric amplitude term	
Δ	Ellipsometric phase term	
I	Irradiance of a wave	[W/m^2]
ω	Angular frequency	[rad./s]
γ	Tension	[N]

Abbreviations in text

AFM	Atomic Force Microscope
CPU	Central Processing Unit
GPU	Graphics Processing Unit
HPF	Human Plasma Fibrinogen
HSA	Human Serum Albumin
LYZ	Lysozyme
PAP	Parallel processing
PCSA	Polarizer-Compensator-Sample-Analyzer (Ellipsometer)
PSA	Polarizer-Sample-Analyzer (Ellipsometer)
RAE	Rotating-Analyzer-Ellipsometer
SEM	Scanning Electron Microscope
SLE	Simple Layer Estimate
SNR	Signal to Noise Ratio
SPR	Surface Plasmon Resonance
TIR	Total Internet Reflectance
VAE	Variable Angle Ellipsometer
VASE	Variable Angle Spectral Ellipsometer
MFS	Multi-Fiber Spectrophotometer

1 Introduction

This chapter seeks to put things into perspective for this study, to provide an underlying path for the progression of the study. Before going into the actual subject, we will discuss the motivation of the study as well as its main aims.

1.1 MOTIVATION

A reason for studying adsorption phenomenon could have various motivations. The aim could be to provide a novel method to observe a phenomenon or to improve an existing method. Furthermore, the commercial potential in nano-detection is both clear and immense.

But an underlying reason for particle detection could generally come from biology. Human biology to be precise. It is of great interest to understand both the biological compatibility of a material and reaction of such a material inside a living organism. Both implant material and drug delivery are of interest through macroscopic and microscopic scale.

Whether the aim is to observe nanoparticle interaction with drugs to provide new drug delivery possibilities or just to observe a new plastic or metal inside a living orgasm, the overall aim is always in the physio-chemical field of adsorption studies. Photonics has been used as a tool to assist in these observations for decades. Still, good deal more will be found as understanding grows slowly. While studies have been conducted for years, the real environment still remains a mystery. More or less. This is because there is a large gap between *in–vivo* (inside living things) and a *in–vitro* (”glass tube”) experiments. Usually, more theoretical studies in laboratories have a much more simplified environment compared to the actual environment of a real biological body. However, it is those studies which provide questions of fundamental processes behind phenomena, studies such as this, that might move things towards

meaningful goals. So, while this study does not deal with ground–breaking novelties, for reasons that should become clear, it will provide a humble but critical approach to the vastness of variables that physics and chemistry kindly provides, and presents them in the perspective of photonics.

1.2 PUTTING THINGS INTO PERSPECTIVE

The main effort to detect proteins and particles in liquid environments using ellipsometry has been ongoing for nearly four decades. Since the 1970s observations have concentrated on kinetics and packing discussion on various surfaces [1–3]. Irwin Langmuir even provided kinetic proposals nearly one hundred years ago [4,5]. These things said, we are mixing a wide variety of multidisciplinary research fields into this study.

While extensive studies have been made to understand protein adsorption, models are not yet perfect. Far from it, since this long research history will create yet more theories about the adsorption of particles into the existing of multidisciplinary studies in this field. This study tries to acknowledge this past research, but due of a combination of several areas of expertise, something still might be missing from the analyses done here. To include background and discussion about the fundamentals of the phenomenon, chapter 2 was written. This chapter includes some of the historical work done towards understanding the adsorption phenomenon of particle adsorption. The main focus in the whole study will be the photonic detection of adsorption in liquid, but as previously stated, we are following in the footsteps of significant researchers.

Figure 1.1 presents an overly simplified schematic of a combination of fields which need to be addressed before delving into the topic of photonic detection of adsorption. This is the minimal image that should be constructed as a concept prior to starting photonic studies in any liquid environment. Moreover, this same trinity comes into play in many research areas when either a liquid or a plasma phase is present. A solid and a gas are friendly as material

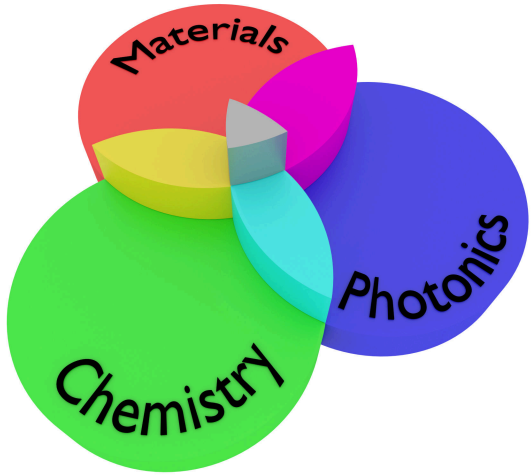

Figure 1.1: *A conceptual visualization of three research field that can overlap in an adsorption study.*

phases because when they coexist, a stable state and interface for the materials usually exists during the measurements. However, once a third phase is introduced, great caution should be shown, because one new material phase might be accompanied by a multitude of variables.

A rather ambiguous field, "materials", is shown in the visualization in Figure 1.1. Materials here represent a general material, usually solid in nature, and provide a clear distinction of thought which should remain between these three entities. A physicist like the author could say that it is ridiculous to differentiate materials from photonics in the same way as separating materials from physics. But again, this is just a one way of observing the phenomenon and hopefully provide a state of mind for what is to come.

Figure 1.1 shows that these three fundamental categories overlap one another, as well as that they can overlap only two at a time, creating many different approaches. When thinking about overlapping chemistry and a material, we are discussing material chemistry and physical chemistry, and when overlapping photonics and

materials, we are naturally discussing the photonic properties of a material. The main thing to comprehend from the Figure 1.1 is that these areas and points of views cannot be defined as fully separable entities in a liquid environment. They are and will play a major part of the particle adsorption detection with photons and thus should be always noted.

Returning to the liquid environment and the challenges of measuring with photons, constantly moving liquids with their swirly refractive indices and internal chemistry are enough of a challenge even without interacting nano-sized particles. However, that is the direction of this study. Discussing and studying this phenomenon can only lead to benefit.

1.3 AIM AND STRUCTURE OF THIS STUDY

It was already noted in 1998, that "Ellipsometry is now a well-established method for the investigation of protein adsorption phenomena at interfaces" [6]. But only recently, in 2012, it was said about adsorption studies that, "The literature is a mess." [7] So, while the phrasing might enable us to note something, it should not be interpreted as a direct discovery of all underlying phenomena.[a]

The aim of this study was to research the underlying phenomenon of adsorption as well as discuss a polarimetric device as a tool for studying the said phenomenon, while providing information about photonic methods. One focus is in describing a minimal setup of polarimetry to study adsorption and discuss any hardware used in the device in greater detail. However, the main focus is in the discussion of the photonic models that has been and are used to evaluate the complex phenomenon of adsorption.

[a] Without belittling any study, for example the "method for the investigation" is rather far from the phrase "method for qualifiably characterizing."

The aims of the work are as listed:

1. To provide:
    - An introductory level of information about the adsorption phenomenon.
    - A collection of work already done in an aspect of photonic detection of adsorption.
    - A minimum theory of polarimetry related to the generally used Ψ and Δ variables of ellipsometry.
2. To compare:
    - Different calculation models and effect of variables.
3. To discuss:
    - Different ellipsometric constructions.
    - The state of photonic research of adsorption.
    - If it is really possible to detect protein adsorption on titanium.
    - Other explanations for detected signals.
    - A signal and light source quality as well as key detector variables.
    - Example signals from real surfaces.

The word *optics* and *optical* both have a strong historical correlation to visual range of photon wavelengths. While the word optics is well–established and has been used for even invisible wavelengths, it must be said that previous usage does not claim to be a good policy. Thus, more general terminology involving photons is used throughout this dissertation. Optical is now photonic and optics correspondingly is photonics. While this might seem odd, it is done because there is no desire to even hint that these methods would just involve the visual range of wavelengths. We understand, that photons could also include, for example, X–rays and far–

infrared methods, which are both outside the scope of this study, but we still believe, that if appropriate and possible, one could still extent many things from this study to different photon energies.

This study aims to cover the basics of adsorption in liquid as well as related photonics. That is not an easy task to do, because existing literature discusses both fundamental and intermediate phenomena, which relate to the adsorption. Furthermore, depending on the research field where these things are discussed, there can be a very different value given to these fundamental and intermediate phenomena. Thus, we will shortly go through the fundamental basics, and after this, we will move to discuss the intermediate phenomena. Mainly, the fundamental discussion in this study contains the interatomic forces and discussion of the liquid media itself. All intermediate effect come from these fundamental sources and are discussed separately. Understandably, interatomic forces and chemistry related to liquid environment is too big of a challenge to include in any individual study, so a lot will be dismissed.

The photonics part of this study will concentrate to describe Ψ and Δ, the ellipsometric parameters commonly associated with any ellipsometric study, but the main aim is to discuss the actual analytic value of these parameters. Or more accurately; how analytic Ψ and Δ really are in a liquid environment? This discussion is done using several different scenarios in the used models.

When the fundamental and intermediate basics has been covered, we should already understand where the conclusions are heading. It should become clear for the reader of this work, how much fundamentals can be dismissed in a photonics study of adsorption. We will conclude, that the complex liquid environment and corresponding vast amount of parameters of interatomic interaction should be interpreted with caution. We will also remark, that the chosen refractive indices and used model can produce a huge variation to the final results. Especially, if absolutely no remarks on the interatomic forces or evaluation of optical models are done.

2 *Adsorption fundamentals and photonic research*

Despite photonics being the main topic in this study, this chapter describes the background of the particle adsorption phenomenon on an introductory level. It will also discuss photonics, but only to collectively state and compare the historical and current status of adsorption research.

This chapter tries to lay out some framework to the adsorption phenomenon. Firstly, few key points are made about biomaterials, interactomic forces, and liquid media (sections 2.2, 2.3, and 2.4). Secondly, the adsorption is discussed through intermediate phenomenon, and related key points, which are commonly seen in adsorption studies (section 2.5). Especially, the section 2.5.2 makes a clear list of the effecting variables in protein adsorption.

2.1 APPROACH TO ADSORPTION IN THIS STUDY

In this part, we are at the crossroads of historical studies and knowledge. We will not fully consider the highest level of discussion, which would be purely atomic. Few words on interatomic forces will be said in section 2.3, but even if atom–level calculations might perhaps solve much of the unknown, there is currently no tools that can do that. Calculation requirements would be astronomical for general adhesion studies with big molecules. Instead, descriptions and explanations usually from lower–level empiric observations and measurements are not only more meaningful but are also easier to comprehend.

Furthermore, this chapter of the work provides both limitations on and opportunities for the interpretation of results of this study. A great deal of work has been made in aim to understand ad-

sorption as phenomenon and all intermediate observations that it produces. There is no single work that could be pointed out, but there are few that stands out when discussing the protein adsorption [3,7,8]. Actually, this is one of the most important things to note. Adsorption as phenomenon, even with proteins, does not directly equal that we are discussing biomaterials. Adsorption is more about the fundamental interatomic forces and anything "bio" is evaluated in different context. No doubt there is a dream to connect the fundamental phenomenon of adsorption and biomaterials, but after sections 2.2 and 2.3, it should be clear, that a great challenge exists in combining these two.

Finally, the adsorption phenomenon is still strongly motivated by the potential for immediate biological applications. Those applications are all kept at minimum in this section and we will only observe adsorption in liquids, as this study is entitled to do. The main aim are the proteins, so that those more strongly connected to chemistry, such as lipids [9], poly(ethylene glycol) (PEG) [10], polymers [11–13], polymer surfaces such as polyelectrode multilayers (PEM) [14,15], self-assembling monolayers (SAM) [16], and platelet adhesion [10,17] are all left out. These are major fields of study, but are too large to cover in detail here. Similarly, we will omit most of the actual biochemistry background for the same reason. The field of biochemistry creates greatly detailed descriptions of each functional group of proteins and induces a whole new level of discussion that is beyond the scope of this study [18,19].

2.2 A FEW WORDS ON BIOMATERIALS

When biomaterials are discussed, there is always constant interest in finding new, cheaper, and more applicable materials. Williams ([20], 2009) has discussed the meaning of the whole word "biomaterial" and concluded the following:

> "A biomaterial is a substance that has been engineered to take a form which, alone or as part of a complex system, is used to direct, by control of interactions with components of living systems, the course of any therapeutic or diagnostic procedure, in human or veterinary medicine."

Williams also included several previous definitions of biomaterial in his paper. This study will not redefine anything. Here we simply state that *a biomaterial is a substance aimed to be used within a living organism*. This usage usually involve engineering bone replacements because bones construct the frame of human body and sometimes need a replacement or redoing [21–24].

2.2.1 Material response and properties

Any material that is in contact with the human body generates a reaction with a human body's immune system. Sometimes this reaction is expected to be minimal, sometimes maximal, depending on the application. For example, if a material is expected to be a delivery agent of some sort, it is understandable that a minimal reaction is desired to increase delivery rates. Similarly, if a material is to be integrated into a body, some reaction would be ideal [25–27]. This reaction with the body depends on how the innate[a] immunity system responds to the material in question. Macrophages and dendritic cells are believed to be one of the initial functional cells that determine the immune system reaction to a substance [26,27]. Despite the body–centrific view, a response of a material is still interesting as any material could have some other biological usages, such as a reaction with bacteria or viruses [28–30].

Depending on the actual need for a material, the material should not only have a positive integration with the body but should also be structurally optimized. For example, scaffolding biomaterials are something which provide increased cell attachment, increased

[a] First line of defense of the immune system.

flow transport, and controlled biodegradability [21,22,31,32]. Biomaterial is usually desired to have [33]

1. Good mechanical properties
2. Chemical and physical durability
3. Biocompatibility
4. "Bone-compatibility" (Osseointegration)

The mechanical properties need to be correct so that any stress moves along the material in the proper way. The material should not corrode in the body nor it should erode too quickly. In addition to being biocompatible, the material should provide osseointegration. Osseintegration involves the material having the ability to be a growth platform for bone cells.

Cell adhesion and osseointegration

The standard for testing a biomaterial is usually cell culturing. It is easy to understand that if a cell can be cultured (grown) on a surface, the surface would be compatible or at least non-toxic to that particular cell. However, the case is not that simple. Cells need to be evaluated in different ways and there are numerous active components in cell–adhesion tests. We should bear in mind that cell–adhesion can and are used to test biomaterials. For example, see one work of Anselme ([34], 1999) for different quantitative cell–adhesion tests. A cell–adhesion test can test toxicology, biocompatibility, and the ossoeintegration of a selected material.

2.2.2 Actual materials

Titanium

When discussing the application of titanium, there is no doubt that bone replacements are one of the first applications that come into mind. Indeed, titanium fills all the required compatibility requirements of a biomaterial and is already widely used. Some of the

compatibility is thought to come from the natural oxidation of the titanium [35,36]. This has created a countless number of different researched titanium alloys which seek to be the next advancement in the use of titanium [33]. As this is the introduction to this topic, the selected material in the experimental section is also titanium [37].

For implant usage review, see the paper of Long and Rack ([38], 1998) which demonstrates a good comparison of titanium and other possible materials. For a truly concrete description of implant usage, see the study of Albrektsson *et al.* ([39], 1981) which illustrates the actual use of implants.

Other materials

The fundamental materials for concept–testing purposes is usually silver (Ag), gold (Au), or platinum (Pt). All are considered biocompatible and have good chemical stability, for example, in detection applications [40]. This even more the case with gold and silver nanoparticles, which also have interesting photonic properties (see section 2.6).[b] Still, an ideal reaction is not enough. The mechanical properties also need to be in order. Thus, a vast number of different materials have been extensively researched: materials such magnesium (and alloys) [41,42], peptides [32], collagen [43], hydrogels [44,45], chitin/chitosan [46], silk [47], zirconia [48], carbon-based materials [49],[c] and numerous porous materials [31]. It could be suggested that any material with reasonable mechanical and structural stability at a room–condition environment has most likely already been tested for a bio-application.

[b] Platinum is an excellent catalyst in chemistry. It is not used so much in adsorption studies since it is one of the most expensive substances on earth.

[c] Hydrogen adsorption/absorption is particularly of interest in potential hydrogen-cell applications [50,51].

2.2.3 Proteins?

The question is what does protein adsorption really tell us? It has been widely studied, so how does it differ from cell–adhesion tests? The initial inflammatory response of the human body originates from the actual blood and thus the first plasma molecules, such as proteins determine the initial cell response [52,53]. Anderson *et al.* ([53], 2005) aptly noted when protein adsorption was mentioned in the implant context.

> "... it is highly probable that the types, levels, and surface conformations of the adsorbed proteins are critical determinants of the tissue reaction to such implants."

The exact causality of protein adsorption is still unknown and very much unique from surface to surface, so there is no direct answer to the questions above. Still, there is no doubt that protein and other particles are of interest when evaluating potential biomaterials even if single protein adhesion wouldn't directly tell if material is biocompatible.

2.3 INTERATOMIC FORCES

In section 2.1 we already stated that atomic level discussion is not in the aim of this work. However, few words must be said about them before we continue. Adsorption, as a phenomenon, is all about *interatomic* (between atoms) and *intermolecular* (between molecules) forces. With large molecules, such as proteins, *intramolecular* (within molecule) forces can even dictate their natural complex structure, and with that, their natural functionality.

2.3.1 Force between charges

Coulombian forces (electric charge) are very important or even fundamental factor in particle behavior. Electrochemistry and electrokinetics is major field of study targeting both inorganic and organic particles. More importantly, charge transfer within atoms as

well as existing ions play important role in all liquid environments. The direct Coulomb's force attracting point charges Q_1 and Q_2 is [54]

$$\mathbf{F}_{12} = \frac{Q_1 Q_2}{4\pi\epsilon_0 r^2}\mathbf{r}_{12}, \tag{2.1}$$

where ϵ_0 is the permittivity of a vacuum ($8.854 \cdot 10^{-12}$ F/m), r the distance between the particles, and $\mathbf{r}_{12}$ the resulting vector between the charges.

We will now make a clear separation. An external field can be used to manipulate particles and analyze the kinetics of these particles. However, in a real environment, such as biological, there are generally no external fields. Thus, electrokinetics could be considered an analytical method for particle detection, separation, or other analysis. The use of external fields is different from the passive environment, for example, of protein adsorption, which usually deal with induced dipoles and corresponding van der Waals forces. While electrokinetics is useful in many analytical methods, we do not consider it in this study.[d] Still, this fundamental force is seen within all particles having a change, which understandably effects adsorption if it is brought into play.

While Equation 2.1 is useful in some models, it is still quite cumbersome for use at the atomic level. Also, atomic calculations are separate from simple Coulombian force calculations. Furthermore, the Coulombian force can be rather difficult to use when, for example, dipoles are discussed. When van der Waals forces come into play with non–permanent and permanent dipole particles, the calculation of the dispersion forces has to be done [55]. While this is a completely different matter, it is shortly discussed in the next section.

2.3.2 van der Waals

It could be bluntly stated, that interatomic forces define the adsorption phenomenon. These short–range forces are, namely, van der

[d] For further information on the electrokinetics, see Morgan and Green, "AC Electrokinetics: colloids and nanoparticles" [54].

Waals forces. The forces are divided to Keesom, Debye, and London dispersion forces, which contribute to dipole–dipole, dipole–induced–dipole, and induced–dipole–induced–dipole interactions correspondingly. Forces between permanent dipoles might follow nicely a theory similar to Coulombian force, but with induced dipoles, the challenge of analysis lies in temporal dynamical nature of the created dipoles.

The list of intermediate factors in adsorption, that we will create in section 2.5.2, could perhaps be directly explained by the van der Waals forces. However, the exact solving of those forces for a complicated liquid environment with interparticle forces would be too much even for modern computers.

Keesom and Debye forces

Keesom and Debye forces are the easier van der Waals forces to understand. If a permanent dipole charge is introduced to a vicinity of another permanent dipole or charge-neutral entity, there will be attraction force between these two entities. This is rather important especially with salt solutions, which are filled with different ions and dipoles.

London dispersion force

London dispersion force counts for many natural phenomena, that cannot be explained with permanent dipoles. If there wouldn't be a force such London–dispersion force, many ideal materials, such as the noble gases in liquid form, wouldn't be held together, as there are no charge–attraction between the atoms. London–dispersion force is created from the coupling of electron through permutations. This is schematically drawn in Figure 2.1. London dispersion force could be thought as electron–orbital imperfection inside single atom, or as a coupling of atom–atom electron orbitals, because those are, in this case, the same.

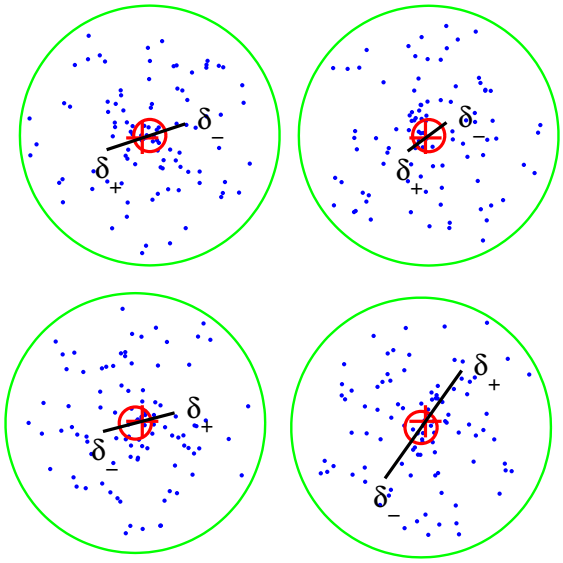

Figure 2.1: *Schematic representation of ideological concept behind London dispersion force. Presented four non–correlated atoms with 50 random electron positions (dots) around an atom center (red cross). The temporal positions of electrons constantly recreate the effective charge center (red circle) which differs from the atom center. This effectively creates a dipole, even within a single atom, with dipole charges δ_+ and δ_-. This very small imperfection will then further couple to surrounding atoms, creating the London–attraction forces.*

2.3.3 Evaluation of the forces

We will now shortly discuss how these forces can be approached. In general, all van der Waals forces are short–range forces with $1/r^6$ relation to distance [56]. The Keesom–contribution is somewhat directly related to the dipole charges of two interacting entities. However, with Debye and London dispersion forces, polarizability term is added to the equations. Understandably this polarizability describes how strongly any atomic entity resists an external field. Hamaker originally introduced ([57]) a method of calculating a single energy value between materials, indicating attraction forces, and

these calculations have been studied ever since that, producing several approximations, and further improvements [55,56,58,59].

However, from a photonic point of view, the polarizability of these evaluated entities (molecules or atoms) can also be expressed with material permittivity [55,56,58,59]. Ideally, when material energy spectrums, or "density of states", are fully known, a Hamaker constant between these materials can be calculated [58]. There are also approximations, which don't need the full energy spectrum. However, this kind of fundamental theory, calculations, and approximations should be a separate study. Thus, they are dismissed from this study. Also, the exact Hamaker calculations become near impossible, when dynamic states of material are discussed. Then, the question is, *what are the energy states of a big buffer-liquid-dissolved organic molecule, that could be reliably used in the evaluation of interatomic forces*? Understandably, this question is not part of this study, but we note the challenge in potential calculations as complex molecules change over time.

2.3.4 Atomic Force Microscopy

When discussing interatomic forces we cannot ignore atomic force microscope (AFM). The principle of AFM is to move a small and sharp tip near a sample surface. This tip is attached to a cantilever, and the movement of this cantilever is usually evaluated with measuring changes in laser beam reflected from the cantilever.[e] Other methods, such as piezo–electric, are also used to detect the cantilever position. The actual movement in the scanning of the tip in three dimensions is done with piezo–elements.

The importance of AFM is in the accuracy of it. Forces as small as 10^{-18} Newtons [60] towards the cantilever can be detected; in air and also in liquid environment. Furthermore, the tip can be charged with electrically which makes it possible to detect charge transfer between the tip and a sample. Different organic films have

[e] Originally, in [60], the cantilever position was evaluated with scanning tunneling microscope.

been successfully measured with AFM for a long time [61], but more importantly, because of the liquid environment possibilities, AFM has been even used to evaluate the water–surface association [62], which would be extremely valuable in all adsorption studies. However, this is again one thing that cannot be covered in this study as the theory as well as the execution of an AFM force measurements would be a whole new ordeal for any study. For more extensive outlook on the fundamentals of AFM, please see, for example, the reviews [56,58,63–65].

2.3.5 Impact on adsorption

The adsorption is defined by the interatomic forces. So there is no question, that they wouldn't have impact on adsorption. Question is; *how much of the interactomic forces one can reveal or evaluate in an individual study*? The numerical approach is still rather big for anyone to handle. Calculations of atomic level systems are emerging [66,67], but extensive temporal and large molecule calculations in a liquid environment, are still just too much for any device to handle. Even few hundred picoseconds of calculation, in more defined environment, is both tedious and could be considered a long time [68]. So, there is much work to cover to model these slower diffusion and adsorption phenomena in complex liquid environments.

This all said, we will try to approach the adsorption phenomenon with more intermediate effects, such as listed in section 2.5 below. However, the key point here is to realize, that all adsorption related phenomena and the intermediate effects emerge from the interatomic forces. For more on the van der Waals forces see, for example, the works of French ([55], 2000) and Butt *et al.* ([56], 2005) as well as the references therein.

2.4 LIQUID MEDIA

Liquid is a very broad word and the author also takes the knowing risk of using it here. Some things could change with deviations

from the obvious water, but only some as the phase would be liquid. Furthermore, many things could be similar even if a radical change in the liquid phase were to occur. Still, this depends highly on the actual media used and how it is evaluated, if at all.

Because the main focus here is on the liquids of the human body and biomaterials, water and human blood become the main subject of our interest. Water is still the general solute in the human body, and with that, a major part of blood. Moreover, blood is always there if outside materials, such as implants, are introduced to the human body. Incidentally, since blood consists of proteins, the adsorption of proteins is generally connected to the biocompatibility of the material [69].

Different ambient media, such as liquids, have been successfully used also in ellipsometry to provide increased accuracy instead of using different incident angles [70]. Also, different adsorption isotherms have been evaluated for simple liquids using ellipsometry [71]. But without going into photonic research more deeply, what is the impact of the surrounding media to particle adsorption? There is no direct answer to this as complex chemical processes could be involved near adsorbent depending of the liquid media. Still, no doubt that any free ions would have an effect if put in this said media, if not through chemical effects, at least in photonics perspective.

The solute for the particles in this study is a phosphate buffered saline (PBS) which is a commonly used buffer in protein studies [7, 72–97]. Exact fractions of the materials of this solution are described later in section 4.2.2, but it is important to note that the solute is not pure water. PBS contains many free ions compared to pure water. It is also closer to the real human body environment, which is understandably an important factor. Because of this reasoning, the background research for this work tries to exclude these pure water solute studies. The author wants to make clear that though water is a very important part of the protein adsorption, it should not be a pure solute for the proteins since it is too far from the real body environment.

The effect of ions in a solution is never a trivial task to solve. Even salt diffusion can be considered a high level research [98] and different salt sorption is very important, for example, in earth soil functions [99]. But if the salt ions can travel freely in a certain volume of a liquid media and the aim is studying, for example, a protein adsorption, through van der Waals forces, the salt ions must effect water–surface, surface–particle, and particle–water forces. And despite the fact that these ions could be considered helping or obstructing the adsorption, there is no universal solution for the ion effect and studies remain very setup specific [100]. The whole topic of salt is rather quietly dismissed in photonic studies even if it might be very important factor. While it would be interesting and even fundamental topic to cover, the sheer amount of background to start the discussion is immense, and thus, the evaluation of the effect of the infused salts is left out from this study.

2.4.1 Hydration forces

In connection to van der Waals forces, the liquid environment, and even the interactions of a simple water molecule is a complex discussion. Even the definition of an interface is not trivial task, because the interface could be thought as *Laplace* or *Poisson* interface. A Laplace–type interface has only two materials and the interface is a binary step, while on the other hand, a Poisson–type interface has a transition stage between the said materials [101]. However, now we will discuss, through illustrations, just the hypothetical behavior of water molecules near interface.

Water has a natural dipole charge and associates with itself through hydrogen bonds. Figure 2.2 shows, according to [101], a schematic representation of so called primary hydration force. Figure 2.2 shows schematically, different strengths of interaction of water very close to an interface. It is clear from the figure, that if we are discussing photonic detection of layers only a few nanometer thick, these fundamental interaction forces could have a huge effect on the measured signals. But we will conclude from Figure 2.2,

that essentially, the hydration force seems to be just the complex interaction between the water molecules, which is a phenomenon that could have an effect even on the photonic signal. Also, this could affect the depth density of water near an adsorbent, which definitely would change photonic signal analyses.

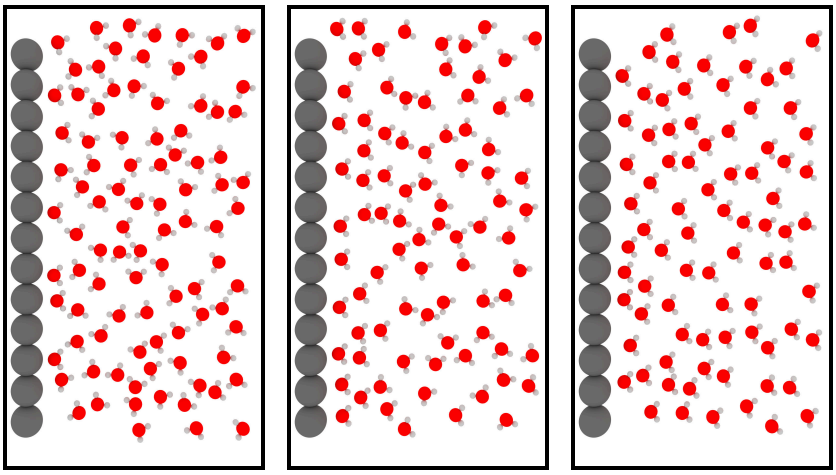

Figure 2.2: *Schematic representation of primary hydration force. Showing water molecules and adsorbent (dark gray). The adsorbent effect on the polar water molecules increases from low to high from a) to c) as the organization of the molecules increases.*

So, despite of the actual reasons for water self–association, such as interface or surface tension, water–molecule and water–material interactions could have defining effect to any particle adsorption. Figure 2.2 showed so called primary hydration force, but when other entities are mixed to the water media, we would have several primary hydration forces. This overlapping of primary hydration forces could be called "secondary hydration force" as they effect each other [101]. Figure 2.3a shows an illustration of possible secondary hydration force.

The primary hydration force applies to all entities in water medium, and much like in Figure 2.3a these interatomic forces can cre-

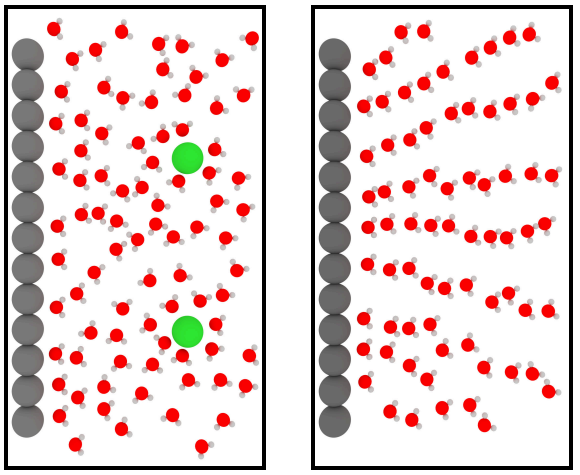

(a) (b)

Figure 2.3: *Schematic representation of a) secondary hydration force deriving from particles that also have association with water and which further affects the primary hydration force. Also shown b) a very strong water association that could be possible with very strong external field on the interface.*

ate situations where particles, water, and the material (adsorbent), all form a complex dynamic system. An external field, such as pure electric potential, or other strong electromagnetic field could also generate dramatic addition to the gentle collection of variables, such as the hypothetical illustration of Figure 2.3b displays. So, all in all, it is not said that a single photon, or a consequent number of photons couldn't affect this delicate system. Despite the continuous "non-contact" claims.

Another thing to consider inside liquid media, related to organization of molecules and particles, is the charge density. When observing both external field, charges, and dipoles, in the liquid media near an interface, it is more than possible, that by time the charge density can change near any interface. This can affect the adsorption or be caused by adsorption. After all, there is an abundance of ions in the commonly used salt media.

Furthermore, *hydrophobic force* or *hydrophobic effect*, are said to be created between organic non-polar molecules in water, which can be nearly ten times stronger than the van der Waals forces, and which create strong aggregation as well as segregation of entities in water solution [102,103].

We can conclude, that the water could have interesting association forces to itself, and with any particles in the water medium, and that there is much work to cover in interfacial research [101]. However, it is curious that questions, for example, about interfacial phenomenon of water association are rarely seen in photonic studies, while the rest of the scientific community might struggle in characterizing fundamental reasons behind these sophisticated phenomena. It could be speculated that this is at least partially due to the discussion of intermediate phenomena instead of the actual interatomic forces. Even if the intermediate forces are just a manifestation of interatomic forces, there might be something missing when moving to intermediate phenomena. But what are these intermediate effects we often see? We will consider them next.

2.5 VARIABLES IN ADSORPTION

The purpose of this section is to provide discussion of intermediate effects that derive from interatomic forces. While this might seem odd approach, the reason to do this is that sometimes there exists only these intermediate phenomenon as a discussion in a single study. The authors might understand the actual fundamental atomic forces, or not. This is because usually these intermediate effects are the ones that are concretely evaluated and measured. For example, it is easy to place a water drop on a surface, measure the water–sample contact angle, and discuss that as a fundamental cause for any further observations, rather than discuss the interatomic forces. While contact angle has an connection to atomic forces, it should be used wisely. In this study we concentrate to photonics and rather hypocritically do exactly this minimal discussion, for example, of the water contact angles, but it might

not be the best approach in general, if the real adsorption as a phenomenon is the aim of the study. Nevertheless, there are also some more macroscopic intermediate effects, such as material porosity or topography, which is a discussion itself and becomes necessary to cover. Because of these reasons, this section was created.

2.5.1 Material porosity

In regard to terminology, a particle is considered to be adsorbed when the particle is on the surface and absorbed when it is inside the surface (see Figure 2.4). It should be understood that these are very much different in the sense of a photonic measurement. If the particle, protein or other substance, somehow becomes part of a porous surface or even hides itself inside the material, photonic methods would be rather redundant. This is the case at least for adsorbents which are opaque in respect to the photon wavelength used. Numerous experiments and explanations can be found regarding porous materials [31,104–115], but to simplify matters this study mainly concentrates on particle adsorption.

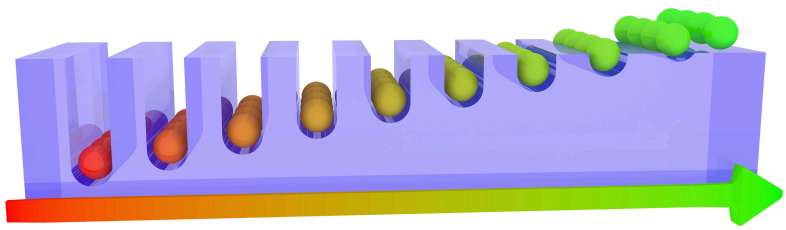

Figure 2.4: *Schematic image of the concept of transtion from an absorbed particle (red) to an adsorbed particle (green).*

While a porous material is generally challenging to deal with, controlled porosity could help in creating different detector applications and facilitate photonic models. These are discussed more in section 2.7. The main idea to keep in mind here is that porosity as well as general topographical changes can be an unknown affecting factor, helping, or both, in adsorption analyses. This is even more

the case in photonics, where the photons can be blind to geometrical changes if the geometry or porosity is not controlled. This is strongly claimed, but depending on the methods a photon might not be sensitive to the absorbed particles due to porosity.

2.5.2 Intermediate factors affecting adsorption

There might be further unknown factorfs in the protein adsorption process, but below is a selected list of the most commonly seen underlying phenomena that can be considered a large part of the protein adsorption. The main effects discussed here are

- (Temperature)
- Solute
- Adsorbent wettability
- Adsorbent topography
- Particle source
- Particle size and weight
- Particle concentration
- Vroman effect

While this list might appear incomplete, the following subsections provide many basic phenomena which might only be titled differently in the list above. We will consider each of the above items individually in the following subsections. One of these items is, however, in brackets.

Temperature is significant factor affecting adsorption of all kinds. In general, it could be one of the most fundamental properties of physics, chemistry, and physical chemistry. With this in mind, a whole new dimension would be added to this study by including temperature in all the different parts of it. However, this is not done. The author recognizes that temperature affects the adsorption rate

(as well as wetting [116]), adsorption amount [71,117], is a catalyst in chemical reactions [118], and affects different material properties such as photonic response [119]. This is just to mention a few broad segments. It is easy to understand that if temperature changes, the fundamental energy state of all involved materials changes which could again affect everything. Thus, in this study the measurements are done in at room temperature and static temperature properties are assumed.

Solute, pH, and ions

As mentioned above, water is the fundamental solution in this study. But the human body and the complexity, for example, of blood is far more diverse than that of mere water. All ion and electron exchange capabilities of the electrolyte, which is the medium for the protein, affect surface-liquid interactions, and therefore adsorption [120]. Thus, the common biologically used phosphate buffered saline (PBS) is used for the protein buffer solution in this study to mimic the natural environment of the human body [82,92, 95,97]. It is understandable to argue that the PBS solution is not the same as that involved with blood and implants, but the important thing is that it is at least closer to the actual situation than pure water, which removes the ionic environment altogether.

Still, the solute plays the biggest role in the mixture. It is the medium in which the studied particles travel. The solute could also directly react with the surface, producing a completely new interface [121].

The acidity of any particle is the electron receiving and donating ability of that particle. In a mixture the acidity is defined as a result of the mixture's properties. This is usually measured as the pH value, which measures the acidity which is the proton (or hydrogen ion H^+) receiving and donating ability. Here we are not so interested in the exact details of the pH, but just in understanding it as an important property of the material, even more as the reactivity of that material. Thus, changing the pH changes the ion-

ization abilities of the material or particle. This naturally affects the adsorption abilities because the chemical as well as the enhanced charge–coupling aspect of the particles and solution are presented.

Studies show that the adsorption rate can be altered by changing the pH (more acidic solution) [117,122]. It was already noted by Irwin Langmuir in 1939 that the exact effect of pH can be protein–specific [5]. This makes it possible to create protein–specific curves which show adsorption rates or adsorption amounts as the function of pH [123]. A more recent study by Imamura *et al.* ([124], 2008) actually shows the effect of pH on the adsorption of nearly 20 proteins on titanium.

pH is also important if the adsorption procedures are observed with different temporal methods such as adjusting pre-adsorption times [125].[f] However, ions and pH can often go hand in hand. If the solution and solute are very pH neutral in regard of each other and the surface, the effect of the existing chemical ions are minimized. While this might be useful in some analyses, the effect and adjustment of the pH can prove more useful in adsorption studies. It is also the reason why all studies should be clear about their solution pH.

Finally, we should clarify some of the terminology. Some of the protein terminology and active groups are explained in Appendix A. The chemistry, such as pH, is again not the main interest of this study, but this appendix entry should indicate general and helpful information about protein terminology.

Adsorbent wettability

Surface and water interactions have probably always been studied in the history of mankind. The source of current water wettability and surface tension research could, however be the work of Young ([127], 1805). Essentially Young discusses vector tensions as well as force and the counter forces. In water droplet test, the key place

[f] Preadsorption has been used to modify a sample surface to change the further adsorption behavior [126].

is the connection point of all of the phases and the corresponding tension of each phase pair; Liquid–gas (LG), solid–liquid (SL), and solid–gas (SG). Much like the schematic representation of Figure 2.5. In equilibrium state, the tensions should sum zero [128] with

$$\gamma_{SG} = \cos(\theta_C)\gamma_{LG} + \gamma_{SL}, \tag{2.2}$$

where θ_C is the water contact angle, the primal direction is along the surface, and the vectors are thus only presented with a numerical expression.

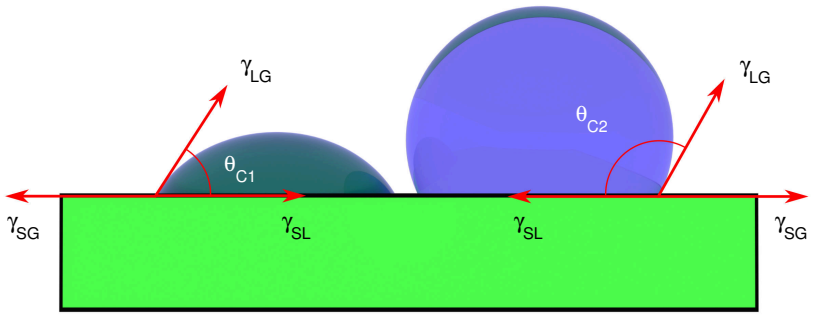

Figure 2.5: *Schematic illustration of two water droplets on a sample surface showing tensions γ_{SG}, γ_{LG}, and γ_{SL}. Angles $\theta_{C1} = 60°$ show a hydrophilic and $\theta_{C2} = 120°$ show a hydrophobic type contact angle.*

While it is useful that this tensiometric measure is still in use, it is rather ambiguous why the measure of the hydrophilic (welcomes water) and hydrophobic (repulses water) surfaces is classified as being separated at specific angle. While the case of $\theta_C = 90°$ creates a balance situation of the three phases, there is a strong case through actual studies towards a limit of $\theta_C = 65°$ as the division between hydrophililcity and phobicity [129,130]. This so–called Berg limit [129] comes from a study where the surface tensions of a controllable polarity liquid and the surfaces were observed. The whole question breaks down into chemical Lewis acid and base association, hydrophobic forces, or to long distance dispersion forces (van der Waals). Hydrophobic forces still exist with $\theta_C = 90°$, while the

$\theta_C = 65°$ is the point where those forces disappear [129]. So perhaps $\theta_C = 65°$ should be the limit between hydrophilic and phobic surfaces (60° in [131]). It is generally simple to literally draw lines on water but we do not want to decide either way.

But the chemical processes, dispersion forces, liquid self assembly and the whole interfacial 3D structure of the liquid interface is far from just a measure of contact angle. With this, perhaps in the case of adsorption, the absolute contact angle values should be used cautiously as the reality might be different.

This all leads to the point where the contact angle becomes only a guideline and the related parameter to water-surface interactions. This does not directly explain everything and it still might not be established well enough from application to application. Still, it is a good place to start, as is the case in this study. In this study we simply discuss water wettability as parameter of particle access to the surface. Because of this approach we will be use the hydrophobic and hydrophilic very loosely because of the complexity of the situation. For example, Figure 5.1 shows a schematic image of two droplets on a surface. One droplet shows a hydrophilic and the other a hydrophobic type of contact angle.

Organic particles such as proteins have been said to carry a water envelope which can easily have the same weight as the protein itself [3]. So it is not possible to ignore the water surface interactions. Figure 2.6 shows the scale of a one nanometer diameter sphere adjacent to a titanium surface while being inside water. Water is rather thick when visualized in this way, and all material near any surface must therefore replace the corresponding volume of water. If the water is tightly bound near the surface, adsorption will certainly not occur.

Similarly, if we extent the scale comparison to proteins, Figure 2.7 shows the same one nanometer sphere adjacent to a small protein of human serum albumin (HSA) [132,133]. It is very easy to note from Figures 2.6 and 2.7 the massive amount of water shifting that must occur with HSA, to say nothing of larger atoms, as seen in Appendix B, which shows both proteins used in this study, human

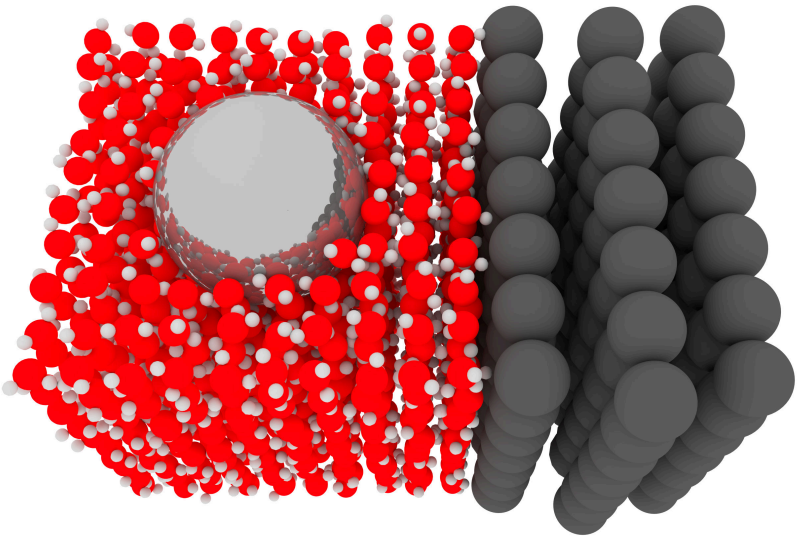

Figure 2.6: *Schematic illustration of the atomic scale of a one nanometer sphere adjacent to a surface (gray). Water molecules are also presented. Red is a oxygen atom and white a hydrogen atom.*

plasma fibrinogen (HPF) and HSA, for further size comparison.[g]

We discuss the phenomenon on a quite macroscopic scale. Very detailed description of water behavior can be found in several sources [85,128,130,136–140], which describe in more detail even the atomic level of water adsorption on surfaces. Interestingly, even water adsorption on surfaces is under study and provides new information, despite the mere three–atom structure of the water molecules [141–143].

To reiterate, we will not discuss the atomic level of the water molecule, only the concept of a water molecule near a surface. We should note that any particle traveling in water must constantly move water to propagate, and if the surface keeps the water tightly

[g]Figure 2.7 and Appendix B both show atom sizes as estimated *van der Waals radii* according to [134] and [135]. For example, hydrogen has selected van der Waals diameter of 0.24 nm and carbon 0.34 nm.

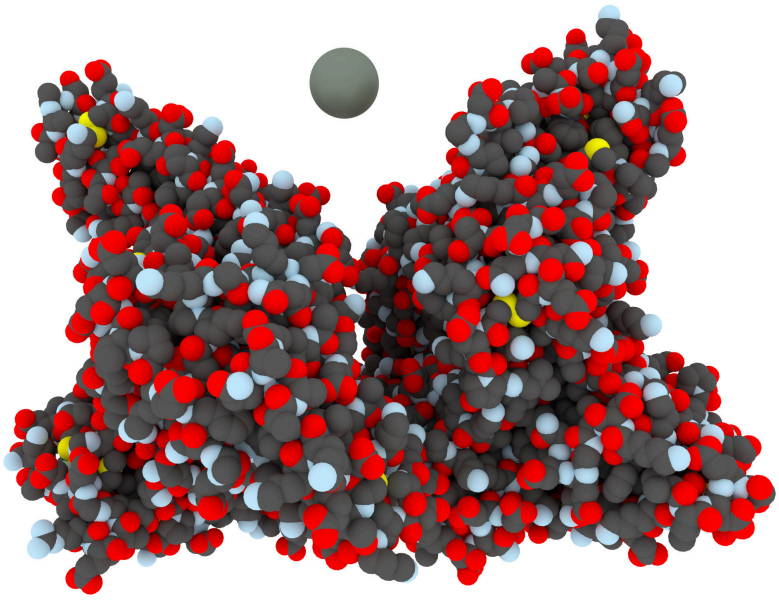

Figure 2.7: *Crystal structure of HSA [132] and a 1 nm diameter sphere. Atoms in the proteins are carbon (gray), nitrogen (blue), oxygen (red), and sulfur (yellow).*

near it, adsorption is not energetically plausible. A more accurate description of water interactions can be found in one of Vogler's review [130]. Reviews by Hodgson and Haq ([117], 2008) and Bonn *et al.* ([140], 2009) should also be noted as a good starting point for wetting studies.

Particle source

Proteins from blood differ from other proteins such as environmental proteins. This limits the protein behavior analysis to only the particular protein being observed. While it might be cheaper to buy the protein that has a source, for example from a rabbit, there can be no extrapolation from this protein to the ones in the human body [7]. It is true that we could determine how much protein is adsorbed, but the proteins should be compared to real human pro-

teins for correct analyses. Similarly, with any particle, a correct type of particle should be used and the source related variables evaluated.

Adsorbent topography

While topography and wetting are connected to each other strongly [138], topography itself should be mentioned as an influential part of adsorption. Studies indicate that topography affects adsorption and even biocompatibility [138,144–148], and that it could be even considered as a method for controlled adsorption [149,150].

One clear terminological factor must be mentioned. Here we consider the more geological term topography in the microscopic scale of a sample surface. Topography is a general 3D environment of a surface; that is, any height change function of a plane. While the roughness of a surface is commonly used as a term to describe a surface, roughness is considered to be more or less a calculated value from a topography. Or at least it should be considered as one because roughness values generally describe a random variation. The average surface roughness R_a is calculated [151]

$$R_a = \frac{1}{N} \sum_{i=1}^{N} |z_i| \,, \tag{2.3}$$

where z_i is the height of the profile in location i.

Equation 2.3 indicates that roughness is a good measure if topographical surface deviations are random and systematic. If the roughness is periodical, this parameter fails more or less to describe the surface. It is easy to see from Equation 2.3 that several very much different surfaces could be generated while maintaining fixed value for R_a.

Because of these reasons, we will not recognize general roughness parameters like R_a as a good general measure of a surface. Today the actual evaluation of a surface is easy, for example, with an atomic force microscope (AFM), and this should be the basic–level study of any surface. Topography is important but the descrip-

tive parameters should be carefully selected and discussed. Despite this, we will use roughness to describe the "random height deviation of the surface" while maintaining the term "topography" as the more general structure of a surface.

As mentioned above, topography effects the adsorption process. Still, the generated surfaces in studies are usually simple. For example, periodic gratings. If the topography of the surface becomes more complicated as with the case of laser ablation [150], the analysis of the result also become more complicated. Thus, one can usually only use a simple periodic structure to control of the surface topography. This facilitate the analyses and models while maintaining control over the surface.

Particle shape and packing

Particle shape is one parameter which is essentially connected to the topographical aspect of particle adsorption. While topography presents the initial structure that any approaching particle encounters, particle shape and size are the other factors of this initial interaction. Packing abilities closely follow particle shape as the surface attracts more particles to it.

Furthermore, organic particles like the previously discussed protein are actually influenced even more by shape as the surface induces conformation changes to these complex structures. Figure 2.8 shows the general principle of this kind of spatial reach and shape–related packing. This principle is geometrical and was already presented decades ago [3,8]. However, it is easy to understand, that particle shape and size could have dramatic effect on the adsorption. As can be understood from Figure 2.8, different surface topographies and particle size distribution might define the final form and packing in the adsorption. Especially, if adsorbing particles have size distribution.

The packing of particles has been studied for a long time but, as mentioned, the long chains of peptides, as proteins, provide an challenge even in controlled environments. To actually state what

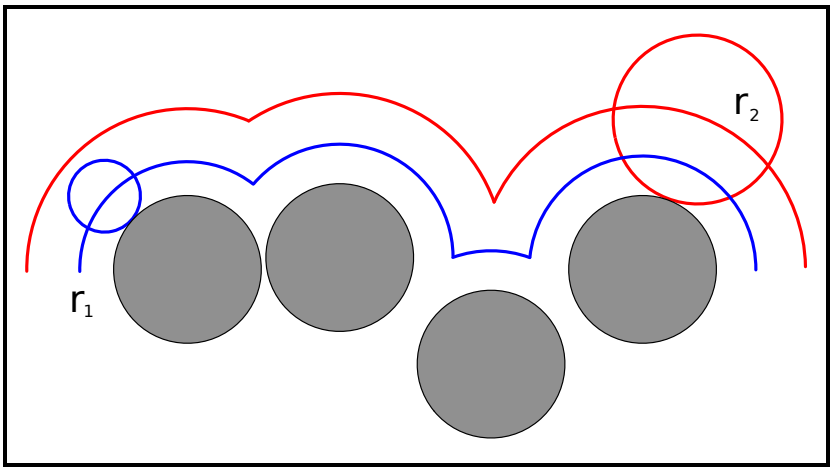

Figure 2.8: *Two–dimensional representation of atom or molecule packing. Entities with radii r*1 *(blue) and r*2 *(red) near surface (gray). Blue and red lines represent the corresponding nearest packing distance.*

accurately occurs during protein packing on complex surfaces is, to this date, more or less a guessing game. Controlled surfaces, however could provide a good way to start studying the packing and adsorption phenomenon.

The actual interpretation of adsorption has been done in 2D over the time [152]. The problem is that many studies deal with adsorption as a surface area model. Countless papers exist resulting in the adsorption of mass per surface area. While this might be really what we are seeking, it does not discuss the actual interfacial three–dimensional (3D) environments. Parhi *et al.* ([152], 2009) describes this as a "2D paradigm" because the real environment is three dimensional. Three–dimensional observation is not new, but has just not been adapted in the history of adsorption studies because it provides a challenging new dimension to analyze [152]. Generally, the packing is assumed to be perfect, but usually "a volumetric packing factor" is later used to estimate the packing efficiency of the adsorbed particles [153,154]. It could be argued if the "packing" in several cases, is just a manifestation of the available sites on

the adsorbent or other surface type properties.

Particle weight and size

After water and surface, the next influential variable is naturally the protein itself. The weight of a protein is usually measured in kilo daltons (kDa $\approx 1.66 \cdot 10^{-24}$ kg). Some studied proteins and corresponding weights are listed in Table 2.1.

The weight itself affects the protein diffusion rate and general activity. It is clear that in a solution very small molecules are slower to diffuse among the water and other molecules, because of the interatomic forces. It has been shown that weight could be directly proportional to the adsorbed amounts [165–167].

Although the size of the protein is relatively small, the protein to protein differences are quite easy to understand, not only from the specifications in Table 2.1, but also from Appendix B, which shows the relative size of the proteins HSA [132], HPF [155] and spherical particles (see Figure B.1 on page 186). This can be thought as the exact reason mass per volume is used in adsorption rather than the number of proteins in volume [166].

Still, it has already been shown that increasing molecule weight increases the theoretical adsorption amount maximum in a logarithmic fashion [168]. At the same time, the molar maximum of the adsorbed amount decreases with increasing protein mass.

Protein concentration

The number of individual proteins detected in human blood is in thousands and more could be found with constantly improved methods [169]. This is a another factor which brings perspective into play. Usually the studies conducted in this field of adsorption are performed with single protein solutions to understand the fundamental process (see section 2.7 for more). However, this does not include the overwhelming number of different proteins and the concept of competitive adsorption. While competitive adsorption is

Table 2.1: *Unit cell ($a \times b \times c$) information of a few common protein crystals as well as a few related studies on those particular proteins and adsorption or kinetics. The visually approximated physical dimensions of the protein shapes ($x \times y \times z$) and the relative volume of protein compared to Human Plasma Fibrinogen are also presented. Protein mass in is atomic units.*

	Human Plasma Fibrinogen (HPF)	Human Serum Albumin (HSA)	Lysozyme (LYZ)
a [nm]	13.52	5.97	5.62
b [nm]	9.49	9.70	6.10
c [nm]	30.08	5.97	3.32
x [nm]	5	10	-
y [nm]	5	10	-
z [nm]	50	10	-
$\frac{1000 \cdot \text{Volume}_X}{\text{Volume}_{HPF}}$	1000.0	89.6	29.5
Mass [kDa]	341 [152]	66 [152]	14.8
Source	[155]	[132]	[156]
Studies	[77,125,157]	[77,158–162]	[72,163,164]

studied, it usually is between two clearly different proteins. Therefore, it hardly approaches the thousands of competing proteins.

The abundance of proteins is an influential parameter. Concentration directly defines the amount of protein per volume unit. The concentration of the molecule not only defines the adsorption ability of the surface, but also defines the saturation of the adsorption saturation for each used protein. This is a very important factor and concentration–wise measurements are always good. The concentration also reveals important factors in the method and equipment used. Because the concentration has a known saturation curve, it reveals erroneous procedures and directly gives estimates on the equipment reliability. [7,91,170,171]

An isotherm is the usual way to observe adsorption amount as the function of gas pressure [4] or particle concentration near the interface. There are numerous, perhaps even sub-optimal, approximations for different adsorption models [152].

One important method involving concentration is the depletion method. In this method the solution that is in contact with the surface is evaluated for particle concentration. It is common to evaluate the concentration at certain time intervals by taking some of the physical solution [137,172–174]. While it might sound tedious, it is very accurate in determining the absolute loss of particles in the solution. This method assumes that the solution concentration is homogenic throughout the solute.

Protein folding

As protein works as a biological reactant, the folding of the protein is an important part of its natural behavior. While some studies are interested more in the denaturation of the protein, it is still of general interest to recognize these procedures to fully understand the behavior of proteins [2,3,175].

The exact general effect in adsorption is rather unknown as the surface possibly induces a unnatural denaturation (folding) of the protein on adsorption. It has been suggested that folding actually affects the packing of the protein on adsorption [176]. Protein folding, however could be said to be part of protein packing, and thus

was excluded from the list above. While protein folding is important for protein functions, it could be said that strongly adsorbed proteins do not in any case behave naturally, so the observed effect would indeed be the protein packing on the surface.

Vroman effect

The Vroman effect [177] is thought to be a different adsorption-displacement type of adsorption where different particles interact with one another essentially creating adsorption competition [166]. It could be argued to be part of interatomic forces, but here we just acknowledge this as a one mentioned intermediate phenomenon from literature [166,177].

Time

While time is excluded from the list above, it has effect on adsorption. It would, however be redundant to include time as a parameter in adsorption, because it is the principle parameter through which adsorption is observed. Usually there are other phenomena which are more influential factors. We could, for example, state that interatomic attraction strength defines an adsorption, but this attraction can be only observed in a time–wise measurement. Because the adsorption isn't a time–independent phenomenon, nothing can be observed without it. For this study we note, that time is just an observation medium.

2.5.3 Reversibility of adsorption

The reversibility of adsorption (desorption) is very difficult but a very real factor in adsorption. It is also related to protein packing, but is usually discussed separately from packing.

It was shown decades ago that under pressure proteins can have both reversible and irreversible forms of packing [5]. While it is true that this was a mechanically created situation, it is always possible to have atomic–level irreversible protein packing. This could further

impede the desorption–readsorption process if it exists. This could also indicate irreversibility of adsorption.

2.5.4 Isotherm and kinetics

This section will follow the general mathematical kinetic notation of Table 2.2. This section (2.5.4) will also observe the general model excellently presented in [178], which combines the two most commonly used models into one theoretical presentation.

Table 2.2: *Notations used in this section for an adsorption kinetic description.*

M	Layer count
a_j	Adsorption rate constant for layer j (mg/l)
b_j	Desorption rate constant for layer j (mg/l)
H_j	Heat adsorption rate for layer j (J/mol)
H_M	Heat adsorption rate for upper layer (J/mol)
K_j	Equilibrium constant for layer j (l/mg)
K_M	Equilibrium constant for upper layer (l/mg)
q	Amount of particle adsorbed on adsorbent (mg/g)
q_m	Amount of particle adsorbed on adsorbent in a full monolayer case (mg/g)
C_{eq}	Equilibrium liquid phase concentration (mg/l)
T	Temperature (K)

The general approach

We will actually follow adsorption as a multilayer model in which each layer has a different adsorption rate and specific parameters, as presented in Table 2.2. Using j layers, the properties of an adsorption (a_j) and a desorption (b_j) rate as well as a heat adsorption rate (H_j), we can write the equilibrium constant for adsorption K_j as [178]

$$K_j = \frac{a_j}{b_j} e^{\frac{H_j}{RT}}. \tag{2.4}$$

According to [178], for M layers, an adsorption amount q can lead to

$$q = q_m \frac{K_1 C_{eq} \left[1 - (M+1)\left(K_M C_{eq}\right)^M + M\left(K_M C_{eq}\right)^{M+1}\right]}{\left(1 - K_M C_{eq}\right)\left[1 + \left(\frac{K_1}{K_M} - 1\right) K_M C_{eq} - \frac{K_1}{K_M}\left(K_M C_{eq}\right)^{M+1}\right]}. \tag{2.5}$$

Langmuir kinetics

The beauty of the multilayer approximation of Equation 2.5 is that it also predicts a Langmuir model for an adsorption. As early as the beginning of 1900s Irwin Langmuir presented a method to observe the surface adsorption coverage of a gas on a surface [4]. While this presentation is for gases, it has been adapted over the course of adsorption studies and still remains the standard and can be safely included in an adsorption study.

A Langmuir-type isotherm describes the surface coverage q to be

$$q = q_m \frac{K_1 C_{eq}}{1 + K_1 C_{eq}} = \frac{C_{eq} \frac{a_1}{b_1} e^{\frac{H_1}{RT}}}{1 + C_{eq} \frac{a_1}{b_1} e^{\frac{H_1}{RT}}}, \tag{2.6}$$

when $M = 1$ in Equation 2.5. That is, a Langmuir-type adsorption is a single layer adsorption model [4,178].

Let us observe an actual isotherm. Table 2.3 lists a few model values for the used kinetics observations. In these calculations the concentration is C and the corresponding C_{eq} is divided by the maximum values of C. That is, C_{eq} always has values from zero to one.

Figure 2.9 shows the Langmuir kinetics of a model where a_1 changes through certain values. Other values are as presented in Table 2.3. The Langmuir isotherm could vary as the adsorption rates change. Nevertheless, the behavior is a saturating function, as in Figure 2.9.

Table 2.3: *Basis of the model values for the used kinetics model of equation 2.5.*

Variable	Value	Unit
T	300	K
a_1	1	mg/l
b_1	0.1	mg/l
H_1	1	J / mol
a_M	1	mg/l
b_M	0.1	mg/l
H_M	1	J / mol
R	8.3144621	J / (mol·K)

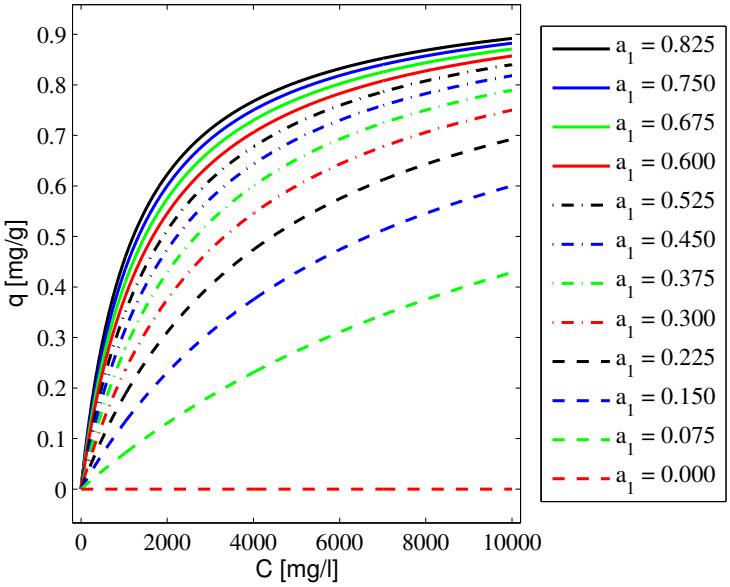

Figure 2.9: *Langmuir model with variation in the a_1 value.*

BET kinetics

The so–called Brunauer, Emmett, and Teller (BET) adsorption isotherm model is an another used in adsorption studies [179]. This is espe-

cially the case with porous material evaluations where a pore filling might create more of a multilayer–style adsorption [180,181]. The BET model can be directly modeled from Equation 2.5 using $M = \infty$. The result according to [178], using the Table 2.2 notation, is

$$q = q_m \frac{K_1 C_{eq}}{\left(1 - K_M C_{eq}\right)\left(1 - K_M C_{eq} + K_1 C_{eq}\right)}. \tag{2.7}$$

Figures 2.10 and 2.11 show a three layer ($M = 3$) and a $M = \infty$ type adsorption isotherm. Figure 2.10 is calculated with Equation 2.5 and Figure 2.11 with Equation 2.7.

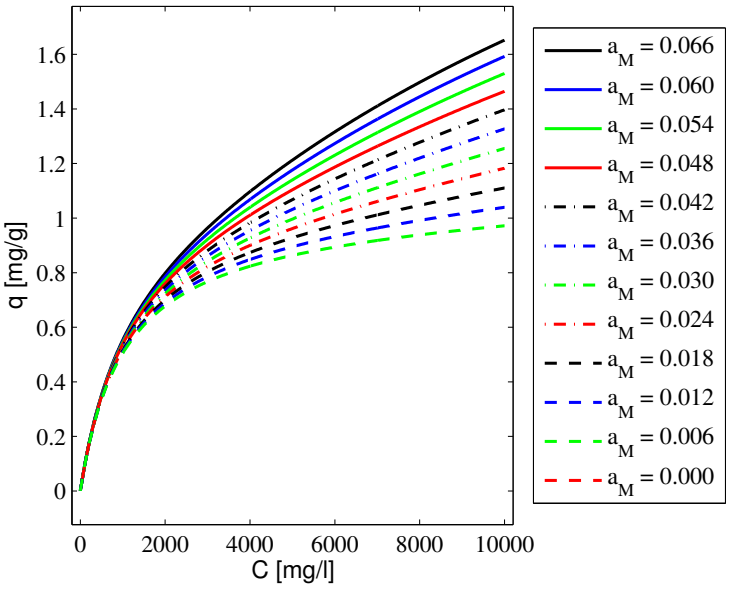

Figure 2.10: *A BET kinetics modeled with a_M variations and using $M = 3$ (Equation 2.5).*

If in Figure 2.10 data were calculated with $M = 10$, there would have been very little difference between the data. That is, a multilayer model with the stated numbers already showed an infinite layer equal to only ten layers. Essentially, the BET model just provides a fit that consists of a several adsorption kinetics seeking to

create one adsorption isotherm that fits most occasions.

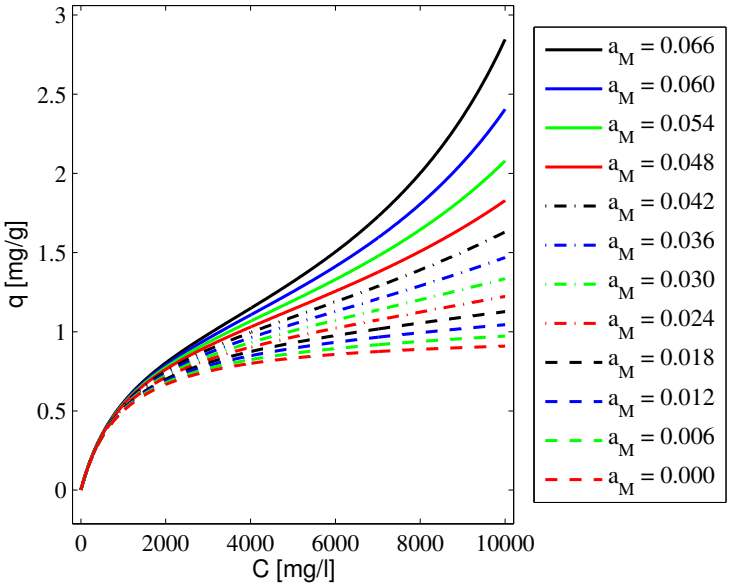

Figure 2.11: *BET kinetics modeled with a_M variations and using $M = \infty$ (Equation 2.7).*

Other isotherm models could be listed, *i.e.* the linear and Freundlich isotherms as well as random sequential adsorption [182], which however, are purposely omitted. The Langmuir and BET can be set defaults as they describe the phenomenon well enough.

It must be reminded that the purpose of all shown Figures 2.9, 2.10, and 2.11 is only to indicate the possibilities, because we already noted the scale of the concentration in these figures. There are numerous different adsorption isotherms, depending on the studied particles and environment. However, these possibilities are something to keep in mind when adsorption data is interpreted [183–185].

2.5.5 Interfering

We need to clearly distinguish the methodology. Adsorption methodology can very simply be separated into two groups. One measurement group interferes with the adsorption and other does not. When we make this sharp separation it is somewhat subjective to state the group to which a single study belongs. There are several methods which seem to be "non–destructive" and "non–contact" methods. However, these are only words if the process is not fully understood. Furthermore, in photonics, it is rather redundant to say that electromagnetic radiation is "non-contact" in the sense of physical contact.

For instance, this study discusses the possibility of photons measuring the adsorption phenomenon. Many might say, without any further thinking, that this method is indeed a non–contact and a non–destructive method. This might be the case, but we must assume that the sensing photon beam does not disturb the adsorption process. Too intensive a beam or photons with too much energy would still interfere with the phenomenon. To say nothing of the possibility of different photon activation of the surface [186]. Thus, the generalized wording, for example, of non-contact should be used carefully and usually this assumption is only true only for a particular measurement device. Therefore, this study does not claim to be a study with a non-contact method.

More dramatic examples of interfering with measurements are, for example, tagging and rinsing studies. Tagging is widely used to detect adsorption with radioactive (usually ^{125}I-labeling [77,187, 188]) indicators or just by using fluorescence [189]. Some key components are attached to the proteins and are later evaluated. This is useful, but there is no certainty that the indicators used would not change the adsorption characteristics and kinetics. Proteins are sensitive particles. The folding and unfolding of protein could determine the future behavior of the protein and even the intermediate states if the folding is studied [160]. Thus, inducing these sensitive factors with foreign connections and claiming, that it is a "natural"

process observation, is always slightly questionable, even if it might provides some results.

Rinsing could be listed as one of the most interfering methods in protein studies, and is defined here as the dipping of samples into solutions and then removing the sample from the solution; even perhaps subsequently washing the sample. The sample is clearly exposed to air before the dry–air evaluation of adsorption [170]. This raises serious questions about the method. What does exposure to air really do to the surface adsorption? This is difficult to answer as the dipping is usually rather open to the method used. Exposure to air and particle solution could occur at any period of time. Many different liquid solutions also involve vast amount of possible reactions and outcomes and it is completely unjustified to assume that the adsorption of the particles is so strong that the sample dipping becomes a valid observation of the complex and environmentally dependent particle adsorption phenomenon.

The mixing or flow [190] of the observed solution is problematic in photonic observations. On one hand, we need to mix the solution to keep the transmitting solution as homogenic as possible. On the other hand, mixing might remove naturally diffusing particles or interfere with the phenomenon in other ways. As this study employs mixing to provide better signals, it is at least one reason for not mentioning non–contact measurement in a liquid environment. It might be claimed that mixing does not influence adsorption, but some constant mixing or flow is essential in photonic measurements since we do not want any unwanted refractive index gradients involved with the observations.

Despite the great number of influential factors discussed, there is another fundamental factor to consider: physical interaction in the sample–protein interphase. One very clear idea here is, do we involve it, or not. That is to say, does the measurement of protein adsorption involve any physical alteration of the sample–protein interphase? Paper [7] divides these research types into Group 1 and Group 2 accordingly. As previously mentioned the interphase should be assumed to be a delicate system and any so-called multi-

layer adsorption could be destroyed if strong forces such as rinsing were involved. The same could be said regarding very strong mixing or exposure to strong fluid currents in the observed solution.

2.5.6 Sample characterization

Previous sections 2.3 and 2.4 combined with the other discussion above, all lead to the necessity of understanding the measured surface. Here, again, we will not go into detailed description of different characterization methods. Instead, we will just acknowledge, that with interatomic forces, it would be beneficial to know the crystal composition and structure of adsorbent.

The most prominent methods are X-ray Photoelectron Spectroscopy (XPS), different mass spectrometers, and X-ray Crystallography. The XPS is used for systematic, repeatable, and quantitative material analysis. Essentially in XPS the sample is radiated with X-rays while analyzing the electrons which come off from the surface. Both kinetic energy and the count of the electrons are recorded. Similarly, mass spectrometers ionize material with electron-beam and the ions, which are created, are ordered by mass-charge-ratios. The equipment of XPS and mass spectrometers might be very different, but both give invaluable information on the material state.

X-ray crystallography is slightly different approach, as it analyzes existing structures. Material in crystal form is radiated with X-rays and the scattering of the X-rays is analyzed. The angular data of the scattering provides information of the crystal lattice order of the material.

All of these method are fundamental ones. They provide repeatable and exact information. For example, the refractive index and permittivity of samples could provide comparable data, but it cannot be generalized as permittivity is an intermediate measure of the atomic properties.

2.5.7 Conclusion

Table 2.4 lists a few interesting review–level papers associated with this topic. We want to note the fact that some additional good papers might exist as the research field is vast, but those presented provide a sufficient introduction to the field of adsorption and to titanium as a material.

Table 2.4: *Review papers on the topic of adsorption offering greater detail.*

subject	**Citation**
Water adsorption and wetting of metals	[116,140]
"The surface science of titanium"	[191]
Photon-activity of titanium	[186,192]
"Structure and reactivity of water at biomaterial surfaces"	[130]
Volumetric adsorption	[152,165–168,174,193,194]

We conclude that one must avoid oversimplifying the liquid environment, since there is a great deal of factors to consider. Furthermore, the exact state of a material becomes a big task to solve even with a solid state measurements. The liquid environment further obstructs the analyses as the state of any matter becomes dynamic. Still, excessive adsorbent analysis would be a great help in solving the interatomic phenomena, but would still require atomic level calculations for being useful.

It must be clearly stated, that the complex variables, that emerge with the liquid state of matter are reality, but this study only scratches the topic. We are discussing the methods and models of photonic sensing of adsorption. All this complexity that could be happening near any adsorbent, is usually estimated to be "a monolayer of homogenic material on the adsorbent." This whole chapter is constructed for discussion, and we already understand, that this estimation, as a general model, is simply preposterous, and we will

return to this below.

2.6 NANOPARTICLES

As mentioned above, the tools for characterization increase in accuracy and become cheaper, so it is only natural that all nano-sized things are targetted by research and applications. This section is devoted to a brief discussion of the applications and creation of nanoparticles. While the discussion here strongly calls the particles as "nano", the same or similar ideas could also be used regarding micro–sized particles.

2.6.1 General

Small particles exist all around us. While they might seem like synthetic human–made toxins, different fine particles keep nature as well as our bodies functioning [195]. Many human body parts such as proteins are essentially nanoparticles, but as they provide, for example, the bodily functions, understandably any additional foreign particles might obstruct or harm these functions.

Human–made parts are generally created with skin products, aerosols and through the combustion engine [196,197]. While nanoparticles are also natural in some way, their production is estimated to dramatically increase and their effects are still generally unknown [197]. Moreover, nanoparticles are used as catalysts in chemistry [198], so their spread is rather extensive in industry.

The biggest positive interest of nanoparticle usage might be their potential use as a delivery agent for medicine and general cancer treatment [199–202]. They are also used in signal enhancement, in general detection or separation, and in imaging fields [203–207]. Even biodegradable versions are produced to provide more "healthy" versions of the particles [208–210].

The materials of interest are usually gold [211,212], silver [213], semiconductors [214], or carbon–based materials [215]. Other inorganic composites are also constantly created and studied [216–220].

The focus is on the size–dependent theory of material, as there are interesting phenomena involved close to single–atom–sized particles [221,222]. For a good general reference, see the review of Niemeyer ([223], 2001).

2.6.2 Synthesis

As previously mentioned, there is a substantial number of sources for nanoparticles because all materials can basically be transformed into nano–sized version. The same is the case with the synthesis of the nanoparticles. Photon–induced [224], chemical synthesis [217,218,225], lithography [226], laser ablation [211,214,224,227–232], and even different microbes [233] have successfully been used in nanoparticle synthesis. The only clear separation is whether the particles are produced bottom–up or top–down [226,233]. In bottom–up the nanoparticles are built up to their final size and in top-down the material is broken down to the desired size [234].

While it matters to some degree what the creation method is, the end result is still dominant and the interest is usually in making cheaper, sustainable as well as repeatable methods instead of actually thinking too much about the method. Thus, we will see more methods developed over the years, but we speculate that one of the most prominent methods might be that which produces biodegradable particles using biological sources,[h] as biological entities creating bio–degradable particles could have immense potential as a working pair. This, again, is understandably connected to human body applications.

A second source–related discussion of course concerns the end result, which varies from method to method and impacts on the functionality of the particles. While some methods might provide a very strict size distribution, some are very broad. However, the application must decide which is best. As nanoparticle interactions

[h]For the biological production of nanoparticles, Narayanan and Sakthivel ([233], 2010) have provided a good review of different possibilities using bacteria and fungi–based nanoparticle synthesis. Despite the slowness of the method, the process is still interesting.

are still quite empiric, it might still be too early to determine if and how the source affects the end application of the particles, or if it even has any meaning.

2.6.3 Toxicology

While nanoparticles provide possibilities, they are somewhat feared due to their effects on the human body. Many modern products include nano-sized particles and the overall effect has only started to be examined. Prow *et al.* ([235], 2011) and the citations therein is a good point of departure for further information on how human skin accepts nanoparticles [236]. The study of Prow *et al.* concentrates on human skin penetration and the uptake of nanoparticles. They state that human skin generally could be considered a barrier to the particles but it might store the particles and skin diseases might affect skin–nanoparticle interactions. Furthermore, different conditions such as ultra violet (UV) radiation exposure seem to have some effect on skin penetration even in relatively short periods of observation [237]. The effect of nanoparticle toxicity and the effect of photon excitation has also been reported [238]. Increased skin penetration also has been observed under mechanical stress of the skin.

Another interesting finding about small particles is that skin penetration might not be completely related to size. There might be several sizes and material–related functions related to toxicology [238]. Furthermore, some particles such as silver nanoparticles are considered generally safe while having low skin penetration and having antibacterial as well as anti-fungal properties [235].[i] It could also be argued that since toxicity is not a simple matter [239] and the effect of the nanoparticle is very unique per organism, this makes the whole question of toxicity hard to determine [240].

Cell penetration is the next clear step in nanoparticle penetration following skin penetration. This is also commonly discussed [241] and even contributing computer simulations start to emerge

[i] For a comprehensive review on silver particles, see [213].

about the penetration of nanoparticles [67]. But while even ambiguous cell penetration might be common knowledge, the long–term effects are still very much unknown. Studies by Moore ([242], 2006) as well as Nowack and Bucheli ([195], 2007) have generated a large discussion on different toxicity effects of nanoparticles and their existence in the environment.

This study uses titanium nanoparticles created through laser ablation. These particles can easily be listed as non-biodegradable and potentially hazardous and safety gloves have been used in handling them. All this is because TiO_2 has been reported to be relatively safe in bacterial studies [240], but also as a potential risk [243]. This indicates that there is disagreement and this should raise awareness in all researchers studying nano as well as microparticles.

2.6.4 Photonic interests

Nanoparticles are also interesting particles to study since they provide photonic signals. They are usually discussed in regard to Raman [244,245], fluorescence [206,246], and as other potential signal enhancing applications [204]. When the size of the nanoparticles decrease to certain point, the particles also start to obey quantum physical properties almost ideally. These particles are called quantum dots.

While nanoparticles have intriguing photonic properties, this study mainly ignores them since a whole new dimension to the study would be needed. A good starting point in literature could, for example, be the review of Willets and Duyne ([247], 2007), which extensively discusses localized surface plasmon spectroscopy (LSPS) as the enabler of surface–enhanced Raman scattering (SERS) as well as other related basics of photonics [248,249]. For metal particle plasmonics, see the review of Pelton *et al.* ([250], 2008).

2.6.5 Atomic models

Different atomic calculation models can in general be constructed in material science. The atomic models generally solve the energy

states of different systems through different Schrödinger–equation estimations.

One note–worthy tool is the Grid Projector Augmented–Wave (GPAW) [251], which uses a uniform real–space grid representation of electron wavefunctions. While there are increasing amounts of open–source tools such as GPAW, the fundamental atomic approximations used are still being reviewed for errors, even for the ground states of crystals [252]. Generally, the evaluated systems in atomic level calculations contain only a few atoms [253], so there is still long way to go for actual studies of volumetric atomic–level adsorption of proteins.

2.6.6 Conclusion

While the toxicology of nano– and microparticles is still ongoing, one thing is certain. Nano–sized particles are significant and show great potential for applications [201,202,204,223,254,255] and should be handled with care. While the aim is, perhaps, not to immediately create the perfect passive drug delivery agent from these particles, there is no need to avoid researching them in environments other than the human body. Nanoparticles provide a solid material to work with as model particles and provide an interesting mix with all kinds of environments. We could claim that the true potential of nanoparticles has yet to be found. Similarly, the calculation approach increases in potential as the level of calculation power becomes capable of making real environments; simplified real environments, of course.

2.7 PHOTONIC METHODS

2.7.1 Method types

Generally, there are numerous combinations of photonic methods and equipment involved in studies of adsorption detection, but here we divide them into three categories.

1. Reflection (Ellipsometry)

2. Total Internal Reflection (TIR)

3. Surface Plasmon Resonance (SPR)

These can be described by the interaction direction of a detecting photon. Figure 2.12 shows the general principle of sensing in these methods. It is obvious from this figure that the categorization done here comes from the photon direction.

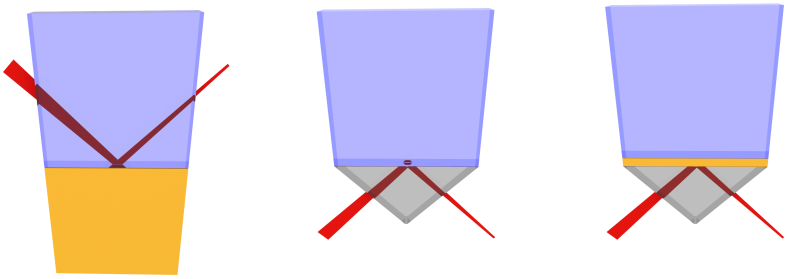

(a) (b) (c)

Figure 2.12: *Schematic representation of the three main photonic studies on adsorption with a) a plain reflection, b) a TIR, and c) a SPR setup. Gray is glass or some other transparent material, blue is liquid, red is a photon path, and yellow represents a sample material.*

One of the most important things to note from Figure 2.12 is the actual physical setup. Figure 2.12a shows the reflection setup which detects particles *on a surface*. This makes it possible to study any reflective surface. Figure 2.12b shows the schematic of a total internal reflection setup. This method studies the particles *behind a surface*. This is an important difference because it forces a studied material to be transparent for detecting photons. The method shows changes in a photon intensity according to the coupling of photons into a liquid. A photon evanescent field extends outside the transparent material into the studied liquid and any changes near this interface affect the reflected photon. That is, any particles on the adsorbend will affect signal intensity.

The third method is similar to a total internal reflection setup, but utilizes a thin layer of metal on a transparent medium. This metal, usually made of gold, can couple photons and create a confined plasmon on the liquid side of the metal which is used to detect any molecules on the liquid. In other words, we are measuring *through a surface*. It is common to alter the gold with organic compounds, nanoparticles, or otherwise physically. These alterations are done to attract a greater amount of particles or specific particles onto the altered material.

These three methods are the main methods that can be established because, historically, they have long been used in the field of adsorption studies. There are a number of other methods that slightly deviate from these main categories, but could be used in a liquid environment. These methods are discussed in section 2.7.5.

2.7.2 Reflection and ellipsometry

If we define a polarimeter as a device that studies the polarization state of photons, then ellipsometry is angular polarimetry of samples in specular angles. A specular angle is a situation where incident and reflected photons have the same angle related to the normal of a sample surface.

Several ellipsometric setups have been constructed to create an efficient polarimeter [256] as well as being used in adsorption studies [6,71,72,81,91,96,123,162,170,257–269]. Figure 2.13 describes schematically different ellipsometer setups. Generally, any ellipsometer consists of 1) a light source, 2) polarization components before the sample, 3) a sample, 4) polarization components after the sample, and 5) a detector. Figure 2.13 shows the parts two to four in them.

The setups in Figure 2.13a and 2.13b can measure the full polarization state of a reflected photon. This makes these setups *complete polarimeters*. Those in Figure 2.13c and 2.13d do not include a wave plate and thus cannot measure the full state of a polarization, which makes them *incomplete polarimeters*. A more accurate description of polarization in general can be found in section 3.2. For now, we just

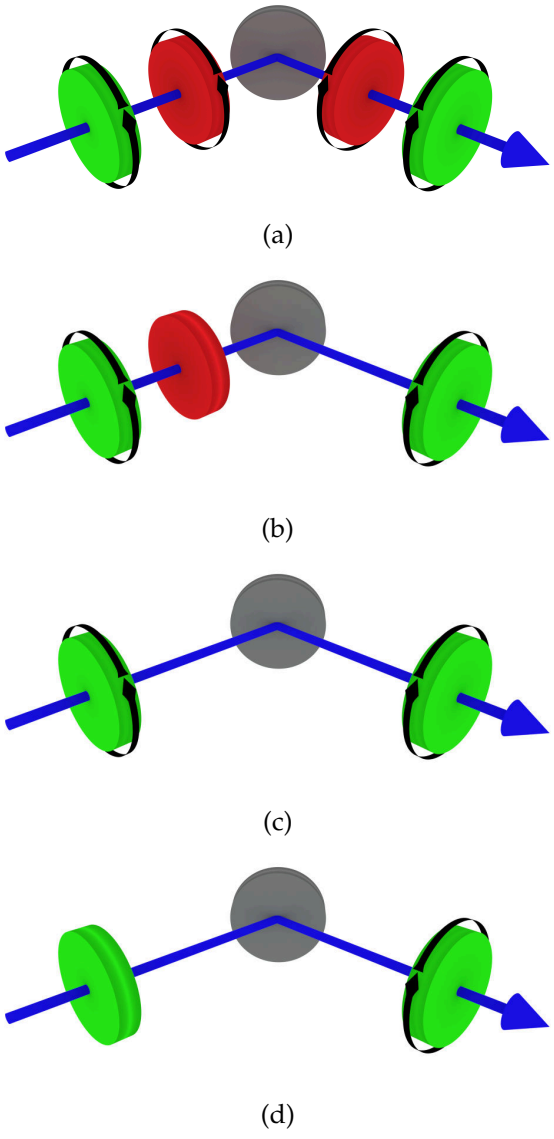

Figure 2.13: *Different polarimeter setups. The blue line is a photon path from left to right, the green disk is a linear polarizer, the red disk is a wave plate, and the gray disk is a sample. The black arrow indicates a rotatable component. Setups shown a) a full option setup, b) a PCSA ellipsometer, c) a PSA, and d) a RAE. [256]*

state that the most common setup is that in Figure 2.13b, a PCSA (Polarizer–Compensator–Sample–Analyzer) ellipsometer. We must also state that a PCSA setup is usually monochromatic, that is, used with one wavelength. In Polarizer–Sample–Analyzer (PSA) setup, the waveplate is removed, and further in RAE (Rotating–Analyser–Ellipsometer), only the polarizer after the sample reflection is a rotating one. Both PSA and RAE setups are more suitable for spectral observations as they do not include a wave plate [270]. A spectral wave plate is not impossible to make, but usually the setup is simplified with a monochromatic wave plate, and uses a single wavelength.

These are the basic components used in ellipsometry, but one can also use a VAE (Variable Angle Ellipsometry) or a spectral version of a VASE (Variable Angle Spectral Ellipsometry) setup in which the actual incident angle is changed. This provides angular data from a sample. A combination of any complete polarimeter and angular measurements provides excellent data for estimations of what happens to the polarization on a photon reflection. However, the angular measurement takes a relatively long time to perform. Thus, a VAE setup is not generally used to study the adsorption phenomenon in a temporal domain. Further, while a VAE setup is informative and easy to use in open air measurements, a liquid environment creates challenging photon paths for this particular setup. It is not a trivial task to design a VAE or a VASE for a liquid environment.

2.7.3 Total Internal Reflection

On an interface, a photon can be fully reflected when the material refractive indices and incident angle are appropriate. In spite of this theoretical total reflection, a photon field actually penetrates to the other material beyond the interface. This is because a photon field is continuous over any interface. The penetrating part of the photon field is called evanescent field. Total internal reflection (TIR) studies of adsorption are based on the theory of an evanescent field. Simi-

larly to this, total internal reflection fluorescence (TIRF) is based on the same thing but also observes a fluorescent part of evanescent coupled photons.

The most prominent benefit of a TIR is its easy setup. Essentially only a light source, a prism, and a detector are needed; much like the schematic presented in Figure 2.12b. Still, a TIR setup basically only observes the effective coupling of the photons through an evanescent field. This provides some changes to the incident photons which are further observed after a reflection. This type of a method can be called an *amount* detector. If we only obtain photon adsorption with each wavelength, the analysis remains rather dull. However, there have been different derivations of a TIR setup, for example, with gratings [271–273], grating transmission applications [274], and combinations of polarimeter setups such as Total Internal Reflection Ellipsometry (TIRE) [267,275,276].

It must be remembered that an evanescent field coupling is very sensitive because of the small distance that an evanescent field penetrates into a material beyond the totally reflecting interface. The evanescent field penetrates the interface in the range of 100 nm depending on the setup and wavelength (100 nm reported in [266,277], 200 nm reported in [278]).

A fluorescent version brings one more information dimension to a TIR setup. As different molecules might fluoresce with a different photon energy, TIRF provides a possibility to separate these molecules. Because the evanescent field is restricted to a very thin layer on the liquid side, an analysis can consist of observations on competitive adsorption. This is an excellent addition to a plain TIR setup. [78,189,263,279]

2.7.4 Surface Plasmon Resonance

Surface plasmon resonance (SPR) is not strictly speaking a photonic method; it occurs only through an intermediate. Still, SPR has been used widely after first being reported [280] in adsorption detection and in signal enhancing studies [73,80,265,281–299].

Let us consider the setup described in Figure 2.12c (on page 52). When an incident photon reflects from a thin metal film, the evanescent field can couple to a metal film plasmon field and provide an attenuation on certain incident/reflection angles [73]. The incident angles are usually provided with a prism and the detector side can be scanned or measured with a line detector to observe the attenuation angle changes. The changes are induced by small changes on the metal/liquid interface like the nano-sized particles that adsorb on the metal.

This is the general idea of an SPR setup. As this system is sensitive to incident angle, reflection angle attenuation, and the wavelength used, there are three main methods to actually detect any SPR–induced changes:

1. Measuring attenuation changes in a static reflection angle of the plasmon resonance [289].

2. Measuring the angular reflection [300].

3. Measuring the wavelength dependent changes [301].

One important requirement for an SPR setup is to have a permittivity sign change in the metal film and liquid interface [289]. Very commonly this is done by using a gold [73] or a silver film [289]. A grating could also be used in creating similar effects. To conclude, while the surface plasmon resonance is not strictly a photonic method, it could be considered one through a medium phenomenon. Indeed, any excitation and the detection are both done photometrically. For a brief review of SPR, see [289].

2.7.5 Other methods

There are many methods that slightly deviate from the direct methods described in sections 2.7.2–2.7.4. Here we will consider some of them.

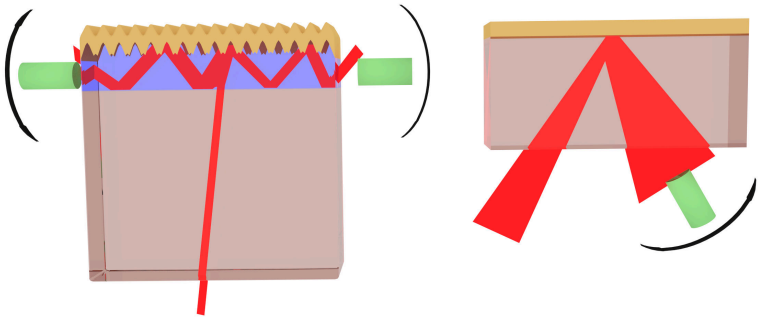

Figure 2.14: *Schematic comparison of a OWLS setup (left inset) and a SPR setup (right inset). Red presents a photon beam, green cylinders are moving detectors, blue is the waveguide, and yellow is a metal film. Studied liquid would be placed on top of the metal film.*

Optical Waveguide Lightmode Spectroscopy (OWLS)

An optical waveguide lightmode spectroscopy (OWLS) is a modified SPR setup where the light is coupled to a thin waveguide with a grating [266,273]. The setup is very similar to the generic structure of the SPR setup shown in Figure 2.12c. Differences arise from the main incident angle of the incident photons and the observation angle of the detector. These changes come from the grating surface of the nano–layer of the used metal. The attenuation angles of the SPR setup are also usually observed from the end of the waveguide.

Generic differences between an SPR setup and an OWLS setup are shown in Figure 2.14. Naturally it is also possible to use a TIR setup with a grating. This would create a very similar scenario to Figure 2.14 (left inset).

Optical Coherence Topography (OCT)

In a sense, coherence topography could be a possible method in observing larger scale adsorption; the ellipsometric approach is often used in evaluating the refractive index changes of the adsorbed layer, and same is the case with OCT.

The drawback of OCT is the resolution and very high sensitivity to the setup. Compared to the nanometer scale of TIR and SPR, coherence topography generally involves things with a resolution of around 1–10 μm and increased spatical resolution creates special needs for the properties of the light source. Still, in some cases the setup could be beneficial and used to detect adsorption layers if the layer size is relatively thick. A good source for OCT and potential applications is, for example, the review of Fercher *et al.* ([302], 2009).

Material alteration

Biomaterials were briefly discussed in section 2.2, but if we specify the usage to adsorption, the aims change slightly. While we can view the material as biomaterial, a great deal of studies still have a controlled enviroment of some sort. By controlled environment we of course consider controlling either the path of the observed particles or the adsorbing material as we aim to somehow change the adsorption behavior.

The controlled particle movement is usually performed with an electric field because it creates a high control over the particles. The material alteration involves some material modifications: chemical etching [36,303], electrical modification [162], Self Assembled Monolayers (SAM) [16,149,282,287,304,305], or creating other modifications which change the physical or chemical nature of a surface [306]. As an example of a modification related to photonics, gratings are the most common alteration as they are generally easy to manufacture and can be customized for a specific application [307,308].

Chemically controlled surfaces are major field of research. If the surface has certain receptors, the surface can be used in very specific detection applications. Chemical assays such as immunoassays are a good example. Immunoassays measure the concentration or presence of an analyte (protein) in a sample liquid. For example biological fluids such as urine and blood plasma are measured for the presence of a certain molecule.

Other deviations

Any other modification to the reflectometry, TIR, and SPR can naturally be achieved.[j] Here we can mention different fiber optical devices [310] which can be easily be built to work even in liquid environments and Fourier Transform Infra-Red (FTIR) methods [124]. One of the TIR applications is Attenuated Total Reflectance (ATR), which uses several bounces of light in a waveguide to produce enhanced attenuation to a TIR signal [311]. As ATR is a branch of TIR, it is not discussed further. Related TIR applications, fiber applications, are also common applications [79,94,190,310,312].

Still unmentioned is Scanning Angle Reflectometry (SAR) [309, 313,314], which is very much ellipsometric method without polarization information, and progressing towards more indirect methods, we find Dynamic Light Scattering (DLS), which measures the scattering of photons which could be used to study adsorption [313,315–319].

Basically any photonic method and device could be considered a potential biological measurement device. Devices measuring a broad spectrum might progress towards higher resolution measuring and imaging [320]. Still, the photonic devices now used in adsorption studies are usually based either on small–scale photon absorption, non–linear phenomena, attenuation, polarization, or coherence.

One of the most common non–photonic methods worth mentioning is Quartz Crystal Microbalance (QCM). In QCM a quartz resonance crystal is used between two metal layers. The one metal layer is often covered with another thin layer of metal which is in contact with the studied particles. The observed parameter is the frequency shift of the quartz crystal under pressure. Essentially QCM is a gravimetric method studied with electric signal [174,321–323]. Neutron Reflection (NR) methods are also used in adsorption studies. In this technique a highly collimated neutron beam is shone towards a thin film and the scattering is then ob-

[j] For short review, see Ramsden ([309], 1997).

served [13,324–326]. Surface–enhanced raman scattering (SERS) is also an often used method in adsorption studies and molecule detection [248]. It has been also used successfully in connection with immunoassays [40].

2.7.6 General photonic results of previous studies

There are two main categories of results for adsorption observations concerning photonics. First are the actual refractive indices of proteins in liquid environment, and second, the observed thicknesses of adsorbed proteins. In the analyses the actual environment is observed as a monolayer, multilayer, or with other estimations, depending on the complexity of the environment. The refractive index is, however the most important to extract from the literature, as we are using a photonic method in this study.

Studies have evaluated the refractive index or even the spectral refractive indices of materials. Table 2.5 lists a number of individual refractive indices used in some photonic studies. Figure 2.15 shows water, PBS[k], quartz and the spectral refractive index of protein in general. The protein spectral refractive index is the mean values extracted from study of Arwin ([328], 1986). We should note here that all these spectra seem to have very similar shapes. This justifies the mean value extraction as well as comparing protein refractive index function shapes to water and PBS.

The other clear result that can be extracted from previous studies is naturally the thickness of the adsorbed protein layer. Table 2.6 lists some studies about the results concerning the function of adsorption target and protein.

Table 2.6 shows a wide variety of surfaces but what is interesting is the deviation on similar surfaces. The model and refractive indices used (Table 2.5) are crucial in photonic studies. Since there is no agreement about the refractive index, the exact layer thickness also becomes ambiguous.

Furthermore, Table 2.6 shows a wide variety of refractive in-

[k]Phosphate buffered saline (PBS) is the buffer solution used in this study.

Table 2.5: *Some evaluated protein refractive indices by source. If no exact information is given in the source, it is marked with a horizontal line. The wavelength is that used in the particular study.*

Wavelength [nm]	**Protein**	**Refractive index**	
401.5	HPF	1.366-1.368	[327]
	IgG	1.390-1.395	
546.1	BSA	1.575	[328]
	Hemoglobin	1.500	
	γ-Globulin	1.544	
620.0	HPF	1.40-1.56	[329]
632.8	HPF	1.365–1.34	[330]
	HSA	1.415–1.445	
	IgG	1.38–1.42	
	LYS	1.475–1.51	
632.8	-	1.45	[294]
632.8	BSA	1.572	[328]
	Hemoglobin	1.485	
	γ-Globulin	1.542	
632.8	-	1.5	[266]
632.8	HSA	1.48	[158]
632.8	HPF	1.465	[278]
632.8	HSA	1.465	
632.8	Hemoglobin	1.465	
-	*various*	1.46–1.90	[257]
200–1000	HPF	1.4	[170]
300–1000	HPF	1.57	[331]

dices, but there is no information about the used liquid media or surfaces. For example, study [327] used hexamethyldisiloxane as adsorbent and PBS media. Very little is generally said about the liquid media or about the surface. Some authors acknowledge this by directly saying that these refractive indices are only for the par-

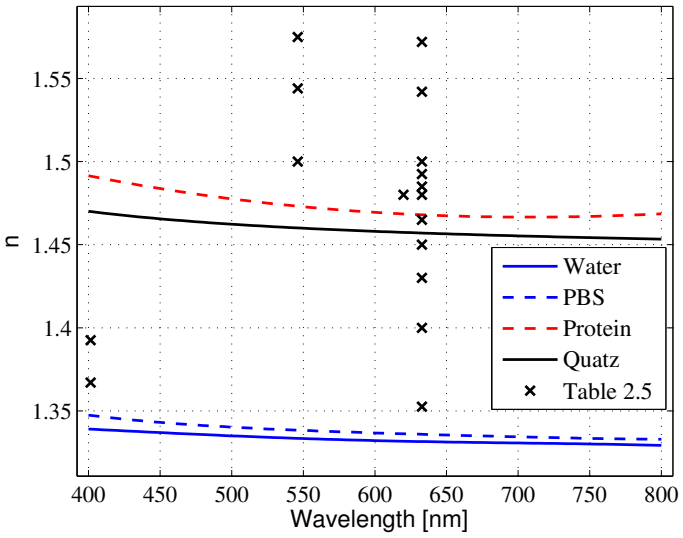

Figure 2.15: *Refractive indices of water [332], PBS, protein [328], and quartz [333].*

ticular used surface. However, questions could be; *what is then the real refractive index of proteins?*; and *is this refractive index a good description of the protein refractive index or just a surface–dependent as well as solution–dependent approximation of dissolved proteins near an interface?*

One thing is certain; Table 2.5 indicates strong disagreement on the used refractive index, which isn't a good starting point for any photonic study. Figure 2.15 also plots these different values, which makes the issue even more visible. It becomes unclear if the discussion is really about true protein refractive index, or about protein packing and surface dependent observations.

de Feijter's equation

De Feijter's approach to adsorption might be one of the most commonly used in photonic studies of adsorption [334]. The equation

itself is

$$M = d_A \frac{n_A - n_s}{dn/ds}, \tag{2.8}$$

where M is the adsorbed mass in ng/mm^2, d_A the thickness of an adsorbed film, n_A the refractive index of the adsorbed film, n_S the refractive index of the surrounding material (liquid), and dn/ds is the "refractive index increment" of the molecules (0.18 cm^3/g [335], 0.182 cm^3/g [330], 0.188 cm^3/g [153]) .

Ball and Ramsten ([335], 1998) succinctly discussed the intricacies of adsorption equations. They note that the commonly used refractive index increment should be a buffer solution dependent value [335]. The refractive index should also be wavelength dependent, which may often be forgotten. Essentially, de Feijter's formula is an effective medium approximation (EMA) of sorts. That is, it is an estimate of the increment to a buffer solution refractive index. EMA is discussed later, in section 4.4.3.

While de Feijter's estimate might be relevant, a problem involves its ambiguous usage. There has been little discussion of the exact value of the increment and how precise the estimate is. It is, however, just commonly used. It also predicts only the case when proteins form exactly d_A thick and homogeneous layer near an adsorbent. While it is not uncommon to do approximation of homogeneous and otherwise photonically ideal behavior of material, we note that it sounds somewhat strong assumption to make for buffer dissolved proteins near an interface.

2.7.7 Conclusion

When discussing a TIR or SPR setup the system is always confined. A SPR requires a specific surface and a TIR requires transparent media. These two methods are more widely used since they seek to detect the molecules on a specific surface. The gain is more accurate detection, but with the cost of a limited setup and samples. A reflection setup is not confined to any specific materials, but when measuring through the liquid and observing only the reflection, accuracy is lost compared to the TIR or the SPR. Still, the

greatest benefit of reflection studies is a sample–wise freedom. Any reflective sample can be used, but very diffuse samples cannot be measured.

Table 2.7 lists shortly the device level comparison for the ellipsometric constructions. The general conclusion is that several of the methods have very specific setups or materials. While ellipsometry loses in absolute sensitivity, polarization makes it possible to analyze even the most complicated situations. The size of an ellipsometric setup is generally large compared to the others, but when designing a lab–on–a–chip type solution, the simplest TIR might be the only solution. It is very convenient because it also can be executed using a simple piece of fiber. However, as the polarization–altering components and other processing methods start to reach nano-scale, these three methods and their setups have their own benefits and could be considered in adsorption detection, even on a smaller scale.

The general sensitivity of the methods should also be considered. This study is not concerning very much the sensitivity of the method used, but has a general interest in providing sensitive methods. While the sensing amount is generally around μg per milliliter (ml), even fg/ml amounts have been observed through photonic measurements [79].

The various values of the refractive indices presented in Table 2.5 seem very ambiguous. While the ellipsometric system is accurate in the evaluation of the refractive index, the actual model has a massive impact on the results and it seems that the values themselves are still not consistent among researchers. It must be stated that there are differences in the setups and the time span of the research is great, but, if ellipsometry is thought to be an accurate method in sensing nano–layer thicknesses, where does the differences come from?

This is also a promising start of for discussion. While the methodology is strong, novel ideas for executing them are, however, difficult because of the fundamental differences in the literature. Is there anything to study then? Surely there is. Especially in the nano–

size range, where the frontier of both biochemistry and photonics are still being established. One might argue that this is an invalid statement because, for example, the Maxwell equations are already established and those have not been disproved in nano-scaled environments. The question of a nano–environment is not that it cannot be solved, but more of what we try to solve. Nanoparticles can be detained and optical tweezers are a reality these days. These are, however controlled and forcefully created scenarios. The natural and passive behavior of such particles in any environment is still not a trivial task to resolve because the questions are not clear.

The *Handbook of Optics* is still a viable source of information on photonic methods [256]. New applications will be found as the fundamental methodology starts to be very strong. The components and computational aspects also become cheaper and cheaper to obtain. This constantly creates new possibilities to use a wider and wider range of wavelengths in applications. Still, the majority of the applications seem to be moving towards detecting molecule concentrations and chiefly to provide answers in detecting a single particle type. While they are generally useful in that, the diversity of applications is very small in this regard. While, for example, fluorescence provides an easy method to perhaps even detect two separate molecules in a competing adsorption, huge underlying processes, structures, and components in a real environment create a major barrier to these otherwise accurate and sensitive methods. We believe that it occasionally seems that researchers have a need to publish rather than being researchers on a quest.

However, we find it relieving, that mixed methods have been used. There are even studies that actually combine the physical chemistry into the photonic methods, and more importantly, acknowledges the depth of adsorption, such as the study of Angelescu *et al.* ([122], 2011). Still, it is sad to see, that despite of the depth analysis in [122], it is not used with photonic data, and instead, homogenic layers and de Feijter's equation is used.

Table 2.6: *Example thicknesses of adsorbed fibrinogen observed in different studies on titanium.*

Method	**Surface**	**Concentration** [mg/ml]	**thickness** [nm]
Ellipsometry	Sputtered titanium on aluminium [331]	3.00	3.5
	Evaporated TiO_2 on Si [329]	0.5	25.8
	Silica [261]	0.1	≈ 15
	Titanium [170]	0.05	3.0 ± 0.6
		1	4.6 ± 0.7
		5	6.6 ± 1.1
QCM	Sputtered titanium on glass [278]	0.08	10.6

Table 2.7: *Pros and cons of the main photonic methods for particle adsorption detection. RAE represents rotating analyzer ellipsometer and PCSA-E Polarizer Compensator Sample Analyzer Ellipsometer (see section 2.7.2).*

Method	**Pros**	**Cons**
RAE	- Cheap - Easy setup - Spectral possibilities	- Incomplete polarimeter
PCSA-E	- Complete polarimeter - Accurate - More analytic	- More expensive - Requires a waveplate
TIR	- Sensitive - Simplest setup - Cheap	- Least analytic - High estimate analysis - Material and setup restrictions - Mainly for ”existence sensing”
TIRF	- TIR with fluorescent data - Competitive adsorption	- Requires high energy photons for fluorescent excitation - Material and setup restrictions
SPR	- Sensitive - Competitive adsorption	- Difficult to setup - Material and setup restrictions

3 Theory

This chapter describes the key components of the photon interaction theory used in this study. As the subject of this study is so broad the theory presents only the exact key points needed in the analysis. The theory can be separated into these main categories:

1. A basic photon description (section 3.1)
2. Polarization of an electromagnetic wave (section 3.2)
3. Ellipsometric parameters (section 3.3)
4. Discussion of the need for raytrace models and the model used in this study (section 4.4)

The constructed ray tracing model is somewhat part of this theory, as it still uses the components presented in this chapter. But for clarity, it is presented in the materials and methods part of this work.

3.1 GENERAL PHOTONICS THEORY

The theory of photon propagation and interaction can be very complex, if necessary and precision is needed. The usual starting point for these theories are the Maxwell equations, which describe the nature and rules governing the quantum of electromagnetic waves, photons. Here we are not as interested in the nature of photons, only their application. In this study, we only need to discuss terms such the interference and consequences of the primal behavior of photons on interfaces.

Thus, we justifiably assume after this, and rightfully so, that a photon electric field can be described with an exponential function [336]

$$\boldsymbol{E}(A, \boldsymbol{k}, \boldsymbol{r}, t, \omega, \phi) = Ae^{\mathrm{i}\left(\boldsymbol{k}\cdot\boldsymbol{r} - t\omega - \phi\right)}, \tag{3.1}$$

where A is amplitude, ω the angular velocity, ϕ phase, $\boldsymbol{k}$ is the wave vector, $\boldsymbol{r}$ propagation vector

$$\boldsymbol{r} = \begin{bmatrix} x\hat{x} \\ y\hat{y} \\ z\hat{z} \end{bmatrix},$$

λ the wavelength, and i is a complex number ($\mathrm{i}^2 = -1$).[a] This wave function can successfully describe the propagation of a photon in numerous cases, with a number of assumptions.

These assumptions are: isotropy, a homogenic material, no scattering, and no absorbtion during photon propagation. This seems to be a strong set of rules, but in most cases this offers a good approximation and a sound set of rules. Despite of the lack of scattering and absorbtion observations in the theory part, the discussion of the effects of the scattering can be found, for example, in [336] (Part2, Chapter 6).

In Equation 3.1, $\boldsymbol{k}$ is the wave vector that describes the directional properties of the propagating phase, but here, we assume isotropy, so that $\boldsymbol{k}$ becomes direction independent scalar

$$k(\lambda) = \frac{2\pi}{\lambda}. \tag{3.2}$$

In the discussion here, we will not generally denote the wavelength dependency of k for notation clarity, but we understand that wavelength defines values of k. As the propagation and wave vector go hand in hand, we will mark the plain coordinates, without unit vectors and partially defining

$$r = \begin{cases} x \\ y \\ z \end{cases}$$

[a] Strictly speaking A, ϕ, and ω could be described individually with the primal coordinate directions (as vectors), but here they are presented as direction independent scalars.

Also, because we assumed isotropy, the Equation 3.1 becomes separable with

$$E(A,k,r,t,\omega,\phi) = \begin{cases} Ae^{\mathrm{i}[kx-t\omega-\phi]} \\ Ae^{\mathrm{i}[ky-t\omega-\phi]} \\ Ae^{\mathrm{i}[kz-t\omega-\phi]}. \end{cases}$$

Further, when assuming a standing wave ($t = 0$), we can transform the field of Equation 3.1 to be simply

$$E(A,k,r,\phi) = \begin{cases} Ae^{\mathrm{i}[kx-\phi]} \\ Ae^{\mathrm{i}[ky-\phi]} \\ Ae^{\mathrm{i}[kz-\phi]}. \end{cases} \tag{3.3}$$

and even more simply, we could describe the field just with scalar phase

$$E(\phi) = e^{\mathrm{i}(-\phi)}, \tag{3.4}$$

which is valid if an observation seeks to evaluate a single point, and the aim is to measure a sum of several fields. This could be the case when observing an interference of sorts, or when calculating the energy of the field. Next, we use Equation 3.4 to do exactly this.

The energy of a field E, which is described as the irradiance[b] I of that wave, can be expressed as

$$I = |E \cdot E^*|, \tag{3.5}$$

where * denotes a complex conjugate

$$(\mathrm{a} + \mathrm{bi})^* = (\mathrm{a} - \mathrm{bi}).$$

Equation 3.5 indicates that the energy of the field E is always in the scale of A^2, when the amplitude A is real. Equation 3.5 for any

[b] Or the "measurable energy", see the discussion that follows.

complex field of Equation 3.3 will produce an irradiance of

$$\begin{aligned} I_{\text{example}} &= |E \cdot E^*| \\ &= E(A,\phi) \cdot E^*(A,\phi) = Ae^{\mathrm{i}\phi} \cdot Ae^{-\mathrm{i}\phi} \\ &= A^2 \left[\cos(\phi) + \mathrm{i}\sin(\phi)\right] \left[\cos(\phi) - \mathrm{i}\sin(\phi)\right] \\ &= A^2\big(\cos^2(\phi) + \sin^2(\phi)\big) \quad \rightarrow 1 \\ &= A^2, \end{aligned}$$

when the whole exponential function is presented with only a single phase ϕ.

This is the case for one photon. It is reasonable that the energy of a single photon is indeed always related to the amplitude of the photon and not the position. In real situations we rarely discuss observing a single photon but rather the time averaged interference of several. One cannot assume that Equation 3.3 would describe the correct energy of a multiple–photon propagation in situations other than that free space propagation when the photons start with same phase. Therefore, one must take into account both the position and the phase term, giving the field the previously described form of Equation 3.3.

Furthermore, it must be noted that the observed irradiance I is indeed a time averaged (marked with $\langle\rangle$) entity with

$$I = \langle |E \cdot E^*| \rangle . \tag{3.6}$$

This will be assumed in further observations dealing with irradiance I. Furthermore, when we discuss photon energy, we discuss the measurable energy which always has dimensions. One cannot measure dimensionless quantities and therefore the irradiance I is always the quantity of power per surface area (W/m^2,[256]), or energy per time per surface area.

Appendix C considers interfering waves with examples and demonstrates why the energy of point–wise interfering static fields can be described with simple cosine function with a phase of ϕ, $\cos(\phi)$. Appendix C indicates that the energy of N interfering fields takes

the form N^2A^2 and that the energy of two interfering photons can be presented with a phase difference ϕ_{dif}

$$\cos(\phi_1 - \phi_2) = \cos(\phi_{dif}). \tag{3.7}$$

While this is not the way the model of this study is later on treated, it is important to note that the interference indeed directly observes the phase components of the interfering photons. Furthermore, this provides a valid reason for using cosine functions in visualizations.

3.2 POLARIZATION

3.2.1 Polarization

Briefly stated polarization describes the direction of electric field amplitude. As polarization is always a property of a photon, we can state that all photons actually propagate more in three–dimensional space than in a geometrically visualized line. The line is usually only visualized as a propagation direction rather than a full presentation of a photon. Let us suppose an electric field propagating along a z-axis. We can express the this field E_z to be a separable combination of x and y components

$$\begin{aligned} \boldsymbol{E}_z(\boldsymbol{A}, \boldsymbol{r}, \boldsymbol{\phi}) &\Rightarrow E_z\left(A_x, A_y, x, y, \phi_x, \phi_y\right) \\ &= E_x(A_x, x, \phi_x) + E_y(A_y, y, \phi_y) \\ &= A_x e^{i[kx-\phi_x]} + A_y e^{i\left[ky-\phi_y\right]}. \end{aligned} \tag{3.8}$$

Wavelength dependence is always present, but can be omitted for simplicity of notation. To express the polarization, we can represent the real part of Equation 3.8 with two primary parts

$$E_x(A_x, x, \phi_x) = A_x \cos\left(kx - \phi_x\right), \tag{3.9}$$

and

$$E_y(A_y, y, \phi_y) = A_y \cos\left(ky - \phi_y\right). \tag{3.10}$$

Equations 3.9 and 3.10 can represent the nature of the polarization and this is exactly what follows. We present wave E_z as a standing wave in the space with

$$\begin{aligned} E_z &= E_x(A_x, x, \phi_x) + E_y(A_y, y, \phi_y) \\ &= A_x \cos(kx - \phi_x) + A_y \cos(ky - \phi_y) \end{aligned} \tag{3.11}$$

Using Equation 3.11, there are two primary types of polarization plotted in Figures 3.1a and 3.1b. Figure 3.1a presents a linear polarization, which is created with $\phi_x = \phi_y = 0$, and $A_x = A_y$. In this case, both primitive components, E_x and E_y are in the same phase and they create a deviation to E_z only in a plane. If a phase difference ($\phi_x \neq \phi_y$) exists, the primitive components E_x and E_y sum each other in such a manner that E_z is expressed by an elliptic trace. If the fields, described in equations 3.9 and 3.10, have a maximal phase difference of $\pi/2$, circular polarization is created. This special case is presented in Figure 3.1b.

It is rather common that the phase difference of E_x and E_y

$$\phi_{xy} = \phi_x - \phi_y, \tag{3.12}$$

is not $\pi/2$ but usually takes some other value.

The polarization directions are created with polarizers which determine the primary directions of the polarization. Components affecting the amplitude of primary components are called linear polarizers.[c] Those polarizers that create a phase delay between the primal polarization directions are called circular polarizers, or waveplates.[d] In reality, there are several types of polarizers and matters might not be this obvious, but these two types create a simple division to keep in mind.

3.2.2 Stokes parameters

Before continuing the discussion of polarization we need to cite four names often associated with material interaction: Fresnel, Stokes,

[c] The A_x and A_y values of Equation 3.9 and 3.10.

[d] Altering the ϕ_{xy}.

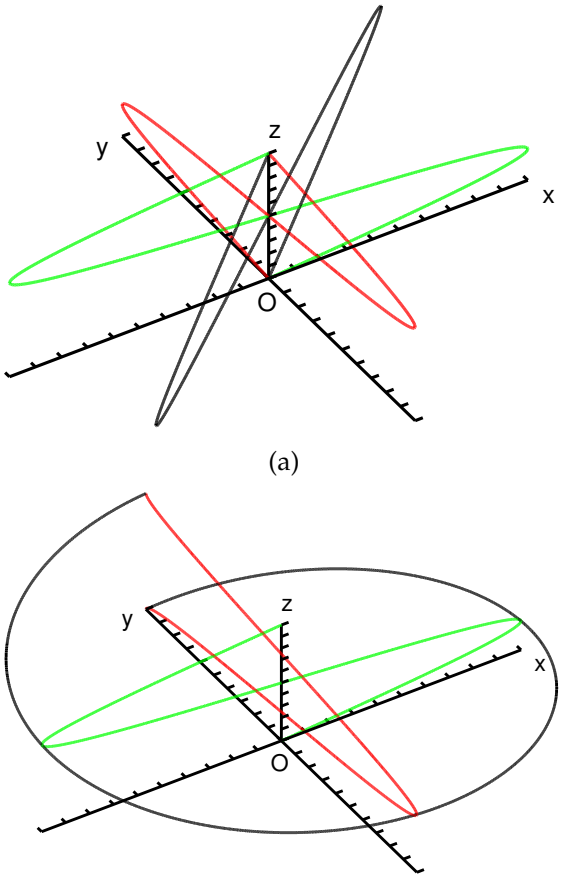

Figure 3.1: *Two polarization states created from Equation 3.11 (black) with two directional amplitudes (gray). (a) linear polarization E_z with $\phi_x = \phi_y = 0$ and (b) circular polarization E_z with $\phi_x = 0$ and $\phi_y = \pi/2$.*

Mueller, and Jones. These names are commonly associated with the "source of invention", but are essential in any discussion of polarization. Here we will consider a polarization state through a simple reflection. This reflection is often described with so–called Fresnel coefficients, which describe a photon reflection from a plane having two separable polarization directions. Fresnel coefficients will be introduced in section 3.2.3.

Table 3.1: *Description of Stokes parameters through linear polarizers P with pass-through in angle α (P_α) [256]. P_R denotes a right–hand circular polarizer and P_L correspondingly a left–hand. For example, P_0 polarization has an amplitude only in the x direction and P_{90} in the y direction.*

Stokes parameter	**Polarizer equivalent**
s_0	$P_0 + P_{90}$
s_1	$P_0 - P_{90}$
s_2	$P_{45} - P_{135}$
s_3	$P_R - P_L$

While Fresnel describes the primitive reflection of a photon, Stokes, Mueller, and Jones are usually spoken of as the description of mathematical approaches of polarization ([256], Part 2, Chapter 22). Stokes parameters describe the polarization of any photon and are presented as a Stokes vector

$$\mathbf{S} = \begin{bmatrix} s_0 \\ s_1 \\ s_2 \\ s_3 \end{bmatrix}. \tag{3.13}$$

Table 3.1 shows all of the four Stokes parameters and the related polarization relations they represent. Furthermore, we can discuss the polarimeters of section 2.7.2 and Figure 2.13 (on page 54). We note that all polarimeters which have no circular polarizers cannot determine the last Stokes parameter s_3. As discussed in the previous section, circular polarization is created with phase a difference between the primal polarization components. Thus, if we do not alter this polarization type, there is no way of distinguishing the phase difference Δ sign (Equation 3.12) or the last Stokes parameter s_3. It will remain unknown. Modern ellipsometers use the Photoelastic Modulators (PEM), which can create controlled elliptical polarization changes with very high rates [78].

The Stokes vector describes the state of polarization of the ob-

served time–averaged photons. Mueller, the Mueller matrix to be precise, describes the possible modifications to that vector through primitives m_{ab}

$$\mathbf{M} = \begin{bmatrix} m_{00} & m_{01} & m_{02} & m_{03} \\ m_{10} & m_{11} & m_{12} & m_{13} \\ m_{20} & m_{21} & m_{22} & m_{23} \\ m_{30} & m_{31} & m_{32} & m_{33} \end{bmatrix}. \tag{3.14}$$

Thus, it is possible to produce any output Stokes vector $\mathbf{S}_1$ from input $\mathbf{S}_0$ by modifying it

$$\mathbf{S}_1 = \mathbf{M}\mathbf{S}_0 = \begin{bmatrix} m_{00} & m_{01} & m_{02} & m_{03} \\ m_{10} & m_{11} & m_{12} & m_{13} \\ m_{20} & m_{21} & m_{22} & m_{23} \\ m_{30} & m_{31} & m_{32} & m_{33} \end{bmatrix} \begin{bmatrix} s_0 \\ s_1 \\ s_2 \\ s_3 \end{bmatrix}. \tag{3.15}$$

Mueller matrix photonics is a completely different matter and here we will limit our observations to systems which have no circular polarization information. That is, when the output of the imperfect system S' is more like

$$\mathbf{S}' = \mathbf{M}'\mathbf{S}_0 = \begin{bmatrix} m_{00} & m_{01} & m_{02} & 0 \\ m_{10} & m_{11} & m_{12} & 0 \\ m_{20} & m_{21} & m_{22} & 0 \\ 0 & 0 & 0 & 0 \end{bmatrix} \begin{bmatrix} s_0 \\ s_1 \\ s_2 \\ 0 \end{bmatrix}. \tag{3.16}$$

Strictly speaking, the zeros in Equation 3.16 remain non-zero unknown, but are set to zero for stating the operators we are dealing with. Since we are dealing with an output such as in Equation 3.16, this output can even be expressed with more simplicity, with Jones formalism. We will consider this in greater detail in section 3.2.5, but we will first discuss Fresnel coefficients.

3.2.3 Fresnel equations and Snell's law

Fresnel equations

Previous sections described polarization as coordinate-wise amplitude differences of the electric field describing a photon. Figure 3.1

showed the separable field of a photon when these directional amplitudes were the same. In reality these primitive components of an electric field are rarely equal, which creates the different polarization states of the field and changes upon propagation and photon–material interaction. Fresnel equations are based on Maxwell equations to describe the changes to these amplitudes on refraction and reflection when the photon interacts with the material. Therefore, Fresnel equations describe the interaction on an interface according to the polarization directions.

We will not show the course of creating Fresnel equations. We only express them as a known tool and discuss what they can measure and analyze if the equipment used is capable of altering polarization before as well as after the interaction.

Two main polarization directions are described in the Fresnel coefficients, p and s. The p directions describe the reflection and transmission coefficient for the case where the electric field amplitude is in the plane of incidence. The s describes case where the amplitude is perpendicular to the incident plane. Both are schematically described in Figure 3.2.

The reflection coefficients r and the transmittance coefficients t are described for both cases as follows

$$r_s = \frac{N_1 \cos(\theta_i) - N_2 \cos(\theta_t)}{N_1 \cos(\theta_i) + N_2 \cos(\theta_t)}, \tag{3.17}$$

$$t_s = \frac{2N_1 \cos(\theta_i)}{N_1 \cos(\theta_i) + N_2 \cos(\theta_t)}, \tag{3.18}$$

$$r_p = \frac{N_2 \cos(\theta_i) - N_1 \cos(\theta_t)}{N_1 \cos(\theta_t) + N_2 \cos(\theta_i)}, \tag{3.19}$$

$$t_p = \frac{2N_1 \cos(\theta_i)}{N_1 \cos(\theta_t) + N_2 \cos(\theta_i)}, \tag{3.20}$$

when N_1 and N_2 are the corresponding complex material refractive indices. Angles θ_i, and θ_t are the incident, and refracted angles, respectively [96].

Next, let us represent the polarization in reflection as schematically drawn in Figure 3.2. We will denote below the polarizations p

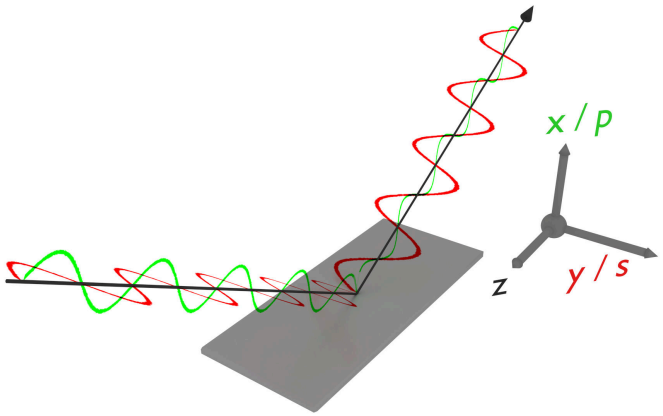

Figure 3.2: *Visualization of polarization components. The green represents the p polarization and red the s polarization (y axis) plane.*

and s with the field primitives E_x and E_y. The polarization state is usually expressed with a number, the relation χ of the two primitive components, with the separable notation of Equation 3.1, as

$$\chi = \frac{E_y}{E_x} = \frac{A_y e^{\mathrm{i}\left(\frac{2\pi}{\lambda}y - t\phi\right)}}{A_x e^{\mathrm{i}\left(\frac{2\pi}{\lambda}x - t\phi\right)}}. \tag{3.21}$$

Let us further denote the relation of input χ_i and output χ_o

$$\frac{\chi_i}{\chi_o} = \frac{\frac{E_{iy}}{E_{ix}}}{\frac{E_{oy}}{E_{ox}}}. \tag{3.22}$$

As this observation focuses on polarization changes, we can not ignore the coordinate system of x and y. This concerns the phase difference between the two polarization primitives ϕ_x and ϕ_y. Therefore, if we open Equation 3.22 with the field notation of Equation 3.4 we obtain

$$\frac{\chi_i}{\chi_o} = \frac{A_{iy} e^{\mathrm{i}\phi_{iy}} A_{ox} e^{\mathrm{i}\phi_{ox}}}{A_{ix} e^{\mathrm{i}\phi_{ix}} A_{oy} e^{\mathrm{i}\phi_{oy}}}. \tag{3.23}$$

Furthermore, we set the phase difference in the input plane to zero $\phi_{xy} = 0$ and assume that the amplitude of the incident or incoming

wave is the same $A_{ix} = A_{iy}$. This produces

$$\frac{\chi_i}{\chi_o} = \frac{A_{ox}}{A_{oy}} e^{\mathrm{i}(\phi_{ox} - \phi_{oy})} = \frac{A_{ox}}{A_{oy}} e^{\mathrm{i}\Delta_{oxy}}. \tag{3.24}$$

Generally this relation of the amplitude terms is marked with

$$\tan(\Psi) = \frac{A_{ox}}{A_{oy}}. \tag{3.25}$$

Combining Equations 3.12, 3.24, and 3.25, we obtain the general ellipsometer equation

$$\frac{\chi_i}{\chi_o} = \tan(\Psi) e^{\mathrm{i}\Delta}. \tag{3.26}$$

The starting point for the Fresnel equation is the multiplier between the input and output fields ($\boldsymbol{E}_o / \boldsymbol{E}_i$). Thus, Equation 3.22 already describes the amplitude relation of the interacting electric field. The actual reflection coefficient r can then be used to describe the ellipsometer Equation 3.26 further to (see [256], Part 3, Chapter 27)

$$\frac{E_i}{E_o} = \frac{r_p}{r_s} = \tan(\Psi) e^{\mathrm{i}\Delta}. \tag{3.27}$$

Equation 3.27 is the most important basic equation of ellipsometry as it states the connection between the Fresnel coefficients and the ellipsometric parameters Ψ and Δ. Fresnel coefficients are defined using electric field changes through interaction, which directly indicates that when the incident and interacted fields are measured, one can study the photonic properties of the said interacting interface.

Snell's law

Another important rule for photon propagation is refraction. Reflection is usually assumed to occur in the same angle as the incident (specular reflection), but the refraction angle is dependent on the refractive index of the material. This refraction is usually described with Snell's law [337]

$$N_1 \sin(\theta_1) = N_2 \sin(\theta_2) \Rightarrow \frac{\sin(\theta_1)}{\sin(\theta_2)} = \frac{N_2}{N_1} \tag{3.28}$$

where θ_1 is the incident angle angle in the material having a refractive index N_1 and θ_2 is the refraction angle of light in the material having a refractive index of N_2.

Snell's law also provides the possibility to calculate the refracted angle from the incident angle and the refractive indices as presented in Equation 3.29. This method is also used in this study to calculate refraction. With complex refractive indices Equation 3.29 produces θ_2 values which also are complex.

$$\theta_2 = \text{asin}\left[\frac{N_1 \sin(\theta_1)}{N_2}\right]. \tag{3.29}$$

3.2.4 Setup in the reflection observations

The previously described polarization measurement setup in this study is much like that in Figure 3.2, only with polarizers added before and after the reflection from the sample surface. The system uses an unpolarized light source, which is then linearly polarized with the first polarizer. Then the surface acts upon the incident wave with Fresnel coefficients r_p and r_s. These Fresnel coefficients have directions which correspond to the x and y directions, respectively, so in later stages p and s will be used for indicating the polarization state. The propagating photon moves to another polarizer and finally to the detector. Thus, there are three operators affecting the system and the general notation of the system output O can be written

$$E_o = \mathbf{J}_{\text{LinPol}}(\alpha_2)\mathbf{J}_r\mathbf{J}_{\text{LinPol}}(\alpha_1)\mathbf{E_i}, \tag{3.30}$$

where $\mathbf{J}_{\text{LinPol}}$ denotes linear polarizer, $\mathbf{J}_r$ the surface, and $\mathbf{E_i}$ is the input field. The $\mathbf{J}$ denotes a Jones matrix, which is an easy notation for expressing essentially paraxial photon paths as is the case here. Equation 3.30 follows so–called Jones formalism, which is operated

from right to left, as do all matrix operations. We will next examine the essential points of Jones formalism in this particular simple system.

3.2.5 Jones formalism

Jones calculus is matrix operation formalism which describes light propagation for the two primal polarization directions [338]. It is especially used in polarization optics because the polarization can be described with these simple principle components.

Jones calculus in general

Jones calculus uses vectors and matrices to describe an optical system. Thus, each matrix is a photonic component in the system and the starting point for the matrix operators are generally vectors. Let us consider a simple standing wave having a phase ϕ in a point which has x and y components. This could be written with vector

$$E = \begin{bmatrix} E_x \\ E_y \end{bmatrix} = \begin{bmatrix} A_x e^{i\phi_x} \\ A_y e^{i\phi_y} \end{bmatrix}. \tag{3.31}$$

The wave described in (3.31) is a very primitive version of a wave, but let us alter it with Jones operators. We now examine the effects of a single Jones operator on the wave defined above. Let us note that the operator

$$\mathbf{J} = \begin{bmatrix} A & B \\ C & D \end{bmatrix} \tag{3.32}$$

is created. We then operate the wave (3.31) to generate an output **O**.

$$\mathbf{O} = \mathbf{JE} = \begin{bmatrix} A & B \\ C & D \end{bmatrix} \begin{bmatrix} E_x \\ E_y \end{bmatrix} = \begin{bmatrix} AE_x + BE_y \\ CE_x + DE_y \end{bmatrix} \tag{3.33}$$

It is clear in Equation (3.33) that the multipliers A and D directly affect the propagation of each component, *i.e.* if $B = C = 0$, then A and D are the amplitude multipliers after the photonic element

which the operator **J** describes. We can therefore alter the amplitude of the primitive directions x and y with these multipliers.

If B and C, in Equation 3.33, are not zero the amplitudes can be rotated. Thus, rotation to a degree of α could be executed with Jones operator

$$\begin{aligned}
&\mathbf{J}_{rot}(\alpha) \\
&= \begin{bmatrix} \cos(\alpha) & -\sin(\alpha) \\ \sin(\alpha) & \cos(\alpha) \end{bmatrix} \begin{bmatrix} 1 & 0 \\ 0 & 0 \end{bmatrix} \begin{bmatrix} \cos(-\alpha) & -\sin(-\alpha) \\ \sin(-\alpha) & \cos(-\alpha) \end{bmatrix} \\
&= \begin{bmatrix} \cos^2(\alpha) & \cos(\alpha)\sin(\alpha) \\ \cos(\alpha)\sin(\alpha) & \sin^2(\alpha) \end{bmatrix}.
\end{aligned} \tag{3.34}$$

It is possible to describe many photonic elements with the general Jones notation of 3.32. Next we will examine the Jones construction of a reflection system with polarizers.

3.2.6 Jones formalism output in PSA reflection

In the PSA (Polarizer–Sample–Analyzer)[e] system equation stated in Equation (3.30) the first polarizer can be thought to be redundant as the used photon source has no known polarization state. Thus, the input polarization and first linear polarizer can be combined and Equation (3.30) can be rewritten as

$$E_o = \mathbf{J}_{\mathrm{LinPol}}(\alpha_2)\mathbf{J}_r\mathbf{E_i}, \tag{3.35}$$

where the incident wave $\mathbf{E_i}$ already includes polarization angle α_1 and can be simply expressed (using Equation 3.31)

$$\mathbf{E_i} = \begin{bmatrix} E_p \\ E_s \end{bmatrix} = \begin{bmatrix} A_x e^{-i\phi_x}\cos(\alpha_1) \\ A_y e^{-i\phi_y}\sin(\alpha_1) \end{bmatrix} = \begin{bmatrix} A_p\cos(\alpha_1) \\ A_s\sin(\alpha_1) \end{bmatrix}. \tag{3.36}$$

Because the aim of this theory is to link it to measured values, one could assume here $A_p = A_s = 1$. This selection could be made if

[e] Note that this is the exact setup from Figure 2.13c on page 54.

the first polarizer is ideal and the light source does not have polarization dependencies. We will, however, just continue with

$$\mathbf{E_i} = \begin{bmatrix} A_p \cos(\alpha_1) \\ A_s \sin(\alpha_1) \end{bmatrix}. \tag{3.37}$$

We can simplify the notation of the output field by multiplying the $\mathbf{J}_r\mathbf{E_i}$ and setting the input field as a reflected field

$$\begin{aligned} \mathbf{E_{ir}} = \mathbf{J_r}\mathbf{E_i} &= \begin{bmatrix} r_p & 0 \\ 0 & r_s \end{bmatrix} \begin{bmatrix} A_p \cos(\alpha_1) \\ A_s \sin(\alpha_1) \end{bmatrix} \\ &= \begin{bmatrix} r_p A_p \cos(\alpha_1) \\ r_s A_s \sin(\alpha_1) \end{bmatrix}. \end{aligned} \tag{3.38}$$

After this the output of the system is simply

$$\begin{aligned} \mathbf{E_o} &= \mathbf{J}_{\text{LinPol}}(\alpha_2)\mathbf{E_{ir}} \\ &= \begin{bmatrix} \cos^2(\alpha_2) & \cos(\alpha_2)\sin(\alpha_2) \\ \cos(\alpha_2)\sin(\alpha_2) & \cos^2(\alpha_2) \end{bmatrix} \begin{bmatrix} r_p A_p \cos(\alpha_1) \\ r_s A_s \sin(\alpha_1) \end{bmatrix}, \end{aligned} \tag{3.39}$$

which will transform as

$$\begin{aligned} \mathbf{E_o} &= \begin{bmatrix} \cos^2(\alpha_2) & \cos(\alpha_2)\sin(\alpha_2) \\ \cos(\alpha_2)\sin(\alpha_2) & \cos^2(\alpha_2) \end{bmatrix} \begin{bmatrix} r_p \cos(\alpha_1) \\ r_s \sin(\alpha_1) \end{bmatrix} \\ &= \begin{bmatrix} r_p A_p \cos(\alpha_1)\cos^2(\alpha_2) + r_s A_s \sin(\alpha_1)\cos(\alpha_2)\sin(\alpha_2) \\ r_p A_p \cos(\alpha_1)\cos(\alpha_2)\sin(\alpha_2) + r_s A_s \sin(\alpha_1)\cos^2(\alpha_2) \end{bmatrix}. \end{aligned}$$

Using redefined markings of Equation 3.38, namely

$$\begin{aligned} E_p &= r_p A_p \cos(\alpha_1) \\ E_s &= r_s A_s \sin(\alpha_1)\ , \end{aligned}$$

the final output of the system will be

$$\mathbf{E_o} = \begin{bmatrix} E_p \cos^2(\alpha_2) + E_s \cos(\alpha_2)\sin(\alpha_2) \\ E_p \cos(\alpha_2)\sin(\alpha_2) + E_s \cos^2(\alpha_2) \end{bmatrix}. \tag{3.40}$$

3.2.7 Irradiance of the reflected field

The energy (irradiance) of the system of (see Equation 3.40) is defined [339] as

$$\begin{aligned} I =& E_o^* E_o \\ & \begin{bmatrix} E_p \cos^2(\alpha_2) + E_s \cos(\alpha_2)\sin(\alpha_2) \\ E_p \cos(\alpha_2)\sin(\alpha_2) + E_s \sin^2(\alpha_2) \end{bmatrix}^* \\ & \begin{bmatrix} E_p \cos^2(\alpha_2) + E_s \cos(\alpha_2)\sin(\alpha_2) \\ E_p \cos(\alpha_2)\sin(\alpha_2) + E_s \sin^2(\alpha_2) \end{bmatrix}. \end{aligned} \tag{3.41}$$

This will produce an output vector with components

$$\begin{aligned} I &= \begin{bmatrix} I_p \\ I_s \end{bmatrix}, \\ I_p = I_x =& E_p^* E_p \cos^4(\alpha_2) + E_p^* E_s \cos^3(\alpha_2)\sin(\alpha_2) \\ & + E_s^* E_p \cos^3(\alpha_2)\sin(\alpha_2) + E_s^* E_s \cos^2(\alpha_2)\sin^2(\alpha_2) \\ I_s = I_y =& E_p^* E_p \cos^2(\alpha_2)\sin^2(\alpha_2) + E_p^* E_s \sin^3(\alpha_2)\cos(\alpha_2) \\ & + E_s^* E_p \sin^3(\alpha_2)\cos(\alpha_2) + E_s^* E_s \sin^4(\alpha_2). \end{aligned} \tag{3.42}$$

Combining these components will show that the overall results looks simpler,

$$\begin{aligned} I = I_p + I_s =& E_p^* E_p \cos^2(\alpha_2) + E_s^* E_s \sin^2(\alpha_2) \\ & + \left[E_p^* E_s + E_s^* E_p\right] \sin(\alpha_2)\cos(\alpha_2), \end{aligned} \tag{3.43}$$

because we know that

$$\cos^2(\alpha) + \sin^2(\alpha) = 1. \tag{3.44}$$

This, however, does not require a linear polarizer. Only the rotation of the coordinates is required after a surface reflection. Thus, in this simple reflection system one could state that $\mathbf{J}(\alpha_2)_{LinPol}$ would be the Jones matrix rotator and polarizer

$$\mathbf{J}_{\text{LinPol}}(\alpha_2) = \begin{bmatrix} 1 & 0 \\ 0 & 0 \end{bmatrix} \begin{bmatrix} \cos(\alpha_2) & \sin(\alpha_2) \\ \sin(\alpha_2) & \cos(\alpha_2) \end{bmatrix}, \tag{3.45}$$

which would provide exactly the same output energy as in (3.43), since the overall energy of the polarized field is not affected by the polarization rotation.

3.3 ELLIPSOMETRIC PARAMETERS

The next step is to rewrite the system output and find the key parameters which describe it. With trigonometric rules [340]

$$\begin{aligned}\cos(\alpha)\sin(\alpha) &= \frac{1}{2}\sin(2\alpha),\\ \sin^2(\alpha) &= \frac{1-\cos(2\alpha)}{2},\\ \cos^2(\alpha) &= \frac{1+\cos(2\alpha)}{2},\end{aligned} \tag{3.46}$$

it is possible to rewrite Equation 3.43 for the output energy I.

$$\begin{aligned}I &= E_p^* E_p \left(\frac{1+\cos(2\alpha)}{2}\right) + E_s^* E_s \left(\frac{1-\cos(2\alpha)}{2}\right)\\ &+ \left(E_p^* E_s + E_s^* E_p\right)\frac{\sin(2\alpha)}{2}\\ &= \frac{1}{2}\Big[E_p^* E_p + E_s^* E_s + E_p^* E_p\cos(2\alpha_2) - E_s^* E_s\cos(2\alpha_2)\\ &+ E_p^* E_s\sin(2\alpha_2) + E_s^* E_p\sin(2\alpha_2)\Big]\\ &= \frac{1}{2}\left[s_0 + s_1\cos(2\alpha_2) + s_2\sin(2\alpha_2)\right]\\ &= I\left(r_p, r_s, \alpha_1, \alpha_2\right),\end{aligned} \tag{3.47}$$

where s_0, s_1, and s_2 are three of the previously mentioned Stokes parameters

$$\begin{aligned}s_0 &= E_p^* E_p + E_s^* E_s\\ s_1 &= E_p^* E_p - E_s^* E_s\\ s_2 &= E_p^* E_s + E_s^* E_p.\end{aligned} \tag{3.48}$$

Thus, the final output of the ellipsometric reflective system can be observed using the four variables r_p, r_s, α_1, and α_2 as in Equation (3.47).

3.3.1 Ellipsometric and Stokes parameters

The Stokes parameters in Equation 3.48 are very useful in describing the output energy in a system where the polarization is considered. Equation 3.47 demonstrates the relation of the Stokes parameters by conveniently choosing $2\alpha_2$ values. Because of the nature of the trigonometric functions, we could select the α_2 values with 45° ($\pi/4$) steps. With this selection all three Stokes parameters can be defined with only three angles

$$\begin{aligned} I(0) &= \frac{1}{2}\left[s_0 + s_1\right] \\ I(45) &= \frac{1}{2}\left[s_0 + s_2\right] \\ I(90) &= \frac{1}{2}\left[s_0 - s_1\right], \end{aligned} \tag{3.49}$$

when the output energy $I\left(r_p, r_s, \alpha_1, \alpha_2\right)$ is marked only by $I(\alpha_2)$. The connection between Stokes parameters and the ellipsometric parameters Ψ and Δ are more closely observed in Appendix D. The ellipsometric parameters describe the output of the system, *i.e.* the detected irradiance when to expressing the ellipsometric variables (Equation D.13 on page 194) with α_2 angle dependent variables in (3.49).

$$\cos(2\Psi') = -\frac{s_1}{s_0} = \frac{\frac{1}{2}(s_0 - s_1) - \frac{1}{2}(s_0 + s_1)}{\frac{1}{2}(s_0 - s_1) + \frac{1}{2}(s_0 + s_1)} = \frac{I(90) - I(0)}{I(90) + I(0)} \tag{3.50}$$

$$\begin{aligned} \sin(2\Psi')\cos(\Delta) = \frac{s_2}{s_0} &= \frac{\frac{1}{2}\left[2(s_0 + s_2) - \left[(s_0 + s_1) + (s_0 - s_1)\right]\right]}{\frac{1}{2}\left[(s_0 - s_1) + (s_0 + s_1)\right]} \\ &= \frac{2 \cdot I(45) - \left[I(0) + I(90)\right]}{I(90) + I(0)} \\ &= \frac{2 \cdot I(45)}{I(90) + I(0)} - 1 \end{aligned} \tag{3.51}$$

Combining (3.50) and (3.51) it is possible to solve Ψ' and Δ directly with measured light field irradiances

$$\begin{aligned}\Psi' &= \frac{1}{2}\text{acos}\left[\frac{I(90)-I(0)}{I(90)+I(0)}\right] \\ \Delta &= \text{acos}\left[\frac{\frac{2\cdot I(45)}{I(90)+I(0)}-1}{\sin(2\Psi')}\right]\end{aligned} \tag{3.52}$$

3.3.2 Discussion of the nature of Ψ and Δ measurements

The selected relation of Equation D.5 (page 192) can be simplified by selecting $\alpha_1 = 45°$. This produces

$$\tan(\Psi') = \frac{\tan\Psi}{\cancelto{1}{\tan(\alpha_1)}} \quad \Rightarrow \quad \Psi' = \Psi, \tag{3.53}$$

which is assumed in future setups to be the default setting. The initial polarization, which the angle α_1 defines, can be selected for an arbitrary angle, in which case the relation

$$\Psi = \text{atan}\left[\tan(\Psi')\tan(\alpha_1)\right] \tag{3.54}$$

holds. If used, this will only slightly change the evaluation of Ψ and Δ.

Equation 3.52 is very convenient because there are only three main irradiances to measure in reflection; they reveal ellipsometric parameters Ψ and Δ, but there is a one major concern in the measurements of Ψ and Δ. This concern is created by the nature of the results of (3.50) and (3.51). Because Ψ has to be calculated first, the nature of trigonometric functions arises. Because the angle is multiplied by two, the left side of (3.50) is defined in the range of $0° \leq \Psi \leq 180°$. Furthermore, because (3.51) has the same double angle of Ψ, this range of definition must be discussed. A great deal of change to Δ can be induced when dealing with Ψ close to $0°$ or $180°$. This would force the $\sin(2\Psi)$ term to be close to zero creating the greatest numerical error to Δ assuming constant errors in $I(\alpha_2)$.

Thus, these areas of Ψ should be kept in mind while performing a ellipsometric analysis.

Equation 3.27 shows the polarization direction relation which connects it to the ellipsometric variables Ψ and Δ. This is only another way to express complex numbers as the division of two complex numbers is still just a single complex number. If we express this complex number with $a + \mathrm{i}b$, Equation 3.27 can be rewritten

$$\begin{aligned}\frac{r_p}{r_s} &= \tan(\Psi)e^{\mathrm{i}\Delta} \\ &= a + \mathrm{i}b,\end{aligned}$$

which can further be written as

$$\begin{aligned} & a + \mathrm{i}b \\ = & \tan(\Psi)\left[\cos(\Delta) + \mathrm{i}\sin(\Delta)\right] \\ & \Rightarrow \\ a = & \tan(\Psi)\cos(\Delta) \\ b = & \tan(\Psi)\sin(\Delta) \\ & \Rightarrow \\ \tan(\Psi) = & \frac{a}{\cos\Delta} \\ b = & \frac{a}{\cos\Delta}\sin(\Delta) = a\tan(\Delta) \end{aligned}.$$

This connects the reflection amplitudes to the Ψ and Δ as

$$\Delta = \operatorname{atan}\left(\frac{b}{a}\right) \tag{3.55}$$

$$\Psi = \operatorname{atan}\left[\frac{b}{\sin(\Delta)}\right] = \operatorname{atan}\left[\frac{a}{\cos(\Delta)}\right], \tag{3.56}$$

and can be used in calculations of the theoretical Ψ and Δ values.

3.3.3 Polarization dependent output of systems

Naturally, the output irradiance of an ellipsometric or any other photonic system is affected by the wavelength of the incident photons, $I_\mathrm{o} = I_\mathrm{o}(\lambda, \cdots)$. The Fresnel coefficient is therefore always a

function of a wavelength λ and consequently any and all interactions of photons should be considered as a function of photon energy. This is not cited in the notation of the previous theory because of readability.

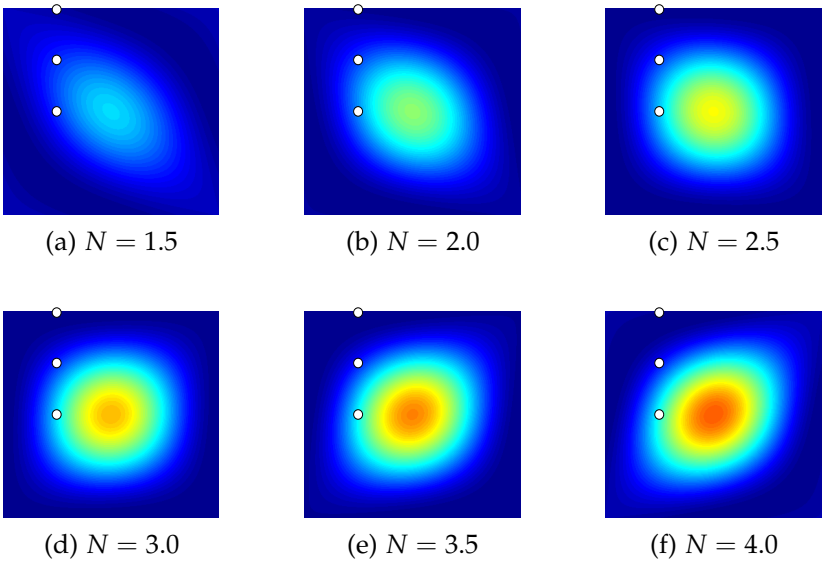

(a) $N = 1.5$ (b) $N = 2.0$ (c) $N = 2.5$

(d) $N = 3.0$ (e) $N = 3.5$ (f) $N = 4.0$

Figure 3.3: *Calculated irradiance of a reflective surface with the marked refractive index. The row position indicates the polarizator 1 angles from 0 to π, and the column position indicates the polarizator 2 angles from 0 to π in each image. Color mapping in the images is shared, having values from zero to one with associated colors from blue to red. White dots indicate the output points of Equation 3.49.*

Let us observe the theoretical output of our ellipsometric system. The calculated irradiances of the PSA system are presented in Figures 3.3 and 3.4. This is done using the calculated output Equation 3.47 and Stokes vector descriptions in Equation 3.48. Figure 3.3 shows the modeled output as a map which analyzes the two polarizer angles from zero to π. The incident angle in the Fresnel equations was 70 degrees. The angle is zero for both polarizers in the upper left–hand corner of the calculated images. The α_1 is increased in a horizontal direction and α_2 in a vertical direction. Both

figures show the output from six different surfaces. This demonstrates the output changes in different cases due to changes in the refractive index.

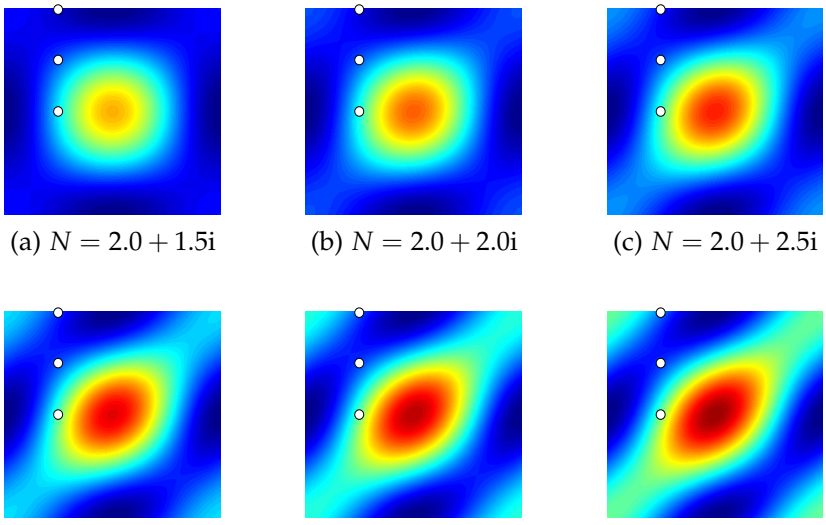

(a) $N = 2.0 + 1.5\text{i}$ (b) $N = 2.0 + 2.0\text{i}$ (c) $N = 2.0 + 2.5\text{i}$

(d) $N = 2.0 + 3.0\text{i}$ (e) $N = 2.0 + 3.5\text{i}$ (f) $N = 2.0 + 4.0\text{i}$

Figure 3.4: *Calculated irradiance of a reflective surface with the marked refractive index. The row position indicates the polarizator 1 angles from 0 to π, and the column position indicates the polarizator 2 angles from 0 to π in each image. Color mapping in the images is shared, having values from zero to one with associated colors from blue to red. White dots indicate the output points of Equation 3.49.*

Figure 3.4 shows the imaginary part induced changes to the observed polarization plane when the sample has a constant real part of the refractive index of 2. This means that both the real and imaginary part can do similar things to the polarization. If the output of a real system of Figures 3.3 and 3.4 were measured, it would be done at three different polarization points.[f] Namely, the points marked in these figures. It is evident that the refractive index of the surface could be analyzed from the polarization data. How-

[f] Assuming the limited requirements of Equations 3.50 and 3.51 (page 87).

ever, the fact that the output is harmonic makes things challenging. Thus, different ellipsometric systems usually provide more accurate knowledge of the full polarization state of photons.

3.4 THIN FILM REFLECTION

The simplest and perhaps the most frequently used application of ellipsometry and polarimetry is the evaluation of a single thin film. This can be either reflection or transmission depending on the interest. There are numerous sources for the theory but the principle is old and simple, as it just uses the Fresnel coefficients.

3.4.1 Single film reflection

The Fresnel coefficients are excellent in describing specular reflection. Thus, they are the common starting point of any simple calculation involving smooth surface reflection. Here we also describe the simplest thin film reflection having two interfaces and three materials, as described in Figure 3.5.

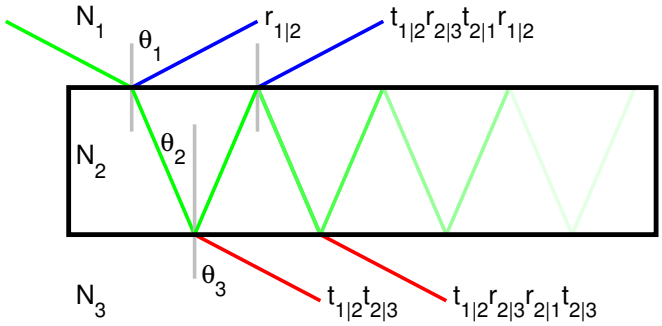

Figure 3.5: *A schematic showing a three refractive index system having complex refractive indices N_1, N_2, and N_3. A photon passes the system from left to right (green). Showing the overall reflection of incident angle θ_1 (blue) and the overall transmission (red) expressed with the associated Fresnel coefficients r and t. Polarization dependence can be observed using the corresponding Fresnel coefficients.*

Let us mark the reflection and transmission amplitude with r and t, respectively. We will then mark the system materials with running numbers from 1 to N. The polarization can essentially be marked at any time, for example, with r_s or r_p but is now omitted. Interfaces will be marked with directions from material to material with a vertical line $|$. Thus, for example, s–polarized reflection from material 5 to material 6 would be marked by $r_{s5|6}$. This is, without polarization, the marking used in Figure 3.5, and the output of that particular reflection would be

$$r = r_{1|2} + t_{1|2}r_{2|3}t_{2|1} + t_{1|2}r_{2|3}r_{2|1}r_{2|3}t_{2|1}\cdots, \tag{3.57}$$

which is a series that can be expressed by [341]

$$r = r_{1|2} + \frac{t_{1|2}t_{2|1}r_{2|3}e^{-2i\sigma}}{1 + r_{1|2}r_{2|3}e^{-2i\sigma}}. \tag{3.58}$$

The solution of Equation 3.58 uses the term $e^{-2i\sigma_{TF}}$, which describes the interference of the summed terms, which can be expressed as being created due to the phase difference ϕ_{TF}

$$\sigma_{TF} = \frac{2\pi}{\lambda} n_{TF} d_{TF} \cos(\phi_{TF}). \tag{3.59}$$

Note that Equation 3.59 is very much the same interference creating term as discussed in section 3.1 (page 69). The transmittance of the schematic shown in Figure 3.5 can be created as easily as the reflection part. This simple single layer estimation will hereafter be referred to as SLE.

3.4.2 Ellipsometric parameters

Based on the ideology of Equation 3.57, we can create any system by following the photon path. When dealing with non-polarizing components the overall path is the same with both polarizations. This means that the detector side of the ellipsometric calculations can be performed directly using Equation 3.30 (page 81).

This provides a direct contact to the actual ellipsometric parameters through the complex polarization primitives r_p and r_s by using

Equations 3.55 and 3.56. Later, in section 4.4, we will calculate these outputs and compare the results to those created by the constructed raytrace model as well as to real measurements.

4 Materials and methods

4.1 DEVICES AND COMPUTER PROGRAMS

This section includes the description of the programs and clarifies all of the performed measurements. We will discuss the devices, materials, and then the measurement procedures. Finally, the numerical models are described.

4.1.1 Devices

To simplify the explanation, Table 4.1 describes the most relevant used devices by their final usage. If any programs have been used, they have been those provided with the device. If a custom program has been created, it is mentioned in the corresponding section of this chapter.

4.1.2 Programs

Generally the program that is provided with the equipment was used to measure any data. However, the model, some visualizations, and the signal to noise measurements were performed with the aid of *Microsoft® Visual Studio®*. Most of the data processing and plotting of data was done with *MathWorks® Matlab®*. The remaining visualizations were performed using *Python®* programming language, the *Blender®* program, *GNU Image Manipulation Program* (GIMP), and *Inkscape®* program.

4.2 SURFACES AND PARTICLES

4.2.1 Surfaces

Sample surfaces were all consistently titanium–based materials. A total of four groups were observed: polished titanium (Ti), heat–treated titanium (Ti_{HT}), roughened titanium (Ti_{P1500}), and hydrocarbon–

Table 4.1: *Devices, by manufacturer and usage.*

Device	**Measurements**
Woollam, Variable Angle Spectral Ellipsometer (WVASE)	• Sample Refractive index • Ψ and Δ references • Titanium heating effects
Specim, Multi–fiber spectrometer (MFS)	Main ellipsometric measurements
Thorlabs, OSL1-EC	Measurement light source
Quantronix Integra C-3.5	THz laser used in nanoparticle production
LEO, Gemini 1550	Scanning electron microscope (SEM) images
Veeco Metrology, AutoProbe M5	Atomic force microscope surface roughness measurements
KSV Instruments, Theta	Contact angle measurements
Bentham, DTMc300	Monochromator used in the signal to noise ratio measurements
Hamamatsu, PMA12	Spectrophotometer for observing the MFS linearity and signal to noise ratio (SNR)

covered titanium (Ti_{CH}). The samples were all disk–shaped, 3 mm thick with a 16 mm diameter. Nanoparticles were measured on polished titanium, but are marked with Ti_{nano} for clarity. The selection of the samples was purely photonic. The nanoparticles provide a different adsorbing particles while Ti_{CH} provides a surface with completely different refractive index. Later on we will discuss the model in more detail, but the overall model is done for proteins and polished titanium, so that Ti_{CH} and Ti_{nano} should provide dif-

ferent results. If Ti_{CH} and Ti_{nano} would provide similar results as Ti–protein pair, the model could be said to be unreliable.

The heat treatment of the titanium was performed in a oven at a 200 °C temperature. The heat treatment duration was five hours. This was done to observe the stability of the titanium surfaces, *i.e.* if air–stored titanium reacts differently with particles than heated titanium. Hereafter, the titanium samples are marked as Ti and the heat–treated (HT) with Ti_{HT}.

Surface topography naturally effects the active surface area and the other parameters of the adsorption. To clarify the small–scale differences in the surfaces, a titanium sample was roughened with standard P1500 sand paper. The resulting surface was a very diffuse titanium surface, which is denoted by Ti_{P1500}. Figure 4.1 shows a scanning electron microscope (SEM) image of a Ti_{HT} and a Ti_{P1500}, where the roughness difference is clear. The liquid environment measurement of this particular roughened surface was not possible as it scattered too much of the incident photons, but it will function as a rough surface reference.

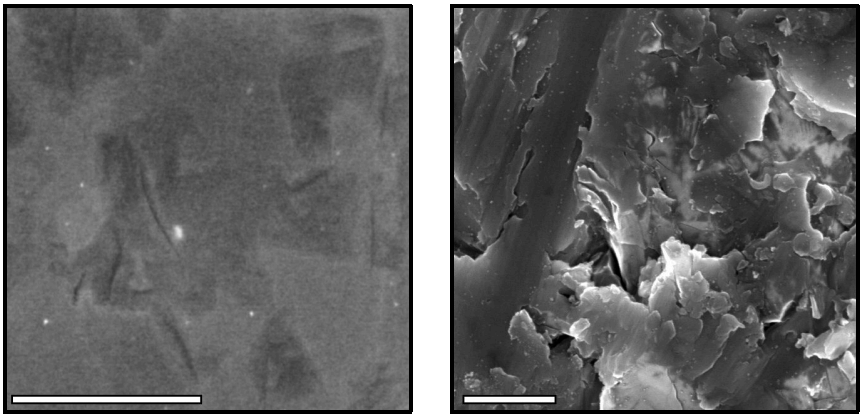

(a) (b)

Figure 4.1: *A scanning electron microscope image of a) polished titanium and of b) sand paper roughened titanium. The white bar indicates a length of 500 nm.*

The selected titanium samples were used only because they provided a completely different attachment surface and roughness compared to plain titanium. Thus, the Ti_{CH} surface was added to the measured samples. The Ti_{CH} samples were purchased commercially and were manufactured through chemical vapor deposition on the titanium. The very precise parameters of production of the Ti_{CH} surfaces is not so important, though it could be the basis of another study since deposition and evaporation are very delicate in regard to the system parameters [342]. With this, chemical vapor deposition could be used as a surface modification in an adsorption study. The interest here, however is merely to see if we can create a different signal from the Ti_{CH} surface and repeat it from sample to sample. The Ti_{CH} also falls into a somewhat medium roughness category, which was possible to measure with the used polarimetric device. Figure 4.2 shows the atomic force microscope (AFM) images of Ti, Ti_{CH}, and Ti_{P1500}.

While the Ti_{P1500} samples are not used in the measurements, as they proved too diffuse to be measured with the ellipsometric setup, the effects of surface roughness are extremely clear from the AFM images in Figure 4.2. They also show the limits of the ellipsometric setup. As the surface roughness increases, both the measurement and analysis of an ellipsometric method becomes more difficult. As in this study, the theory is usually for solid and perfectly flat surfaces. This does not promote the usage of the rough surfaces. Especially in the liquid environment, where the adsorbed particles can become absorbed particles inside the material grooves.

4.2.2 Particles, molecules, and solutions

Phosphate buffered saline (PBS)

Purified water (10 $M\Omega/cm^{-1}$) was used as the basis for the PBS solution and was prepared with 8 mM Na_2HPO_4, 1.8 mM KH_2PO_4, 140 mM NaCl, and 2.7 mM KCl. The M indicates the molarity in moles per liter. While it is common to use sodium citrate as an additional particle separator inside the liquid, it was not added in

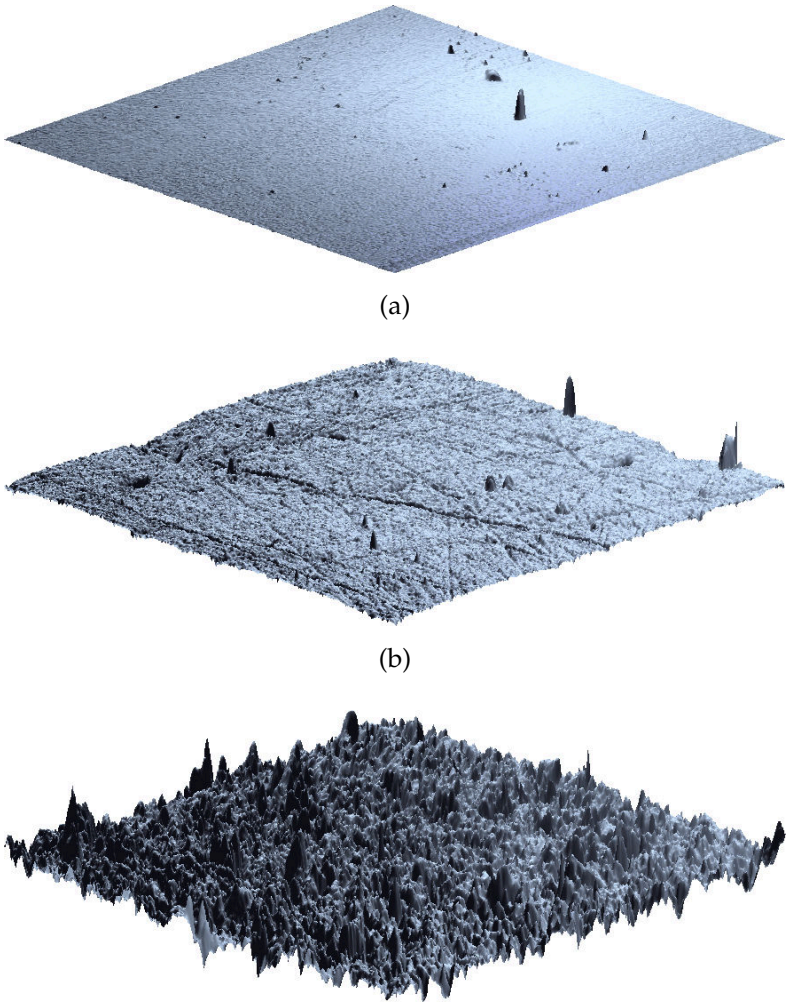

(a)

(b)

(c)

Figure 4.2: *Atomic Force Microscope (AFM) images of (a) polished titanium, (b) Ti_{CH}, and (c) Ti_{P1500} surfaces. All images share a common vertical axis and are comparable to each other. Subplot (c) shows values in the range of zero to 2.5 µm. The sides of the shown plane cover an area of 100 µm × 100 µm.*

this case, as we now know, that more buffer–liquid altering only adds variables. The end pH of the PBS solution was near neutral 7.

Proteins

Two target proteins were used in the study. A smaller particle shows smaller changes as the adsorption strength is connected to particle size (weight). Thus, a smaller protein, Human Serum Albumin (HSA), was used in the isotherm observations. In this part, a static selection of concentrations from 88 to 5000 nM were used. During the measurements the proteins were stored in cold and in crystal form, and were not in liquid form for more than 48 hours at a time.

The second measured protein was Human Plasma Fibrinogen (HPF). Because the sample to sample comparison was important, the HPF measurements were executed with a constant molarity of 500 nM. Both proteins, HPF (fraction I, type III) and HSA (97-99%), were purchased commercially from *Sigma-Aldrich*. The actual difference between the proteins is evident, and the crystal structure of both proteins is shown in Appendix B (see page 186).

The corresponding molarities are rather ambiguous as discussed in the theory. Depending on the situation, either the molarity or the weight is more important. The corresponding density for HSA the isotherm measurements of 88 nM and 5000 nM corresponds to 6 $\mu g/ml$ and 333 $\mu g/ml$. Similarly, the 500 nM of HPF corresponds to 170 $\mu g/ml$.

Nanoparticles

The nanoparticles were created with a Quantronix Integra C-3.5, which provided a 2.1 mJ per pulse, 120 fs pulse duration, 790 nm center wavelength, and 1 kHz repetition rate. The pulses were guided in purified water (10 MΩ·cm), where the titanium base sample was placed. The sample was irradiated for 10 minutes in the focused pulse laser beam for us to extract the particles from the sample. The focal point moved while the liquid filled with particles, but the sample container was moved constantly to provide the best pulse connection to the surface. The biggest factor in the sample movement was the actual sound emitted from the pulse laser

ablation. It was kept at maximum for the 10–minute period. Figure 4.3 shows a colored Scanning Electron Microscope (SEM) image of the resulting particles.

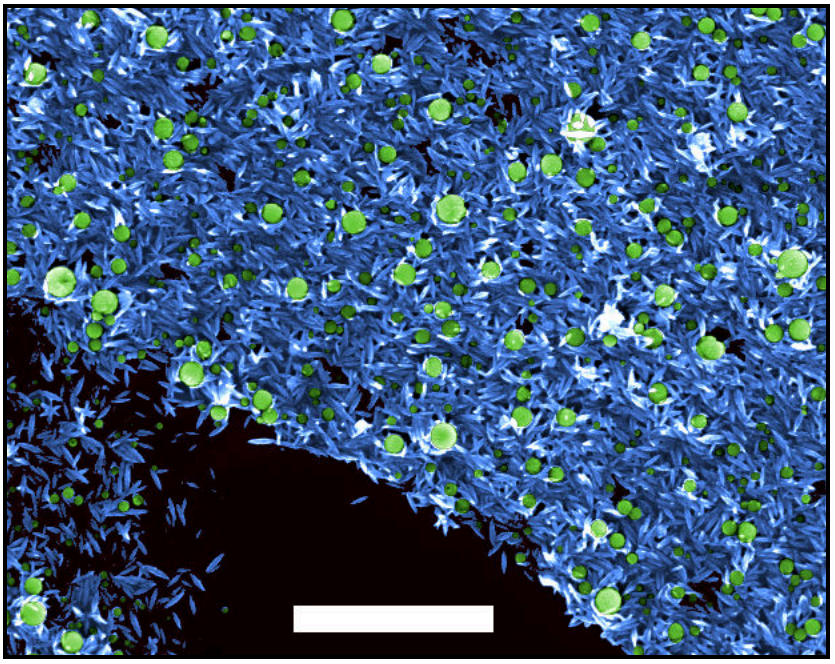

Figure 4.3: *Colored SEM image of the used particles. The image shows spherical particles in green, cylindrical particles in blue, and the silicone substrate in black. The bar shows a length of 1 µm.*

The ablation created two types of particles: spherical and cylindrical. In fact, the cylindrical ones were more spear–like, as seen in Figure 4.3. The size distribution of the cylindrical particles was relatively constant, but the size distribution of the spherical ones was determined separately. Both nanoparticle types were determined with (1) drying a known volume droplet containing the nanoparticles onto a substrate, (2) imaging it with a scanning electron microscope, (3) counting the particles and measuring the diameter distribution of the spherical particles, and finally (4) calculating the volume–mass of the particles. Figure 4.4 shows the counted size distribution of the spherical nanoparticles.

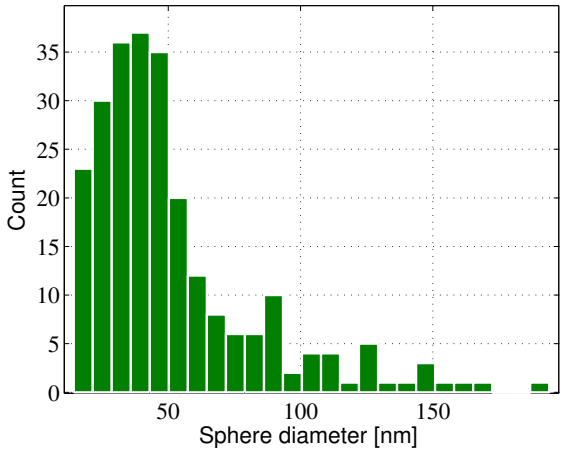

Figure 4.4: *Distribution of the spherical nanoparticles created with pulse laser ablation. The overall counted particle number was 248.*

As the actual amount of the particles is important, the size distribution of the spherical particles and the number of both particles were used to calculate the mass per volume ratio of the particles. Because of the uneven distribution of the particles during the drying of the solution droplet containing the nanoparticles, the mass calculations are only estimates. Table 4.2 lists the estimates gathered from the SEM imaging of the nanoparticles.

This solution concentration is totally an estimate of the concentration. This is chiefly because an imaging solution was used to study the amount from relatively high concentrations. Some of the particles might still be hidden in the observations. This is, however close to the optimal concentration since the number of particles provides better statistics and reduces the need for actually searching for the particles in the SEM images. It also offers a good estimate of the coverage that the nanoparticles create on the surface. The study of nanoparticle formation as well as the concentration effects on adsorption would be a fascinating study. However, here we only note that this concentration ($\approx$ 50 μg/ml) seems rather low since even single milligrams per milliliter seems to be the common concentration range [83,174]. Still, with the proteins, μg range is not

Table 4.2: *Estimates used to characterize the produced nanoparticles. The abbreviation CN stands for a cylindrical nanoparticle and SN a spherical nanoparticle. Overall particle concentration was measured to be 54.7 ug/ml.*

Estimate	**Value**
Area	3017204 μm^2
Density, CN	206.09 units/μm^2
Density, SN	39.29 units/μm^2
Single volume, CN	158.55 $10^{-6}\mu$m^3
Single volume, SN	183.23 $10^{-6}\mu$m^3
Volume, CN	98586 μm^3
Volume, SN	21721 μm^3
Density, CN & SN	4.23 mg/mm^3 [343]
Weight, CN	417.01 ng
Weight, SN	91.87 ng
Droplet, Volume	10 mm^3
Concentration, CN	417.01 ng/10 mm^3 $\approx$ 41.7 ng/μl = 41.7 μg/ml
Concentration, CN	91.87 ng/10 mm^3 $\approx$ 9.2 ng/μl = 9.2 μg/ml

an oddity. It would be always possible to centrifuge the particle solutions or evaporate the liquid, but the low concentration was a good benchmark to observe if the adsorption or presence of these particles was possible with the constructed setup, and to determine the signal compared to the proteins.

4.3 MEASUREMENTS

4.3.1 Measurement setup

Figure 4.5 shows the final setup in the measurements with all the components described. The linear polarizer was a *Heliopan SH-PMC ES 55* linear polarizer. A high–quality calcite polarizer was also available, but the visual range of light source favored the camera polarizer. The camera polarizer would have already been optimized for the light source wavelength range and have been be easier to use than a calcite version. The only drawback was that any interference solutions in the camera polarizer could have distorted the results, but that was thought to be negligible. Although, it must be stated that another excellent reason for not choosing the calcite polarizers was their high angular sensitivity. They have a very small working input angle and might not be the most suitable in liquid environment measurements.

The measurement device is an imperfect polarimeter with a concurrent light source and cuvette signal measurement. Despite the cuvette beam having a different measurement geometry through the liquid cuvette, it provides a perspective on the changes in the cuvette as well as the measuring glass windows of the cuvette. If the reference beam can detect categorized sample signals, we may conclude that the sample itself adds nothing to the equation and adsorption cannot be detected from the sample surface. Consequently be compare the cuvette signal to the one reflected from the sample surface.

The first polarizer in the Figure 4.5 setup was positioned in a static angle of 45° ($\pi/4$) and the second polarizer was rotated to three angles, 0°, 45°, and 90°, to solve the first three Stokes parameters and then Ψ and Δ from the reflected photon beam. The fiber that measured the light source was used to correct the sample signal. The signal and the effect of this correction will be shown later in the results section 5.2.1.

Figure 4.6a shows a typical spectrum of the light source measured with the Hamamatsu spectrometer. It can be noted that

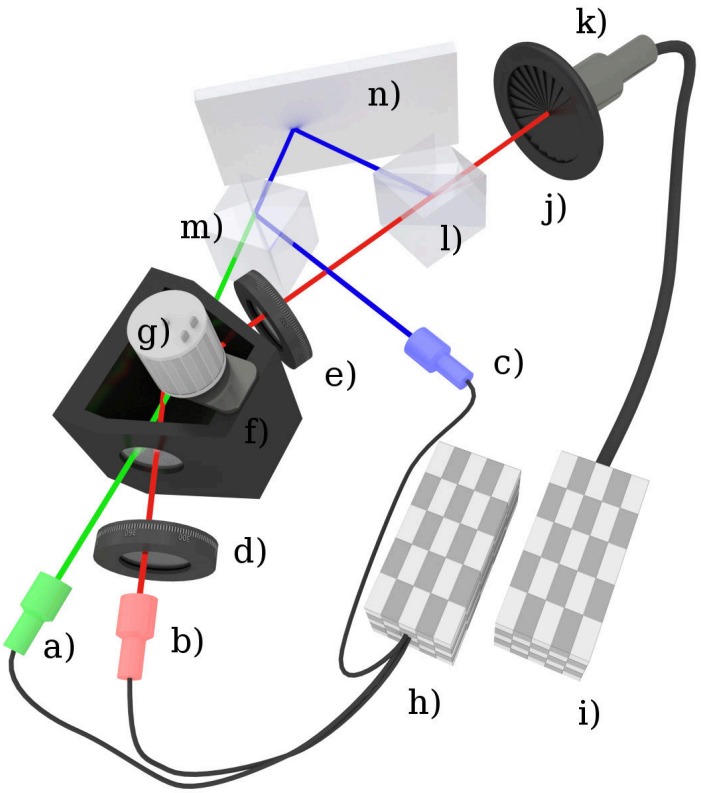

Figure 4.5: *Schematic presentation of the photonic measurement setup with a) reference detector fiber, b) sample detector fiber, c) light source detector fiber, h) multi-fiber photometer, i) light source, d) second polarizer, f) liquid cuvette, e) first polarizer, m) second beam–splitter, n) mirror, l) first beam–splitter, j) aperture, k) light input, and g) liquid mixing motor.*

the light source has a daylight filter that cuts the halogen source spetrum at higher wavelengths. The effect of the filter is shown in Figure 4.6b, where the amount of harmonic oscillation increases towards higher wavelengths. Essentially, it has no effect in general amplitude measurements, but here it seems that the filter could be interferometric. If the light source already has interfering photons, it could affect the system or explain some observation.

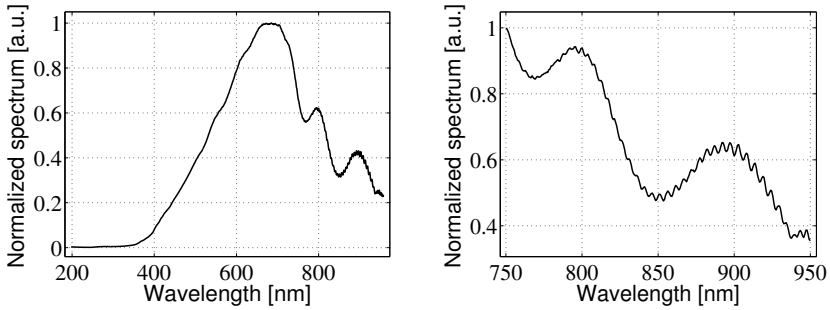

Figure 4.6: *Normalized spectrum of the lightsource in a) the wavelength range covering the measurements and b) showing the near infra-red area.*

4.3.2 Quality of the sensor used

Lee ([344], 2005) lists several noise contributors to a CCD array such as transfer noise, dark current, fixed patter noise, high energy radiation, thermal noise, shot noise, noise from analog-to-digital converter, and noise from electrical interference. All of them can be present on the sensor at any time, as in the multi-fiber spectrophotometer used in this study. We do not concentrate on all, but note that there are many different noise sources available to a sensor.

In general, we can divide the noise of any sensor to include two main components; 1) signal–dependent noise and 2) signal–independent noise. Both of these create a superposition of noise which cannot entirely be removed in a general case, but some effort can be made to increase the quality of a signal. The signal–independent part can be evaluated with a time–wise measurement in the dark. While this is not a perfect solution, it most likely produces a non-zero level that could be considered noise and can later be removed from the signal. The signal–dependent noise part is always measured with the actual signal. It is always in a superposition with the signal–independent noise, but could be considered being a single component.

This superposition of the signal–dependent and the signal–independent

noise is generally one discussed as the signal to noise ratio (SNR) of a signal when the dark signal level is subtracted. Still, even if we remove the average of the signal–independent part, temporal fluctuations still exist together with the signal–dependent part. In this study we do not discuss the nature of noise in more detail. We assume that the dark–level subtraction and the observations of the actual signal are sufficient to evaluate the noise. We also assume that sensor dynamics are sufficient after the dark–level subtraction to analyze the signal. We define a measured signal as I_0, and the noise I_{noise} as the standard deviation of the temporally measured signal. Thus, the decibel notation of the signal to noise ratio (SNR_{dB}) can be written as [344]

$$SNR_{\text{dB}} = 10 \cdot \log_{10}\left(\left[\frac{I_{\text{noise}}}{I_0}\right]^2\right) = 20 \cdot \log_{10}\left(\frac{I_{\text{noise}}}{I_0}\right).$$

The Specim MFS was tested together with a *Hamamatsu PMA-12* photometer using ten repeats per wavelength and the *Bentham* monochromator to produce individual wavelengths. The resulting SNR_{dB} is presented in Figure 4.7. In the actual measurement part we discuss a temporal signal to noise ratio as well as the measured quality of the light source of the setup.
The measured SNR is always some sort of time–wise function of a system. There may be fast and slow processes in both sensor and in light source that interfere with the observations of a phenomenon.

4.3.3 Liquid environment measurements

Measurement sequence

The main measurements were performed in a liquid cuvette, as schematically shown in Figure 4.5 (page 105). The overall measurement took around three hours and the measurement procedure was divided into three main stages. The first stage was to align the sample. This took between one to ten minutes.

The system was aligned with purified water and added phosphate buffered saline (PBS) inside the cuvette. It is generally un-

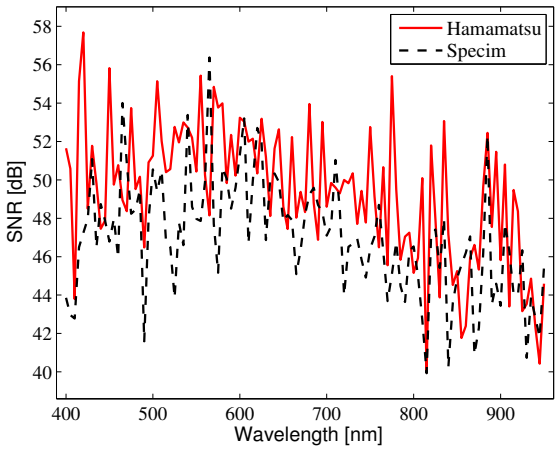

Figure 4.7: *Signal to noise ratio of the two devices from 400 nm to 950 nm.*

known how different liquids react with each sample. Consequently, the saline was allowed to simmer for around thirty minutes before the addition of the proteins. This was the second stage of the measurement. The third phase started when actual particles, proteins or nanoparticles were injected into the cuvette. Then a measurement was recorded for approximately 60 minutes before being terminated.

The overall liquid amount inside the cuvette (20 ml) already covered the sample fully in the PBS waiting phase. At this point the container had 18 ml of PBS liquid in it. The addition of the molecules was performed from a larger molarity liquid by adding a further 2 ml of the protein liquid. This meant that the particles had only one–tenth the molarity after the injection.[a] The injection of particles was done with 10 ml Finnpipette with a disposable tip. A tip end was carefully lowered inside the liquid before injecting the particles.

[a] But matched the given molarities, such as 500 nM for HPF.

Water contact angle

The water contact angle was measured with 5 μl droplets using a commercial device and an associated program. The measurement included a minimum of 10 samples and a maximum of 20 samples for each measured sample type. The overall discussion of the water contact angles will be just to describe the different behavior of water on surface. Because of this, the contact angles are not further, for example, surface roughness corrected.

4.4 MODELS

As discussed above (see section 2.7), spectral ellipsometry requires a model to evaluate the layers it detects. It not uncommon to see a theoretical model as well as a real measurement in ellipsometric studies. We believe this is a good policy to follow. Thus, the ellipsometric parameters Ψ and Δ are evaluated through a model to draw a conclusion about the actual adsorbed nanoparticles.

This chapter concentrates on explaining the core structure of the model. It also explains *how* the model was created. Later, in section 4.4.5, we discuss *what* was done with the created model.

4.4.1 What is a model anyway?

Before discussing models, it is useful to clarify what model actually means. A model in general is a well–defined frame of approach to a problem. This might seem ambiguous, but all scientific work could be defined as a collection of different models. There is always a well–defined frame which makes the work in hand discrete. One model can't solve everything. A frame also implies that the tools need to be defined and explained. Furthermore, at the core, a model always tries to describe something, or filling a frame. The model may be created for a problem or some more abstract entity.

The goodness of the model usually consists of three main things. Firstly, how well the frame of the problem is defined. Secondly, how

well the tools used are defined, and finally, how well the model describes the approached entity. Usually they basically go hand in hand. After a model is constructed, the model often becomes a persistent entity which describes something in the given frame. We wish to note, that this section is also only a model, which hopefully makes the frame of the word "model" clearer since it is often used in the literature. We also understand, that testing the model goodness testing, or at least some evaluation, should be a part of model building.

4.4.2 Need for mathematical modeling

The need for models such as tracing photons usually comes from industry which provides the equipment. That is, basically industrial fields concerned with optics. Optics is category of photonics in the range of wavelengths (380 nm – 780 nm) responsive to the human eye. This interest is understandable since there is a massive market for consumer goods and a great deal of money is involved. In addition to consumers always want bigger and better quality products, this need continues. Besides consumer products, another main area includes non-optics modeling, usually related to academic research, which can include anything from X–ray diffraction to radio wave models.

Traditional optical models usually include the modeling of environments such as lens packs and nano–scale structure measured in air. Nano– and microtechnology is now commonplace and there are common models for optics with combined nano– and micro–structured components. This is because technology has the tendency to decrease in size as more functions are desired in a smaller area. Nowadays, with a growing number of personal computer and other devices, there is also an increasing interest in improving display and camera technology with custom directional reflection profiles, such as designing non–reflecting and other filter coatings for different technologies.

As discussed in chapter 2, the liquid environment has a vast

number of variables. This makes the environment in this study complicated, at least when compared to traditional ray tracing, which usually only involves a static environment and a set of static refractive indices for the system components. Figure 4.8 shows the general layers involved in the simplest possible liquid environment reflection measurement. It also presents the simplest environment schematic of a liquid environment which has some particles included in the liquid. The description of the numbered layers of Figure 4.8 are listed in Table 4.3.

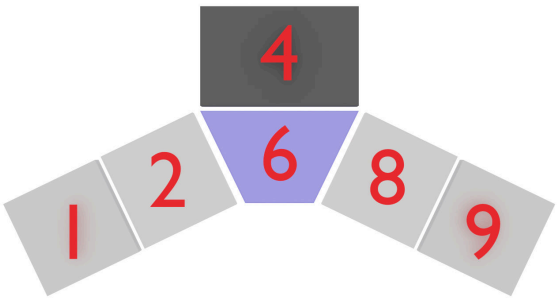

(a)

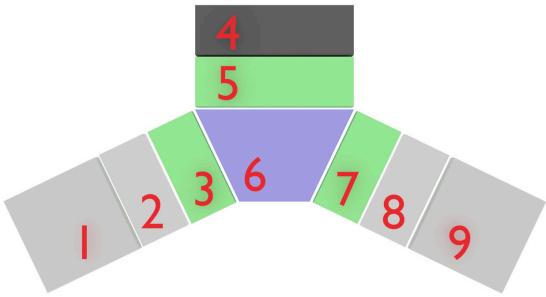

(b)

Figure 4.8: *Schematic diagram of the existing material layers in a liquid cuvette. The descriptions of the layers by number are found in Table 4.3.*

Figure 4.8 and the layer description in Table 4.3 demonstrate the need for some evaluation of a liquid system. There are several interfaces, which themselves all are parameters in photonics. In ad-

dition, the layers that the particles alter are more or less unknown and can change as a function of the time. This does not help, but requires a numerical evaluation aside from the real measurements. Indeed, it is nearly standard procedure to include some layer thickness estimates with an optical measurement, not only to evaluate a protein layer but also to check the stability of the photonic system.

Table 4.3: *The material layers presented in Figure 4.8. Also, the cross marks if the material is considered to have a time-wise variable refractive index $N(\lambda, t)$, or a static refractive index $N(\lambda)$.*

Layer	**Description**	$N(\lambda)$	$N(\lambda, t)$
1,9	Air	x	
2,8	Cuvette window	x	
3,7	Possibly attached particles on the cuvette window		x
4	Sample	x	(x)
5	Adsorbed particles		x
6	The liquid environment which contains the particles		x

Let us once more consider Table 4.3. This study assumes that both cuvette windows have a potential to adsorb the investigated particles. This is usually completely ignored, especially in the ellipsometric theory as the measurement beam hits the cuvette window at a zero angle incident. This usually will show a researcher that polarization observations can be ignored for the cuvette windows. This is because the polarization relation r_p/r_s of p and s polarized photons remains if we multiply r_p or r_s with same and constant number. If we consider the refractive index of a liquid itself to be a time-wise function $N(\lambda, t)$, a sensing beam of photons will have propagation direction changes and even the Fresnel–coefficients can be affected. If a measuring photon beam is put to a zero angle for all of the input rays, we cannot generally assume that the output beam through the cuvette window would be always polarization

independent.

If we assume a variable refractive index of a liquid, an analytic solution could be far too time–consuming to perform. This is because the modeling is usually simple if the individual photon can be seen through the paraxial assumption. In the paraxial assumption, the photon is always considered to travel through a single line in space. Generally this is good estimation, because even in thin–layer calculations, the geometrical differences are negligible since a detector has very macroscopic size compared to single–photon geometric shifts in a system.

When the geometrical modeling is performed, as in this study, the model can also provide beam shift estimates. This helps to define the effects on the detector side, if the measurement beam is shifted. In conclusion, we understand, that the liquid environment, in complexity, has the potential to match all the available resources.

4.4.3 Models in different photonic systems

What is possible with a model? This is a valid question but the answer is broad since all real systems can essentially be approximated with a numerical calculus. When discussing the adsorption phenomenon, all data is presented through some sort of model. This usually indicates some exactly known environment or in which approximations and suppositions about the reality are made. Sadly, it seems that adsorption studies are mainly about suppositions as seen in section 2.7. If there is no agreement on the general refractive indices of proteins in a liquid, it indicates major disagreement about ambiguous models. The refractive index is deeply involved with photonic models and if there is disagreement, then there is very little to discuss.

But let us consider the photonic models of adsorption in a liquid. Generally, in ellipsometry, models are single thin–layer approximations [96,158,188,261,331,345,346]. Very little effort has been put into an actual three–dimensional environment. It is refreshing to occasionally see even discussion about three–dimensional ad-

sorption [347,348], or a particle gradient near an adsorbent.

One of the discussed models is the Effective Medium Approximation (EMA), in which a material is considered to have gradients [347]. The EMA model combines permittivities of materials by brutally combining them with some factor. This seems to be a reasonable model as the permittivity performs alterations directly to an interacting electric field, such as a photon, and the measured spectra seem to follow the models [109,347].

Is there, however any reason to use EMA or similar mixed permittivity models? We believe that the answer is yes, and no. Yes, if there is reason to believe that the EMA model has only a statistical effect, such as materials with large pores (non–diffracting) [105,110,111]. That is, when the adsorbent is a mix of materials and it is justified to assume a highly controlled periodic structure. The 'no' answer to the use of EMA, however comes from the reasoning that EMA should be employed with care as it is only for certain surfaces. More importantly, very little is noted about adsorption in three dimensions, because for example the pore filling factors are generally suppositions and only a single property of a generated layer.

If we recall Figure 2.15 on page 63, we can see that proteins, as a vast amount of biological particles inside water, have refractive index much like water or surrounding buffer. It is estimated that proteins carry water–like envelopes that can easily be the same weight as the protein itself [3], depending, of course, on the protein hydryphobicity. Essentially, the question of models is whether, in the adsorption phenomenon, the adsorbed protein removes all water from the adsorbed layer or are the photonic properties of the water still dominant, despite the adsorption?

Let us further consider the Figure 4.9, which shows two possible cases for protein adsorption as a material density near adsorbent. The figure shows monolayer and a multilayer adsorption scenarios. The single–layer adsorption estimates a rather unnatural step of the material near the adsorbent. It raises the question of why the single–layer estimate is still dominant? We could spec-

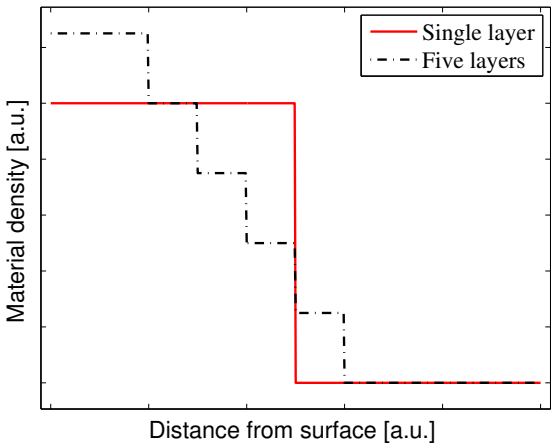

Figure 4.9: *Arbitrary unit presentation of material near adsorbent (left side), and two approaches, with a single layer and five layers of material.*

ulate that it is much simpler and researchers still think that any three–dimensional adsorption phenomenon can be correctly estimated with an effective monolayer. While a single layer is totally valid with solid materials, there should also be more discussion about a three–dimensional adsorption environment in photometric studies.

Still, if we create transition states[b] for any adsorbing particle, it must be justified. While natural particles such as proteins have a strong ideal and real connection to water, we cannot claim this of all particles, such as of inorganic nanoparticles. A complex entity such as protein might be enveloped with water, but this is not always the case and deviations from protein to protein might also occur with dramatic effects to the observed density (*i.e.* permittivity/refractive index). We still believe that using monolayer in a liquid environment is plainly the wrong approach as it completely ignores the three–dimensional environment of adsorption. Instead of changing the monolayer thickness on adsorption, perhaps a constant dimension with multilayer evaluations could be a more natural approach

[b]Such as plot in Figure 4.9 having five layers.

to the adsorption of natural particles such as proteins. It is, however true that the multilayer system becomes analytically, and even numerically unsolvable in many cases. However, the greater difficulty of the model should not be a reason to avoid its use if it could be more plausible. We will discuss this more in section 5.3.3 (page 171).

4.4.4 Models used in this study

Numerical approach

In section 4.4.2 we mentioned the setup and the multitude of interfaces that it may be involved. Here we will discuss the photonic calculations performed with parallel processing (PAP). The model is constructed with PAP processing of *NVIDIA® CUDA®*. Compute Unified Device Architecture (*CUDA®*) is a programming library which harnesses the graphics processing unit (GPU) of a common and a commercial PC.[c] The benefits of using PAP are evident. While the existing processors in computers only use one or a few threads at a time, GPU can use millions simultaneously. The processing power of a single GPU processor is smaller than that in a normal PC processor, but the vast number of processors in GPU easily surpasses a normal CPU (Central Processing Unit) in tasks that can be executed in parallel. Here, it is used to calculate a sample reflection for both polarization primitives (s and p) and wavelengths at the same time.

The power of PAP comes from the parallel processing, but the drawback is the limited amount of possible environments. Where normal CPU programming has all of the computer at hand, PAP uses a graphics unit, which limits the possibilities. It is understandable that a GPU can handle parallel computing but the rest of the computer is more or less linear, with a single execution at a time. This is why most GPU processing is executed as a function and the result then is retrieved after the process finishes.

[c] Other solutions are also available for PAP.

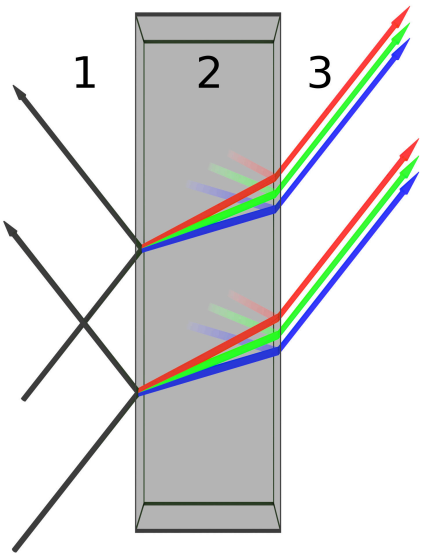

Figure 4.10: *Parallel challenge of the ray–tracing for a single layer of material in transmission: 1) input and reflected parts, 2) wavelength division through Fresnel coefficients and Snell's law, and 3) output.*

Pure ray–tracing is an interface by interface procedure since Snell's law (angle) and the Fresnel coefficients (complex amplitude) dictate the further propagation of a photon. There is no perfect way to divide the different steps of a ray–tracing procedure, as demonstrated in Figure 4.10.[d] The steps cannot be performed fully in parallel because the state of the previous step defines the next. However, in photonics, the polarization and wavelengths, which often are systematically different from each other, can be separated and performed in parallel. Much like done in this work.

Figure 4.11 shows the principle of the ray trace. A 3D environment is created with an external program. This program creates an environment in triangles which act as collision primitives. When collision occurs, the ray is divided into a new reflected and

[d]This is geometric ray–tracing which presents different challenges than, for example, Fourier modal methods [349].

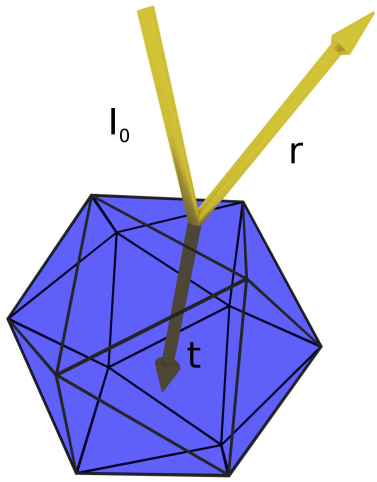

Figure 4.11: *Model system principle. Each object is recreated with triangles and all rays I_0 are checked for collision and divided into corresponding reflection r and transmission t.*

transmitted ray which are again propagated. All numerical theory follows the Fresnel coefficients on each interaction.

The amount of interaction with the triangles was the limited variable in the tracing program. In this case, a maximum of 14 interactions were allowed for the program. While, this seems like a quite low number, if the ray divides into two new rays on each interaction, the amount of processed rays for N allowed interactions becomes $2^N + 1$.[e] For 14 interactions this represents a maximum of 16385 processed possible rays. Figure 4.12 shows a work flow following the European Computer Manufacturers Association (ECMA) standard (ECMA-4) for the executed ray trace [350]. Each ray is tracked until it collides with a bounding box triangle or a detector triangle and is processed accordingly. On every interface, the ray is also divided into new rays for reflection r and transmission t, respectively ("r" and "t" in Figures 4.11 and 4.12).

[e]The additional one is for the input ray before the first interaction

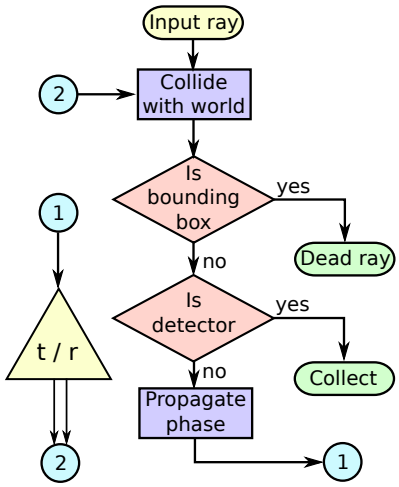

Figure 4.12: *Program flow chart for the ray–trace calculations. The "r / t" indicates the division of a ray into a reflected and a transmitted part.*

Result extraction from the models

As discussed above, the basis for the evaluated model is interfacial Fresnel raytrace. The actual results that are extracted in this study come from comparing the theoretical calculations to the measured. It was noted, that the overall theoretical signal changes in all evaluated cases are rather small; only around few percents. Furthermore, these changes seem more or less flat in the function of wavelength. Because of this, the theoretical system was evaluated with several possible outcomes, and then a linear fit was used to describe the system, per wavelength. For example, if a certain particle type was thought to form a single layer of material on the adsorbent, the linear fit would predict, by wavelength, the particle layer thickness in the function of signal change. These signals were namely the relative changes of Ψ and Δ, which were calculated using procedure described in section 3.3.2 (page 88).

This is not uncommon approach, as both incomplete and complete polarimeters always need some environmental model, which is used to calculate the results. Also, it is understandable that the

model type and used refractive indices defines the outcome of the results. This is why several approaches were used to make this model and refractive index dependence clear. Next, we explain these different type of approaches.

4.4.5 Photometric evaluations

The numerical evaluations simulate the environment seen in Figure 4.5 (Page 105). Let us further discuss the polarization dependence of the interfaces presented in section 4.4.2. While an excess amount of layers might create some energy loss for passing photons, a zero angle incidence essentially creates no polarization changes. Therefore, we can simplify the numerical evaluation of the polarimetric environment.

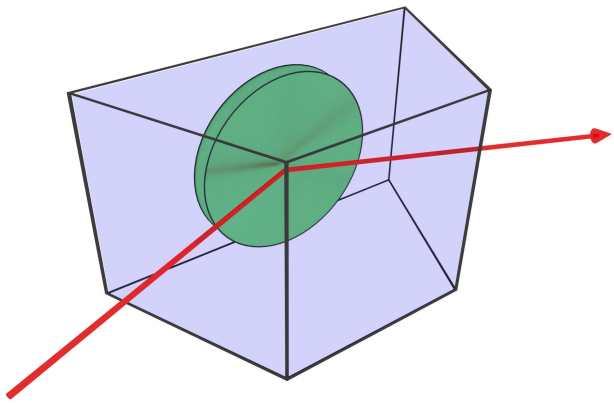

Figure 4.13: *Schematic image of a minimized ray–trace environment with a measurement beam (red), a liquid environment (blue), and a sample (green).*

Figure 4.13 shows a minimalistic environment that can be used in this case. A ray passes into the liquid environment with a zero incident angle so it does not effect the polarization, but the liquid environment must be present for the sample calculations to be cor-

rect.

Traditional approach – monolayer

As discussed above, the more traditional approach to adsorption is monolayer estimation. While it ignores the three–dimensional environment, it is the easiest way to evaluate an adsorbed particle layer. Figure 4.14 schematically represents a sample (green) in a liquid environment (blue) having different particle monolayers on it (red).

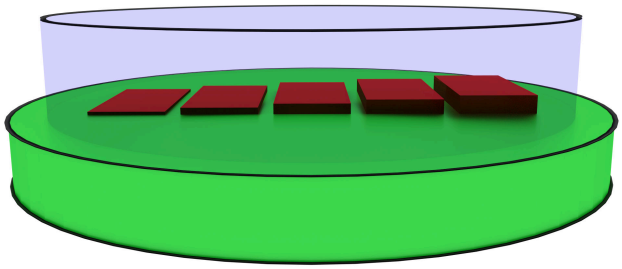

Figure 4.14: *Schematic image of several adsorbed monolayer thicknesses (red) on a sample (green) in a liquid environment (blue).*

This traditional approach could be calculated with numerous different refractive indices. Naturally, the refractive index is spectral, but some research might claim even a single constant refractive index for the models used. Generally, the evaluation concerns either a layer thickness or a refractive index. The purpose of using several refractive indices in this study is to determine the effect on the results. While there is no general rule for a water– or buffer–immersed particle refractive index, the effect of using different refractive indices should be clear after we use, in this study, three different spectral indices which are called $n_1(\lambda)$, $n_2(\lambda)$, and $n_3(\lambda)$ below.

The refractive indices $n_1(\lambda)$ and $n_2(\lambda)$ are PBS–based refractive indices, while $n_3(\lambda)$ is presented in section 2.7.6 (page 61). The

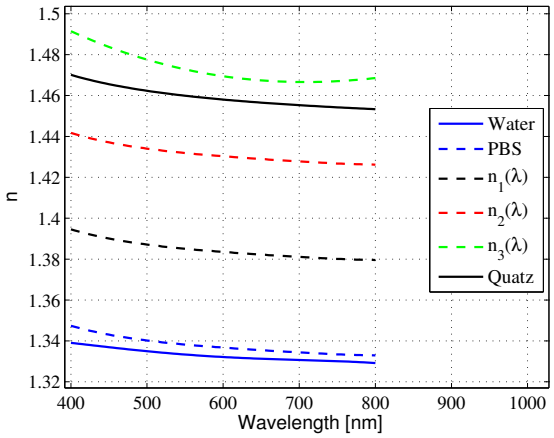

Figure 4.15: *Three evaluated refractive indices, $n_1(\lambda)$, $n_2(\lambda)$, and $n_3(\lambda)$ in respect to water, PBS, and quartz refractive indices.*

buffer–based, or PBS–based, refractive indices $n_1(\lambda)$ and $n_2(\lambda)$ follow the buffer refractive index in shape, but the values fit nicely between PBS and $n_3(\lambda)$. The reference refractive indices of quartz presented in Figure 4.15 is an average refractive index of birefringent quartz and only demonstrate the refractive index scale in the plot.

We must note one important thing of the $n_1(\lambda)$ and $n_2(\lambda)$ refractive index selection. As literature is very ambiguous about the protein refractive index, we are using several ones. Table 2.5 already showed an abundance of different refractive indices that are used. There are even studies which brutally use a constant refractive index over all wavelengths. We understand, that spectrally constant refractive index is rather error–prone approach. So, instead, we approximate that PBS immersed particles could create a small overall increase to PBS refractive index, and with that, would retain the shape of PBS's spectral refractive index function. With this, arbitrarily selected multipliers were selected, and with these, $n_1(\lambda)$ as well as $n_2(\lambda)$ were created, as presented in Figure 4.15. In any study, the dominant effect of PBS might be sufficient approximation, but after a certain amount of packed molecules, this model could fail. How-

ever, understandably, it is still more plausible model rather than using constant refractive index over all wavelengths.

In the Ψ and Δ analyses changes in the calculated model are observed. The changes in Ψ and Δ from a known monolayer environment is used to calculate layer thicknesses of an adsorbed layer in the actual measurements. Despite fact that Ψ and the Δ are the main values evaluated, in the results mainly relative and percentual changes have been observed because they are easier to discussed.

Three–dimensional adsorption

While this traditional monolayer approach is the most common one, it still completely ignores the environment. It assumes the formation of sharp borders of material. To observe a different scenario, a three–dimensional adsorption was calculated for a constant thickness of a material on a sample and the layer densities were changed; this thickness is divided using refractive index gradients from PBS towards $n_3(\lambda)$. The selected constant layer thickness was 20 nm and the scenario is represented in Figure 4.16.

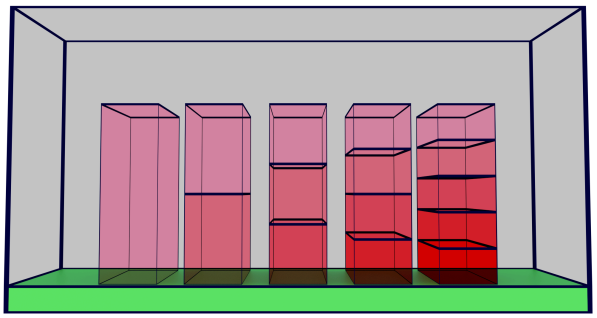

Figure 4.16: *Three–dimensional illustration of the multilayer adsorption approach, using constant observation thickness and dividing the layer into one to five density layers. A stronger red color indicates increased density, and the overall density in this constant layer thus increases from left to right.*

In Figure 4.16, the left-most layer model is equal to a monolayer model, but when the division is increased from left to right, we understand, that this could not only be a separate collection of layer models, but also a plausible model for temporal behavior of adsorption. Figure 4.16 presents densities with colors, having five different values. The strongest density represents refractive index $n_3(\lambda)$ and the change from density to density is just done with refractive index increments $[n_3(\lambda) - n_{\mathrm{PBS}}(\lambda)]/5$. We understand, for example, that permittivity could be better gradient calculation basis, but here the concept is the only thing we are interested in.

Effect of the geometrical setup

Geometrical effects were also calculated for the discussion. In this experiment a measurement beam is tilted ± 5 degrees in the incident plane to observe effects that are induced in the ellipsometric parameters Ψ and Δ. This simple modification to a rays path is represented in Figure 4.17.

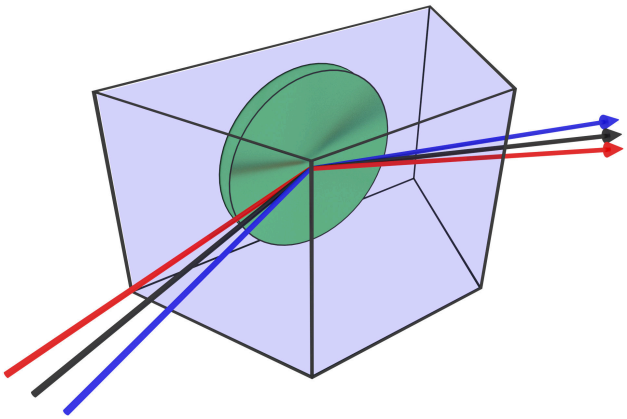

Figure 4.17: *Incident ray (black) alteration, showing two altered angles of +5 (red) and -5 (blue).*

4.4.6 Model challenges

Photonics

The physical challenge to these models is usually either accuracy or speed. However, the parallel programming presented here and increasing computational power in future might eliminate this challenge. An approximating full–field theory such as discrete Fourier methods could perhaps give more accurate estimations for the propagating field in the nano–scale, but we will be satisfied with the Fresnel–model. While comparing methods in an unknown environment sounds quite valueless, it would be interesting to see methodological comparisons in adsorption studies.

Physical models can always be more accurate. Here we do not include an evanescent field, scattering, or birefringence, all of which could be important with particle adsorption. This is very common in adsorption studies, to ignore all of these matters, but, this is the dilemma. If there is no exact structural knowledge of the environment, more accurate calculations would be bound to fail. Still, it would be beneficial to understand the adsorption phenomenon by actually trying to create more complex analyses.

Programming and numerical dispersion

Without going deeply into programming details, the ray–trace performed in this study provided a great challenge, especially in the GPU environment, where the dynamics are limited. Generally, any photon that interacts with any interface disperses into a minimum of two parts.[f] This makes any dynamic ray trace with a free geometric approach essentially impossible because of mathematical dispersion. The allowed interactions must somehow be limited so that the system has a discrete size in parallel execution.

A solution for this mathematical diversity could be in some cases to only allow transmissions for a ray. If the actual path or po-

[f] In birefringent materials there would be four parts. Diffractive surfaces could have even greater ray division.

sition were not important, a single ray could be followed for as long as needed without any issues of the system being too great for the computer memory. For example, a paraxial lens system could be traced with huge throughput if the output would be the only thing required. In this study we observe the interference in thin films, so the phases and positions need to be known. Figure 4.18 shows this challenge in the system previously described in Figure 4.16, which is one of the models. There is a need for allowed interactions for each ray, but diversity becomes a challenge with increasing demand on the needed memory. Because of the ray–tracing nature, the parallelization of the ray trace broadens the need for memory so that all interfering photon paths could be accounted for.

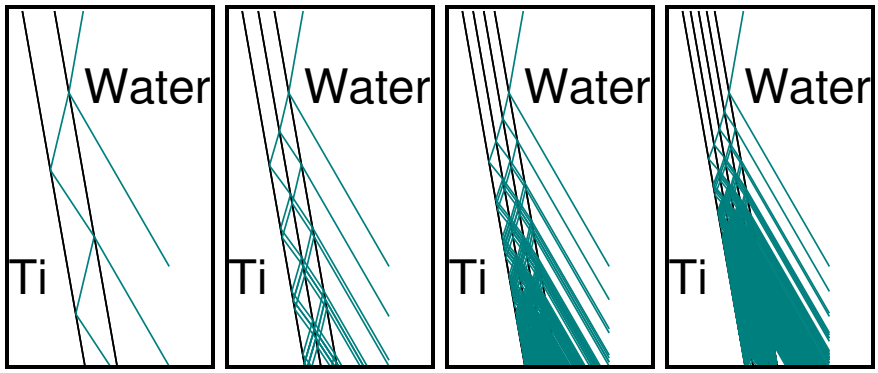

Figure 4.18: *Multilayer system on titanium with a) one, b) two, c) three, and d) four layers with each increasing refractive index towards the titanium. Rays propagate from the top to bottom of the image.*

Furthermore, it must be stated that GPU programming in general is a significant challenge for even the experienced programmer. The parallel execution creates a whole new level of needs. not only because the parallel programming can be a nightmare in parallel memory access, but it also creates a performance challenge which could be pursued forever. This is, because GPU programming is not just magically faster than CPU but it requires optimization starting from planning for it to even be an efficient solution. To increase

GPU execution speed, the task is to always optimize and plan. This generates a greater time requirement for the construction of the system. Finally, the direct transfer of code from plain C++ is generally not possible and requires rewriting on the GPU part which makes the parallel processing a challenge to create. Still, despite all the challenges, varieties parallel processing will be a part of future computing and can be very rewarding if the planning and execution are done properly.

4.4.7 Conclusion

Overall, three types of tests were performed numerically to discuss the photonic sensing of adsorption. Firstly, monolayer adsorption is observed with different protein refractive indices while reflecting these results into the measured results in a real environment. Secondly, the model is extended into three dimensions, observing the amount of gradient layers with constant adsorbed thickness to provide a discussion on the goodness of the monolayer model. Finally, the geometrical effects are discussed in a case where the measuremente beam is slightly tilted to demonstrate the effects of a misaligned measurement beam.

5 Results and discussion

5.1 CHARACTERIZATION OF THE USED SAMPLES

5.1.1 Contact angle and topography

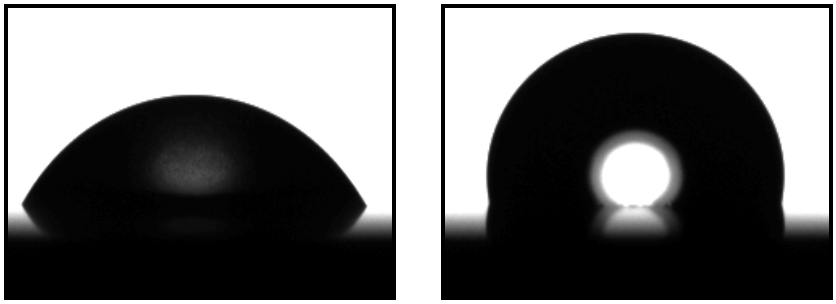

(a) (b)

Figure 5.1: *Water droplet on titanium. Subfigures show a) a low contact angle, and b) a high contact angle.*

As discussed in section 2.5.2, the surface–water interaction could not only affect but be a fundamental factor in particle adsorption [76]. That is the case with particles that are enveloped with water, such as protein.

Figure 5.1 shows measurement example from two different types of observations and Table 5.1 collectively shows all of the measured contact angles. We can immediately note that the samples might be challenging. In a sense, all these surfaces statistically show hydrophilic behavior. In other words, the surface demonstrates hydrophilic behavior, which could in turn indicate an increased water adsorption to the surface and then impede the water-enveloped particle adsorption. Still, a high deviation of the titanium contact angles could also indicate some contamination since the Ti_{HT} surface shows much lower deviations in the contact angles.

However, the exact measurement of the contact angle in air is

rather difficult. While it might be very easy, for example, on perfectly flat evaporated surfaces, the few scratches and local tilts in the surface do not help. Even the smallest topographical surface changes immediately increase the errors and deviations in the contact angle measurements. Different liquid contact angle measurements in different liquid environments could be possible, but an alien liquid could further contaminate the adsorbent, so this cannot be a general solution.

Table 5.1: *Measured contact angles, mean values, median values, standard deviations (Std.) as well as minimum (Min.) and maximum (Max.) value in degrees. Surface roughness and some literature values for a comparison, are also presented.*

Name	**Mean**	**Median**	**Std.**	**Min.**	**Max.**	R_a [nm]
Ti	69.78	67.85	15.48	47.93	115.96	3.66
Ti_{HT}	58.68	57.52	4.09	54.04	65.31	5.20
Ti_{CH}	76.90	76.38	4.07	69.43	47.3	47.3
Ti_{1500P}	51.98	56.69	10.97	34.44	64.34	141
Ti [146]	53.9	-	5.1	-	-	< 15
Ti [170]	81.2	-	4.1	-	-	-
Ti [351]	86	-	4	-	-	-

The measured contact angles for the titanium are rather low compared to some of the literature values (Table 5.1). Furthermore, a deviation from sample to sample and from study to study is also rather large. There is, perhaps, some stabilization from the heat treatment but there is nothing to be excited about. The Ti_{CH} shows clearly larger contact angles but the roughened Ti_{P1500} shows smaller ones which is due to topographical changes. Regarding this set, there are no expected further analyses concerning the contact angle other than the fact that the surfaces were seen to be somewhat scratched. This could totally explain the variations and large minima to maxima observations of the contact angle, and renders the overall results somewhat unreliable. Also, the droplet size here was

5 μl, which still might be too sensitive to a gravitational effect as even as small a volume as 1 μl is not uncommon [352]. Sometimes in studies the droplet size is not even mentioned which increases the uncertainty among water contact angle study comparisons.

Still, the titanium surfaces show quite similar contact angles. Also, as discussed above, the surface could show stronger water binding on the surface, which could impede the adsorption of the particles. Even if the surface scratches might distort the results, the adsorption signal could be smaller than with hydrophobic surfaces, or that the adsorption might not even occurring. We will discuss this later on.

5.1.2 Atomic force microscope observations

The measured titanium samples are quite smooth. This is one of the disadvantages of the ellipsometric setup as the theory of ellipsometry generally involves a perfectly smooth surface. As discussed above, topography and the accompanying roughness are already connected with the reactivity of the surface, for both chemical and physical adsorption. This is easy to understand because of increased active surface area. Ellipsometry is, however rather blind to topographical variations. It can certainly be used but a rough surface still deters the analysis. While even nanoscale thin layers can be evaluated with ellipsometry, extremely rough surfaces could hide the adsorption phenomenon.

Both the physio–chemical activity and the background for photometric analysis are good reasons to evaluate surface roughness before the measurements. Figure 4.2a shows a surface profile of one of the Ti surfaces. Figure 4.2c also presents the profile of a $\mathrm{Ti}_{\mathrm{P1500}}$ surface which has been roughened with sand paper. It is clear that the photonic behavior of a rougher surface could be rather difficult to model or perhaps even measure. Indeed, the rougher surface was too diffuse to be measured with the constructed device. It must be noted here that the measurement of $\mathrm{Ti}_{\mathrm{P1500}}$ could certainly have been performed, but the indicated low detection dynamics would

have created too much an error in the end results, and the Ti_{P1500} was omitted.

The surfaces roughness from AFM measurements for each of the surface is listed in Table 5.1. We note, that the roughness might not directly indicate water contact angle values, but this is understandable, as the material crystal structure should be the primary effecting factor in contact angle (surface energy). There are methods for correcting contact angles from surface roughness, but it is not done here, as we merely wanted to see the water contact strength and physical roughness.

5.1.3 Titanium heating

Because titanium has a natural tendency to form a thin oxide layer [35,36], this property was investigated if it affects adsorption in any way. If the pure titanium reacted inside the liquid environment, this could create super–positioned changes which would make it difficult to observe the actual adsorption phenomenon. Therefore, the Ti_{HT} samples were exposed to slightly extreme conditions compared to normal room conditions. A few titanium samples were exposed to 200 °C for five hours and the surface was inspected with WVASE.

Figure 5.2 shows the effects to the measured sample surface reflection per polarization. It can be noted that some reaction occurs to the surface during the heat treatment. The refractive indices were measured and the results are presented in Figure 5.3. The difference between monotonic refractive indices and ellipsometric parameters should also be noted. In this case, the Ψ values show clear shape differences between Ti and Ti_{HT} samples.

The reference used in Figure 5.3 is for evaporated thin films [353]. It is not uncommon to see such references which only state the base material regardless of the method. Inspite of this reference using evaporated Ti, there is a high resemblance to the refractive index measured here. These similarities might be from oxidation or from general crystal structure changes in the titanium as a bulge at

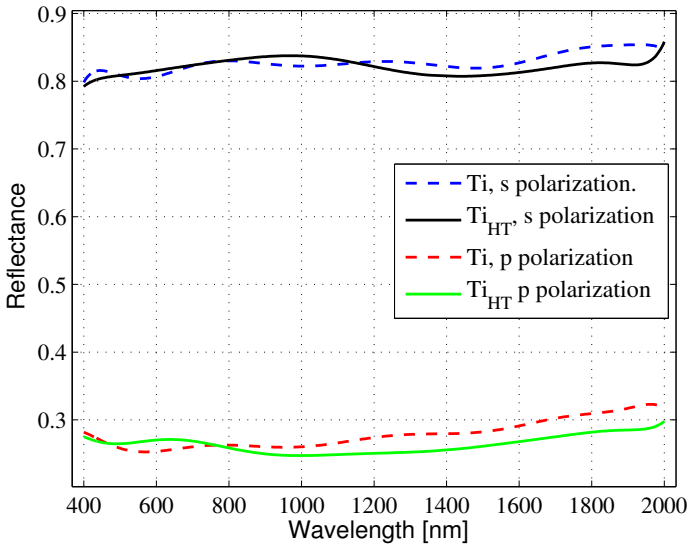

Figure 5.2: *Reflectance of s and p polarization from Ti and Ti_{HT} in the range of 400 to 2000 nm.*

750 nm appears, much like that in the evaporated thin films [353]. Here we do not concentrate too much on the oxidation process of titanium,[a] but simply note that the surface chemistry of titanium makes this oxidation possible, and some change happened through the heating. Consequently, there might even be a thin oxide layer on the assumed pure titanium which could affect the photonic observations. The observed changes might be due to the natural oxidation layer thickening or a new one forming. The main reason, however, for the Ti_{HT} was to determine the effect on adsorption, which will be discussed later.

[a] *The surface chemistry of titanium dioxide* is incidentally the name of one work of Diebold ([191], 2003). This huge review has nearly 200 pages and 800 citations in it and covers most there is to know about titanium dioxide.

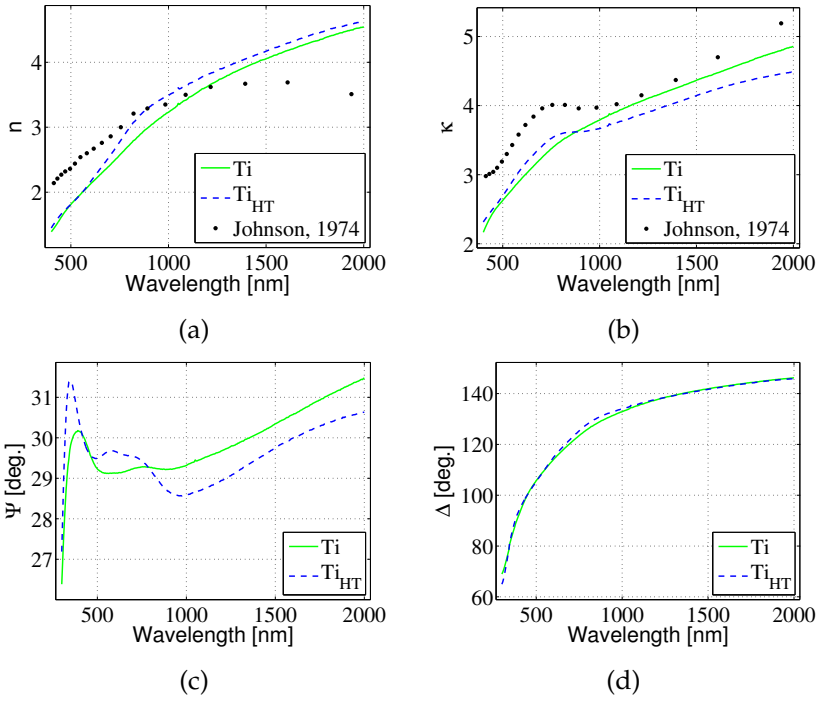

Figure 5.3: *Refractive index: a) real part n, b) imaginary part κ. Also showing c) Ψ, and d) Δ for both Ti and Ti_{HT}. Literature values by Johnson [353], are also presented.*

5.1.4 Justifying the numerical models

The ray–trace model (RTM) calculation for a thin–layer evaluation was constructed. This was done in aim to connect theoretical adsorption with real measurements for further analyses. Evaporated quartz samples were measured with the WVASE and the numerical model was compared using the ellipsometric parameters Ψ and Δ.

Figure 5.4 shows a single–layer equation (LSE), a measured (WVASE), and a ray–trace model (RTM) for a pure evaporated copper surface. Reason for using the copper surface is the certainty to get accurate base–material refractive index. As discussed above, titanium could have naturally occurring thin layer of oxide on them, which could create error between measured and calculated signals. Thus, the

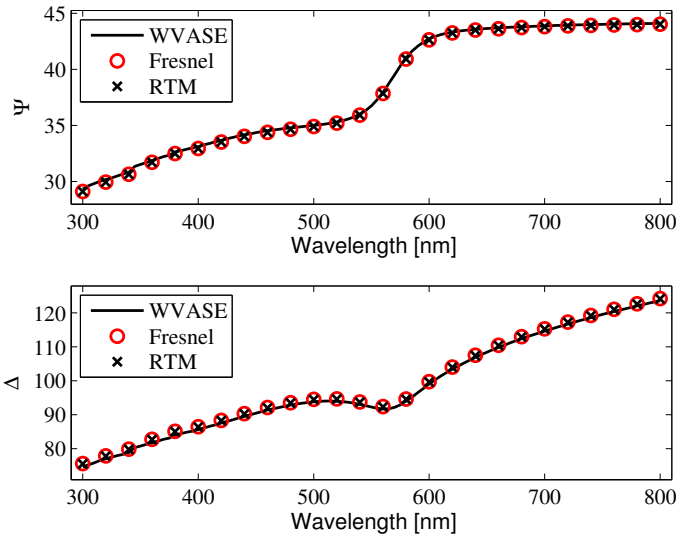

Figure 5.4: *Comparison of measured (WVASE), and calculated* Ψ *and* Δ *values from a pure copper surface. Calculations show a Fresnel equation and built ray trace model (RTM) evaluated values.*

justification was done using a freshly evaluated evaporation of a copper layer. The copper layer was 100 nm of copper on a glass substrate, which was thought to represent a bulk material.

The pure copper surface show great agreement of calculated and measured data in Figure 5.4. The second surface was a 55.5 nm of evaporated quartz on the firstly evaluated layer of copper. Measured and calculated reflection, as Ψ and Δ, are shown in Figure 5.5. The theory used in this case, was the simple layer estimate (SLE) from Equation 3.59 (on page 3.59). All of the data match nicely, but that said, Figure 5.5 also shows the supposed 55.5 nm evaporated surface. However, the model clearly shows similarities to a 74 nm evaporated layer thickness of quartz.

Two justifications were presented for the ray–trace model: a copper surface, and a quartz thin layer further evaporated on that. While the theories concur, the reality of the evaporation is another matter. The thickness difference between the quartz layer thickness

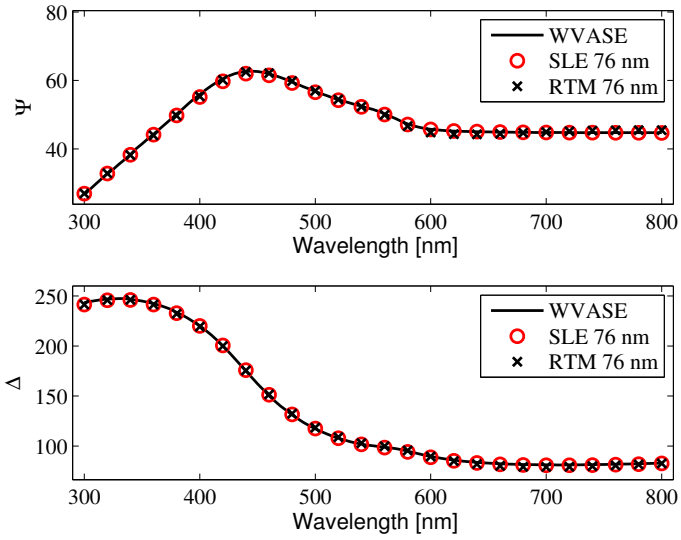

Figure 5.5: *Comparison of measured (WVASE), and calculated* Ψ *and* Δ *values from copper with an evaporated thin layer of quartz, showing both the single–layer estimate (SLE) and the constructed ray trace model (RTM) results for 74 nm quartz layer.*

and the manufactured surface is thought to be from the evaporator device and the chosen refractive indices. The crystal that detects an evaporation process was seen to be very lazy in the status update frequency and the electron beam controller in the evaporator was a manual one. We have no doubt the thickness error could be due to the evaporation process and that the thickness of the quartz layer is actually the amount that the model predicts rather than what the device indicated during the evaporation. However, another reasonable explanation for the variance would be the difference in the theoretical refractive indices and the actual evaporated surface, because quartz is birefringent material and only a single spectral refractive index for the quartz was used in the numerical evaluation.

Still, the overall average error between measured and theoretical values was around two percents. Also, the ideological dif-

ference in the models should not be forgotten; the SLE is a single equation constructed from a sum series and the other a complex coordination–based C++ program that is constructed from the ground up. All in all, the error seems tolerable and provides information, that the ray tracing works sufficiently for further analyses.

Performance

Because we deal with parallel computing, we must naturally comment on the performance of the model. As discussed in section 4.4.6 (page 125), the parallel processing (PAP) power provides only some benefits to this particular model. It is very powerful tool and the model benefits from some of the properties of parallel computing. As discussed above, the challenge to the system is the number of interactions. The number of interactions increase the size need of an individual traced ray, which is the limiting factor in the numerical construction. Figure 5.6a shows this dilemma numerically. Figure 5.6a indicates the increase in allowed interactions and the calculation time is observed.[b] The number of allowed interactions N created $2^N + 1$ elements in the calculation vector and Figure 5.6a clearly shows this polynomial increase in trace time, when the allowed interactions are increased.

Compared to the increased interactions, Figure 5.6b shows excellent performance results. The required time for a perfect parallel calculation is flat for any added calculated elements, and the performance of the ray–trace is very close to that. In addition to the wavelength count shown in Figure 5.6b, the numerical evaluations are performed for both polarizations at the same time.

As discussed in section 4.4.6, the ray trace execution has problems in dealing with the numerical dispersion of the individual ray. Each interaction divides the light into two additional components and if a position is recorded, it creates an increasing need for stor-

[b] In the performance part, the model was a 10 nm layer of molecules on titanium inside a water block and the full environment contained 26 triangles in the collision detection.

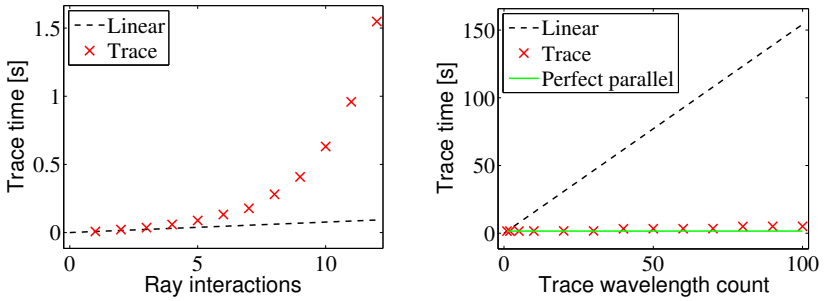

(a) (b)

Figure 5.6: *Time required by a ray trace environment according to a) increased ray interactions and b) increased wavelength count.*

age space to store and processing time. A paraxial system with only a transmitting rays could highly benefit from this performance, if it were calculated using parallel computing.

We also understand, that the built system could be interpreted as rather overly complex for the evaluated environments. However, we are not indicating, that the simple systems should be used, and the benefits could be immense in more complex calculations. The complexity of system models is discussed below.

5.2 OBSERVED KINETICS

The measurement and discussion of the kinetic behavior of particles is one of the objects of this study. There are several points to consider and measurements to show. Firstly, we check the signal of the light source detector and discuss the temporal signals recorded. Only then will we continue with the actual adsorption kinetics. Once we have observed the changes in the photonic signals, we will estimate the adsorption.

In the following we will refer to the real measurements; there are also three important signal sources to recall from the previous chapter. The measurement system recorded signal through three fibers at the same semiconductor sensor. These three signal sources

will be referred to as fibers or signals. The word "detector" for each fiber is avoided since all these fibers were guided to the same detector. We should recall from section 4.3.1 (page 104) that the light fiber is the fiber recording the light source, the reference fiber records the signal which passes through the cuvette, and the third fiber, the sample fiber, records the reflection from the sample inside the cuvette.

5.2.1 Temporal signal challenges

Light source

When discussing any photonics system the light source should always be one of the first matters to consider. Not only for an emission range, but also for quality. This is not always easy. In this case the multifiber device enabled concurrent measurements of a light source while the actual kinetics were observed.

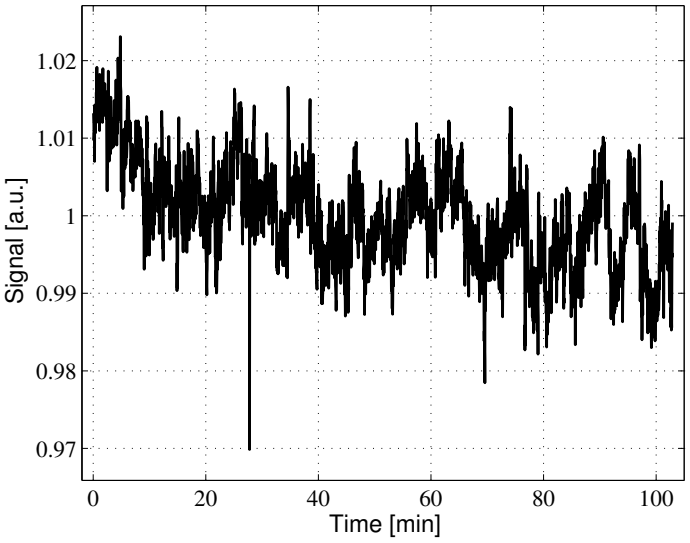

Figure 5.7: *Normalized measured signal from a light detector fiber from a measurement. The shown signal wavelength is 631 nm.*

Figure 5.7 shows a light signal from a measurement. While the

light source was always stabilized for two hours before any measurements, there is always temporal noise in the light signal. The noise in Figure 5.7 is not only a fast changing signal, but it seems that two noise signals, slower and faster, overlap.

The deviations shown in Figure 5.7 are very real. The light source signal shows one percent deviations nearly constantly over time. In this particular measurement the light source also shows a descending trend. This trend represents some signal changes having even longer period deviations, as in some measurements the same trend was ascending. As the aim of this study is nanodetection, we will most likely discuss small changes, which could be difficult, if the the light source has a lot of constant changes.

Signal noise and correction

Indeed, the light source signal proved not only useful observation but a mandatory addition to this study, because of parallel recording, some of the fast temporal changes of the light source fiber and sample fiber signals were the same. This enabled the correction of the sample signal deviations on a whole new level. It could be assumed that any semiconductor device has a different fast–changing signal–independent noise compared to others. If we measure a light source signal and a signal through a sample, these signals would have independent fast deviations, though not in this case, as the multifiber system shares some of the noise properties among the measurement fibers.

Because of the parallel recording, all of the signals were actually divided by the light signal before the final analyses. This corrected the light source deviations quite a bit. As the photons pass through the system and the liquid cuvette, this correction is certainly imperfect as there is an arbitrary level of difference between the light source and sample signals. In other words, the light source could be considered to have a signal–independent noise while the other also has a signal from the liquid cuvette. The sample signal was fixed by dividing it with the light source signal, and with this, there is

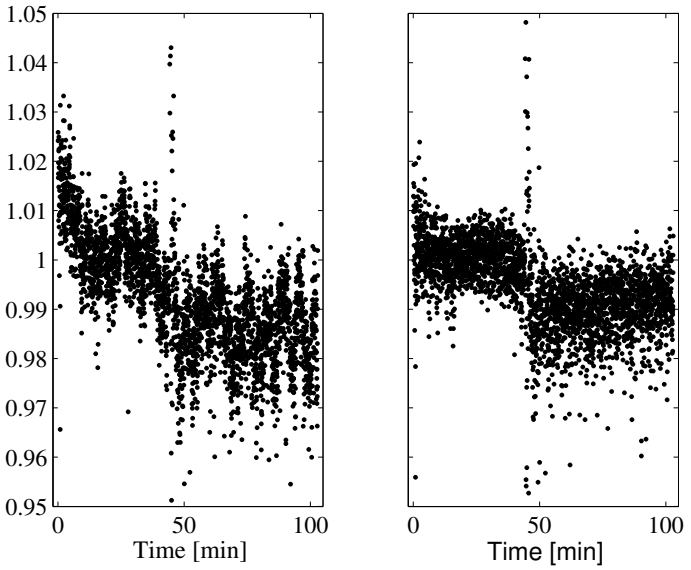

Figure 5.8: *Measured and a normalized signal point swarm from a reference fiber without light correction (left inset) and with light correction (right inset). The measurement wavelength was 631 nm. Particles were injected into the measurement cuvette at around 45 min.*

bound to be some error. However, as mentioned above, this enabled the measurements. As an correction example, Figure 5.8 shows a signal passing through the measurement cuvette (reference fiber) and the same signal divided by the corresponding normalized light source signal, as in Figure 5.7.

The effect of the light signal division was immense, even to the point that it indicates a clear change occuring in the signal on particle addition. Indeed, Figure 5.8 shows a signal where at approximately 45 minutes, the molecules are injected into the liquid cuvette. It is not obvious in unfixed signal.

The correction can also be evaluated with two numerical observations. First, fast temporal signal deviations can be observed with the signal to noise ratio SNR_{dB}. This is expressed in Figure 5.9, with a constant observation window of five minutes (150 points).

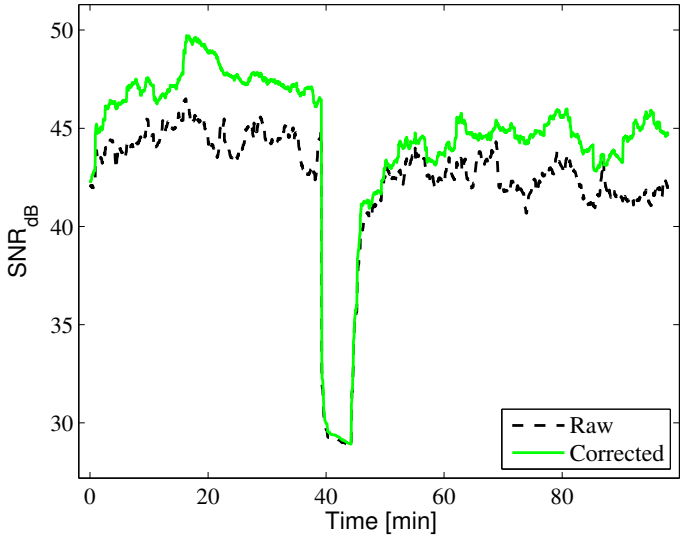

Figure 5.9: *Signal to noise ratio of a raw and a light–corrected signal with a five–minute observation window at 631 nm. Higher values indicate lower noise.*

Even decibel improvements as high as ten can be seen in this signal to noise observation between a corrected and a raw signal. Please note, that the high signal to noise ratio comes from the observed small time window, which is not so visible in Figure 5.8.

A second numerical estimation could be done to describe the overall stability of a signal. While there might be several possibilities, the sum of a derivate was selected here to be an evaluator. Hence, a signal was derivated and a ten–minute observation window used. The sum of the absolute value of the derivate describes how much the overall signal varies in that observation window, or if there are larger trends in the data. The evaluated signal increases if the signal grows unstable. Figure 5.10 shows the derivate sum and further shows that a corrected signal not only has better signal to noise ratio but is also more stable than a raw signal.

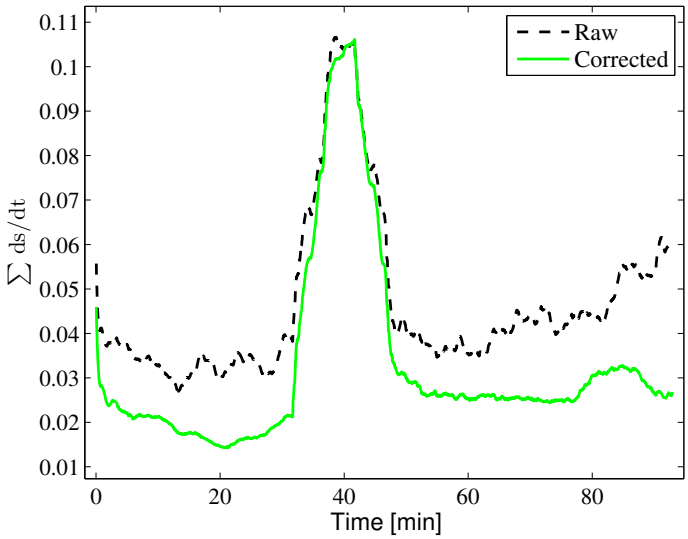

Figure 5.10: *Sum of the absolute values of the derivate of a raw and a light–corrected temporal signal with a ten–minute observation time t window at 631 nm. Lower values indicate better temporal stability.*

5.2.2 HSA protein isotherm

Similar to Figure 5.8, the particle injection induced measured signal changes from the sample fiber which could be evaluated. So, several concentrations of HSA were measured on titanium surfaces, and the changes recorded. Figure 5.11 shows such changes as isotherm. This isotherm is usually shown by an ascending saturating curve, but Figure 5.11, in contrast was chosen to show the descending trend related to descending photonic signal.

The isotherm presented in Figure 5.11 is calculated from a signal change with a five–minute average three minutes after the protein injection. The observed signal change is calculated from Δ. Ψ values did not show as strong a correlation. As only one protein was evaluated for the isotherm, no further parametrization for the function is done. From the isotherm, it could be possible to observe particle differences, as well as the adsorption saturation. Here we only note that Figure 5.11a fit indicates signal saturation after 4 μM

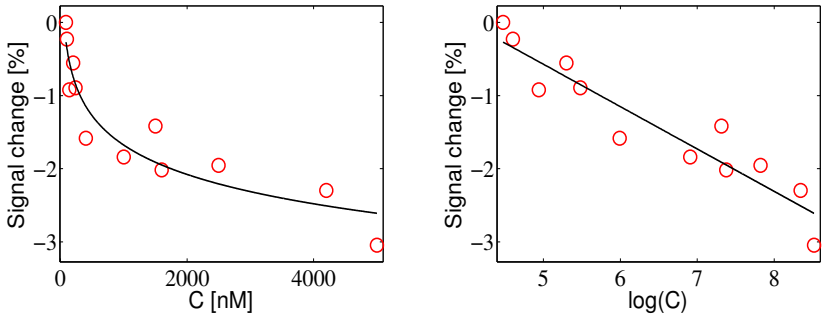

Figure 5.11: *Measured HSA concentration and amount of adsorption evaluated from Δ values having a) the theoretical shape of a logarithmic–shape isotherm, and b) a linear correlation of this logarithmic isotherm showing a linear correlation coefficient of -0.94.*

concentration. This is to be expected as 4 μM is already rather high concentration.

As one of the research aims was to determine if it is really possible to measure an adsorption of proteins, we could discuss this matter here. This further creates the need to present a sample signal and a reference signal through the measurement cuvette. As the theory indicates, the isotherm could indeed present a logarithmic behavior of signal changes. Here we will assume that this is an actual signal change from the proteins that are injected and adsorbed. Figure 5.11 shows a single wavelength observation and a linear fit of the isotherm. Figure 5.12 shows the linear fit correlation similar to Figure 5.11b, by wavelength, calculated between photonic signal change and logarithm of concentration, of all of the 12 HSA concentration measurements.

There are a number of clear factors to consider regarding the graphs in Figure 5.12. The first is similarities. This demonstrates that the signals are from the same environment, and despite that, the wavelength–dependent shape similarities are interesting. The higher positive correlation indicates that the signal generally increases as a function of the protein concentration, or follows the

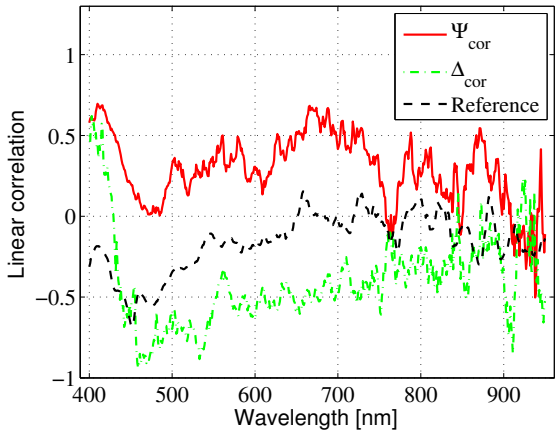

Figure 5.12: *By wavelength, the linear correlation between logarithm of concentration and* Ψ, Δ, *as well as raw reference signal change.*

isotherm model. Similarly, a negative correlation indicates decreasing isotherm and signal.

As discussed in section 4.3.1, the light source may contain interferometric filtering. At least Figure 4.6, on page 106, was a strong indication of that. Furthermore, it might not simple be coincidence that the Ψ_{cor} correlation interestingly dips at around 770 nm, 850 nm, and 930 nm in Figure 5.12, as these are the observed local minima of the emission spectrum of the light source. Some filtering could also affect Ψ_{cor} and Δ_{cor} towards higher wavelengths. This makes it clear that there might be some unreliable regions in the spectrum for adsorption observations. Indeed, when we look at the Ψ_{cor} and Δ_{cor} correlation functions in Figure 5.12, we note that the sum of the Ψ_{cor} and Δ_{cor} correlation is near one. This seems logical as these parameters are connected is some way and calculated from the same signal.[c] The sum of the absolute values $|\Psi_{cor}| + |\Delta_{cor}|$ was plotted (Figure 5.13). The exact idea of this plot was; *assuming that* Ψ_{cor} *and* Δ_{cor} *are mathematically inseparable, to determine how suitable these two variables together are in describing the concentration C*

[c]More so because the Ψ and Δ theory strongly connects the relation between these two parameters.

induced changes S to the photonic signal assuming that the change follows the linear correlation of the relation of log(C) and S. While this plot is noisy from wavelength to wavelength, the sum is stable in the range of 450 nm to 750 nm and dramatically then dips at higher wavelengths. If the plot of Figure 5.12 were stable, the wavelength could be said to have a balanced explanation effect. However, the clear dip after the 750 nm could indicate that the spectrum should perhaps be considered unbalanced. Because of this particular observation, wavelengths higher than 750 nm should be separately considered if they show inconsistent results.

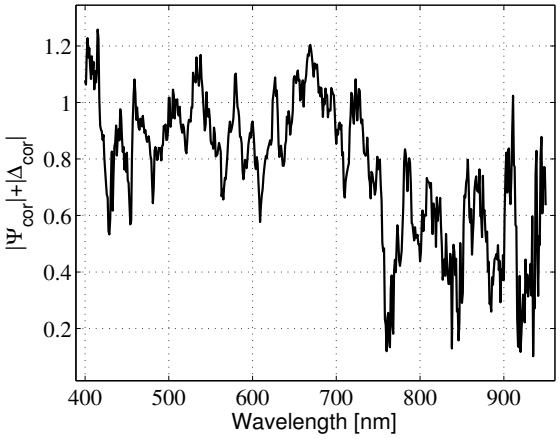

Figure 5.13: *Sum of* $|\Psi_{cor}|$ *and* $|\Delta_{cor}|$ *correlation as a function of a wavelength.*

So, it seems that particles are also observed in the signal changes from the titanium surface, but the wavelengths are open to interpretation. The adsorption seems to be explained fully at 460 nm (Figure 5.11) from the Δ_{cor} with a isotherm correlation coefficient of -0.94, but, on the other hand, the validity of the explanation decreases from there. The light source already provides light (Figure 4.6) from wavelengths below 400 nm, but it seems that the valid analyzing range starts after around 450 nm (Figure 5.12). However, the reference signal has a small correlation to the added proteins at the 460 nm wavelength. Furthermore, the reference photon path

through the cuvette is tilted by design. The reference beam enters the cuvette with a large angle of incidence and the reference signal should have the largest amplitude changes, if the effective liquid refractive index changes, or there are adsorbed particles in the liquid cuvette window. This would indicate, that the high correlation is indeed from the particles near the titanium sample surface and that the adsorption can be detected.

Although, one more consideration should be mentioned. Measurements and numerical observations in this section are only for a human serum albumin (HSA) protein, setup, and titanium sample. It cannot be directly claimed that all proteins follow these same trends and rules. Thus, a benefit of this section is that we could conclude that the adsorption can be measured and that we indeed receive different responses from different wavelengths.

It could be speculated, because of the additional spectral information shown, that we are seeing the physical movement of the measurement beam or the Fresnel coefficients get effected due to small refractive index changes of the buffer itself, not the adsorbing particles.[d] Incidentally, this is again rarely spoken of. The liquid environment brings, not only variables that affect the adsorption itself, but also adds to the fundamental photonic variables. Here, we will continue with the assumption, that the signal change indeed comes from the adsorbing particles, but also understand that other explanations could cover for the small changes. Indeed, the signal might still show adsorbing particles, but the signal could also be consisting of several overlapping changes where the adsorption is only part of it. This could, for example, explain the device–to–device differences and could be one explanation for the literature refractive index variety.

[d]The measurement beam is not spatially flat, so even very small changes in spatial movement might be detected.

5.2.3 HPF protein kinetics

HPF vs. HSA adsorption

Section 5.2.2 claimed that the observation of protein adsorption could be possible but the wavelength response should be observed with caution, if it shows any oddities. In this section, we change the measured particles to human serum fibrinogen (HPF).

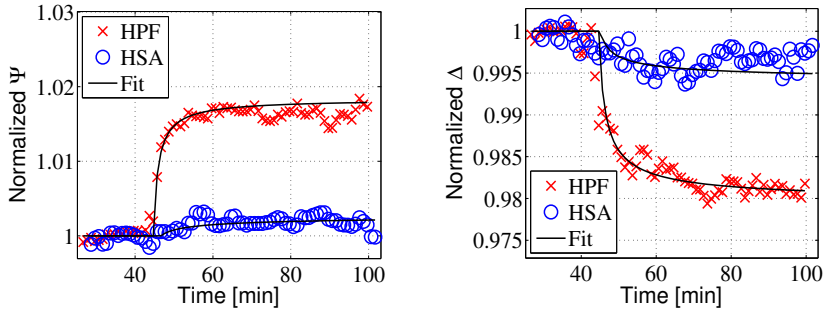

(a) (b)

Figure 5.14: *Signal of different protein on a sample surface to normalized* Ψ *and* Δ *from a measurement at 638 nm.*

Initially, from Figure 5.14, we note the signal change differences between an HSA and an HPF measurement. According to theory, there should be clear amplitude difference in the changes when comparing the kinetics of a smaller and a larger molecule on same surface with the same concentration. Figure 5.14 shows a single wavelength signal from a titanium surface. Both proteins have the same concentration but because of the mass difference, the HPF signal is significantly larger. For clarity, the figure plots only one point per minute.

Figure 5.14 also shown the kinetic behavior of both proteins. While HSA has much smaller signal, the time–wise saturation seems to happen somewhat at the same time. It is interesting to see, that long–term signal recording might not be all useful as the observed signals starts to oscillate. We note that the first 20–30 minutes of the measurement the signal saturates with clear signal changes before

the oscillation occur. Furthermore, it is not uncommon to see different temporal trends within a single measurement. For example, there is clearly visible approximately a ten minute interval oscillation during the measurements, which occurred with all samples. This waviness of the signals could be from adsorption desorption or from the mixer creating turbulences into the cuvette. This behavior was observed in all measurements and similar behavior has been seen in the literature [329].

Furthermore, the signal changes immediately after the injection of the proteins could be interpreted as very simple adsorption, where all possible adsorbing sites for the protein are filled. After this, the interpretation becomes more or less speculative. The signal changes could be, for example, from protein packing, where there is higher disorder in some point of the adsorption, after which the adsorbed layer readjusts.

HPF kinetics

As mentioned above, a total of 12 samples were measured in the HPF measurements, three repeats per type. More could have been measured, but this was seen irrelevant due to the fact that each measurement took time and because each measurement was observed to be highly repeatable. It must also be noted that the cuvette was quite large in size so the protein consumption was rather large per measurement, and it was financially wiser to make only a few carefully selected fundamental measurements.

Figure 5.14 shows an example of an observed signal for a single wavelength. Since these measurements have two dimensions, time and wavelength, any presentation of data can be tricky. One attempt to show the Ψ and Δ signal changes for all of the measurements concurrently, can be seen in Figures 5.15 and 5.16.

Figures 5.15 and 5.16 both show same axes. The wavelength increases from top to bottom and time increases from left to right. The overall time frame is 35 minutes and the injection is in the left–hand side. Single row of images represents one sample type.

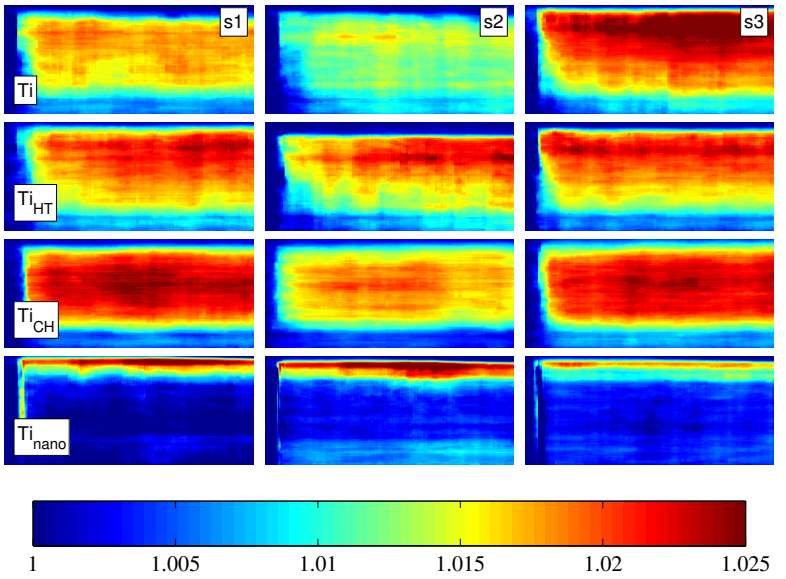

Figure 5.15: Ψ *change visualization of all of the samples. In subfigures, each row has a sample type and columns are repeats. The horizontal axis presents an overall timeframe of 35 minutes while injection is in left–hand side. The vertical axis shows wavelengths from 456 nm to 810 nm from top to bottom and the colors slide from blue to red showing normed values from 1.0 to 1.025. Each column represents a repetition sample s1, s2, and s3, respectively.*

Each type could be separated, except for the Ti and Ti_{HT}, which show very much the same signal changes. Already on this basis we could assume that Ti_{HT} has not gained or lost any specific properties during the heating process and these measurements could be essentially interpreted as similar.

Overall changes on Ti and Ti_{HT} are an increasing Ψ and a decreasing Δ, which is in accordance with the literature on adsorption studies of protein on titanium [331]. The signal change after injection seem rather rapid with all surfaces as particles quickly saturates the surface. As Figures 5.15 and 5.16 cover a time span of more than half an hour, we can see that most signals calm down 10–20 minutes after the particle injection. Even after the change sta-

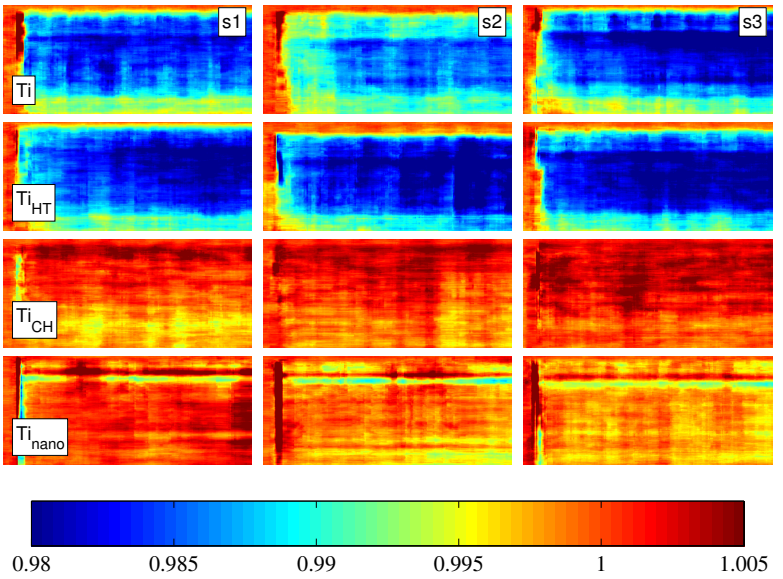

Figure 5.16: *Visualization of Δ change in all of the samples. In subfigures, each row has a sample type and columns are repeats. The horizontal axis presents an overall time frame of 35 minutes while injection is in left–hand side. Vertical axis is wavelength from 456 nm to 810 nm from top to bottom. Each column represents a repetition sample s1, s2, and s3, respectively.*

bilizes, the signal continues to vary over time. Still, all change types are very clear and systematic to sample type.

Naturally, the statistical changes were evaluated from the data in Figures 5.15 and 5.16. If we mark the injection time as t_{inj}, the starting period signal level was evaluated as a signal median of t_{inj} minus 10 minutes to t_{inj} minus one minute range. Similarly, this time interval was evaluated against a median of signal in a time range t_{inj} plus 10 minutes to t_{inj} plus 20 minutes.

Figure 5.17 plots these changes in Ψ and Figure 5.18 the changes in Δ. One common factor noted in the HSA isotherm measurements is a sudden dip after 700 nm wavelengths. While the light source still has intensity in that region, and also the plots of Figure 5.17 seem to show this discontinuity of spectral trend in the higher

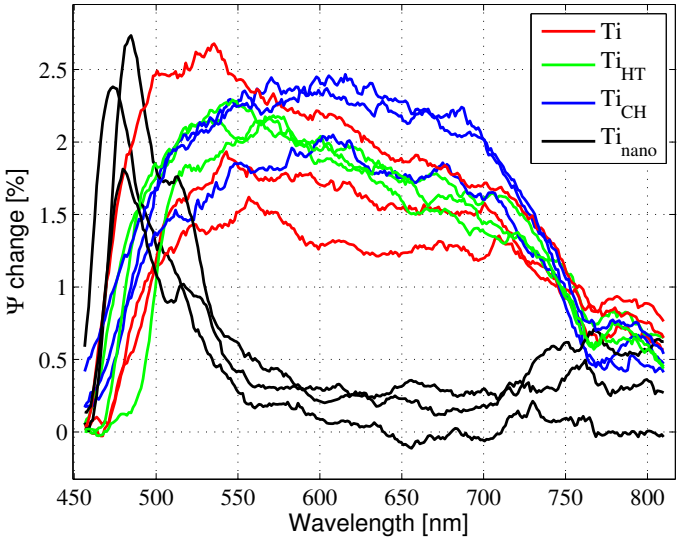

Figure 5.17: Ψ *changes, in percent, following a HPF injection by sample type.*

wavelength area.[e]

Overall, the Ψ change is positive. This shows that the polarization amplitude relation changes. Similarly, the phase–descriptive variable Δ shows negative phase changes. Naturally, we want to determine if a reference signal[f] demonstrates the same trends. While some follow similar trends, the sample types no longer group, as they do with the sample signal Ψ and Δ. Figure 5.19 shows an important set of signals measured from the reference fiber. Firstly, the changes are larger than with Ψ and Δ, and secondly, the changes both show a similar trend. This is most likely because all of the signals need to follow the spectral shape of the refractive index of the used buffer. The ellipsometric parameters Ψ and Δ are generated from the polarization changes occurring on the sample surface

[e] A certain part of the spectrum would be a *range*, but here we also discuss the temporal dimension which generates an overall *area*.

[f] A *Reference fiber* or a *reference signal* was measured from the beam that traveled through the liquid cuvette.

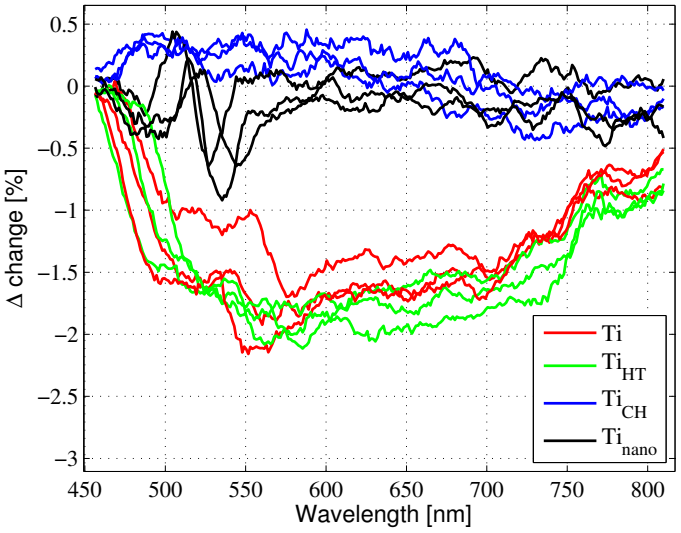

Figure 5.18: Δ *changes, in percent, following a HPF injection by type.*

while the reference signal changes are generated by changes in the liquid refractive index and possible adsorption on the cuvette windows. An important matter to note here is the lack of systematic results measured from the reference fiber. While it might still be possible that the proteins are detected on the cuvette window, the lack of polarization knowledge makes this impossible to verify, or even repeat.

The manual alignment of the measurement fibers must play a major role in this study. Every time the sample was aligned, the geometry was slightly adjusted, which could explain the sample to sample differences observed with the reference fiber. All plots in Figure 5.19 should essentially be the same. There is no reason why one of the plots should be different from another. Still, some differences exists. Changes are seen as similar spectral shapes, but, for example, the smaller wavelength position shifts. The liquid environment in this setup acts as a prism that divides the light into components in the case of the reference beam (see the setup in Figure 4.5 on page 105). This could easily explain the different changes

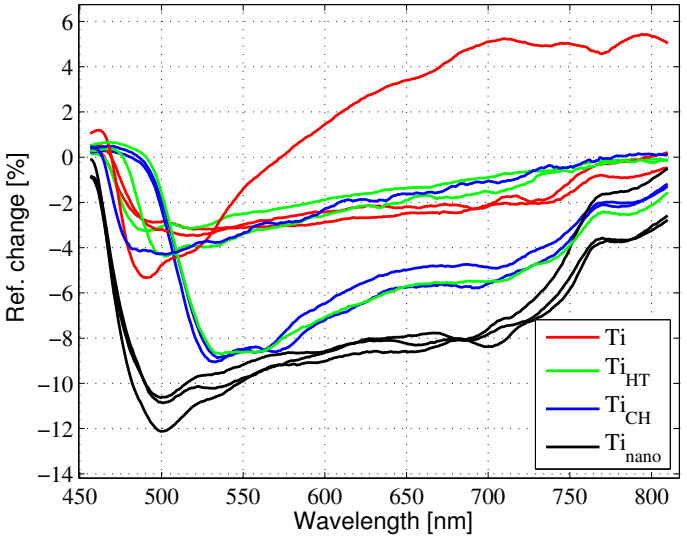

Figure 5.19: *Changes, in percent, in a reference fiber signal following a HPF injection by type. Plots are smoothed to better show those that overlap.*

since the initial position of the measurement fiber for the photon beam was manually aligned. But through this, we also understand why the ellipsometer can be said to be robust and repeatable, as the Ψ and Δ are so repeatable.

Finally, it must be noted, that the valid range for wavelengths vary, and the 475 nm to 525 nm range becomes important. In Figure 5.12 (page 145), the correlation was the highest in this area. We also note the similarities between Δ correlation in Figure 5.12 and Figure 5.19. The high correlation of Ψ in Figure 5.12 and low correlation of Δ could be a telling tale about physical, photonics–related changes in the cuvette, and not as detected adsorption. But, then again, we must keep in mind, that while these signals are correlated, they are very much different, and we are now discussing two different proteins. Like previously mentioned, the sample and the reference fiber measure very different geometry, despite they are measuring the same environment. Reason we are not going into

more details about the reference signal, because it would essential require adsorption analyses of the cuvette windows, which would be a whole another study. So comparing the reference and sample fiber is not fully justified, but could provide extremely valuable information, and should be included in adsorption study. Here we note, that the reference fiber cannot explain the sample signals, and that the samples analyzed with reference fiber don't have changes that could be identifiable.

5.2.4 Signal from numerical models

Monolayer

As the changes in the ellipsometric signals are shown and seem systematic, let us observe how in theory the signal would change. Firstly, a monolayer model is observed. The monolayer was used with the three different refractive indices presented in Figure 4.15 (page 122). The reason for using several refractive indices is the previous discussion of mismatching literature values (see section 2.7.6, page 61) for the refractive indices, and to really observe how the selection effects the numeric values.

Figures 5.20 and 5.21 show Ψ and Δ changes in percent. The percentage is compared to the plain surface without the monolayer. Both figures show an increasing layer thickness, having thickness on horizontal axis from 0 to 40 nm. The data is presented with as few colors as possible to make the changes more visible.

The simplest thing to observe in Figures 5.20 and 5.21 is that each shows increasing Ψ and decreasing Δ as the function of increasing layer thickness. We must bear in mind that this is generally true only for thin layers as is the case here. The layer thicknesses are very small. Still, they are also the layer scales that the literature deals with, so there is no point in evaluating vastly overly thick protein layers.

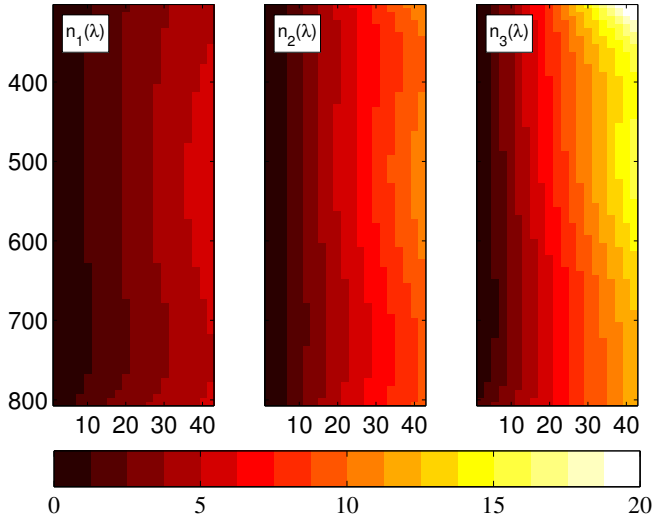

Figure 5.20: *Model–predicted* Ψ *changes, in percent, as the function of monolayer thickness for the each refractive index (left to right):* $n_1(\lambda)$, $n_2(\lambda)$, *and* $n_3(\lambda)$. *Vertical axis shows wavelength in nanometers, and horizontal is layer thickness from 0 to 40 nm.*

Multilayer

In comparison to the monolayer, the multilayer model estimated a constant thickness of adsorbed molecules having increased density over time. The density increasing was made increasing the layer count and the density was modeled to increase more near the adsorbent (titanium) surface. Figure 5.22 shows the results, as a relative change, for both Ψ and Δ.

We can see, that there is constant increase in both Ψ and Δ when the layer count (density) of the fixed thickness of proteins is increased. Furthermore, when compared to the results of monolayer presented in Figures 5.20 and 5.21, we notice, that the changes are far more greater with the multilayer model. Indeed, the gradient actually couples the photons more strongly towards the adsorbent and larger changes in polarization are generally observed.

This again is excellent result to discuss. If the model is changed

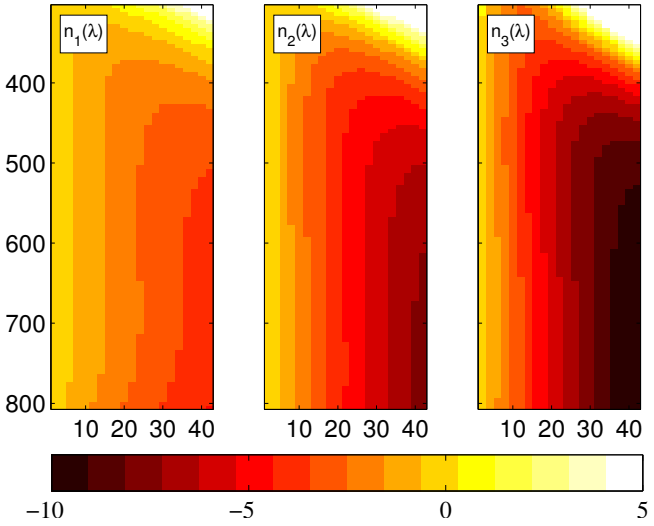

Figure 5.21: *Model–predicted* Δ *changes, in percent, as the function of monolayer thickness for the each refractive index (left to right):* $n_1(\lambda)$, $n_2(\lambda)$, *and* $n_3(\lambda)$. *Vertical axis shows wavelength in nanometers and horizontal is layer thickness from 0 to 40 nm.*

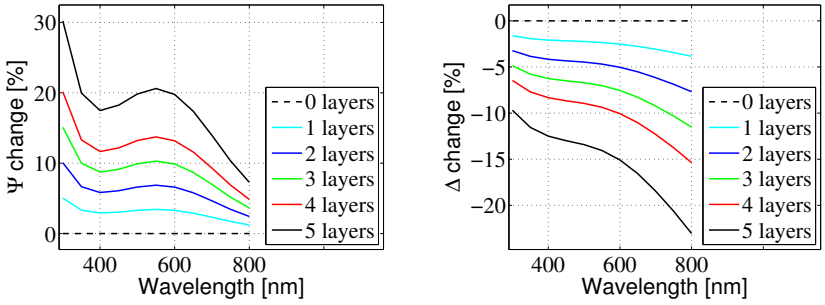

Figure 5.22: *Five layer models and their respective signal change, in percent, to a)* Ψ *and to b)* Δ.

to a gradient version of the adsorption, the changes to polarization are bigger. This would indicate, that using a gradient model to calculate the adsorbed amount of particles, the result would show

smaller adsorbed thicknesses than the corresponding monolayer model.

Geometry

One of the calculational models was to model the situation where a measurement beam is actually tilted in the incident plane. Naturally, the goal is always to aim the beam as much as possible in the zero incident angle towards the liquid cuvette window, but as the alignment work is generally done by hand, it not so common to have some degree of tilt in the beam. Here we calculated the induced changes of a five–degree tilt on either side of the measurement beam (sample fiber) in the incident plane.

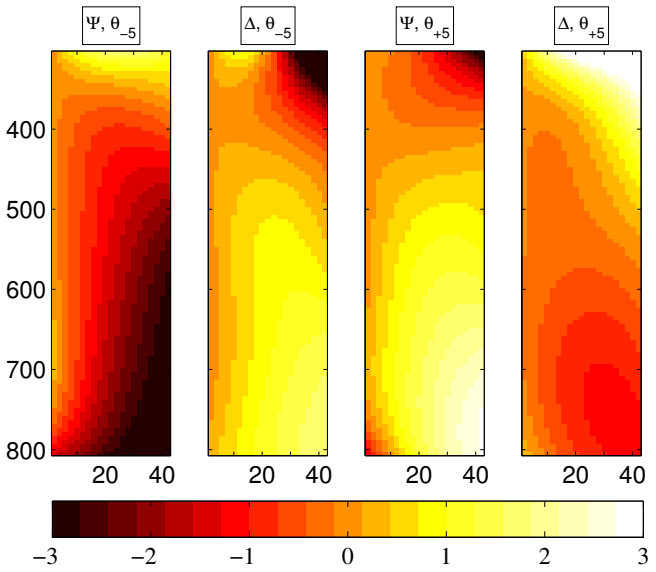

Figure 5.23: *Effect of the measurement beam angle. The two on the left are for a -5 degree tilt (θ_{-5}) and on the right for a +5 degree tilt (θ_{+5}). a) and c) show Ψ change difference while c) and d) the Δ change difference. In each sub-figure, vertical axis presents wavelength in nanometers, and horizontal axis presents the monolayer thickness.*

This model is constructed in a similar manner to the monolayer

calculations. The refractive index for the protein layer modeled was $n_3(\lambda)$ (to induce the largest changes) and the layer thickness was evaluated from zero to 40 nm. Figure 5.23 shows the percentual changes of both tilt directions on both Ψ and Δ. It can be noted that the directions have similar amplitudes but opposite effects. The θ_{-5} shows smaller than expected values for Ψ and larger for Δ. The effect is the opposite for the θ_{+5} direction.

This holds for the $n_3(\lambda)$ refractive index, and this is the reason for the results being presented in percent. The change is not that great, but misalignment in the incident plane could generate false results as either larger or smaller adsorption amounts depending on the very small error of five degrees in the alignment. And as we have seen, the signal changes are not that big to begin with. So even a small misalignment could play a part in the final results.

5.2.5 Model–predicted adsorption and model goodness

The model for the predicted amount of adsorption was constructed as described in section 4.4.4. Essentially, it is just a linear fit of calculated monolayer thicknesses in relation to Ψ and Δ changes. This fit, facilitates calculating the actual thickness of the material when observing the signal change of both Ψ and Δ.

The fit for the value change is performed for both Ψ and Δ. Thus, each measurement can generate a thickness estimate per wavelength and per time. Figure 5.24 shows the Ψ evaluated thickness for each sample measured. Unlike the original signals in Figures 5.15 and in 5.16, Figure 5.24 shows a vertical axis from 500 nm to 700 nm for more accurate estimations. Figure 5.24 evaluations are made using refractive index $n_3(\lambda)$ in the model fit.

The goodness of the fit could be estimated with different methods. Because both Ψ and Δ can be used to evaluate the adsorbed particle layer thickness, the difference in the thickness, they individually estimate, can be observed. If the basic model is correct, Ψ and Δ should agree on the particle monolayer thicknesses. That is, the difference of Ψ and Δ predicted thicknesses can be used as one

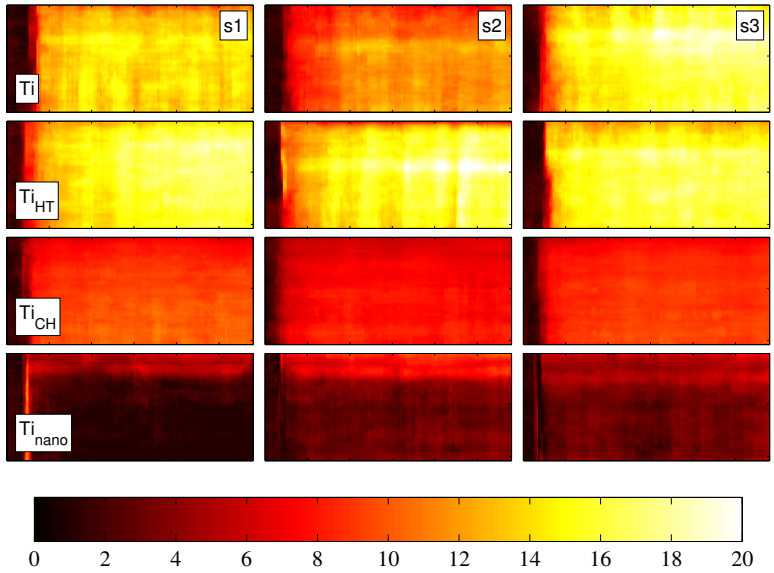

Figure 5.24: *Predicted temporal thickness of protein from the monolayer model. Each vertical axis shows wavelengths from 500 nm to 700 nm from top to bottom. Colors represent nanometers of protein thickness.*

model goodness evaluator.

Figure 5.25 presents the difference of Ψ and Δ predicted differences by wavelength. Essentially, values near zero predict a good fit and, correspondingly, increasing values are an indication of the model failing. Note that all samples are purposely displayed. The calculated model is for proteins and the titanium surface, despite we also present the Ti_{CH} and Ti_{nano} measurements here. In Figure 5.25 the third row shows the Ti_{CH} surface measurements. We can clearly see that there is a systematic disagreement between Ψ and Δ in the model. This is not surprising as the model has not been suitably constructed for the Ti_{CH} surface while Ti and Ti_{HT} both show suitability for the used model. The function of measuring the very different Ti_{CH} surface was to see that the photonic signals are different and to evaluate the model goodness with "wrong kind of" surface.

Similarly, the measured nanoparticles are another good example

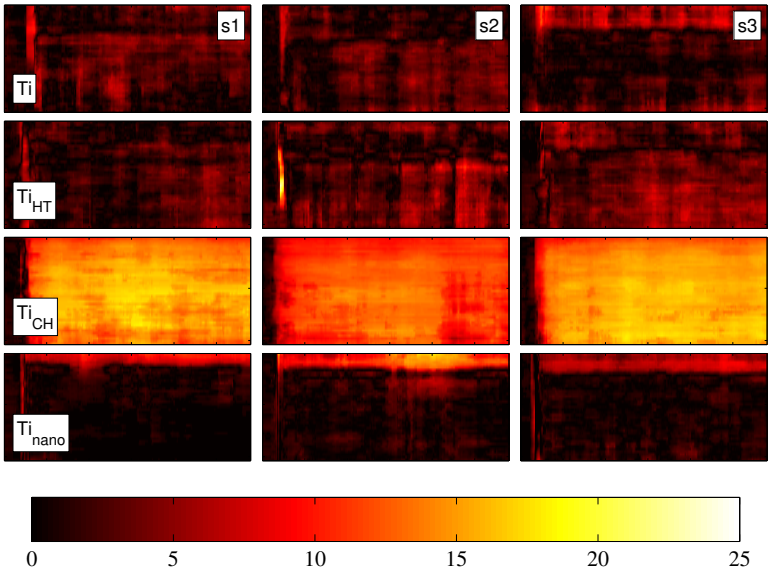

Figure 5.25: *Difference in* Ψ *and* Δ *predicted temporal thickness of protein from the monolayer model. Each vertical axis shows wavelengths from 500 nm to 700 nm from top to bottom. Colors represent nanometers of protein thickness. Smaller value indicates better fit.*

of the model suitability evaluation. Ti_{nano} shows consistently good fit of the model. Still, this might indicate that the model evaluation is more sensitive to the sample material as all surfaces Ti, Ti_{HT}, and Ti_{nano} are essentially measured on titanium. However, we must note that the Figure 5.24 shows low thickness values for Ti_{nano}. If the changes are small, this type of evaluation of goodness of the fit is not reliable.

On the basis of data in Figure 5.24, there is some access to the spectral statistics of the formation of temporal monolayer. Each horizontal line in the sub–images of Figure 5.24 show a temporal thickness evaluation for one wavelength. If we assume that the model is correct, then all such lines should statistically describe a temporal monolayer thickness. Thus, all samples were evaluated by calculating a median of all the temporal signals over the wavelengths. Figure 5.26 shows such statistics for Ti and Ti_{HT} surfaces,

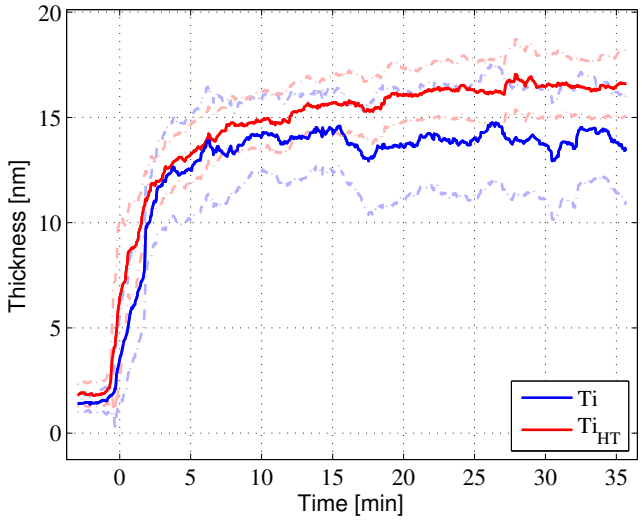

Figure 5.26: *Statistical thickness calculated from all measured temporal spectra for Ti and Ti_{HT} samples. Time axis shows time from HPF injection. The lighter plots show the standard deviation per sample.*

the valid model surfaces. Both a median signal and standard deviation contours are shown. As we can see, very little difference could be in the titanium surfaces; despite some of the spectral differences, the surfaces behave statistically the same. This, however, could be a misinterpretation. As the theory concerns pure titanium, the model could predict small differences while this particular model could indicate that the surfaces are quite equal regarding adsorption. While the errors seem the same, this is not sufficient data indicating that the model would be perfect for both. This is due to the underlying changes that could have been caused by the heat treatment (see Figure 5.3 on page 134). However, for clarity, we will assume the Ti and Ti_{HT} surface equal as adsorbent from now on.

Finally, the statistical observation of model goodness can be performed for all samples. Figure 5.27 shows one such a plot. Standard deviations are not shown for clarity, but what is clear is the fact that the error (Ψ and Δ predicted thickness difference) is smallest for all of the titanium samples. This is not surprising, as the adsorbent

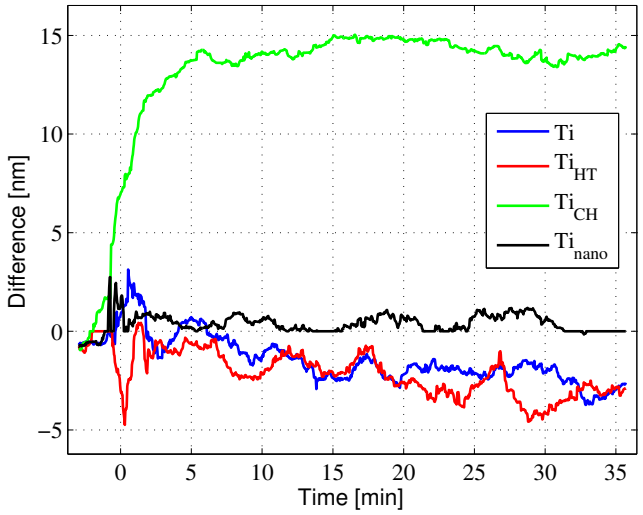

Figure 5.27: *Difference if* Ψ *and* Δ *predicted adsorbed protein thickness in the monolayer model.*

refractive index in dominant in any liquid environment photonic model, but what is interesting is that there is a trend in this goodness evaluation. One interpretation could be that if the model is for monolayer, there might be some transition states, that occur before the final adsorption state is formed. Other indication of Figure 5.27 is, that a monolayer is not a sufficient model in temporal domain. The values of Ti_{nano} are very low, but also cutting to zero in several places. This is explained with the small overall signal values with Ti_{nano} measurements. It also indicates that this goodness evaluation fails with extremely small signal changes, but if there is no signal, we can also conclude, that the nanoparticles are just not adsorbing from the cuvette volume onto the titanium, or that our device cannon detect them.

Similarly, the statistical difference of the Ψ and Δ calculated monolayer thicknesses, after 30 minutes from injection, is presented in Figure 5.28, for each evaluated refractive index. This figure indicates that statistically all the used different refractive indices appear to be more or less the same. However, the Ti_{CH} shows sys-

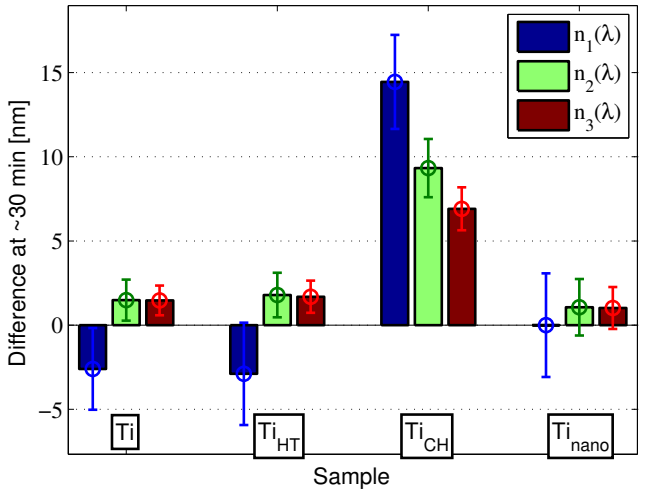

Figure 5.28: *Thickness differences of* Ψ *and* Δ *calculated thicknesses 30 min after the particle injection, for all of the three refractive indices. Smaller values indicate better* Ψ *and* Δ *agreement.*

tematically bad agreement to the model (high difference values), which was to be expected. Furthermore, from Figures 5.15 and 5.16 (pages 150 and 151), we note that the nanoparticles induce overall extremely small changes to Ψ and Δ, which explains the seemingly good model goodness. A possible fix for this could be the usage of inverse of the signal levels as a multiplier. With that, the goodness would always be bad with small signals, which is a fair approximation, because poor signals shouldn't even be considered in the first place.

What can be stated about the three different refractive indices used for the protein monolayer calculations? The calculated end thicknesses after 30 minutes are presented in Figure 5.29, for each sample, using the same titanium based monolayer model with the refractive indices $n_1(\lambda)$, $n_2(\lambda)$, and $n_3(\lambda)$. Recalling from Figures 5.20 and 5.21 (page 156), the increased refractive index for the proteins induced larger changes to Ψ and Δ. And because all of the adsorption results are carried from the numerical model, it

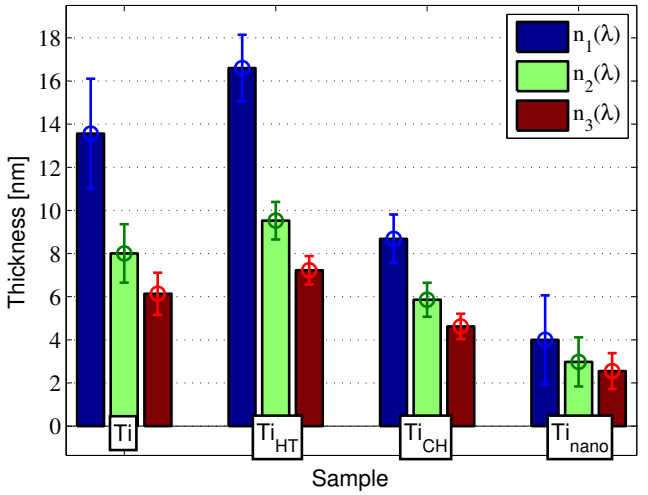

Figure 5.29: *Thickness of the protein monolayer 30 min after from the particle injection, using the three different refractive indices for the proteins.*

is not surprising to see, that the linear fit between signal change and monolayer thickness predicts the largest adsorption towards the surface estimated with $n_1(\lambda)$. In other words, a less dense layer of proteins requires more thickness to induce a certain amount of signal change.

Are the results plausible? As discussed in section 2.7, there can be a wide variety of layer thicknesses in literature, so comparing to those seems irrelevant. But how about, when we compare to the particle dimensions? Now we understand, that our "monolayer" might be a misleading name. We understand it as a monotonic or homogenic layer, rather than a single adsorbed layer of particles. We are not indicating that the particles couldn't adsorb to several layers with density distribution. Figure 5.29 indicates the actual layer thicknesses for Ti and Ti_{HT}, and they seem to be reasonable. The crystal form of HPF is around 5 nm thick in the narrow side,[g] so the monolayer thickness is plausible for both Ti and Ti_{HT}. The

[g]See Figure B.1 on page 186.

Ti_{CH} and Ti_{nano} are both showing incorrect values as they served as a model goodness discussion, but how about if the adsorbed thickness would be unreasonably low? For example, the case of Ti_{nano} has been calculated with the protein refractive indices. Protein refractive index is much lower than of titanium nanoparticles, which indicates that the layer can be said to be near zero with the nanoparticles, because in general, we can list three explanations for a very low adsorbed layer thicknesses; 1) the adsorption does not occur, 2) the adsorption cannot be sensed, or 3) the adsorption sites are limited. These are all plausible explanations for the case of Ti_{nano} samples. In the case of limited adsorption sites, we might see a few particles on the surface, but due to the low coverage, we could statistically observe much lower monolayer thickness values, than the diameter of a single particle.

5.3 DISCUSSION

5.3.1 Errors and possible contamination sources

The purity of the samples and liquids is the first thing to consider as an error source. Still, a great deal of care was taken during the measurement steps. Samples were stored in a closed container before the measurements and always handled with nitrile gloves which were initially washed in purified water. The water was clean with a conductivity of 10 $M\Omega/cm^{-1}$ and the water storage was performed in sealed glass bottles of 100 ml which were changed every day. The same PBS solution was used throughout the measurements and could be one source of contamination, but a static PBS source was thought to be more important than creating a new one every day. The proteins were stored in a liquid no more than 48 hours and were generally stored in a cold environment and in a crystal form when possible.

Section 5.2.4 presented some discussion on geometric errors, but this needs to be addressed again, especially in regard to the sensor. It used a fiber to couple any signal into the spectrometer sensor. There is a possibility that some error is generated from a misalign-

ment of the fibers. This is because the coupling angle to a small fiber end could be a sensitive factor during any measurement. Similarly, no large scale polarization analyses were performed for the used photonic components. This is not a desired approach as the componets could reveal surprising factors. Due to signal integrity and repeatability, we are sure that the device work, but further optimization through component characterization could be possible.

One clear error source could be the actual thin oxide layer on the titanium. It could create interference with signals, internally with Ti sample, as well as when comparing Ti and Ti_{HT} samples to each other. In general, this would not be an issue, but due to very small signal changes and small layer thicknesses, it could play a role in the analyses.

There is also very little discussion about the actual liquid. The liquid was mixed with a mixer at a slow speed throughout the measurement. This could have some effect on the adsorption phenomenon, on both the attachment and the temporal kinetics of the adsorbing particles.

However, when discussing the liquid itself, the buffer solution must be the biggest error source for the photonic signals. Again, one thing that is left aside. The salt can effect both polarization as well as the adsorption. It is not said, that after the PBS addition, the system is not anymore a pure sample–liquid environment. However, as mentioned above, atomic level evaluation on ions and adsorption, and covering those in the context of photonics, would be quite an endeavor.

Notes on the injection

There are several factors in the injection of particles that can affect the observed kinetics. This is simple to understand because a faster injected particle could show a faster attachment as the liquid generally mixes faster. This again provides a faster particle concentration saturation near the adsorbent surface. At the same time the more slowly injected particles could show a less aggressive kinetic behav-

ior. The injection is very important, especially in studies like this. The cuvette volume is large and the measurements are performed through the actual liquid. All variations and heterogenicity in the liquid could be falsely interpreted in a measured signal.

Some studies avoid this by fully separating the sample from the particle injection. Generally this is done with a flow system where the particles are put into a separate area in a system or by simply having a separate container and valves for the particles. This could, however be a more expensive setup and only solves the injection portion for the adsorption study. Also, more elaborate constructions provide more room for contamination as the system becomes harder to clean. Only thing to do, is to say that the effects of both artificial liquid movements, mixing and injection, are negligible in regard to the end results.

Environment

The environment and used models are the biggest challenge in photonic adsorption detection. Usually all of the effect of ions, such as the ones from salt buffer, are ignored in photonic studies. The only effecting factor claimed are the added particles. But it should be understood that the resulting environment is delegate system with salt and particles, if a salt buffer is used, much like in this study, and especially with photonic signals. However, reason for ignoring the environment is simply the factorial complexity of the system. Thus, in all honesty, the environment can have even strong unforeseen effects to the photonic results.

5.3.2 Results

Device and setup

The first clear results were presented in section 5.2.1 (page 139). There the temporal signal of the fiber spectrometer was introduced. An important note was made about the device. The multi–fiber spectrometer actually enabled small particle observations. As the

observed changes were very low, the signal–level change might not be visible if the light source correction were impossible. We also noted that signal correction is a very good operation because the sample signal and light source signals are measured with the same semiconductor detector. The correction in the data was estimated to be very good, because the noise and the shape improvements were imminent.

The light source was also observed for spectral performance with the HSA isotherm measurements. Interestingly the light source might have some unforeseen properties as the explanation rates for the exponential adsorption isotherm drops after around 750 nm for the light source. This was taken into account in the HPF adsorption part so that only the narrow range of 500 nm to 700 nm was used in calculations. While this is unfortunate since the wavelengths are "lost", it could be given as one result, that the quality and performance of a light source should be the first thing to consider in any photonic measurement, without blindly using the full spectrum of the device. Moreover, the input signal rarely has the same quality than the actual signal that is gone through the measured system.

Adsorption kinetics

The observed adsorption kinetics were rather dull. Only one example was shown in Figure 5.14, which showed the real kinetic signal of assumed adsorption. The observed saturation of the surface seemed to follow a logarithmic trend without dramatic sample to sample differences.

The actual interesting part was found to be after around 20 minutes of particle injection. The signal seemed to evolve, following a different trend. This was not further analyzed, but these long term behaviors could be also helpful in a study where the adsorption behavior, as a phenomenon, is of interest.

Numerical methods

The calculated model was constructed with parallel processing (PAP), which provided a fast way to trace any desired system, albeit with the few limitations discussed (section 4.4.6). Here we also created a multilayer model which indicated that one reason for the historical monolayer observations could be that a the monolayer model is uniquely defined and thus easy to use. Still, a monolayer with a solid interface as adsorption model appears to be a very unnatural approach to adsorbed particles. Despite this, the monolayer approach was further evaluated with several spectral refractive indices. As there was disagreement in the literature on the spectral indices, basically any desired result would be possible to obtain. For example, using three different spectral refractive indices, this study calculated a human plasma fibrinogen (HPF) monolayer of around 14 nm, 8 nm, and 6 nm adsorbed on titanium, depending on the selected refractive indices.

The monolayer model goodness was estimated from the agreement of the Ψ and Δ predicted layer thickness. Only one fixed model was evaluated against proteins and nanoparticles as well as two very much different surfaces. The heat treated surface was not statistically different adsorbent, but the carbon treated sample showed much more different signals. Again, this was done just to check if the model works as intended for the protein and titanium adsorbent and served as an example for model goodness evaluations. Using single model of different particles and surfaces was a second kind of model goodness estimation after the Ψ and Δ agreement. These goodness values were estimated to be reasonable and expected. More goodness estimates would be welcome in adsorption studies, even primitive ones, as the disagreement was also observed to change over time.

Both multilayer and monolayer model showed, that Ψ and Δ changes increase when the density of the layer is increased. Either with different refractive index selection in monolayer model, or with increasing density through multilayer model. This is un-

derstandable, but is also rarely discussed in literature. It would be extremely interesting if, for example, the water association to a adsorbent were found to be dominant in a way, that it would require a very thin layer of water to be modeled on the adsorbent surface, in all cases. This is just an example, but because it is challenging to determine nano–scale atomic and molecular adsorption rules, it could be a possibility. Increasingly so, if a wide variety of samples with different surface energies were under research.

5.3.3 Effect of the model

The effect of the model is the main focus in this study, so we must discuss it in more detail. We have already seen the effect of the selected refractive index, difference of monolayer and multilayer model, as well as some geometrically induced changes. However, what is the environment really like? To discuss this, we consider different hypothetical particle probability distributions P, with distance d_a from an imaginary adsorbent $P(d_a)$. Figure 5.30 shows two monolayer models with altered density (5.30a) and thickness (5.30b).

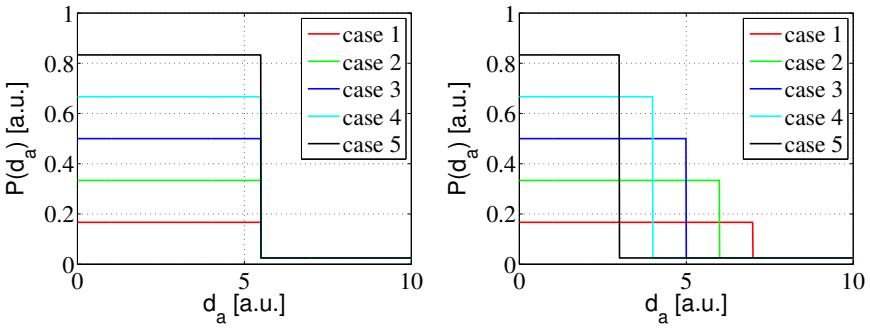

Figure 5.30: *Representation of hypothetical monolayer distribution of particle location probability P near adsorbent $P(d_a)$, with particle distance of d_a from the adsorbent.*

Because the Figure 5.30 shows particle probabilities $P(d_a)$ with

arbitrary units, they must be clarified. We could think, that the surrounding media in the plots of Figure 5.30 is any buffer liquid. We also notice, that in this kind of speculation, the probability of particles is always above zero, and places showing larger probability of particles $P(d_a)$, leads to lower values of buffer probability $P_{\text{buffer}}(d_a)$ so, that the volume is filled with either buffer or particles, with $P(d_a) + P_{\text{buffer}}(d_a) = 1$.

Figure 5.30 also shows different cases for discussion purposes. Indeed, both figures show traditional monolayer models. If the cases shown would be considered in time–wise order, Figure 5.30a would show, reflected to photonic models, a case where the refractive index of adsorbed monolayer thickness increases from case 1 to 5. Similarly, in Figure 5.30b, we could be observing a temporal shift of particle density from the buffer towards the adsorbent, having changing particle density, monolayer thickness, or both, from case 1 to 5. It is clear, that while a photonic model could be easily created from the illustrations of Figure 5.30, we quickly understand that the monolayer might be a silly approximation. Essentially, a monolayer model defines a static predefined limit of interatomic forces, because somehow, in the monolayer model, these forces seem to stop after a certain monolayer thickness or other variable is "satisfied."

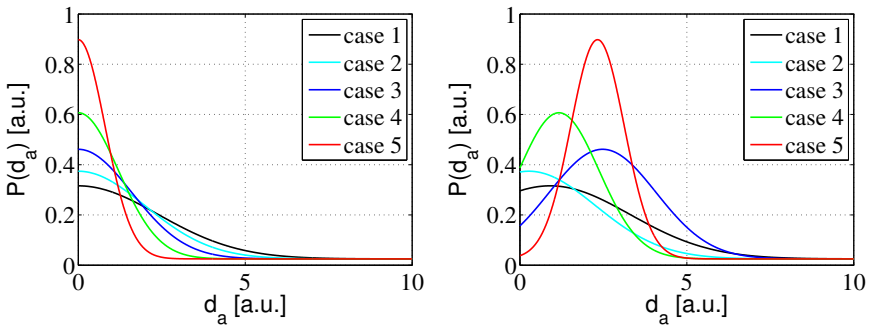

Figure 5.31: *Representation of hypothetical normal (Gaussian) distribution of particle location probability P near adsorbent $P(d_a)$, with particle distance of d_a from the adsorbent.*

Figure 5.31 illustrates more of similar cases as shown in Figure 5.30. We notice, that Figures 5.30b and 5.31a actually represents similar cases. However, the big difference is, that the situation of the particle probability near the adsorbent is more natural in Figure 5.31b. Indeed, the distributions seen in Figure 5.31a are zero–centered normal distributions. With the more natural continuous distribution near the adsorbent, we note, that this could be a natural case, where the adsorbent attracts (from case 1 to 5) the particles near it, through interatomic forces. Unlike in monolayer, here the adsorbed particles could fulfill the requirements of interatomic attraction forces with increased coverage near the adsorbent, thus creating a continuous particle density gradient.

After this we consider, arguably the most realistic model [122], which is presented in Figure 5.31b. We notice, that the particle probability is not necessarily maximized near the surface, but could located elsewhere. This could be the effect of buffer ions, or simply induced by water, as discussed in chapter 2. If the surface would welcome water near it, the probability density center of the particles could remain relatively far from the surface. And if we discuss photonic models, Figure 5.31b comes rather far from the traditional monolayer model of Figure 5.30a. It is also needless to add, that even in the approach of Figure 5.31b, the cases could go in temporal order from 1 to 5, and that the complexity would just increase more.

The commonly seen de Feijter's equation (Equation 2.8, page 64) or similar possible monolayer models, calculate the adsorbed mass by multiplying the cases of Figure 5.30 with a single selected multiplier. But when looking Figure 5.31b, we understand, why it's more plausible and why we are not showing the adsorption as a mass.

Sure, it could be argued, that monolayer is "sufficient" approximation, but the question is, *sufficient for what*? Monolayer will systematically generate error, because it doesn't consider any interatomic basics as well as understandably might generate huge variations between methods and samples. We only conclude, that a monolayer is just a very crude approximation, and if only arbitrary

numbers are searched, it might be "sufficient."

5.3.4 Device selection

Device selection can have an effect on the actual signals that are evaluated, but as this study essentially covers different polarimeters, the theory base is rather the same with all devices. The ellipsometric parameters are describing the state of the photons. This means, that different ellipsometric devices should be comparable to this study. Selection of the different ellipsometers would affect the accuracy and the way, for example, how Ψ and Δ would be revealed.

Still, the selected device might define both the measured environment and used photonic models. Namely, when discussing the three types of photonic devices listed in section 2.7 (starting from page 51), the device selection could effect the results immensely, through the adsorption models. For example, if comparing total internal reflection to surface reflection ellipsometry (this study), we note that even if the electromagnetic field system is completely different, the adsorption system will remain complex, and the detection methods could show differences between them.

Thus, a comparison of different system would be beneficial. One work like this could be the one of Höök *et al.* ([278], 2002). They used both monolayer and *random sequential adsorption* (RSA) model for the theoretical calculations. The study measured adsorbed amount of albumin, fibrinogen, and hemoglobin on titanium surface. Table 5.2 shows the collected results from this work. We note, from Table 5.2 and from discussion in [278], that there are still a lot to cover for really solving the real adsorption environment. Despite of the huge, and seemingly random differences in the results in Table 5.2 between theory and measured values, we think that it is still good, because there is at least effort towards combining the results given with different devices and models. But it is just more proof of the strong device and model dependencies in photonic adsorption studies.

Table 5.2: *Adsorption amounts observed in study of [278]. Showing the theory predicted (Monolayer and RSA) as well as average of measured OWLS and ellipsometry (OWLS/E) protein mass on adsorbent [278]. Number presented in ng/cm^2.*

	Monolayer	RSA	OWLS/E
Albumin	226	129	188 ± 22
Fibrinogen	1050	540	424 ± 19
Hemoglobin	298	170	359 ± 41

Finally, we consider the actual possibilities and sensing type of different photonic devices. As we recall from the Figure 5.31, adsorbed particles could have rather tedious distributions. Then, what should we demand from the equipment? Short answer is, that the sensing should go trough the evaluated distribution of adsorbed particles. That is the only way to make sure that the possible particle gradient is fully interacted by photons. Thus, even if total internal reflection and plasmons might be extremely sensitive, they might not be able to fully explain the particles on the adsorbent. That said, even the reflection methods like ellipsometry are still in the beginning of liquid environment sensing, because the used adsorption models remain ambiguous. Even with ellipsometry, the approach should perhaps be with simplified buffers and particles as well as assumptions of other than monolayer–type adsorption.

5.3.5 Surface characterization

We need to make one important note on the sample surfaces. As discussed above, knowing the adsorbent is one key element in an adsorption study. That said, only a little of that is done in this study. This is actually common photonic approach. Just to visualize with electron and atomic force microscope. However, vast amount of analysis could be possible through more sophisticated surface analysis. Atomic composition of the surface could be further evaluated, for example, with x–ray photoelectron spectroscopy (XPS), and the

atomic force microscopy (AFM) could be extended to measure actual forces.

However, all these things would also require in–depth analysis. We understand, that it is not sufficient to state about titanium surface, that it is, indeed titanium. It is far different to characterize the atom composition to provide a throughout discussion of physical chemistry, rather than studying adsorption with photonic methods. In material science, the interest is to characterize the manufactured surfaces, but in an adsorption study, the analysis should be continued to more complex chemical, and to dispersion force discussion. While this study also misses this analysis, we can already conclude, that it wouldn't be an easy task, and should be the initial focus of the study as well as using appropriately selected devices and simplified buffer solutions.

5.3.6 Accuracy and repeatability of the study

Firstly, sample to sample signals seem very repeatable in this study. The differences are most likely due to small changes in the setup. The ideal situation would a motorized automatic accurate alignment of the measurement beam for all samples. Here the setup is finalized by hand for all samples. The fiber size is so small that even a small change in surface position or surface finishing of the sample in the sample holder allows some photons to avoid the detector fiber. This is not generally a problem, but it can explain small differences from sample to sample.

Secondly, the particle signals: we could claim that the measured signal really comes from the particles, not just from another source such as the HPF protein and the nanoparticles induce different spectral changes in the signal. Not many studies actually do this but the usage of several particle types, would be beneficial to determine if the observed signal is from the particles or some other related change. That is, using both organic and non–organic particles. If, for example, in this stydy, the nanoparticles had created a similar change to that of the organic protein, it would have been an

indication that the particles are not the source of a signal.

Thirdly, it should be mentioned, that the constructed device is extremely simple. Essentially, it contains only two camera polarizers, halogen light source, and detector. For example, it doesn't use waveplate, which would be included in PCSA ellipsometer. It could be argued, that the multi–fiber detector made these measurements possible, because of the signal quality corrections of the parallel signal recording, but it is not uncommon to see a photodiode in PCSA ellipsometers evaluating the light source signal level. So, we conclude, that with cheap elements, you might not get the best result to signal quality, but it is still possible. It should also be noted, that there is no evaluation of data during the measurements, such as rotating optical components to find signal minima (null ellipsometry), and because of this, the constructed device can be said to be functional and robust.

Furthermore, accuracy and repeatability are always key points of any study. Not only internally, but in a way that peers should be able to repeat it. We are confident that the device and models works correctly and the overall results are in fact correct. This, however, does not account for accuracy in any study. For example, the nature of Ψ and Δ direction ambiguity and possible human errors must be considered. This is not, however, so important. It should be clear to the reader that it is not about the accuracy of one study, but more about the goodness of the model. What was the environment? What was the actual model? How was the model goodness estimated? If the goodness has zero evaluation, there is nothing more to say. Figure 5.29 listed several possible monolayer adsorption thicknesses. This was the case because the literature cannot agree on the refractive index of proteins (Table 2.5, page 62). Even if we already understood, that the refractive index could be a surface dependent, there seems to be a trend in shifting these potentially system dependent variables readily, without justification, from system to system.

The aims of this study were listed in section 1.3 and at this point, should have been covered in the discussion. Still, if ideas

about parameters in the particle adsorption still lack clarity, it is not surprising as the literature itself still struggles with the underlying variables. But it is now clear, why the system model shouldn't be a monolayer, but perhaps something more advanced and surface dependent.

5.3.7 Future

Though we are not clairvoyant, biggest progress in the future of photonic liquid environment adsorption detection is still most likely to be seen. The overall aim still seems to focus on the very fundamental properties of model environment, such as liquid self–association and to liquid–to–sample interaction. While some research still focuses on particle–surface interaction, there is no escaping the environment, that surrounds the particles.

The complexity of the whole subject of adsorption might arise from the overlapping of different phenomena. Skimming through the literature of journal papers is sometimes also mind numbing because there are so many studies about the adsorption, that actually provide very little new information about adsorption, but concentrate on sample novelty, devices, and observed signals. Thankfully, not all studies are like this. In particular, work on the systematic and known alteration of surfaces with at least two parallel methods could actually help us to determine the needed parameters. Still, these parameters are usually quite unique per surface and a general solution for surface–buffer interactions with particle adsorption is not likely to emerge, as there are so many system dependent variables. This again highlights the model goodness evaluation importance in a single study.

Seeing the extent of this introduction–level study and discussion of photonics, addition of chemistry and further atomic physics seems unreasonable. Indeed, we could speculate, that a single study or person shouldn't perhaps try to approach the adsorption as a phenomenon. It might be possible, but trying to fully cover all these fundamental variables is troublesome, to say the least.

However, the challenge is, that all of the fundamental phenomenon should always be kept in mind, no matter how small of a slide the study covers, which could prove to be challenging. Finally, and most importantly, if photonic methods are being deployed, both device, and the model approach should be matching the phenomenon, not just using something that is very convenient.

6 Conclusions

This study provided an extensive and critical look at the history of the photonic adsorption detection. The current main points of the phenomena were presented and discussed, covering several decades of research centering on photonic detection. Furthermore, the main photonic methods were introduced and discussed.

In the experimental part, the simplest spectral ellipsometric setup, a rotating analyzer ellipsometer (RAE), was built to study the adsorption of different concentrations of both Human Serum Albumin (HSA) and Human Plasma Fibrinogen (HPF) proteins. The adsorption kinetics in phosphate buffered saline (PBS) buffer solution were measured for those particles as well as for one concentration of nanoparticles. The isotherm of the HSA was observed to validate the device in measuring the protein adsorption while the heavier HPF protein was observed on three different surfaces for discussion. Several other explanations for the photonic signal changes after protein injection were also discussed. The discussion was extended to time and surface types while reflecting the measurements to numerical models of the system.

The numerical method consisted of a ray–tracing system using parallel computing of the Graphics Processing Unit (GPU). It showed remarkable potential in the photonic part, but due to the linearity of ray–tracing the benefits could be even greater in more theoretical field theory calculations in both chemistry and photonics. The constructed imperfect polarimeter was greatly improved by the used detector, multi-fiber spectrometer, which proved to have excellent signal to noise possibilities due to the parallel recording of data on the same semiconductor detector.

The results and theory correspond very well, but this is by no means startling. The constructed models and discussion is sturdily founded on the idea that a more systematic approach to three–dimensional adsorption models is needed even if measuring on

more simplified flat surfaces. The plain monolayer model of adsorption should be abandoned and a greater focus placed on the depth analyses of adsorption. While three–dimensional adsorption study is no easy task to perform, perhaps after all this time, it could be at least time to start.

A On protein chemical compound names

This appendix describes and visualizes some common compounds often related to proteins and particle adsorption. Chemistry is sometimes somewhat difficult to follow because of these non-trivial names. For readers working both in chemistry and in physics Figure A.1 presents the most common compounds related to proteins and their corresponding names.

In this appendix we mark atoms by their corresponding chemical characters. For the sake of reading, all atoms are colored in the visualizations. A grayish color indicates a bond between atoms and a violet square indicates any organic group attaching to that position.

Figure A.1 shows the four most important joining molecules and their names: primary amine, amide, carboxylic acid, and amino acid. They are basic to many compounds, moreso in biology.

When two carboxylic acids form a bond, the resulting $-C(O)NH-$ bond between them is called a peptide bond (the name of the amide in Figure A.1b becomes peptide bond). Similarly, the resulting molecule is a peptide. Proteins and peptides are very long amino acid chains. Not easing the naming, a protein is only separated from peptides by its size. So, essentially, proteins are large combination of peptides. The way amino acids are joined to the long string of acids defines the folding of the protein and identifies it. This also defines its biological function.

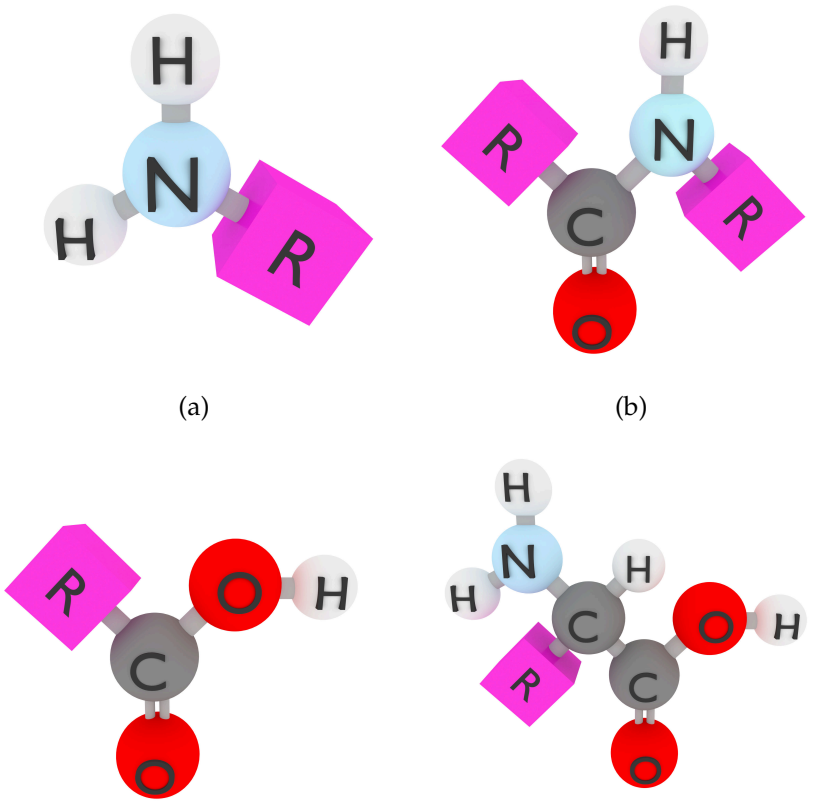

Figure A.1: *Primary chemical compounds of proteins. a) Primary amine, b) amide, c) carboxylic acid, and d) amino acid.*

B Protein shape and scale

Figure B.1 illustrates the scale and shape of a crystal form of two rather commonly used proteins, Human Serum Albumin (HSA) and Human Plasma Fibrinogen (HPF). In the figure, hydrogen atoms are omitted for convenience but otherwise it shows atoms by color. One and ten nanometer diameter spheres for scale are also shown in Figure B.1.

If we are interested in protein structure and functions, the *RCSB Protein Data Bank* is an excellent source for gathering information. There are also numerous existing visualization tools for PC and mobile devices such as *BioJava*. The data bank also provides text files following a certain standard, which makes it possible to create individual visualizations. The visualizations are usually for active chemical groups and certain protein areas, but, for example, Figure B.1 was created by extracting atom data from these text files with a custom program.

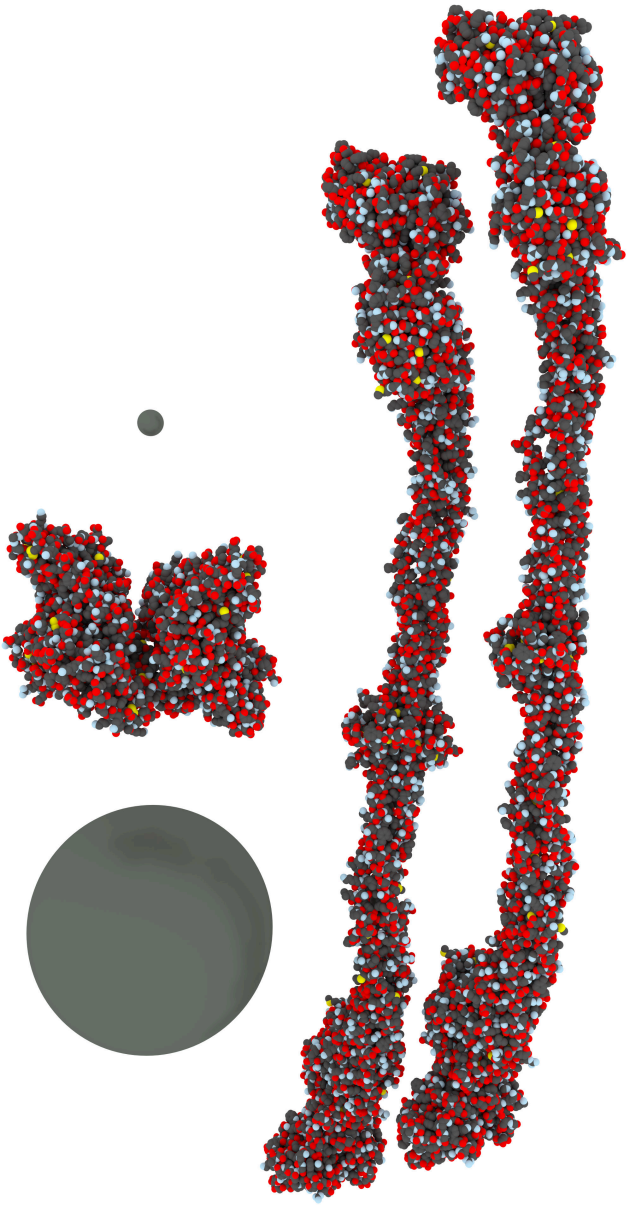

Figure B.1: *The two reported crystal structures of HPF and HSA with a 1 nm and a 10 nm diameter sphere for scale. Atoms in the proteins are carbon (gray), nitrogen (blue), oxygen (red), and sulfur (yellow).*

C Interfering electric fields

Let us assume a electric field of Equation 3.1 (page 69). If we describe this electric field with only the phase ϕ, we can describe it to be a time–independent field

$$E(A,\phi) = E_e = Ae^{\mathrm{i}\phi}. \tag{C.1}$$

Then, the sum E_s of these two fields E_e can be written

$$E_{s2} = E_{e1} + E_{e2} = Ae^{i\phi_1} + Ae^{i\phi_2}, \tag{C.2}$$

which would have the energy (irradiance) of

$$\begin{aligned} I_{s2} = E_s E_s^* &= (Ae^{\mathrm{i}\phi_1} + Ae^{\mathrm{i}\phi_2})(A^*e^{-\mathrm{i}\phi_1} + A^*e^{-\mathrm{i}\phi_2}) \\ &= (Ae^{i\phi_1} + Ae^{\mathrm{i}\phi_2})(A^*e^{-\mathrm{i}\phi_1} + A^*e^{-\mathrm{i}\phi_2}) \\ &= A^*A\left(2 + e^{\mathrm{i}(\phi_1-\phi_2)} + e^{\mathrm{i}(\phi_1+\phi_2)}\right) \\ &= A^*A\left(2 + \cos(\phi_1-\phi_2) + \cancel{\mathrm{i}\sin(\phi_1-\phi_2)}\right. \\ &+ \left.\cos(\phi_2-\phi_1) + \cancel{\mathrm{i}\sin(\phi_2-\phi_1)}\right) \\ &= 2A^*A\left(1 + \cos(\phi_1-\phi_2)\right), \end{aligned}$$

where * denotes a complex conjugate. This creates the final irradiance of these two interfering waves

$$I_{s2} = 2A^*A\left(1 + \cos(\phi_1-\phi_2)\right). \tag{C.3}$$

The irradiance of C.3 is $2A^*A$ as an average, with a minimum of zero, and a maximum of $4A^*A$. Thus, if we desire the scaling of the irradiance to be between zero and one, the E_s should be divided by the square of the number of the photon count. Moreover, the result of C.3 explains why photon fields are often modeled with only a cosine function; both the irradiance and the wave can be described with that approximation. This will create, for example, an

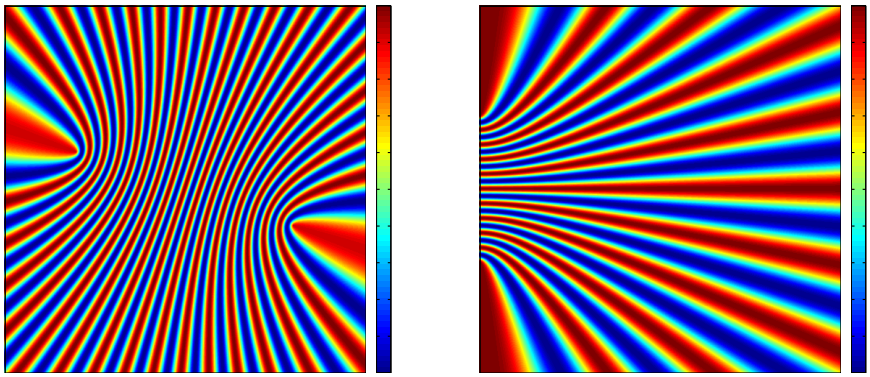

(a) (b)

Figure C.1: *Two dimensional illustration of two electric fields interfering with* $\lambda_{P1} = \lambda_{P2} = 40$. *(a) shows the interference with* $(x_1, y_1) = (100, 200)$ *and* $(x_2, y_2) = (400, 300)$. *(b) shows the interference with* $(x_1, y_1) = (1, 350)$ *and* $(x_2, y_2) = (1, 150)$.

interference of two waves which only discusses the phase difference ϕ_{dif}, because the irradiance can be described as $\cos \phi_{dif}$.

This simple approximation is applicable to a vast number of applications when interfering waves are thought to have no absorbtion or scattering in the observed medium. Figure C.1 shows 500 pixel times 500 pixel images where the horizontal direction is thought to be the x-axis and vertical the y-axis. The figure is shows two waves interfering when the coordinates (x_1, y_1) and (x_2, y_2) are thought to be the point sources. The energy is calculated with Equation C.3 while the phases ϕ_1 and ϕ_2 are thought to have values according to

$$\begin{aligned} \phi_1(x,y) &= \frac{2\pi}{\lambda_{P1}} \left(\sqrt{(x-x_1)^2 + (y-y_1)^2} \right) \\ \phi_2(x,y) &= \frac{2\pi}{\lambda_{P2}} \left(\sqrt{(x-x_2)^2 + (y-y_2)^2} \right), \end{aligned}$$

where x and y are the image coordinates and wavelengths λ_{P1} and λ_{P2} are measured in pixels.

Another interesting feature of Equation C.3 is that the corre-

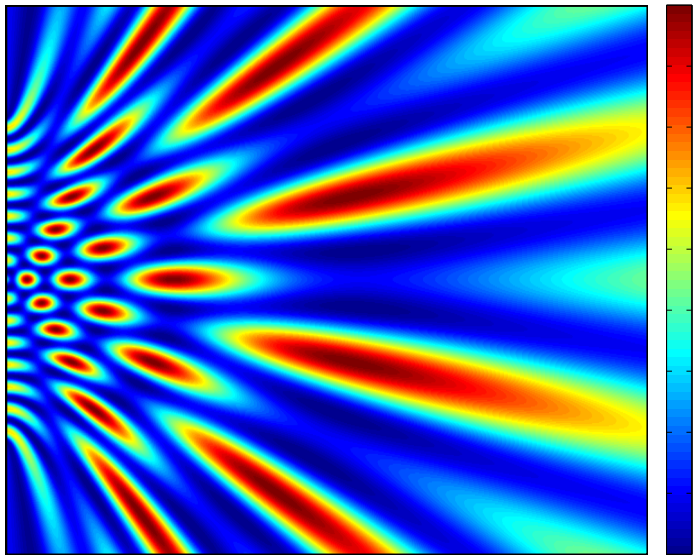

Figure C.2: *Illustration of the spatial irradiance of the interference of three waves where* λ_{P1}=λ_{P2}=$\lambda_{P3} = 40$ *and, correspondingly, the three source locations (x,y) are (1,100), (1,250), and (1,400).*

sponding result with three waves would be

$$I_{s3} = A^2 \left(3 + \cos(\phi_1 - \phi_2) + \cos(\phi_1 - \phi_3) + \cos(\phi_2 - \phi_3)\right). \quad \text{(C.4)}$$

A quick glance at this irradiance could indicate it to be faulty as the static part is 3 and the number two is the multiplier for the cosine functions. Because the range of the cosine is from minus one to plus one, this would indicate an I_{s3} energy range of the A^2 times range $[-3, 9]$. Because all of the angles are evaluated there cannot be a combination of ϕs which would give a phase of $-\pi$ to all terms. Therefore, the energy stays positive at all times. Figure C.2 shows an example of Equation C.4 where all points are indeed positive.

The general form for the interfering wave energy will always have a form $A^2\,(N + [\cdots])$, where N is the number of waves interfering with each other and the $[\cdots]$ part corresponds to all the existing $(N^2 - N)/2$ cosine terms, and real amplitude A is assumed.

If Equation C.2 were defined with realistic fields, there would be

a slight changes. This would mean situation when the amplitudes of two different fields were not the same and always complex. If so, the sum of two fields would be

$$E_{s2} = E_{e1} + E_{e2} = A_1 e^{i\phi_1} + A_2 e^{i\phi_2},$$

which would yield a carried energy of

$$\begin{aligned} I_{s2} &= E_s E_s^* && \text{(C.5)} \\ &= A_1^* A_1 + A_2^* A_2 + (A_1^* A_2 + A_2^* A_1) \cdot \cos(\phi_1 - \phi_2) && \text{(C.6)} \end{aligned}$$

This is very similar to the previous versions. In essence, the field always has the amplitude pairs $A_\mathrm{a}^* A_\mathrm{a}$ and the interference is created with $\left(A_\mathrm{a}^* A_\mathrm{b} + A_\mathrm{b}^* A_\mathrm{a}\right) \cos(\phi_\mathrm{a} - \phi_\mathrm{b})$ when summed over all possible waves a and b. It is important to note is that even in the case of Equation C.5, the field energy is still directly related to the cosine of the field phase differences as the amplitude terms are static.

D Ellipsometric equations

Let us follow Equation (3.47) by opening the components E_p and E_s in reflection

$$\begin{aligned} E_p &= r_p \cos(\alpha_1) A_\mathrm{i} \\ E_p^* &= r_p^* \cos(\alpha_1) A_\mathrm{i}^* \\ E_s &= r_s \sin(\alpha_1) A_\mathrm{i} \\ E_s^* &= r_s^* \sin(\alpha_1) A_\mathrm{i}^*, \end{aligned} \tag{D.1}$$

when the amplitude of the incident field is selected to be A_i. Then (3.47) becomes

$$\begin{aligned} I =& \frac{1}{2}\Big[E_p^* E_p + E_s^* E_s + E_p^* E_p \cos(2\alpha_2) - E_s^* E_s \cos(2\alpha_2) \\ &+ E_p^* E_s \sin(2\alpha_2) + E_s^* E_p \sin(2\alpha_2)\Big] \\ \frac{2I}{A_\mathrm{i}^* A_\mathrm{i}} =& r_p^* r_p \cos^2(\alpha_1) + r_s^* r_s \sin^2(\alpha_1) \\ &+ \cos(2\alpha_2)\left[r_p^* r_p \cos^2(\alpha_1) - r_s^* r_s \sin^2(\alpha_1)\right] \\ &+ r_p^* r_s \sin(2\alpha_2)\cos(\alpha_1)\sin(\alpha_1) \\ &+ r_s^* r_p \sin(2\alpha_2)\cos(\alpha_1)\sin(\alpha_1) \\ \frac{2I}{A_\mathrm{i}^* A_\mathrm{i}} =& \left[r_p^* r_p \cos^2(\alpha_1) + r_s^* r_s \sin^2(\alpha_1)\right] \\ &\left[1 + \cos(2\alpha_2)\frac{r_p^* r_p \cos^2(\alpha_1) - r_s^* r_s \sin^2(\alpha_1)}{r_p^* r_p \cos^2(\alpha_1) + r_s^* r_s \sin^2(\alpha_1)}\right. \\ &\left. + \sin(2\alpha_2)\frac{\cos(\alpha_1)\sin(\alpha_1)\left[r_p^* r_s + r_s^* r_p\right]}{r_p^* r_p \cos^2(\alpha_1) + r_s^* r_s \sin^2(\alpha_1)}\right] \end{aligned} \tag{D.2}$$

The result of (D.2) is convenient because the terms all can be

written easily.

$$\frac{r_p^* r_p \cos^2(\alpha_1) - r_s^* r_s \sin^2(\alpha_1)}{r_p^* r_p \cos^2(\alpha_1) + r_s^* r_s \sin^2(\alpha_1)} = \frac{\frac{r_p^* r_p \cos^2(\alpha_1)}{r_s^* r_s \sin^2(\alpha_1)} - \frac{r_s^* r_s \sin^2(\alpha_1)}{r_s^* r_s \sin^2(\alpha_1)}}{\frac{r_p^* r_p \cos^2(\alpha_1)}{r_s^* r_s \sin^2(\alpha_1)} + \frac{r_s^* r_s \sin^2(\alpha_1)}{r_s^* r_s \sin^2(\alpha_1)}}, \tag{D.3}$$

which is important to note, because we can connect the $(r_p^* r_p)/(r_s^* r_s)$ relation with (3.27) to be

$$\frac{\frac{r_p^* r_p \cos^2(\alpha_1)}{r_s^* r_s \sin^2(\alpha_1)} - \frac{r_s^* r_s \sin^2(\alpha_1)}{r_s^* r_s \sin^2(\alpha_1)}}{\frac{r_p^* r_p \cos^2(\alpha_1)}{r_s^* r_s \sin^2(\alpha_1)} + \frac{r_s^* r_s \sin^2(\alpha_1)}{r_s^* r_s \sin^2(\alpha_1)}} = \frac{\frac{\tan^2(\Psi) e^{j\Delta} e^{-j\Delta}}{\tan^2(\alpha_1)} - 1}{\frac{\tan^2(\Psi) e^{j\Delta} e^{-j\Delta}}{\tan^2(\alpha_1)} + 1} \tag{D.4}$$

By introducing a new relation

$$\tan(\Psi') = \frac{\tan(\Psi)}{\tan(\alpha_1)} \tag{D.5}$$

we can convert

$$\begin{aligned}
\frac{\tan^2(\Psi') - 1}{\tan^2(\Psi')) + 1} &= \frac{\tan^2(\Psi') - \sin^2(\Psi') - \cos^2(\Psi')}{\tan^2(\Psi')) + 1} \\
&= \frac{\tan^2(\Psi') - \cos^2(\Psi') - \sin^2(\Psi')}{\tan(\Psi') + 1} \\
&= \frac{\tan^2(\Psi') - \cos^2(\Psi') - \tan^2(\Psi')\cos^2(\Psi')}{\tan(\Psi') + 1} \\
&= \frac{\tan^2(\Psi')\left[1 - \cos^2(\Psi')\right] - \cos^2(\Psi')}{\tan(\Psi') + 1} \\
&= \frac{\tan^2(\Psi')\sin^2(\Psi') - \cos^2(\Psi')}{\tan(\Psi') + 1} \\
&= \frac{\left[\sin^2(\Psi') - \cos^2(\Psi')\right]\left[\tan^2(\Psi') + 1\right]}{\tan(\Psi') + 1} \\
&= \sin^2(\Psi') - \cos^2(\Psi')
\end{aligned} \tag{D.6}$$

Using (3.46) this can finally be converted to

$$\begin{aligned}
\frac{\tan^2(\Psi') - 1}{\tan^2(\Psi')) + 1} &= \sin^2(\Psi') - \cos^2(\Psi') \\
&= \sin^2(\Psi') - 1 + \sin^2(\Psi') \\
&= 1 - \cos(2\Psi') - 1 \\
&= -\cos(2\Psi')
\end{aligned} \tag{D.7}$$

There is a similar case with the second fraction of (D.2), which can be edited to

$$
\begin{aligned}
&\frac{\cos(\alpha_1)\sin(\alpha_1)\left[r_p^* r_s + r_s^* r_p\right]}{r_p^* r_p \cos^2(\alpha_1) + r_s^* r_s \sin^2(\alpha_1)} \\
=&\frac{r_p^* r_s \cos^2(\alpha_1)\tan(\alpha_1) + r_s^* r_p \cos^2(\alpha_1)\tan(\alpha_1)}{r_p^* r_p \cos^2(\alpha_1) + r_s^* r_s \sin^2(\alpha_1)} \\
=&\frac{\frac{r_p^* r_s \cos^2(\alpha_1)\tan(\alpha_1)}{r_s^* r_s \sin^2(\alpha_1)} + \frac{r_s^* r_p \cos^2(\alpha_1)\tan(\alpha_1)}{r_s^* r_s \sin^2(\alpha_1)}}{\frac{r_p^* r_p \cos^2(\alpha_1)}{r_s^* r_s \sin^2(\alpha_1)} + \frac{r_s^* r_s \sin^2(\alpha_1)}{r_s^* r_s \sin^2(\alpha_1)}} \\
=&\frac{\frac{\cancel{r_p^* r_s} \cos^2(\alpha_1)\tan(\alpha_1)}{\cancel{r_s^* r_s} \sin^2(\alpha_1)} + \frac{\cancel{r_s^*} r_p \cos^2(\alpha_1)\tan(\alpha_1)}{\cancel{r_s^*} r_s \sin^2(\alpha_1)}}{\frac{r_p^* r_p \cos^2(\alpha_1)}{r_s^* r_s \sin^2(\alpha_1)} + \frac{r_s^* r_s \sin^2(\alpha_1)}{r_s^* r_s \sin^2(\alpha_1)}} \\
=&\frac{\frac{1}{\tan(\alpha_1)}\left[\tan(\Psi)e^{-j\Delta} + \tan(\Psi)e^{j\Delta}\right]}{\frac{\tan^2(\Psi)}{\tan^2(\alpha_1)} + 1} \\
=&\frac{\frac{1}{\tan(\alpha_1)}\left[2\tan(\Psi)\cos(\Delta) - \tan(\Psi)\sin(\Delta) + \tan(\Psi)\sin(\Delta)\right]}{\frac{\tan^2(\Psi)}{\tan^2(\alpha_1)} + 1}
\end{aligned}
\tag{D.8}
$$

Using the relation (D.5) and we obtain

$$
\begin{aligned}
\frac{2\tan(\Psi')}{\tan(\Psi')+1} &= 2\cos(\Delta)\frac{\tan(\Psi')\left[\cos^2(\Psi') + \sin^2(\Psi')\right]}{\tan(\Psi')+1} \\
&= 2\cos(\Delta)\frac{\frac{\sin(\Psi')}{\cos(\Psi')}\cos^2(\Psi') + \tan(\Psi')\sin^2(\Psi')}{\tan^2(\Psi')+1} \\
&= 2\cos(\Delta)\frac{\sin(\Psi')\cos(\Psi') + \tan(\Psi')\sin^2(\Psi')}{\tan^2(\Psi')+1} \\
&= 2\cos(\Delta)\frac{\sin(\Psi')\cos(\Psi')\left[\tan^2(\Psi')+1\right]}{\tan^2(\Psi')+1} \\
&= 2\cos(\Delta)\sin(\Psi')\cos(\Psi') \\
&= \cancel{2}\cos(\Delta)\frac{\cancel{1}}{\cancel{2}}\sin(2\Psi') \\
&= \cos(\Delta)\sin(2\Psi')
\end{aligned}
\tag{D.9}
$$

With the cleaned ratios (D.7) and (D.9) we can rewrite (D.2). Bearing in mind (D.1), the system output energy will become

$$\begin{aligned} I =& \frac{1}{2}\left[1-\cos(2\alpha_2)\cos(2\Psi')+\sin(2\alpha_2)\cos(\Delta)\sin(2\Psi')\right] \\ & \left[E_p^* E_p + E_s^* E_s\right] \end{aligned} \tag{D.10}$$

Because the Stokes parameter defines (3.48), page 86, the output can be written to

$$I = \frac{1}{2} s_0 \left[1-\cos(2\alpha_2)\cos(2\Psi')+\sin(2\alpha_2)\cos(\Delta)\sin(2\Psi')\right] \tag{D.11}$$

Furthermore, when comparing this result to the output (3.47) calculated on page 86 the relation between the Stokes parameters and the ellipsometric parameters Ψ and Δ can be clarified.

$$\begin{aligned} I &= \frac{1}{2}\left[s_0 + s_1\cos(2\alpha_2) + s_2\sin(2\alpha_2)\right] \\ I &= \frac{1}{2}\left[s_0 - s_0\cos(2\alpha_2)\cos(2\Psi') + s_0\sin(2\alpha_2)\cos(\Delta)\sin(2\Psi')\right] \end{aligned} \tag{D.12}$$

$$\begin{aligned} \cos(2\Psi') &= -\frac{s_1}{s_0} \\ \cos(\Delta)\sin(2\Psi') &= \frac{s_2}{s_0} \end{aligned} \tag{D.13}$$

It is evident that the ellipsometric parameters also support the imperfect polarimeter as the Stokes parameter s_3 is absent from Equations D.13.

Bibliography

[1] P. Cuypers, W. Hermens, and H. Hemker, "Ellipsometry as a tool to study protein films at liquid-solid interfaces," *Analytical biochemistry* **84,** 56–67 (1978).

[2] R. L. Baldwin, "Intermediates in protein folding reactions and the mechanism of protein folding," *Annual review of biochemistry* **44,** 453–475 (1975).

[3] F. M. Richards, "Areas, volumes, packing, and protein structure," *Am. Rev. Biophys. Bioeng.* (1977).

[4] I. Langmuir, "The adsorption of gases on plane surfaces of glass, mica and platinum.," *Journal of the American Chemical society* **40,** 1361–1403 (1918).

[5] I. Langmuir and V. J. Schaefer, "Properties and Structure of Protein Monolayers.," *Chemical Reviews* **24,** 181–202 (1939).

[6] H. Elwing, "Protein absorption and ellipsometry in biomaterial research," *Biomaterials* **19,** 397–406 (1998).

[7] E. A. Vogler, "Protein adsorption in three dimensions," *Biomaterials* **33,** 1201–1237 (2012).

[8] C. Chothia, "Structural invariants in protein folding," *Nature* **254,** 304–308 (1975).

[9] H. Andree, C. Reutelingsperger, R. Hauptmann, H. C. Hemker, W. T. Hermens, and G. Willems, "Binding of vascular anticoagulant alpha (VAC alpha) to planar phospholipid bilayers.," *Journal of Biological Chemistry* **265,** 4923–4928 (1990).

[10] E. A. Scott, M. D. Nichols, L. H. Cordova, B. J. George, Y.-S. Jun, and D. L. Elbert, "Protein adsorption and cell adhesion on nanoscale bioactive coatings formed from poly (ethylene glycol) and albumin microgels," *Biomaterials* **29,** 4481–4493 (2008).

[11] V. Shubin, "Adsorption of cationic polymer onto negatively charged surfaces in the presence of anionic surfactant," *Langmuir* **10,** 1093–1100 (1994).

[12] P. Alexandridis, "Amphiphilic copolymers and their applications," *Current Opinion in Colloid & Interface Science* **1,** 490–501 (1996).

[13] E. Murphy, J. Lu, A. Lewis, J. Brewer, J. Russell, and P. Stratford, "Characterization of protein adsorption at the phosphorylcholine incorporated polymer-water interface," *Macromolecules* **33,** 4545–4554 (2000).

[14] G. Ladam, P. Schaad, J. Voegel, P. Schaaf, G. Decher, and F. Cuisinier, "In situ determination of the structural properties of initially deposited polyelectrolyte multilayers," *Langmuir* **16,** 1249–1255 (2000).

[15] A. P. Ngankam, G. Mao, and P. R. Van Tassel, "Fibronectin adsorption onto polyelectrolyte multilayer films," *Langmuir* **20,** 3362–3370 (2004).

[16] N. Sheller, S. Petrash, M. Foster, and V. Tsukruk, "Atomic force microscopy and X-ray reflectivity studies of albumin adsorbed onto self-assembled monolayers of hexadecyltrichlorosilane," *Langmuir* **14,** 4535–4544 (1998).

[17] H. Nygren, C. Eriksson, and J. Lausmaa, "Adhesion and activation of platelets and polymorphonuclear granulocyte cells at TiO 2 surfaces," *Journal of Laboratory and Clinical Medicine* **129,** 35–46 (1997).

[18] J. C. Schmit and S. Brody, "Biochemical genetics of Neurospora crassa conidial germination.," *Bacteriological reviews* **40,** 1 (1976).

[19] R. Urfer and K. Kirschner, "The importance of surface loops for stabilizing an eightfold $\beta\alpha$ barrel protein," *Protein Science* **1,** 31–45 (1992).

[20] D. F. Williams, "On the nature of biomaterials," *Biomaterials* **30,** 5897–5909 (2009).

[21] K. Rezwan, Q. Chen, J. Blaker, and A. R. Boccaccini, "Biodegradable and bioactive porous polymer/inorganic composite scaffolds for bone tissue engineering," *Biomaterials* **27,** 3413–3431 (2006).

[22] D. W. Hutmacher, "Scaffolds in tissue engineering bone and cartilage," *Biomaterials* **21,** 2529–2543 (2000).

[23] K. J. Burg, S. Porter, and J. F. Kellam, "Biomaterial developments for bone tissue engineering," *Biomaterials* **21,** 2347–2359 (2000).

[24] D.-A. Wang, S. Varghese, B. Sharma, I. Strehin, S. Fermanian, J. Gorham, D. H. Fairbrother, B. Cascio, and J. H. Elisseeff, "Multifunctional chondroitin sulphate for cartilage tissue–biomaterial integration," *Nature materials* **6,** 385–392 (2007).

[25] M. Lampin, R. Warocquier-Clérout, C. Legris, M. Degrange, and M. Sigot-Luizard, "Correlation between substratum roughness and wettability, cell adhesion, and cell migration," *Journal of biomedical materials research* **36,** 99–108 (1997).

[26] J. E. Babensee, "Interaction of dendritic cells with biomaterials," in *Seminars in immunology*, Vol. 20 (Elsevier, 2008), pp. 101–108.

[27] S. Franz, S. Rammelt, D. Scharnweber, and J. C. Simon, "Immune responses to implants–a review of the implications for the design of immunomodulatory biomaterials," *Biomaterials* **32,** 6692–6709 (2011).

[28] Y. H. An and R. J. Friedman, "Concise review of mechanisms of bacterial adhesion to biomaterial surfaces.," *Journal of biomedical materials research* 338–48 (1998).

[29] Y.-L. Ong, A. Razatos, G. Georgiou, and M. M. Sharma, "Adhesion Forces between E. c oli Bacteria and Biomaterial Surfaces," *Langmuir* **15,** 2719–2725 (1999).

[30] F. Furno, K. S. Morley, B. Wong, B. L. Sharp, P. L. Arnold, S. M. Howdle, R. Bayston, P. D. Brown, P. D. Winship, and H. J. Reid, "Silver nanoparticles and polymeric medical devices: a new approach to prevention of infection?," *Journal of Antimicrobial Chemotherapy* **54,** 1019–1024 (2004).

[31] V. Karageorgiou and D. Kaplan, "Porosity of 3D biomaterial scaffolds and osteogenesis," *Biomaterials* **26,** 5474–5491 (2005).

[32] T. C. Holmes, "Novel peptide-based biomaterial scaffolds for tissue engineering," *TRENDS in Biotechnology* **20,** 16–21 (2002).

[33] M. Geetha, A. Singh, R. Asokamani, and A. Gogia, "Ti based biomaterials, the ultimate choice for orthopaedic implants–a review," *Progress in Materials Science* **54,** 397–425 (2009).

[34] K. Anselme, "Osteoblast adhesion on biomaterials," *Biomaterials* **21,** 667–681 (2000).

[35] Y.-T. Sul, C. B. Johansson, Y. Jeong, and T. Albrektsson, "The electrochemical oxide growth behaviour on titanium in acid and alkaline electrolytes," *Medical engineering & physics* **23,** 329–346 (2001).

[36] X. Liu, P. K. Chu, and C. Ding, "Surface modification of titanium, titanium alloys, and related materials for biomedical applications," *Materials Science and Engineering: R: Reports* **47,** 49–121 (2004).

[37] H. Nygren, P. Tengvall, and I. Lundstroem, "The initial reactions of TiO2 with blood," *Journal of biomedical materials research* **34,** 487–492 (1997).

[38] M. Long and H. Rack, "Titanium alloys in total joint replacementa materials science perspective," *Biomaterials* **19,** 1621–1639 (1998).

[39] T. Albrektsson, P.-I. Brånemark, H.-A. Hansson, and J. Lindström, "Osseointegrated titanium implants: requirements for ensuring a long-lasting, direct bone-to-implant anchorage in man," *Acta Orthopaedica* **52,** 155–170 (1981).

[40] D. S. Grubisha, R. J. Lipert, H.-Y. Park, J. Driskell, and M. D. Porter, "Femtomolar detection of prostate-specific antigen: an immunoassay based on surface-enhanced Raman scattering and immunogold labels," *Analytical chemistry* **75,** 5936–5943 (2003).

[41] M. P. Staiger, A. M. Pietak, J. Huadmai, and G. Dias, "Magnesium and its alloys as orthopedic biomaterials: a review," *Biomaterials* **27,** 1728–1734 (2006).

[42] F. Witte, "The history of biodegradable magnesium implants: a review," *Acta Biomaterialia* **6,** 1680–1692 (2010).

[43] K. H. Stenzel, T. Miyata, and A. L. Rubin, "Collagen as a biomaterial," *Annual review of biophysics and bioengineering* **3,** 231–253 (1974).

[44] M. P. Lutolf, G. P. Raeber, A. H. Zisch, N. Tirelli, and J. A. Hubbell, "Cell-Responsive Synthetic Hydrogels," *Advanced Materials* **15,** 888–892 (2003).

[45] S. Kiyonaka, K. Sada, I. Yoshimura, S. Shinkai, N. Kato, and I. Hamachi, "Semi-wet peptide/protein array using supramolecular hydrogel," *Nature materials* **3,** 58–64 (2004).

[46] E. Khor and L. Y. Lim, "Implantable applications of chitin and chitosan," *Biomaterials* **24,** 2339–2349 (2003).

[47] G. H. Altman, F. Diaz, C. Jakuba, T. Calabro, R. L. Horan, J. Chen, H. Lu, J. Richmond, and D. L. Kaplan, "Silk-based biomaterials," *Biomaterials* **24,** 401–416 (2003).

[48] C. Piconi and G. Maccauro, "Zirconia as a ceramic biomaterial," *Biomaterials* **20,** 1–25 (1999).

[49] M. Shim, N. W. Shi Kam, R. J. Chen, Y. Li, and H. Dai, "Functionalization of carbon nanotubes for biocompatibility and biomolecular recognition," *Nano Letters* **2,** 285–288 (2002).

[50] A. Chambers, C. Park, R. T. K. Baker, and N. M. Rodriguez, "Hydrogen storage in graphite nanofibers," *The journal of physical chemistry B* **102,** 4253–4256 (1998).

[51] Y. Ye, C. Ahn, C. Witham, B. Fultz, J. Liu, A. Rinzler, D. Colbert, K. Smith, and R. Smalley, "Hydrogen adsorption and cohesive energy of single-walled carbon nanotubes," *Applied physics letters* **74,** 2307–2309 (1999).

[52] C. J. Wilson, R. E. Clegg, D. I. Leavesley, and M. J. Pearcy, "Mediation of biomaterial-cell interactions by adsorbed proteins: a review," *Tissue engineering* **11,** 1–18 (2005).

[53] J. M. Anderson, A. Rodriguez, and D. T. Chang, "Foreign body reaction to biomaterials," in *Seminars in immunology*, Vol. 20 (Elsevier, 2008), pp. 86–100.

[54] H. Morgan and N. G. Green, *AC Electrokinetics: colloids and nanoparticles* (Research Studies Press LTD., 2003).

[55] R. H. French, "Origins and applications of London dispersion forces and Hamaker constants in ceramics," *Journal of the American Ceramic Society* **83,** 2117–2146 (2000).

[56] H.-J. Butt, B. Cappella, and M. Kappl, "Force measurements with the atomic force microscope: Technique, interpretation and applications," *Surface science reports* **59,** 1–152 (2005).

[57] H. Hamaker, "The Londonvan der Waals attraction between spherical particles," *Physica* **4,** 1058 – 1072 (1937).

[58] R. French, R. Cannon, L. DeNoyer, and Y.-M. Chiang, "Full spectral calculation of non-retarded Hamaker constants for ceramic systems from interband transition strengths," *Solid State Ionics* **75,** 13–33 (1995).

[59] J. B. Rosenholm, K.-E. Peiponen, and E. Gornov, "Materials cohesion and interaction forces," *Advances in colloid and interface science* **141,** 48–65 (2008).

[60] G. Binnig, C. F. Quate, and C. Gerber, "Atomic force microscope," *Physical review letters* **56,** 930 (1986).

[61] J. P. Peltonen, P. He, and J. B. Rosenholm, "Order and defects of Langmuir-Blodgett films detected with the atomic force microscope," *Journal of the American Chemical Society* **114,** 7637–7642 (1992).

[62] A. Weisenhorn, P. Maivald, H.-J. Butt, and P. Hansma, "Measuring adhesion, attraction, and repulsion between surfaces in liquids with an atomic-force microscope," *Physical Review B* **45,** 11226 (1992).

[63] L. Bergström, "Hamaker constants of inorganic materials," *Advances in Colloid and Interface Science* **70,** 125–169 (1997).

[64] B. Cappella and G. Dietler, "Force-distance curves by atomic force microscopy," *Surface science reports* **34,** 1–104 (1999).

[65] R. Garcıa and R. Pérez, "Dynamic atomic force microscopy methods," *Surface science reports* **47,** 197–301 (2002).

[66] G. Raffaini and F. Ganazzoli, "Molecular modelling of protein adsorption on the surface of titanium dioxide polymorphs," *Philosophical Transactions of the Royal Society A: Mathematical, Physical and Engineering Sciences* **370,** 1444–1462 (2012).

[67] H.-m. Ding, W.-d. Tian, and Y.-q. Ma, "Designing nanoparticle translocation through membranes by computer simulations," *Acs Nano* **6,** 1230–1238 (2012).

[68] O. Berger, O. Edholm, and F. Jähnig, "Molecular dynamics simulations of a fluid bilayer of dipalmitoylphosphatidylcholine at full hydration, constant pressure, and constant temperature.," *Biophysical journal* **72,** 2002 (1997).

[69] D. G. Castner and B. D. Ratner, "Biomedical surface science: Foundations to frontiers," *Surface Science* **500,** 28–60 (2002).

[70] M. Landgren and B. Joensson, "Determination of the optical properties of silicon/silica surfaces by means of ellipsometry, using different ambient media," *The Journal of Physical Chemistry* **97,** 1656–1660 (1993).

[71] M. Malmsten and B. Lindman, "Ellipsometry studies of the adsorption of cellulose ethers," *Langmuir* **6,** 357–364 (1990).

[72] M. Wahlgren, T. Arnebrant, and I. Lundström, "The adsorption of lysozyme to hydrophilic silicon oxide surfaces: comparison between experimental data and models for adsorption kinetics," *Journal of colloid and interface science* **175,** 506–514 (1995).

[73] J. Rahn and R. Hallock, "Antibody binding to antigen-coated substrates studied with surface plasmon oscillations," *Langmuir* **11,** 650–654 (1995).

[74] S. Sousa, M. M. Brás, P. Moradas-Ferreira, and M. Barbosa, "Dynamics of fibronectin adsorption on TiO2 surfaces," *Langmuir* **23,** 7046–7054 (2007).

[75] J. C. Riboh, A. J. Haes, A. D. McFarland, C. Ranjit Yonzon, and R. P. Van Duyne, "A nanoscale optical biosensor: real-time immunoassay in physiological buffer enabled by improved nanoparticle adhesion," *The Journal of Physical Chemistry B* **107,** 1772–1780 (2003).

[76] P. Cha, A. Krishnan, V. F. Fiore, and E. A. Vogler, "Interfacial energetics of protein adsorption from aqueous buffer to surfaces with varying hydrophilicity," *Langmuir* **24,** 2553–2563 (2008).

[77] F. Liu, M. Zhou, and F. Zhang, "125I labelling of human serum albumin and fibrinogen and a study of protein adsorption properties on the surface of titanium oxide film," *Applied radiation and isotopes* **49,** 67–72 (1998).

[78] S. A. Hall, P. A. Covert, B. R. Blinn, S. Shakeri, and D. K. Hore, "Rapid and sensitive polarization measurement for characterizing protein adsorption at the solid–liquid interface," *The Journal of Physical Chemistry C* **117,** 1796–1803 (2013).

[79] A. Leung, P. Shankar, and R. Mutharasan, "Real-time monitoring of bovine serum albumin at femtogram/mL levels on antibody-immobilized tapered fibers," *Sensors and Actuators B: Chemical* **123,** 888–895 (2007).

[80] A. J. Haes and R. P. Van Duyne, "A nanoscale optical biosensor: sensitivity and selectivity of an approach based on the localized surface plasmon resonance spectroscopy of triangular silver nanoparticles," *Journal of the American Chemical Society* **124,** 10596–10604 (2002).

[81] J. Noordmans, H. Wormeester, and H. J. Busscher, "Simultaneous monitoring of protein adsorption at the solid–liquid interface from sessile solution droplets by ellipsometry and axisymmetric drop shape analysis by profile," *Colloids and Surfaces B: Biointerfaces* **15,** 227–233 (1999).

[82] A. Lewis, M. Kilburn, I. Papageorgiou, G. Allen, and C. Case, "Effect of synovial fluid, phosphate-buffered saline solution, and water on the dissolution and corrosion properties of CoCrMo alloys as used in orthopedic implants," *Journal of Biomedical Materials Research Part A* **73,** 456–467 (2005).

[83] P. Roach, D. Farrar, and C. C. Perry, "Interpretation of protein adsorption: surface-induced conformational changes," *Journal of the American Chemical Society* **127,** 8168–8173 (2005).

[84] S. He, K.-K. Liu, S. Su, J. Yan, X. Mao, D. Wang, Y. He, L.-J. Li, S. Song, and C. Fan, "Graphene-based high-efficiency surface-enhanced Raman scattering-active platform for sensitive and multiplex DNA detection," *Analytical chemistry* **84,** 4622–4627 (2012).

[85] C. Freij-Larsson, T. Nylander, P. Jannasch, and B. Wesslén, "Adsorption behaviour of amphiphilic polymers at hydrophobic surfaces: effects on protein adsorption," *Biomaterials* **17,** 2199–2207 (1996).

[86] M. Khan, R. Williams, and D. Williams, "The corrosion behaviour of Ti–6Al–4V, Ti–6Al–7Nb and Ti–13Nb–13Zr in protein solutions," *Biomaterials* **20,** 631–637 (1999).

[87] P. Soman, Z. Rice, and C. A. Siedlecki, "Measuring the time-dependent functional activity of adsorbed fibrinogen by atomic force microscopy," *Langmuir* **24,** 8801–8806 (2008).

[88] J.-Y. Zheng, R. M. Pasternack, and N. N. Boustany, "Optical scatter imaging with a digital micromirror device," *Opt. Express* **17,** 20401–20414 (2009).

[89] S. R. Kim, M. S. Rhee, B. C. Kim, H. Lee, and K. H. Kim, "Modeling of the inactivation of¡ i¿ Salmonella typhimurium¡/i¿ by supercritical carbon dioxide in physiological saline and phosphate-buffered saline," *Journal of microbiological methods* **70,** 132–141 (2007).

[90] J. J. Storhoff, S. S. Marla, P. Bao, S. Hagenow, H. Mehta, A. Lucas, V. Garimella, T. Patno, W. Buckingham, W. Cork, et al., "Gold nanoparticle-based detection of genomic DNA targets on microarrays using a novel optical detection system," *Biosensors and Bioelectronics* **19,** 875–883 (2004).

[91] L. Lindh, T. Arnebrant, P.-E. Isberg, and P.-O. Glantz, "Concentration dependence of adsorption from human whole resting saliva at solid/liquid interfaces: an ellipsometric study," *Biofouling* **14,** 189–196 (1999).

[92] E. Brynda, M. Houska, A. Brandenburg, and A. Wikerstål, "Optical biosensors for real-time measurement of analytes in blood plasma," *Biosensors and Bioelectronics* **17,** 665–675 (2002).

[93] A. Klomp, G. Engbers, J. Mol, J. Terlingen, and J. Feijen, "Adsorption of proteins from plasma at polyester non-wovens," *Biomaterials* **20,** 1203–1211 (1999).

[94] C.-Y. Chiang, M.-L. Hsieh, K.-W. Huang, L.-K. Chau, C.-M. Chang, and S.-R. Lyu, "Fiber-optic particle plasmon resonance sensor for detection of interleukin-1β in synovial fluids," *Biosensors and Bioelectronics* **26,** 1036–1042 (2010).

[95] N. Huang, P. Yang, Y. Leng, J. Chen, H. Sun, J. Wang, G. Wang, P. Ding, T. Xi, and Y. Leng, "Hemocompatibility of titanium oxide films," *Biomaterials* **24,** 2177–2187 (2003).

[96] P. Tengvall, I. Lundström, and B. Liedberg, "Protein adsorption studies on model organic surfaces: an ellipsometric and infrared spectroscopic approach," *Biomaterials* **19,** 407–422 (1998).

[97] B. Brando, W. Göhde, B. Scarpati, and G. D'Avanzo, "The vanishing counting bead phenomenon: Effect on absolute CD34+ cell counting in phosphate-buffered saline-diluted leukapheresis samples," *Cytometry* **43,** 154–160 (2001).

[98] M. S. McAfee, H. Zhang, and O. Annunziata, "Amplification of salt-induced polymer diffusiophoresis by increasing salting-out strength," *Langmuir* **30,** 12210–12219 (2014).

[99] H. Li, T. R. Pereira, B. J. Teppen, D. A. Laird, C. T. Johnston, and S. A. Boyd, "Ionic strength-induced formation of smectite quasicrystals enhances nitroaromatic compound sorption," *Environmental science & technology* **41,** 1251–1256 (2007).

[100] P. Somasundaran and L. Huang, "Adsorption/aggregation of surfactants and their mixtures at solid–liquid interfaces," *Advances in colloid and interface science* **88,** 179–208 (2000).

[101] V. Parsegian and T. Zemb, "Hydration forces: Observations, explanations, expectations, questions," *Current Opinion in Colloid & Interface Science* **16,** 618–624 (2011).

[102] J. Israelachvili and R. Pashley, "The hydrophobic interaction is long range, decaying exponentially with distance," *Nature* 341–342 (1982).

[103] D. Chandler, "Interfaces and the driving force of hydrophobic assembly," *Nature* **437,** 640–647 (2005).

[104] R. B. Bjorklund and H. Arwin, "Ellipsometric study of anionic surfactant adsorption on apatite and calcite ore surfaces," *Langmuir* **8,** 1709–1714 (1992).

[105] R. B. Bjorklund, S. Zangooie, and H. Arwin, "Adsorption of surfactants in porous silicon films," *Langmuir* **13,** 1440–1445 (1997).

[106] S. Zangooie, R. Bjorklund, and H. Arwin, "Protein adsorption in thermally oxidized porous silicon layers," *Thin Solid Films* **313,** 825–830 (1998).

[107] D. van Noort and C.-F. Mandenius, "Porous gold surfaces for biosensor applications," *Biosensors and Bioelectronics* **15,** 203–209 (2000).

[108] A. Álvarez-Herrero, R. L. Heredero, E. Bernabeu, and D. Levy, "Adsorption of water on porous Vycor glass studied by ellipsometry," *Applied optics* **40,** 527–532 (2001).

[109] H. Arwin, "Spectroscopic ellipsometry for characterization and monitoring of organic layers," *physica status solidi (a)* **188,** 1331–1338 (2001).

[110] L. Karlsson, P. Tengvall, I. Lundström, and H. Arwin, "Penetration and loading of human serum albumin in porous silicon layers with different pore sizes and thicknesses," *Journal of colloid and interface science* **266,** 40–47 (2003).

[111] L. Karlsson, M. Schubert, N. Ashkenov, and H. Arwin, "Protein adsorption in porous silicon gradients monitored by spatially-resolved spectroscopic ellipsometry," *Thin solid films* **455,** 726–730 (2004).

[112] C. Pacholski, M. Sartor, M. J. Sailor, F. Cunin, and G. M. Miskelly, "Biosensing using porous silicon double-layer interferometers: reflective interferometric Fourier transform spectroscopy," *Journal of the American Chemical Society* **127,** 11636–11645 (2005).

[113] Z. Chen, J. Jiang, G. Shen, and R. Yu, "Impedance immunosensor based on receptor protein adsorbed directly on porous gold film," *Analytica chimica acta* **553,** 190–195 (2005).

[114] N. A. Yebo, P. Lommens, Z. Hens, and R. Baets, "An integrated optic ethanol vapor sensor based on a silicon-on-insulator microring resonator coated with a porous ZnO film," *Optics Express* **18,** 11859–11866 (2010).

[115] C. Boissiere, D. Grosso, S. Lepoutre, L. Nicole, A. B. Bruneau, and C. Sanchez, "Porosity and mechanical properties of mesoporous thin films assessed by environmental ellipsometric porosimetry," *Langmuir* **21,** 12362–12371 (2005).

[116] A. Hodgson and S. Haq, "Water adsorption and the wetting of metal surfaces," *Surface Science Reports* **64,** 381–451 (2009).

[117] T. Kopac, K. Bozgeyik, and J. Yener, "Effect of pH and temperature on the adsorption of bovine serum albumin onto titanium dioxide," *Colloids and Surfaces A: Physicochemical and Engineering Aspects* **322,** 19–28 (2008).

[118] M. Haruta, "Size-and support-dependency in the catalysis of gold," *Catalysis Today* **36,** 153–166 (1997).

[119] V. Shibaev, A. Bobrovsky, and N. Boiko, "Photoactive liquid crystalline polymer systems with light-controllable structure and optical properties," *Progress in Polymer Science* **28,** 729–836 (2003).

[120] C. M. Roth and A. M. Lenhoff, "Electrostatic and van der Waals contributions to protein adsorption: comparison of theory and experiment," *Langmuir* **11,** 3500–3509 (1995).

[121] K. E. Healy and P. Ducheyne, "The mechanisms of passive dissolution of titanium in a model physiological environment," *Journal of Biomedical Materials Research* **26,** 319–338 (1992).

[122] D. G. Angelescu, T. Nylander, L. Piculell, P. Linse, B. Lindman, J. Tropsch, and J. Detering, "Adsorption of Branched-Linear Polyethyleneimine–Ethylene Oxide Conjugate on Hydrophilic Silica Investigated by Ellipsometry and Monte Carlo Simulations," *Langmuir* **27,** 9961–9971 (2011).

[123] W. M. de Vos, P. M. Biesheuvel, A. de Keizer, J. M. Kleijn, and M. A. Cohen Stuart, "Adsorption of the protein bovine serum albumin in a planar poly (acrylic acid) brush layer as measured by optical reflectometry," *Langmuir* **24,** 6575–6584 (2008).

[124] K. Imamura, M. Shimomura, S. Nagai, M. Akamatsu, and K. Nakanishi, "Adsorption characteristics of various proteins to a titanium surface," *Journal of bioscience and bioengineering* **106,** 273–278 (2008).

[125] M. Malmsten, D. Muller, and B. Lassen, "Sequential adsorption of human serum albumin (HSA), immunoglobulin G (IgG), and fibrinogen (Fgn) at HMDSO plasma polymer surfaces," *Journal of colloid and interface science* **193,** 88–95 (1997).

[126] C. Maechling-Strasser, P. Déjardin, J. C. Galin, and A. Schmitt, "Preadsorption of polymers on glass and silica to reduce fibrinogen adsorption," *Journal of Biomedical Materials Research* **23,** 1385–1393 (1989).

[127] T. Young, "An essay on the cohesion of fluids," *Philosophical Transactions of the Royal Society of London* 65–87 (1805).

[128] N. Churaev, "Contact angles and surface forces," *Advances in Colloid and Interface Science* **58,** 87–118 (1995).

[129] J. M. Berg, L. T. Eriksson, P. M. Claesson, and K. G. N. Borve, "Three-component Langmuir-Blodgett films with a controllable degree of polarity," *Langmuir* **10,** 1225–1234 (1994).

[130] E. A. Vogler, "Structure and reactivity of water at biomaterial surfaces," *Advances in Colloid and Interface Science* **74,** 69–117 (1998).

[131] Y. Sugita, K. Ishizaki, F. Iwasa, T. Ueno, H. Minamikawa, M. Yamada, T. Suzuki, and T. Ogawa, "Effects of pico-to-nanometer-thin TiO¡ sub¿ 2¡/sub¿ coating on the biological properties of microroughened titanium," *Biomaterials* **32,** 8374–8384 (2011).

[132] S. Sugio, A. Kashima, S. Mochizuki, M. Noda, and K. Kobayashi, "Crystal structure of human serum albumin at 2.5 Å resolution," *Protein Engineering* **12,** 439–446 (1999).

[133] S. Meng, E. Wang, and S. Gao, "Water adsorption on metal surfaces: A general picture from density functional theory studies," *Physical Review B* **69,** 195404 (2004).

[134] R. S. Rowland and R. Taylor, "Intermolecular nonbonded contact distances in organic crystal structures: Comparison with distances expected from van der Waals radii," *The Journal of Physical Chemistry* **100,** 7384–7391 (1996).

[135] A. Bondi, "van der Waals volumes and radii," *The Journal of physical chemistry* **68,** 441–451 (1964).

[136] P. Adlercreutz, "On the importance of the support material for enzymatic synthesis in organic media," *European Journal of Biochemistry* **199,** 609–614 (1991).

[137] L. Shi and K. D. Caldwell, "Mucin adsorption to hydrophobic surfaces," *Journal of colloid and interface science* **224,** 372–381 (2000).

[138] J. Kijlstra, K. Reihs, and A. Klamt, "Roughness and topology of ultra-hydrophobic surfaces," *Colloids and Surfaces A: Physicochemical and Engineering Aspects* **206,** 521–529 (2002).

[139] N. Churaev and V. Sobolev, "Wetting of low-energy surfaces," *Advances in colloid and interface science* **134,** 15–23 (2007).

[140] D. Bonn, J. Eggers, J. Indekeu, J. Meunier, and E. Rolley, "Wetting and spreading," *Reviews of modern physics* **81,** 739 (2009).

[141] J. Phillips, D. Kelly, L. Radovic, and F. Xie, "Microcalorimetric study of the influence of surface chemistry on the adsorption of water by high surface area carbons," *The Journal of Physical Chemistry B* **104,** 8170–8176 (2000).

[142] C. D. Hatch, J. S. Wiese, C. C. Crane, K. J. Harris, H. G. Kloss, and J. Baltrusaitis, "Water adsorption on clay minerals as a function of relative humidity: Application of BET and Freundlich adsorption models," *Langmuir* **28,** 1790–1803 (2012).

[143] H. Furukawa, F. Gandara, Y.-B. Zhang, J. Jiang, W. L. Queen, M. R. Hudson, and O. M. Yaghi, "Water adsorption in porous metal–organic frameworks and related materials," *Journal of the American Chemical Society* **136,** 4369–4381 (2014).

[144] H. Rønold, S. Lyngstadaas, and J. Ellingsen, "Analysing the optimal value for titanium implant roughness in bone attachment using a tensile test," *Biomaterials* **24,** 4559–4564 (2003).

[145] K. Rechendorff, M. B. Hovgaard, M. Foss, V. Zhdanov, and F. Besenbacher, "Enhancement of protein adsorption induced by surface roughness," *Langmuir* **22,** 10885–10888 (2006).

[146] L. Ponsonnet, K. Reybier, N. Jaffrezic, V. Comte, C. Lagneau, M. Lissac, and C. Martelet, "Relationship between surface properties (roughness, wettability) of titanium and titanium alloys and cell behaviour," *Materials Science and Engineering: C* **23,** 551–560 (2003).

[147] L.-H. Li, Y.-M. Kong, H.-W. Kim, Y.-W. Kim, H.-E. Kim, S.-J. Heo, and J.-Y. Koak, "Improved biological performance of Ti implants due to surface modification by micro-arc oxidation," *Biomaterials* **25,** 2867–2875 (2004).

[148] K. Cai, J. Bossert, and K. D. Jandt, "Does the nanometre scale topography of titanium influence protein adsorption and cell proliferation?," *Colloids and surfaces B: Biointerfaces* **49,** 136–144 (2006).

[149] F. A. Denis, P. Hanarp, D. S. Sutherland, J. Gold, C. Mustin, P. G. Rouxhet, and Y. F. Dufrêne, "Protein adsorption on model surfaces with controlled nanotopography and chemistry," *Langmuir* **18,** 819–828 (2002).

[150] M. Bereznai, I. Pelsöczi, Z. Toth, K. Turzo, M. Radnai, Z. Bor, and A. Fazekas, "Surface modifications induced by ns and sub-ps excimer laser pulses on titanium implant material," *Biomaterials* **24,** 4197–4203 (2003).

[151] G. Chinga, P. O. Johnsen, R. Dougherty, E. L. Berli, and J. Walter, "Quantification of the 3D microstructure of SC surfaces," *Journal of microscopy* **227,** 254–265 (2007).

[152] P. Parhi, A. Golas, N. Barnthip, H. Noh, and E. A. Vogler, "Volumetric interpretation of protein adsorption: capacity scaling with adsorbate molecular weight and adsorbent surface energy," *Biomaterials* **30,** 6814–6824 (2009).

[153] D. Clerc and W. Lukosz, "Real-time analysis of avidin adsorption with an integrated-optical output grating coupler: adsorption kinetics and optical anisotropy of adsorbed monomolecular layers," *Biosensors and Bioelectronics* **12,** 185–194 (1997).

[154] L. L. Conte, C. Chothia, and J. Janin, "The atomic structure of protein-protein recognition sites," *Journal of molecular biology* **285,** 2177–2198 (1999).

[155] J. M. Kollman, L. Pandi, M. R. Sawaya, M. Riley, and R. F. Doolittle, "Crystal structure of human fibrinogen," *Biochemistry* **48,** 3877–3886 (2009).

[156] Y. Joti, M. Nakasako, A. Kidera, and N. Go, "Nonlinear temperature dependence of the crystal structure of lysozyme: correlation between coordinate shifts and thermal factors," *Acta Crystallographica Section D: Biological Crystallography* **58,** 1421–1432 (2002).

[157] M. M. Dudek, T. L. Lindahl, and A. J. Killard, "Development of a point of care lateral flow device for measuring human plasma fibrinogen," *Analytical chemistry* **82,** 2029–2035 (2010).

[158] P. Ying, A. S. Viana, L. M. Abrantes, and G. Jin, "Adsorption of human serum albumin onto gold: a combined electrochemical and ellipsometric study," *Journal of colloid and interface science* **279,** 95–99 (2004).

[159] L. Galantini, C. Leggio, and N. V. Pavel, "Human serum albumin unfolding: a small-angle x-ray scattering and light scattering study," *The Journal of Physical Chemistry B* **112,** 15460–15469 (2008).

[160] J. A. Kamal, L. Zhao, and A. H. Zewail, "Ultrafast hydration dynamics in protein unfolding: human serum albumin," *Proceedings of the National Academy of Sciences of the United States of America* **101,** 13411–13416 (2004).

[161] X. Wang, L. Yu, C. Li, F. Zhang, Z. Zheng, and X. Liu, "Competitive adsorption behavior of human serum albumin and fibrinogen on titanium oxide films coated on LTI-carbon by IBED," *Colloids and Surfaces B: Biointerfaces* **30,** 111–121 (2003).

[162] A. Tsargorodskaya, A. Nabok, and A. Ray, "Ellipsometric study of the adsorption of bovine serum albumin into porous silicon," *Nanotechnology* **15,** 703 (2004).

[163] C. Postel, O. Abillon, and B. Desbat, "Structure and denaturation of adsorbed lysozyme at the air–water interface," *Journal of colloid and interface science* **266,** 74–81 (2003).

[164] J. R. Lu, M. J. Swann, L. L. Peel, and N. J. Freeman, "Lysozyme adsorption studies at the silica/water interface using dual polarization interferometry," *Langmuir* **20,** 1827–1832 (2004).

[165] N. Barnthip, P. Parhi, A. Golas, and E. A. Vogler, "Volumetric interpretation of protein adsorption: kinetics of protein-adsorption competition from binary solution," *Biomaterials* **30,** 6495–6513 (2009).

[166] H. Noh and E. A. Vogler, "Volumetric interpretation of protein adsorption: competition from mixtures and the Vroman effect," *Biomaterials* **28,** 405–422 (2007).

[167] H. Noh and E. A. Vogler, "Volumetric interpretation of protein adsorption: partition coefficients, interphase volumes, and free energies of adsorption to hydrophobic surfaces," *Biomaterials* **27,** 5780–5793 (2006).

[168] N. Barnthip, H. Noh, E. Leibner, and E. A. Vogler, "Volumetric interpretation of protein adsorption: kinetic consequences of a slowly-concentrating interphase," *Biomaterials* **29,** 3062–3074 (2008).

[169] K. A. Resing, K. Meyer-Arendt, A. M. Mendoza, L. D. Aveline-Wolf, K. R. Jonscher, K. G. Pierce, W. M. Old, H. T. Cheung, S. Russell, J. L. Wattawa, et al., "Improving reproducibility and sensitivity in identifying human proteins by shotgun proteomics," *Analytical chemistry* **76,** 3556–3568 (2004).

[170] Z. Bai, M. Filiaggi, and J. Dahn, "Fibrinogen adsorption onto 316L stainless steel, Nitinol and titanium," *Surface Science* **603,** 839–846 (2009).

[171] B. Zdyrko, P. B.-Y. Ofir, A. M. Alb, W. F. Reed, and M. M. Santore, "Adsorption of copolymers aggregates: From kinetics to adsorbed layer structure," *Journal of colloid and interface science* **322,** 365–374 (2008).

[172] J. J. Ramsden, "Experimental methods for investigating protein adsorption kinetics at surfaces," *Quarterly Reviews of Biophysics* **27,** 41–105 (1994).

[173] K. Nakanishi, T. Sakiyama, and K. Imamura, "On the adsorption of proteins on solid surfaces, a common but very complicated phenomenon," *Journal of Bioscience and Bioengineering* **91,** 233–244 (2001).

[174] P. Kao, P. Parhi, A. Krishnan, H. Noh, W. Haider, S. Tadigadapa, D. L. Allara, and E. A. Vogler, "Volumetric interpretation of protein adsorption: interfacial packing of protein adsorbed to hydrophobic surfaces from surface-saturating solution concentrations," *Biomaterials* **32,** 969–978 (2011).

[175] K. Murayama and M. Tomida, "Heat-induced secondary structure and conformation change of bovine serum albumin investigated by Fourier transform infrared spectroscopy," *Biochemistry* **43,** 11526–11532 (2004).

[176] P. Roach, D. Farrar, and C. C. Perry, "Surface tailoring for controlled protein adsorption: effect of topography at the nanometer scale and chemistry," *Journal of the American Chemical Society* **128,** 3939–3945 (2006).

[177] L. Vroman, A. Adams, G. Fischer, and P. Munoz, "Interaction of high molecular weight kininogen, factor XII, and fibrinogen in plasma at interfaces," *Blood* **55,** 156–159 (1980).

[178] A. Ebadi, J. S. S. Mohammadzadeh, and A. Khudiev, "What is the correct form of BET isotherm for modeling liquid phase adsorption?," *Adsorption* **15,** 65–73 (2009).

[179] S. Brunauer, P. H. Emmett, and E. Teller, "Adsorption of gases in multimolecular layers," *Journal of the American Chemical Society* **60,** 309–319 (1938).

[180] B. Coasne, K. E. Gubbins, and R. J.-M. Pellenq, "A grand canonical Monte Carlo study of adsorption and capillary phenomena in nanopores of various morphologies and topologies: testing the BET and BJH characterization methods," *Particle & Particle Systems Characterization* **21,** 149–160 (2004).

[181] K. S. Walton and R. Q. Snurr, "Applicability of the BET method for determining surface areas of microporous metal-organic frameworks," *Journal of the American Chemical Society* **129,** 8552–8556 (2007).

[182] J. Talbot, G. Tarjus, P. Van Tassel, and P. Viot, "From car parking to protein adsorption: an overview of sequential adsorption processes," *Colloids and Surfaces A: Physicochemical and Engineering Aspects* **165,** 287–324 (2000).

[183] J. Scheutjens and G. Fleer, "Statistical theory of the adsorption of interacting chain molecules. 1. Partition function, segment density distribution, and adsorption isotherms," *Journal of Physical Chemistry* **83,** 1619–1635 (1979).

[184] Y.-S. Ho and G. McKay, "Sorption of dye from aqueous solution by peat," *Chemical Engineering Journal* **70,** 115–124 (1998).

[185] R. Eriksson, J. Merta, and J. B. Rosenholm, "The calcite/water interface: I. Surface charge in indifferent electrolyte media and the influence of low-molecular-weight polyelectrolyte," *Journal of colloid and interface science* **313,** 184–193 (2007).

[186] A. Fujishima, X. Zhang, and D. A. Tryk, "TiO¡ sub¿ 2¡/sub¿ photocatalysis and related surface phenomena," *Surface Science Reports* **63,** 515–582 (2008).

[187] S. Moulton, J. Barisci, A. Bath, R. Stella, and G. Wallace, "Investigation of protein adsorption and electrochemical behavior at a gold electrode," *Journal of colloid and interface science* **261,** 312–319 (2003).

[188] T. Berlind, P. Tengvall, L. Hultman, and H. Arwin, "Protein adsorption on thin films of carbon and carbon nitride monitored with in situ ellipsometry," *Acta Biomaterialia* **7,** 1369–1378 (2011).

[189] D. Axelrod, T. P. Burghardt, and N. L. Thompson, "Total internal reflection fluorescence," *Annual review of biophysics and bioengineering* **13,** 247–268 (1984).

[190] T.-C. Chang, C.-C. Wu, S.-C. Wang, L.-K. Chau, and W.-H. Hsieh, "Using A Fiber Optic Particle Plasmon Resonance Biosensor To Determine Kinetic Constants of Antigen–Antibody Binding Reaction," *Analytical chemistry* **85,** 245–250 (2012).

[191] U. Diebold, "The surface science of titanium dioxide," *Surface science reports* **48,** 53–229 (2003).

[192] O. Carp, C. L. Huisman, and A. Reller, "Photoinduced reactivity of titanium dioxide," *Progress in solid state chemistry* **32,** 33–177 (2004).

[193] H. Noh and E. A. Vogler, "Volumetric interpretation of protein adsorption: mass and energy balance for albumin adsorption to particulate adsorbents with incrementally increasing hydrophilicity," *Biomaterials* **27,** 5801–5812 (2006).

[194] H. Noh, S. T. Yohe, and E. A. Vogler, "Volumetric interpretation of protein adsorption: ion-exchange adsorbent capacity, protein pI, and interaction energetics," *Biomaterials* **29,** 2033–2048 (2008).

[195] B. Nowack and T. D. Bucheli, "Occurrence, behavior and effects of nanoparticles in the environment," *Environmental pollution* **150,** 5–22 (2007).

[196] D. B. Kittelson, "Engines and nanoparticles: a review," *Journal of aerosol science* **29,** 575–588 (1998).

[197] N. Lewinski, V. Colvin, and R. Drezek, "Cytotoxicity of nanoparticles," *small* **4,** 26–49 (2008).

[198] A. T. Bell, "The impact of nanoscience on heterogeneous catalysis," *Science* **299,** 1688–1691 (2003).

[199] F. Caruso, R. A. Caruso, and H. Möhwald, "Nanoengineering of inorganic and hybrid hollow spheres by colloidal templating," *Science* **282,** 1111–1114 (1998).

[200] S. Oldenburg, R. Averitt, S. Westcott, and N. Halas, "Nanoengineering of optical resonances," *Chemical Physics Letters* **288,** 243–247 (1998).

[201] I. Brigger, C. Dubernet, and P. Couvreur, "Nanoparticles in cancer therapy and diagnosis," *Advanced drug delivery reviews* **54,** 631–651 (2002).

[202] M. E. Davis, D. M. Shin, et al., "Nanoparticle therapeutics: an emerging treatment modality for cancer," *Nature reviews Drug discovery* **7,** 771–782 (2008).

[203] T. A. Taton, C. A. Mirkin, and R. L. Letsinger, "Scanometric DNA array detection with nanoparticle probes," *Science* **289,** 1757–1760 (2000).

[204] A. N. Shipway, E. Katz, and I. Willner, "Nanoparticle arrays on surfaces for electronic, optical, and sensor applications," *ChemPhysChem* **1,** 18–52 (2000).

[205] Y. C. Cao, R. Jin, and C. A. Mirkin, "Nanoparticles with Raman spectroscopic fingerprints for DNA and RNA detection," *Science* **297,** 1536–1540 (2002).

[206] X. Gao, Y. Cui, R. M. Levenson, L. W. Chung, and S. Nie, "In vivo cancer targeting and imaging with semiconductor quantum dots," *Nature biotechnology* **22,** 969–976 (2004).

[207] M.-C. Daniel and D. Astruc, "Gold nanoparticles: assembly, supramolecular chemistry, quantum-size-related properties, and applications toward biology, catalysis, and nanotechnology," *Chemical reviews* **104,** 293–346 (2004).

[208] K. S. Soppimath, T. M. Aminabhavi, A. R. Kulkarni, and W. E. Rudzinski, "Biodegradable polymeric nanoparticles as drug delivery devices," *Journal of controlled release* **70,** 1–20 (2001).

[209] M. Hans and A. Lowman, "Biodegradable nanoparticles for drug delivery and targeting," *Current Opinion in Solid State and Materials Science* **6,** 319–327 (2002).

[210] J. Panyam and V. Labhasetwar, "Biodegradable nanoparticles for drug and gene delivery to cells and tissue," *Advanced drug delivery reviews* **55,** 329–347 (2003).

[211] F. Mafuné, J.-y. Kohno, Y. Takeda, T. Kondow, and H. Sawabe, "Formation of gold nanoparticles by laser ablation in aqueous solution of surfactant," *The Journal of Physical Chemistry B* **105,** 5114–5120 (2001).

[212] J. Pérez-Juste, I. Pastoriza-Santos, L. M. Liz-Marzán, and P. Mulvaney, "Gold nanorods: synthesis, characterization and applications," *Coordination Chemistry Reviews* **249,** 1870–1901 (2005).

[213] C. Marambio-Jones and E. M. Hoek, "A review of the antibacterial effects of silver nanomaterials and potential implications for human health and the environment," *Journal of Nanoparticle Research* **12,** 1531–1551 (2010).

[214] F. E. Kruis, H. Fissan, and A. Peled, "Synthesis of nanoparticles in the gas phase for electronic, optical and magnetic applicationsa review," *Journal of Aerosol Science* **29,** 511–535 (1998).

[215] S. Gupta and A. Saxena, "Nanocarbon materials: probing the curvature and topology effects using phonon spectra," *Journal of Raman Spectroscopy* **40,** 1127–1137 (2009).

[216] E. A. Meulenkamp, "Synthesis and growth of ZnO nanoparticles," *The Journal of Physical Chemistry B* **102,** 5566–5572 (1998).

[217] J. P. Cason and C. B. Roberts, "Metallic copper nanoparticle synthesis in AOT reverse micelles in compressed propane and supercritical ethane solutions," *The Journal of Physical Chemistry B* **104,** 1217–1221 (2000).

[218] C. L. Carnes and K. J. Klabunde, "Synthesis, isolation, and chemical reactivity studies of nanocrystalline zinc oxide," *Langmuir* **16,** 3764–3772 (2000).

[219] R. S. Underhill and G. Liu, "Triblock nanospheres and their use as templates for inorganic nanoparticle preparation," *Chemistry of materials* **12,** 2082–2091 (2000).

[220] S. Sun, H. Zeng, D. B. Robinson, S. Raoux, P. M. Rice, S. X. Wang, and G. Li, "Monodisperse MFe2O4 (M= Fe, Co, Mn) nanoparticles," *Journal of the American Chemical Society* **126,** 273–279 (2004).

[221] C. Q. Sun, "Size dependence of nanostructures: Impact of bond order deficiency," *Progress in solid state chemistry* **35,** 1–159 (2007).

[222] G. Gouadec and P. Colomban, "Raman Spectroscopy of nanomaterials: How spectra relate to disorder, particle size and mechanical properties," *Progress in Crystal Growth and Characterization of Materials* **53,** 1–56 (2007).

[223] C. M. Niemeyer, "Nanoparticles, proteins, and nucleic acids: biotechnology meets materials science," *Angewandte Chemie International Edition* **40,** 4128–4158 (2001).

[224] T. Asahi, T. Sugiyama, and H. Masuhara, "Laser fabrication and spectroscopy of organic nanoparticles," *Accounts of chemical research* **41,** 1790–1798 (2008).

[225] J. M. Thomas and R. Raja, "Nanopore and nanoparticle catalysts," *The Chemical Record* **1,** 448–466 (2001).

[226] C. L. Haynes and R. P. Van Duyne, "Nanosphere lithography: a versatile nanofabrication tool for studies of size-dependent nanoparticle optics," *The Journal of Physical Chemistry B* **105,** 5599–5611 (2001).

[227] W. Marine, L. Patrone, B. Luk'Yanchuk, and M. Sentis, "Strategy of nanocluster and nanostructure synthesis by conventional pulsed laser ablation," *Applied surface science* **154,** 345–352 (2000).

[228] S. Dolgaev, A. Simakin, V. Voronov, G. Shafeev, and F. Bozon-Verduraz, "Nanoparticles produced by laser ablation of solids in liquid environment," *Applied surface science* **186,** 546–551 (2002).

[229] C. H. Bae, S. H. Nam, and S. M. Park, "Formation of silver nanoparticles by laser ablation of a silver target in NaCl solution," *Applied Surface Science* **197,** 628–634 (2002).

[230] R. Wood, J. Leboeuf, K.-R. Chen, D. Geohegan, and A. Puretzky, "Dynamics of plume propagation, splitting, and nanoparticle formation during pulsed-laser ablation," *Applied surface science* **127,** 151–158 (1998).

[231] M. Ullmann, S. K. Friedlander, and A. Schmidt-Ott, "Nanoparticle formation by laser ablation," *Journal of Nanoparticle Research* **4,** 499–509 (2002).

[232] S. Amoruso, G. Ausanio, R. Bruzzese, M. Vitiello, and X. Wang, "Femtosecond laser pulse irradiation of solid targets as a general route to nanoparticle formation in a vacuum," *Physical Review B* **71,** 033406 (2005).

[233] K. B. Narayanan and N. Sakthivel, "Biological synthesis of metal nanoparticles by microbes," *Advances in colloid and interface science* **156,** 1–13 (2010).

[234] B. Nikoobakht and M. A. El-Sayed, "Preparation and growth mechanism of gold nanorods (NRs) using seed-mediated growth method," *Chemistry of Materials* **15,** 1957–1962 (2003).

[235] T. W. Prow, J. E. Grice, L. L. Lin, R. Faye, M. Butler, W. Becker, E. M. Wurm, C. Yoong, T. A. Robertson, H. P. Soyer, et al., "Nanoparticles and microparticles for skin drug delivery," *Advanced drug delivery Reviews* **63,** 470–491 (2011).

[236] B. Baroli, "Penetration of nanoparticles and nanomaterials in the skin: fiction or reality?," *Journal of pharmaceutical sciences* **99,** 21–50 (2010).

[237] L. J. Mortensen, G. Oberdorster, A. P. Pentland, and L. A. DeLouise, "In vivo skin penetration of quantum dot nanoparticles in the murine model: the effect of UVR," *Nano letters* **8,** 2779–2787 (2008).

[238] L. K. Adams, D. Y. Lyon, and P. J. Alvarez, "Comparative eco-toxicity of nanoscale TiO 2, SiO 2, and ZnO water suspensions," *Water research* **40,** 3527–3532 (2006).

[239] S. Hussain, K. Hess, J. Gearhart, K. Geiss, and J. Schlager, "In vitro toxicity of nanoparticles in BRL 3A rat liver cells," *Toxicology in vitro* **19,** 975–983 (2005).

[240] M. Heinlaan, A. Ivask, I. Blinova, H.-C. Dubourguier, and A. Kahru, "Toxicity of nanosized and bulk ZnO, CuO and TiO 2 to bacteria Vibrio fischeri and crustaceans Daphnia magna and Thamnocephalus platyurus," *Chemosphere* **71,** 1308–1316 (2008).

[241] B. D. Chithrani, A. A. Ghazani, and W. C. Chan, "Determining the size and shape dependence of gold nanoparticle uptake into mammalian cells," *Nano letters* **6,** 662–668 (2006).

[242] M. Moore, "Do nanoparticles present ecotoxicological risks for the health of the aquatic environment?," *Environment International* **32,** 967–976 (2006).

[243] T. C. Long, N. Saleh, R. D. Tilton, G. V. Lowry, and B. Veronesi, "Titanium dioxide (P25) produces reactive oxygen species in immortalized brain microglia (BV2): implications for nanoparticle neurotoxicity," *Environmental Science & Technology* **40,** 4346–4352 (2006).

[244] S. Nie and S. R. Emory, "Probing single molecules and single nanoparticles by surface-enhanced Raman scattering," *science* **275,** 1102–1106 (1997).

[245] G. P. Kumar, "Gold nanoparticle-coated biomaterial as SERS micro-probes," *Bulletin of Materials Science* **34,** 417–422 (2011).

[246] S. Kim, H. E. Pudavar, A. Bonoiu, and P. N. Prasad, "Aggregation-Enhanced Fluorescence in Organically Modified Silica Nanoparticles: A Novel Approach toward High-Signal-Output Nanoprobes for Two-Photon Fluorescence Bioimaging," *Advanced Materials* **19,** 3791–3795 (2007).

[247] K. A. Willets and R. P. Van Duyne, "Localized surface plasmon resonance spectroscopy and sensing," *Annu. Rev. Phys. Chem.* **58,** 267–297 (2007).

[248] K. Kneipp, Y. Wang, H. Kneipp, L. T. Perelman, I. Itzkan, R. R. Dasari, and M. S. Feld, "Single molecule detection using surface-enhanced Raman scattering (SERS)," *Physical review letters* **78,** 1667 (1997).

[249] K. Kneipp, H. Kneipp, I. Itzkan, R. R. Dasari, and M. S. Feld, "Ultrasensitive chemical analysis by Raman spectroscopy," *Chemical reviews* **99,** 2957–2976 (1999).

[250] M. Pelton, J. Aizpurua, and G. Bryant, "Metal-nanoparticle plasmonics," *Laser & Photonics Reviews* **2,** 136–159 (2008).

[251] J. Enkovaara, C. Rostgaard, J. J. Mortensen, J. Chen, M. Duak, L. Ferrighi, J. Gavnholt, C. Glinsvad, V. Haikola, H. A. Hansen, H. H. Kristoffersen, M. Kuisma, A. H. Larsen, L. Lehtovaara, M. Ljungberg, O. Lopez-Acevedo, P. G. Moses, J. Ojanen, T. Olsen, V. Petzold, N. A. Romero, J. Stausholm-Mller, M. Strange, G. A. Tritsaris, M. Vanin, M. Walter, B. Hammer, H. Hkkinen, G. K. H. Madsen, R. M. Nieminen, J. K. Nrskov, M. Puska, T. T. Rantala, J. Schitz, K. S. Thygesen, and K. W. Jacobsen, "Electronic structure calculations with GPAW: a real-space implementation of the projector augmented-wave method," *Journal of Physics: Condensed Matter* **22,** 253202 (2010).

[252] K. Lejaeghere, V. Van Speybroeck, G. Van Oost, and S. Cottenier, "Error estimates for solid-state density-functional theory predictions: an overview by means of the ground-state elemental crystals," *Critical Reviews in Solid State and Materials Sciences* **39,** 1–24 (2014).

[253] D. Matthey, J. Wang, S. Wendt, J. Matthiesen, R. Schaub, E. Lægsgaard, B. Hammer, and F. Besenbacher, "Enhanced bonding of gold nanoparticles on oxidized TiO2 (110)," *Science* **315,** 1692–1696 (2007).

[254] P. K. Jain, X. Huang, I. H. El-Sayed, and M. A. El-Sayed, "Noble metals on the nanoscale: optical and photothermal properties and some applications in imaging, sensing, biology, and medicine," *Accounts of Chemical Research* **41,** 1578–1586 (2008).

[255] E. Katz and I. Willner, "Integrated nanoparticle–biomolecule hybrid systems: synthesis, properties, and applications," *Angewandte Chemie International Edition* **43,** 6042–6108 (2004).

[256] P. Amirtharaj, R. Azzam, L. Beiser, J. Bennett, E. Betensky, G. Boreman, R. Breault, T. Brown, I. Chang, R. Chipman, K. Creath, M. Cronin-Golomb, M. Farn, N. Goldberg, P. Hariharin, T. Harris, J. Harvey, B. Henderson, L. Huff, S. Inoue, R. Johnson, L. Jones, M. Klein, T. Koch, M. Kreitzer, F. Leonberger, J. Lytle, D. Malacara, Z. Malacara, T. Maldonado, T. Milster, D. Moore, J. Moskovich, R. Olderbourg, J. Palmer, R. Paquin, S. Pompea, D. Seiler, J. Stover, P. Suchoski, C. Tang, M. Thomas, W. Tropf, W. Veldkamp, W. Wetherell, W. Wolfe, S.-T. Wu, J. Wyant, E. Zalewski, and G. Zissis, *Handbook of Optics, Volume II: Devices, Measurements, and Properties* (McGraw-Hill, Inc., 1995).

[257] P. A. Cuypers, J. W. Corsel, M. P. Janssen, J. Kop, W. T. Hermens, and H. C. Hemker, "The adsorption of prothrombin to phosphatidylserine multilayers quantitated by ellipsometry.," *Journal of Biological Chemistry* **258,** 2426–2431 (1983).

[258] C. F. Mandenius and L. Ljunggren, "Ellipsometric studies of plasma protein adsorption on membrane polymers for blood purification," *Biomaterials* **12,** 369 – 373 (1991).

[259] H. A. Andree, W. T. Hermens, and G. M. Willems, "Testing protein adsorption models by off-null ellipsometry: Determination of binding constants from a single adsorption curve," *Colloids and Surfaces A: Physicochemical and Engineering Aspects* **78,** 133 – 141 (1993).

[260] M. Malmsten, "Ellipsometry studies of protein adsorption at lipid surfaces," *Journal of colloid and interface science* **168,** 247–254 (1994).

[261] M. Malmsten, "Ellipsometry studies of the effects of surface hydrophobicity on protein adsorption," *Colloids and Surfaces B: Biointerfaces* **3,** 297–308 (1995).

[262] M. Malmsten, "Protein adsorption at phospholipid surfaces," *Journal of colloid and interface science* **172,** 106–115 (1995).

[263] B. Lassen and M. Malmsten, "Competitive protein adsorption studied with TIRF and ellipsometry," *Journal of colloid and interface science* **179,** 470–477 (1996).

[264] K. Spaeth, A. Brecht, and G. Gauglitz, "Studies on the biotin–avidin multilayer adsorption by spectroscopic ellipsometry," *Journal of colloid and interface science* **196,** 128–135 (1997).

[265] R. Green, J. Davies, M. Davies, C. Roberts, and S. Tendler, "Surface plasmon resonance for real time¡ i¿ in situ¡/i¿ analysis of protein adsorption to polymer surfaces," *Biomaterials* **18,** 405–413 (1997).

[266] R. Kurrat, B. Wälivaara, A. Marti, M. Textor, P. Tengvall, J. Ramsden, and N. Spencer, "Plasma protein adsorption on titanium: comparative in situ studies using optical waveguide lightmode spectroscopy and ellipsometry," *Colloids and Surfaces B: Biointerfaces* **11,** 187–201 (1998).

[267] M. Poksinski and H. Arwin, "Protein monolayers monitored by internal reflection ellipsometry," *Thin Solid Films* **455,** 716–721 (2004).

[268] K. Sakai, M. Vamvakaki, E. G. Smith, E. J. Wanless, S. P. Armes, and S. Biggs, "Adsorption characteristics of zwitterionic diblock copolymers at the silica/aqueous solution interface," *Journal of colloid and interface science* **317,** 383–394 (2008).

[269] S. Reichelt, K.-J. Eichhorn, D. Aulich, K. Hinrichs, N. Jain, D. Appelhans, and B. Voit, "Functionalization of solid surfaces with hyperbranched polyesters to control protein adsorption," *Colloids and Surfaces B: Biointerfaces* **69,** 169–177 (2009).

[270] J. Den Boer, G. Kroesen, and F. De Hoog, "Measurement of the complex refractive index of liquids in the infrared using spectroscopic attenuated total reflection ellipsometry: correction for depolarization by scattering," *Applied optics* **34,** 5708–5714 (1995).

[271] A. Bernard and H. R. Bosshard, "Real-Time Monitoring of Antigen-antibody Recognition on a Metal Oxide Surface by an Optical Grating Coupler Sensor," *European Journal of Biochemistry* **230,** 416–423 (1995).

[272] W. Lukosz, "Integrated optical chemical and direct biochemical sensors," *Sensors and Actuators B: Chemical* **29,** 37–50 (1995).

[273] J. Vörös, J. Ramsden, G. Csucs, I. Szendrő, S. De Paul, M. Textor, and N. Spencer, "Optical grating coupler biosensors," *Biomaterials* **23,** 3699–3710 (2002).

[274] F. Caruso, P. S. Vukusic, K. Matsuura, R. S. Urquhart, D. N. Furlong, and Y. Okahata, "Investigation of immuno-reactions in a flow-injection system using surface plasmon resonance," *Colloids and Surfaces A: Physicochemical and Engineering Aspects* **103,** 147–157 (1995).

[275] J.-C. Lai, Y.-Y. Zhang, Z.-H. Li, H.-J. Jiang, and A.-Z. He, "Complex refractive index measurement of biological tissues by attenuated total reflection ellipsometry," *Applied optics* **49,** 3235–3238 (2010).

[276] I. Baleviciute, Z. Balevicius, A. Makaraviciute, A. Ramanaviciene, and A. Ramanavicius, "Study of antibody/antigen binding kinetics by total internal reflection ellipsometry," *Biosensors and Bioelectronics* **39,** 170–176 (2013).

[277] N.-P. Huang, R. Michel, J. Vrs, M. Textor, R. Hofer, A. Rossi, D. L. Elbert, J. A. Hubbell, and N. D. Spencer, "Poly (L-lysine)-g-poly (ethylene glycol) layers on metal oxide surfaces: surface-analytical characterization and resistance to serum and fibrinogen adsorption," *Langmuir* **17,** 489–498 (2001).

[278] F. Höök, J. Vörös, M. Rodahl, R. Kurrat, P. Böni, J. Ramsden, M. Textor, N. Spencer, P. Tengvall, J. Gold, et al., "A comparative study of protein adsorption on titanium oxide surfaces using in situ ellipsometry, optical waveguide lightmode spectroscopy, and quartz crystal microbalance/dissipation," *Colloids and Surfaces B: Biointerfaces* **24,** 155–170 (2002).

[279] A. Toscano and M. M. Santore, "Fibrinogen adsorption on three silica-based surfaces: conformation and kinetics," *Langmuir* **22,** 2588–2597 (2006).

[280] E. Kretschmann and H. Raether, "Radiative decay of non-radiative surface plasmons excited by light," *Z. Naturforsch. a* **23,** 2135–2136 (1968).

[281] H. Räther, *Surface Plasmons on Smooth and Rough Surfaces and on Gratings*, Vol. 111 of *Springer Tracts in Modern Physics* (Springer Berlin Heidelberg, 1988).

[282] R. J. Green, R. A. Frazier, K. M. Shakesheff, M. C. Davies, C. J. Roberts, and S. J. Tendler, "Surface plasmon resonance analysis of dynamic biological interactions with biomaterials," *Biomaterials* **21,** 1823–1835 (2000).

[283] T. Atay, J.-H. Song, and A. V. Nurmikko, "Strongly interacting plasmon nanoparticle pairs: from dipole-dipole interaction to conductively coupled regime," *Nano Letters* **4,** 1627–1631 (2004).

[284] Q. Tang, X. Su, and K. P. Loh, "Surface plasmon resonance spectroscopy study of interfacial binding of thrombin to antithrombin DNA aptamers," *Journal of colloid and interface science* **315,** 99–106 (2007).

[285] F. Tam, G. P. Goodrich, B. R. Johnson, and N. J. Halas, "Plasmonic enhancement of molecular fluorescence," *Nano Letters* **7,** 496–501 (2007).

[286] D. Schaadt, B. Feng, and E. Yu, "Enhanced semiconductor optical absorption via surface plasmon excitation in metal nanoparticles," *Applied Physics Letters* **86,** 063106 (2005).

[287] C. Boozer, Q. Yu, S. Chen, C.-Y. Lee, J. Homola, S. S. Yee, and S. Jiang, "Surface functionalization for self-referencing surface plasmon resonance (SPR) biosensors by multi-step self-assembly," *Sensors and Actuators B: Chemical* **90,** 22–30 (2003).

[288] O. Siiman and A. Burshteyn, "Preparation, microscopy, and flow cytometry with excitation into surface plasmon resonance bands of gold or silver nanoparticles on aminodextran-coated polystyrene beads," *The Journal of Physical Chemistry B* **104,** 9795–9810 (2000).

[289] J. Homola, S. S. Yee, and G. Gauglitz, "Surface plasmon resonance sensors: review," *Sensors and Actuators B: Chemical* **54,** 3–15 (1999).

[290] S.-Y. Chen, J. J. Mock, R. T. Hill, A. Chilkoti, D. R. Smith, and A. A. Lazarides, "Gold nanoparticles on polarizable surfaces as raman scattering antennas," *ACS nano* **4,** 6535–6546 (2010).

[291] K.-S. Lee and M. A. El-Sayed, "Gold and silver nanoparticles in sensing and imaging: sensitivity of plasmon response to size, shape, and metal composition," *The Journal of Physical Chemistry B* **110,** 19220–19225 (2006).

[292] B. Nguyen, F. A. Tanious, and W. D. Wilson, "Biosensor-surface plasmon resonance: quantitative analysis of small molecule–nucleic acid interactions," *Methods* **42,** 150–161 (2007).

[293] P. K. Jain, W. Huang, and M. A. El-Sayed, "On the universal scaling behavior of the distance decay of plasmon coupling in metal nanoparticle pairs: a plasmon ruler equation," *Nano Letters* **7,** 2080–2088 (2007).

[294] G. B. Sigal, C. Bamdad, A. Barberis, J. Strominger, and G. M. Whitesides, "A self-assembled monolayer for the binding and study of histidine-tagged proteins by surface plasmon resonance," *Analytical Chemistry* **68,** 490–497 (1996).

[295] T. Wink, S. J. van Zuilen, A. Bult, and W. P. Van Bennekom, "Liposome-mediated enhancement of the sensitivity in immunoassays of proteins and peptides in surface plasmon resonance spectrometry," *Analytical chemistry* **70,** 827–832 (1998).

[296] B. Schneider, E. Dickinson, M. Vach, J. Hoijer, and L. Howard, "Highly sensitive optical chip immunoassays in human serum," *Biosensors and Bioelectronics* **15,** 13–22 (2000).

[297] A. Ono, M. Kikawada, R. Akimoto, W. Inami, and Y. Kawata, "Fluorescence enhancement with deep-ultraviolet surface plasmon excitation," *Optics express* **21,** 17447–17453 (2013).

[298] H. Kano and S. Kawata, "Two-photon-excited fluorescence enhanced by a surface plasmon," *Optics letters* **21,** 1848–1850 (1996).

[299] J. N. Anker, W. P. Hall, O. Lyandres, N. C. Shah, J. Zhao, and R. P. Van Duyne, "Biosensing with plasmonic nanosensors," *Nature materials* **7,** 442–453 (2008).

[300] K. Matsubara, S. Kawata, and S. Minami, "Optical chemical sensor based on surface plasmon measurement," *Applied Optics* **27,** 1160–1163 (1988).

[301] L.-M. Zhang and D. Uttamchandani, "Optical chemical sensing employing surface plasmon resonance," *Electronics Letters* **24,** 1469–1470 (1988).

[302] A. F. Fercher, W. Drexler, C. K. Hitzenberger, and T. Lasser, "Optical coherence tomography-principles and applications," *Reports on progress in physics* **66,** 239 (2003).

[303] M. N. Sela, L. Badihi, G. Rosen, D. Steinberg, and D. Kohavi, "Adsorption of human plasma proteins to modified titanium surfaces," *Clinical oral implants research* **18,** 630–638 (2007).

[304] M. Martins, C. Fonseca, M. Barbosa, and B. Ratner, "Albumin adsorption on alkanethiols self-assembled monolayers on gold electrodes studied by chronopotentiometry," *Biomaterials* **24,** 3697–3706 (2003).

[305] K. E. Sapsford and F. S. Ligler, "Real-time analysis of protein adsorption to a variety of thin films," *Biosensors and Bioelectronics* **19,** 1045–1055 (2004).

[306] A. Sethuraman, M. Han, R. S. Kane, and G. Belfort, "Effect of surface wettability on the adhesion of proteins," *Langmuir* **20,** 7779–7788 (2004).

[307] J. Dübendorfer and R. Kunz, "Compact integrated optical immunosensor using replicated chirped grating coupler sensor chips," *Applied optics* **37,** 1890–1894 (1998).

[308] N. K. Viswanathan, S. Balasubramanian, L. Li, J. Kumar, and S. K. Tripathy, "Surface-initiated mechanism for the formation of relief gratings on azo-polymer films," *The Journal of Physical Chemistry B* **102,** 6064–6070 (1998).

[309] J. J. Ramsden, "Optical biosensors," *Journal of Molecular Recognition* **10,** 109–120 (1997).

[310] W.-T. Hsu, W.-H. Hsieh, S.-F. Cheng, C.-P. Jen, C.-C. Wu, C.-H. Li, C.-Y. Lee, W.-Y. Li, L.-K. Chau, C.-Y. Chiang, et al., "Integration of fiber optic-particle plasmon resonance biosensor with microfluidic chip," *Analytica chimica acta* **697,** 75–82 (2011).

[311] K. K. Chittur, "FTIR/ATR for protein adsorption to biomaterial surfaces," *Biomaterials* **19,** 357–369 (1998).

[312] J. Rayss and G. Sudolski, "Ion adsorption in the porous sol–gel silica layer in the fibre optic pH sensor," *Sensors and Actuators B: Chemical* **87,** 397–405 (2002).

[313] M. R. Böhmer, E. A. van der Zeeuw, and G. J. Koper, "Kinetics of particle adsorption in stagnation point flow studied by optical reflectometry," *Journal of colloid and interface science* **197,** 242–250 (1998).

[314] C. Picart, G. Ladam, B. Senger, J. Voegel, P. Schaaf, F. Cuisinier, and C. Gergely, "Determination of structural parameters characterizing thin films by optical methods: A comparison between scanning angle reflectometry and optical waveguide lightmode spectroscopy," *Journal of Chemical Physics* **115,** 1086–1094 (2001).

[315] J. Zhao and W. Brown, "Comparative study of the adsorption of nonionic surfactants: triton X-100 and C12E7 on polystyrene latex particles using dynamic light scattering and adsorption isotherm measurements," *The Journal of Physical Chemistry* **100,** 3775–3782 (1996).

[316] T. Okubo and M. Suda, "Absorption of polyelectrolytes on colloidal surfaces as studied by electrophoretic and dynamic light-scattering techniques," *Journal of colloid and interface science* **213,** 565–571 (1999).

[317] O. Santos, T. Nylander, M. Paulsson, and C. Trägårdh, "Whey protein adsorption onto steel surfaceseffect of temperature, flow rate, residence time and aggregation," *Journal of food engineering* **74,** 468–483 (2006).

[318] M. Amirkhani, S. Volden, K. Zhu, W. R. Glomm, and B. Nyström, "Adsorption of cellulose derivatives on flat gold surfaces and on spherical gold particles," *Journal of colloid and interface science* **328,** 20–28 (2008).

[319] R. Sigel, "Light scattering near and from interfaces using evanescent wave and ellipsometric light scattering," *Current Opinion in Colloid & Interface Science* **14,** 426–437 (2009).

[320] T. Hirvonen, N. Penttinen, M. Hauta-Kasari, M. Sorjonen, and K.-E. Peiponen, "A Wide Spectral Range Reflectance and Luminescence Imaging System," *Sensors* **13,** 14500–14510 (2013).

[321] P. Roach, N. J. Shirtcliffe, D. Farrar, and C. C. Perry, "Quantification of surface-bound proteins by fluorometric assay: comparison with quartz crystal microbalance and amido black assay," *The Journal of Physical Chemistry B* **110,** 20572–20579 (2006).

[322] M. Berglin, E. Pinori, A. Sellborn, M. Andersson, M. Hulander, and H. Elwing, "Fibrinogen adsorption and conformational change on model polymers: novel aspects of mutual molecular rearrangement," *Langmuir* **25,** 5602–5608 (2009).

[323] L. Richert, F. Variola, F. Rosei, J. D. Wuest, and A. Nanci, "Adsorption of proteins on nanoporous Ti surfaces," *Surface Science* **604,** 1445–1451 (2010).

[324] D. Bendedouch and S. H. Chen, "Structure and interparticle interactions of bovine serum albumin in solution studied by small-angle neutron scattering," *The Journal of Physical Chemistry* **87,** 1473–1477 (1983).

[325] J. Lu, T. Su, and R. Thomas, "Structural conformation of bovine serum albumin layers at the air–water interface studied by neutron reflection," *Journal of Colloid and Interface Science* **213,** 426–437 (1999).

[326] X. Liu, A. Dedinaite, T. Nylander, A. P. Dabkowska, M. Skoda, R. Makuska, and P. M. Claesson, "Association of anionic surfactant and physisorbed branched brush layers probed by neutron and optical reflectometry," *Journal of colloid and interface science* **440,** 245–252 (2015).

[327] B. Lassen and M. Malmsten, "Structure of protein layers during competitive adsorption," *Journal of Colloid and Interface Science* **180,** 339–349 (1996).

[328] H. Arwin, "Optical properties of thin layers of bovine serum albumin, γ-globulin, and hemoglobin," *Applied spectroscopy* **40,** 313–318 (1986).

[329] P. Silva-Bermudez, S. Muhl, and S. Rodil, "A comparative study of fibrinogen adsorption onto metal oxide thin films," *Applied Surface Science* **282,** 351–362 (2013).

[330] J. Vörös, "The density and refractive index of adsorbing protein layers," *Biophysical journal* **87,** 553–561 (2004).

[331] T. Byrne, S. Trussler, M. McArthur, L. Lohstreter, Z. Bai, M. Filiaggi, and J. Dahn, "A new simple tubular flow cell for use with variable angle spectroscopic ellipsometry: A high throughput in situ protein adsorption study," *Surface Science* **603,** 2888–2895 (2009).

[332] G. M. Hale and M. R. Querry, "Optical constants of water in the 200-nm to 200-μm wavelength region," *Applied optics* **12,** 555–563 (1973).

[333] I. Malitson, "Interspecimen comparison of the refractive index of fused silica," *JOSA* **55,** 1205–1208 (1965).

[334] J. A. De Feijter, J. Benjamins, and F. A. Veer, "Ellipsometry as a tool to study the adsorption behavior of synthetic and biopolymers at the airwater interface," *Biopolymers* **17,** 1759–1772 (1978).

[335] V. Ball and J. J. Ramsden, "Buffer dependence of refractive index increments of protein solutions," *Biopolymers* **46,** 489–492 (1998).

[336] D. S. Goodman, J. E. Greivenkamp, A. S. Marathay, W. H. Carter, J. M. Bennett, C. F. Bohren, E. L. Church, P. Z. Takacs, B. Henderson, A. Miller, A. LaRocca, W. T. Silfvast, R. H. Haitz, M. G. Craford, R. H. Weissman, P. L. Derry, L. Figueroa, C. S. Hong, X. M. Zhao, J. C. Diels, P. R. Norton, A. M. Joshi, G. H. Olsen, J. E. Bowers, Y. G. Wey, J. R. Willison, W. L. Wolfe, P. W. Kruse, J. H. Altman, C. B. Johnson, L. D. Owen, T. J. Tredwell, L. J. Kozlowski, W. F. Kosonocky, W. N. Charman, W. S. Geisler, M. S. Banks, D. H. Brainard, W. Cowan, S. A. Burns, R. H. Webb, D. G. Pelli, B. Farell, J. W. Goodman, M. Mansuripur, W. J. Smith, D. C. O. . Shea, M. E. Harrigan, D. C. Sinclair, R. R. Shannon, R. R. Shannon, P. R. Y. Jr., R. P. Breault, P. J. Rogers, M. Roberts, R. E. Parks, R. L. Rhorer, C. J. Evans, J. A. Dobrowolski,

C. D. Mobley, D. K. Killinger, J. H. Churnside, and L. S. Rothman, *Handbook of Optics, Volume 1, Fundamentals, Techniques, and Design, Second Edition* (McGraw-Hill , Inc, 1995).

[337] D. S. . Goodman, *Handbook of Optics, Volume 1, Chapter 1*, Second edition ed. (McGraw-Hill, Inc., 1995).

[338] R. Azzam, "Modulated generalized ellipsometry," *JOSA* **66,** 520–524 (1976).

[339] A. Robles-Kelly and C. Huynh, *Imaging Spectroscopy for Scene Analysis* (Springer-Verlag New York Incorporated, 2012).

[340] C. I. Palmer and C. W. Leigh, *Plane and Spherical Trigonometry* (McGraw-Hill Book Company, Inc., 1934), Fourth Edition, Ninth Impression.

[341] S. Kim, "Simultaneous determination of refractive index, extinction coefficient, and void distribution of titanium dioxide thin film by optical methods," *Applied optics* **35,** 6703–6707 (1996).

[342] K. Cai, M. Müller, J. Bossert, A. Rechtenbach, and K. D. Jandt, "Surface structure and composition of flat titanium thin films as a function of film thickness and evaporation rate," *Applied Surface Science* **250,** 252–267 (2005).

[343] D. Lide, *CRC handbook of chemistry and physics : a ready-reference book of chemical and physical data* (CRC Press, Boca Raton, Fla, 2004).

[344] H.-C. Lee, *Introduction to color imaging science* (Cambridge University Press, 2005).

[345] R. Collins, I. An, C. Chen, A. Ferlauto, and J. Zapien, "Advances in multichannel ellipsometric techniques for in-situ and real-time characterization of thin films," *Thin solid films* **469,** 38–46 (2004).

[346] G. Droulers, A. Beaumont, J. Beauvais, and D. Drouin, "Spectroscopic ellipsometry on thin titanium oxide layers grown on titanium by plasma oxidation," *Journal of Vacuum Science & Technology B* **29,** 021010 (2011).

[347] J. Maartensson and H. Arwin, "Interpretation of spectroscopic ellipsometry data on protein layers on gold including substrate-layer interactions," *Langmuir* **11,** 963–968 (1995).

[348] S. Lousinian and S. Logothetidis, "Optical properties of proteins and protein adsorption study," *Microelectronic Engineering* **84,** 479–485 (2007).

[349] H. Kim, J. Park, and B. Lee, *Fourier Modal Method and Its Applications in Computational Nanophotonics* (CRC Press, 2012).

[350] European Computer Manufacturers Association, "Standard ECMA-4 Flow Charts," (1966).

[351] S. Takemoto, T. Yamamoto, K. Tsuru, S. Hayakawa, A. Osaka, and S. Takashima, "Platelet adhesion on titanium oxide gels: effect of surface oxidation," *Biomaterials* **25,** 3485–3492 (2004).

[352] A. Abdulagatov, Y. Yan, J. Cooper, Y. Zhang, Z. Gibbs, A. Cavanagh, R. Yang, Y. Lee, and S. George, "Al2O3 and TiO2 atomic layer deposition on copper for water corrosion resistance," *ACS applied materials & interfaces* **3,** 4593–4601 (2011).

[353] P. Johnson and R. Christy, "Optical constants of transition metals: Ti, V, Cr, Mn, Fe, Co, Ni, and Pd," *Physical Review B* **9,** 5056 (1974).

Niko Penttinen

Photonic adsorption studies in liquid

devices, models, and an ellipsometric approach

This thesis discusses of the necessity of correct model variables in photonic sensing of adsorption. A wide outlook on this challenging phenomenon as well as to the existing approaches and literature serves as a reference point to the discussion. An ellipsometric device is constructed and related theory is shown. Finally, a set of example measurements are discussed and reflected to theoretical calculations in an overall aim to reveal what is and isn't a plausible model for liquid environment adsorption.

UNIVERSITY OF EASTERN FINLAND

Publications of the University of Eastern Finland
Dissertations in Forestry and Natural Sciences

ISBN: 978-952-61-1818-5 (printed)
ISSNL: 1798-5668
ISSN: 1798-5668
ISBN: 978-952-61-1819-2 (PDF)
ISSN: 1798-5676 (PDF)